Universidade de Aveiro
2020

Bruno João
da Fonseca
Barroqueiro

Metodologias para projeto mecânico ótimo de estruturas espaciais obtidas por fabrico aditivo

Methodologies for an optimum mechanical design of space structures obtained from additive manufacturing

Universidade de Aveiro
2020

Bruno João da Fonseca Barroqueiro

Metodologias para projeto mecânico ótimo de estruturas espaciais obtidas por fabrico aditivo

Methodologies for an optimum mechanical design of space structures obtained from additive manufacturing

Dissertação apresentada à Universidade de Aveiro para cumprimento dos requisitos necessários à obtenção do grau de Doutor em Engenharia Mecânica, realizada sob orientação científica de António Gil D'Orey de Andrade Campos, Professor Auxiliar com Agregação do Departamento de Engenharia Mecânica da Universidade de Aveiro, e de Robertt Ângelo Fontes Valente, Professor Associado do Departamento de Engenharia Mecânica da Universidade de Aveiro.

o júri / the jury

presidente / president

Doutor Fernando Manuel dos Santos Ramos
Professor Catedrático da Universidade de Aveiro

vogais / members

Doutor Pedro Samuel Gonçalves Coelho
Professor Auxiliar da *Faculdade de Ciências e Tecnologia da Universidade Nova de Lisboa*

Doutor Jorge Américo de Oliveira Pinto Belinha
Professor Adjunto da Instituto Superior de Engenharia do Instituto Politécnico do Porto

Doutora Ana Daniela Isidoro Brandão
Investigadora da European Space Technology and Research Centre (ESTEC), European Space Agency (ESA)

Doutora Isabel Maria Alexandrino Duarte
Investigadora Auxiliar da Universidade de Aveiro

Doutor António Gil D'Orey de Andrade Campos
Professor Auxiliar com Agregação da Universidade de Aveiro (orientador)

agradecimentos / acknowledgements

The work presented in this doctoral thesis was only possible thanks to the collaboration and support of some people.
I am grateful for the support given by my supervisors, Professor António Gil D'Orey de Andrade Campos and Professor Robertt Angelo Fontes Valente, who gave me the necessary guidance and support during these years.
I thank all the colleagues that contributed to my work.
I am grateful for the support given by Centre for Mechanical Technology & Automation of the University of Aveiro and grateful for the opportunity given to me that made developing my research possible.
I want to thank the support given by Active Space Technologies and all the resources made available that contributed to the development of my research work.
I am grateful for the support given by my family and friends.

This thesis is sponsored by a scientific research grant from the Portuguese Foundation for Science and Technology (FCT) with reference SFRH/BD/120779/2016. It was also supported by the FCT projects CENTRO-01-0145-FEDER-029713 by UE/FEDER through the programs CENTRO 2020 and COMPETE 2020, and UID/EMS/ 00481/2013-FCT under CENTRO-01-0145-FEDER-022083. Financial support of program CENTRO 2020 and UE/FEDER is acknowledged through the project CENTRO-01-0247-FEDER-024039, designated as ADVANSS.

keywords Additive Layer Manufacturing; Selective Laser Melting; Topology Optimization; Design for ALM; Laplacian Smoothing; Heterogeneous Specimens; Mechanical Testing; Ti6Al4V; Space Industry; Case Studies

abstract Additive Layer Manufacturing (ALM) is growing rapidly due to the unprecedented design freedom. Thus, the structures' complexity can be drastically increased without significant raises in costs. However, the economic viability of ALM is strongly dependent on the full exploration of the referred design freedom. In fact, the ALM is only cost-effective in highly customized parts. Moreover, the mechanical behavior of materials processed via ALM is an ongoing challenge due to defects, uncertainties in material characterization, and verification methods. Thus, the goal of the present work is the development of a robust methodology for the mechanical optimum design of metallic space structures obtained from additive manufacturing. Thus, two main tasks were established.

The first task is related to the mechanical characterization of a Ti6Al4V alloy, processed via Selective Laser Melting (SLM). Therefore, an experimental testing campaign of Ti6Al4V samples is presented using homogeneous macroscopic testing (tensile, compression, density, hardness, and fatigue) and microscopic testing (defects detection via microcomputed tomography). These samples show better static properties than the other counterparts, obtained by traditional manufacturing processes. However, the repeatability of the SLM samples is still a challenge (particularly in its fatigue behavior) and more testing is needed. Furthermore, these campaigns are expensive and, consequently, more information per test is required. With the development of full-field measurement methods, material model calibration strategies call upon the use of heterogeneous testing specimens. In the scope of this work, an indirect TO methodology is presented, being capable of designing a wide range of different heterogeneous specimens. Then, a stress states performance indicator is also presented to help the selection of the most promising geometry.

The second task is related to the definition of the engineering cycle for ALM structures in its mains phases: (i) design for ALM, (ii) bridging between Topology Optimization (TO) and ALM, (iii) process simulation and structural verification, and (iv) manufacturing. Concerning the first phase, ALM provides great geometric freedom however, there are some design limitations. Therefore, a systematic design methodology is presented, being based on a topology optimization algorithm capable of incorporating the main ALM design limitations (minimum member size and overhang angle). Furthermore, the non-trivial task of bridging between TO and the final smooth geometry is also studied (second phase). The referred task uses a Laplacian smoothing algorithm, which is based on the new concept of mutable diffusion. This new concept shows better properties than the classic algorithms, giving promising results. Furthermore, a new volume constraint is presented, which exhibits a less detrimental impact on the chosen struc-

tural indicators. Regarding the remaining phases, these were analyzed via industrial case studies. For instance, process simulation can provide crucial insight into the optimum manufacturing direction and might dictate the difference between success and failure upon manufacturing.

The impact of this Ph.D. is related with some improvements in (i) the characterization of ALM-produced materials as well as the geometry of the specimens used for their characterization; and in (ii) the engineering cycle of ALM structures, allowing higher efficiency in the structural solutions for the space industry with lower costs.

palavras-chave

Fabrico Aditivo por Camadas; Fusão Seletiva a Laser; Otimização topológica; Design para manufatura aditiva por camadas; Suavização Laplaciana; Provetes heterogéneos; Testes Mecânicos; Ti6Al4V; Indústria espacial; Casos de Estudo

resumo

O uso do fabrico aditivo por camadas está a crescer a um elevado ritmo devido à elevada liberdade de projeto de estruturas. Assim, a complexidade das estruturas pode ser aumentada significativamente sem incrementos significativos nos custos. Todavia, a viabilidade económica do fabrico aditivo por camadas é fortemente dependente de uma exploração inteligente da liberdade de projeto estrutural. Na verdade, o fabrico aditivo por camadas só é rentável em peças de elevada complexidade e valor acrescentado. Adicionalmente, o comportamento mecânico de materiais processados através do fabrico aditivo por camadas é ainda um desafio por resolver devido à existência de defeitos, incertezas na caraterização de materiais e nos seus métodos de verificação. Deste modo, o objetivo deste trabalho é o desenvolvimento de uma metodologia robusta que permita o projeto mecânico ótimo de estruturas obtidas por fabrico aditivo para a indústria espacial. Para isso, foram estabelecidas duas tarefas principais.

A primeira tarefa está relacionada com a caracterização mecânica da liga Ti6Al4V, processada através da fusão seletiva a laser. Portanto, foi realizado uma campanha de testes experimentais com provetes da liga Ti6Al4V composta por testes macroscópicos homogéneos (tração, compressão, densidade, dureza e fadiga) e testes microscópicos (deteção de defeitos usando uma análise com recurso à tomografia microcomputorizada). Foi verificado que estas amostras exibem melhor propriedades estáticas que amostras idênticas produzidas através de processos tradicionais. Contudo, a sua repetibilidade ainda é um desafio (particularmente o comportamento à fadiga), sendo necessário mais testes. Adicionalmente, estas campanhas experimentais são onerosas e, consequentemente, é crítico obter mais informação por cada teste realizado. Dado o desenvolvimento dos métodos de medição *full-field*, as estratégias de calibração de modelos de material propiciam o uso de provetes heterogéneos em testes mecânicos. No âmbito deste trabalho apresenta-se uma metodologia de otimização topológica indireta capaz de projetar uma grande variedade de provetes heterógenos. Posteriormente apresenta-se um indicador de desempenho baseado na quantidade de estados de tensão para selecionar o provete mais promissor.

A segunda tarefa está relacionada com a definição do ciclo de engenharia para o fabrico aditivo por camadas de estruturas metálicas nas suas fases principais: (i) projeto para fabrico aditivo por camadas, (ii) transição entre a otimização topológica e o fabrico aditivo por camadas, (iii) simulação do seu processo de fabrico e sua verificação estrutural e (iv) fabrico. Relativamente à primeira fase, o fabrico aditivo por camadas proporciona uma grande liberdade geométrica, contudo existe limitações ao design. Portanto é apresentada uma metodologia de projeto sistemática, baseada num algo-

ritmo de otimização topológica capaz de incorporar as principais limitações de projeto do fabrico aditivo por camadas tais como a espessura mínima e ângulo do material sem suporte. Adicionalmente, a tarefa complexa de efetuar a transição entre os resultados da otimização topológica e uma geometria final suave também é objeto de estudo. A tarefa anteriormente referida baseia-se na suavização Laplaciana que por sua vez se baseia no novo conceito de difusão mutável. Este novo conceito apresenta melhores e mais promissores resultados que os algoritmos clássicos. Adicionalmente, é apresentado uma nova restrição de volume que proporciona um menor impacto nos indicadores estruturais escolhidos. Relativamente às restantes fases, estas são analisadas através de casos de estudo industriais. A título exemplar, a simulação do processo de fabrico pode fornecer informações crucias para a escolha da direção de fabrico que, por sua vez, pode ditar a diferença entre o sucesso ou o insucesso durante o fabrico.

O impacto deste trabalho está relacionado com melhorias na (i) caraterização de materiais produzidos através de fabrico aditivo por camadas assim como nas geometrias de provetes usados durante a sua caraterização e no (ii) ciclo de projeto em engenharia de estruturas obtidas através do fabrico aditivo por camadas, permitindo soluções estruturais com maior eficiência e menor custo para indústria espacial.

Contents

Intentionally blank page.

Chapter 1

Thesis Outline

1.1 Motivation

Additive Manufacturing (AM) is growing more rapidly than ever and has the potential to revolutionize the way products are designed and manufactured. However, there is a high variety of processes, each one with its own disadvantages and advantages. Furthermore, each process has its specific details and, when combined with the material's distinct characteristics, it poses a challenging problem. Thus, the mechanical behavior prediction of AM structure is an ongoing challenge due to defects, uncertainties in material characterization, and verification methods.

From a design perspective, Additive Layer Manufacturing (ALM) allows unprecedented design freedom and the possibility of raising the complexity of a structure without raising the costs. However, there are still several design limitations, which shall be considered to obtain an economically competitive design. The referred knowledge barrier can be minimized using a computational method (*i.e.* Topology Optimization (TO)), which can include its design limitations and provide solid initial designs. However, the use of the computational method raises another non-trivial issue related to bridging between TO and a final smooth geometry, which can be tacked in different ways.

1.2 Objectives

The ultimate goal of the present work is the development of a robust methodology for the mechanical optimum design of metallic space structures obtained from ALM. In order to achieve such a challenging goal, two main tasks were established. The first task is related to the mechanical characterization of materials obtained from Selective Laser Melting (SLM - an ALM process). The second task is related to the definition of the engineering cycle for ALM structures. Furthermore, the referred task studied the inclusion of SLM limitations into the optimization process and the non-trivial task of bridging between TO and the final smooth geometry. Thus, the impact of this Ph.D. is related with some improvements in (i) the characterization of ALM-produced materials as well as the geometry of the specimens used for their characterization; and in (ii) the engineering cycle of ALM structures, allowing higher efficiency in the structural solutions for the space industry with lower costs.

1.3 Outline

The present document is organized into four main chapters. The first chapter entitled "Literature Review" is composed of a published review article. The referred article, entitled "Metal Additive Manufacturing Cycle in Aerospace Industry: A Comprehensive Review", describes the AM processes and design optimization approaches. Furthermore, several successful case studies of the aerospace industry are enumerated and some research interests of the European Space Agency (ESA) are listed [P1].

The second chapter entitled "Material Characterization" is divided in two sections, each one has an original article. The first article entitled "Experimental mechanical characterization of Ti6Al4V SLM samples via a comparative study", reports an experimental testing campaign using SLM Ti6Al4V specimens from three different suppliers to establish comparisons and evaluate the process stability and repeatability [P2]. After testing tens of specimens and spending tens of thousand euros, the amount of information retrieved is still far from a full characterization, more tests would be needed. In addition, there are other different directions that also needed to be thoroughly tested. However, the cost and time of such campaign make it unviable for many projects. In order to reduce costs and time, each test should provide more information and the heterogeneous specimens may have the potential to play an important role, being the scope of the second article, entitled "Design of mechanical heterogeneous specimens using topology optimization" [P3].

The third chapter entitled "Design for Additive Layer Manufacturing (ALM)" is composed of three sections. The first section is focused on establishing methodologies for finding effective engineering solutions from an industrial perspective. Fortunately, OHB participated in this work, providing relevant technical guidance, and evaluating the quality of the work developed in the process. Thus, this section contains two industrial papers published in conference proceedings. The goal of the first article entitled "Designing Additively Manufactured Parts via Topology Optimization - a space industry case study", is the systematization of the ALM engineering cycle and provide preliminary results of the aerospace industry case study defined by OHB [C1]. The second article entitled "Development of ALM Technology for Space Structures. An opto-mechanical case study", reports the final results of the previous case study in all phases including manufacturing [C2]. The second section is composed of an original published article entitled "Designing Self Supported SLM Structures via Topology Optimization". This article lists the current limitations of the SLM process and proposes a topology optimization algorithm capable of including its main design limitations [P4]. The last section addresses the non-trivial issue related to the bridging between TO and a final smooth geometry via Laplacian smoothing, where the main algorithms were evaluated, and an innovative algorithm was proposed in the original article entitled "Bridging between topology optimization and Additive Manufacturing via Laplacian smoothing" [P5].

The last chapter entitled "Final Remarks" is composed of three sections. The first section (Conclusions) intends to briefly summarize the main contributions of the presented work and perform the global assessment. The second section summarizes the efforts made towards methodology integration. The codes that resulted from the previous sections were rewritten, optimized, and published in the open software community as an integrated part of a broader project. The final section (Future work) intends to give the reader useful guidelines to continue the presented research.

Appendix A presents a summarized business model proposal. In the beginning of this work, a market assessment was performed to identify the needs of the community (scientific and industrial), providing valuable guidelines for future work. The referred proposal is presented in the referred appendix as an article.

Appendix B introduces the life cycle of a startup and the funding mechanisms in Europe in the form of an article. The goal of this section is to provide complementary information to the business case with particular emphasis on the space industry. Since most startups (independently of the business model) will have to find funding and seek support from institutions such as incubators or accelerators. Thus, the referred article provides an overview of the existing mechanisms, providing lists of institutions per type of funding.

Finally, Appendix C provides functional versions of some interactive models. The publications [P4] and [P5] contain interactive models that are not functional in the present document. Their functionality is lost during their inclusion in the present document. Thus, Table C.1 provides functional versions of the referred interactive models.

1.4 List of publications

A collaboration agreement between the University of Aveiro and the company Active Space Technologies allowed the realization of this Ph.D. program. In the scope of this work, several contributions to the scientific community were made via international journals and conference proceedings. Figure 1.1 describes the main stages of the ALM engineering cycle and their correlation with the list of publications below. Thus, the topic of contribution of each article becomes clearer.

The international journal publications correspond to review and original research papers at the fundamental level, being listed below:

[P1] Barroqueiro, B.; Andrade-Campos, A.; Valente, R.A.F.; Neto, V. Metal Additive Manufacturing Cycle in Aerospace Industry: A Comprehensive Review. J. Manuf. Mater. Process. 2019, 3, 52.

[P2] Barroqueiro, B.; Andrade-Campos, A.; Valente, R.A.F. Experimental mechanical characterization of Ti6Al4V SLM samples via a comparative study. To be submitted.

[P3] Barroqueiro, B.; Andrade-Campos, A.; Valente, R.A.F. Design of mechanical heterogeneous specimens using topology optimization. J. Mech. Science. International Journal of Mechanical Sciences. 2020, 181, 105764.

[P4] Barroqueiro, B.; Andrade-Campos, A.; Valente, R.A.F. Designing Self Supported SLM Structures via Topology Optimization. J. Manuf. Mater. Process. 2019, 3, 68.

[P5] Barroqueiro, B.; Andrade-Campos, A.; Valente, R.A.F. Bridging between topology optimization and additive manufacturing via Laplacian smoothing. ASME. J. Mech. Des. Under review in the journal second iteration.

In contrast, the conference publications correspond to industrial papers focused on establishing methodologies and finding engineering solutions at a high-level perspective, being listed below:

[C1] Barroqueiro, B.; Andrade-Campos, A.; Valente, R.A.F. Designing additively manufactured parts via topology optimization -a space industry case study. In Proceedings of Second International Conference on Simulation for Additive Manufacturing, Pavia, Italy, 11-13 September 2019.

[C2] Barroqueiro, B.; Bola, I.; Santos, A., Andrade-Campos, A.; Valente, R.A.F.; Senese. S.; Sedlmaier, T; Widhammer, A. Development of ALM Technology for Space Structures. An optomechanical case study. In Proceedings of 16th European Conference on Spacecraft Structures, Materials and Environmental Testing, Braunschweig, Germany, 8-12 June 2020 (postponed to March 2021 due to Covit-19 pandemic).

[C3] Barroqueiro, B.; Andrade-Campos, A.; Valente, R.A.F. Integrated Methodology for Designing Structures coming from Additive Layer Manufacturing. In Proceedings of 23rd International Conference on Material Forming, Cottbus, Germany, 4-6 May 2020.

[C4] Barroqueiro, B.; Andrade-Campos, A.; Valente, R.A.F. Design of an Additive Manufactured Part by Topology Optimization. In Proceedings of 2nd International Conference of TEMA: Mobilizing Projects, Aveiro, Portugal, 11-12 July 2019.

[C5] Barroqueiro, B.; Andrade-Campos, A.; Valente, R.A.F. Integrated Methodology for Designing ALM Structures. In Proceedings of 3nd International Conference of TEMA: Mobilizing Projects, Aveiro, Portugal, 23 January 2020.

Still, in the scope of this work, other publications were made as a secondary author and, therefore, these are not listed in the present section.

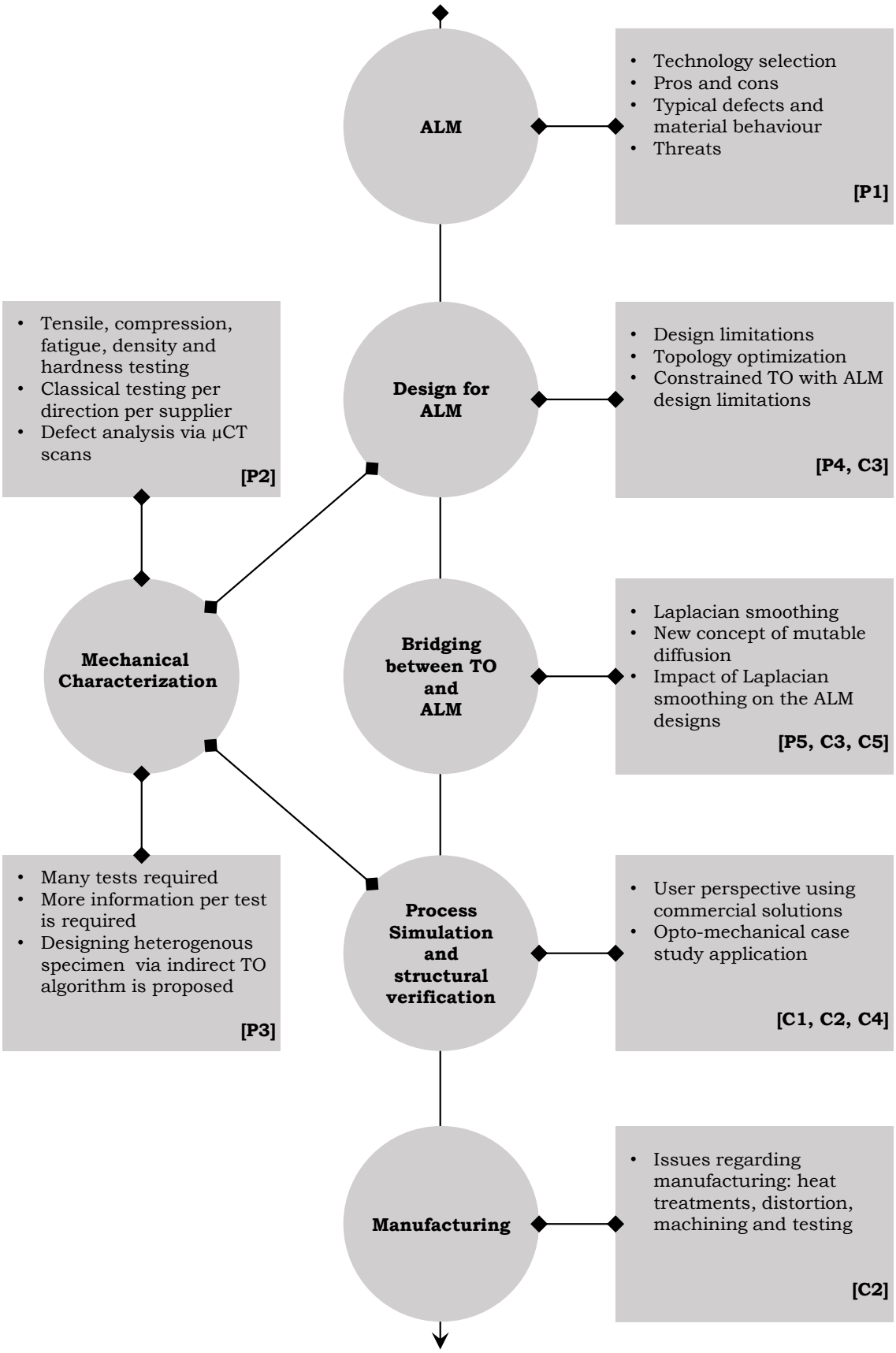

Figure 1.1: Description of the main stages of the ALM engineering cycle and their correlation with the presented publications.

Chapter 2

Literature review

In this chapter, a comprehensive review of the most import AM process is presented. The revision article starts with process categorization ((i) Powder Bed Fusion (PBF), (ii) Direct Energy Deposition (DED), and (iii) Hybrid Manufacturing) and a comparison in terms of advantages, disadvantages, and suppliers. Then, a brief overview of AM defects and their origin is discussed as well as the typical behavior of some materials (*e.g.* Ti6Al4V, AISI316, AlSi10Mg, Invar, Inconel). In the next section, the AM design optimization cycle is discussed in terms of threats to its widespread and the design limitations that shall be considered during the designing process of an AM structure. The final section presents some research interests of the European Space Agency (ESA) and concludes with several successful examples of AM parts in the aerospace industry [P1].

Journal of
Manufacturing and Materials Processing

MDPI

Article

Metal Additive Manufacturing Cycle in Aerospace Industry: A Comprehensive Review

B. Barroqueiro [1,2,*], A. Andrade-Campos [1], R. A. F. Valente [1] and V. Neto [1]

[1] Department of Mechanical Engineering, Centre for Mechanical Technology & Automation, University of Aveiro, 3810-193 Aveiro, Portugal
[2] Active Space Technologies, Actividades Aeroespaciais S.A., Parque Industrial de Taveiro, Lote12, 3045-508 Coimbra, Portugal
* Correspondence: bjfb@ua.pt

Received: 29 May 2019; Accepted: 21 June 2019; Published: 26 June 2019

Abstract: Additive Manufacturing (AM) is the forefront of advanced manufacturing technologies and has the potential to revolutionize manufacturing, with a dramatic change in the design and project paradigms. A comprehensive review of existent metal AM processes, processable materials, respective defects and inspection methods (destructive and non-destructive) is presented in a succinct manner. Particularly, the AM design optimization methodologies are reviewed and their threats and constraints discussed. Finally, an aerospace industry case study is presented and several cost-effective examples are enumerated.

Keywords: metal AM processes; inspection methods; AM defects; design optimization; aerospace structures

1. Introduction

Metal-based Additive Manufacturing (AM) is a rapidly growing industry, exceeding $1030M in 2016 with a $7150M revenue being forecasted by 2026 [1]. For instance, titanium additive manufactured parts are expected to reach a revenue of $350M in 2020 and $1030M in 2024 [2]. From an economic perceptive, paradigms are changing from mass production to mass customization and personalization due to technological developments [3–5]. Advanced manufacturing technologies are important promoters of this change of paradigm, which are likely to improve productivity. Moreover, the drastic increase of flexibility allows some industries to offer personalization options and reduce the overall time to market [3].

Additive Manufacturing, in particular Selective Laser Melting (SLM) and Electron Beam Melting (EBM), is at the forefront of the advanced manufacturing technologies [6]. Recently, important AM patents (e.g., [7–12]) have expired. Therefore, new companies in the field are emerging and the competition is increasing. Nowadays, the list of AM processes is long and many alternative processes are emerging on the market [13]. Metal-based AM processes consist in the manufacturing of a 3D object layer by layer, providing great design freedom. However, how to fully explore this freedom should be further developed, with the AM engineering cycle rethought [14].

Current design optimization tools do not allow to take full advantage of AM capabilities and several threats are still present. These particularities need to be accounted for in the design optimization, process simulation and structural verification stages [14]. Figure 1 shows a typical AM engineering cycle, where the symbiotic and iterative nature between the stages is also represented.

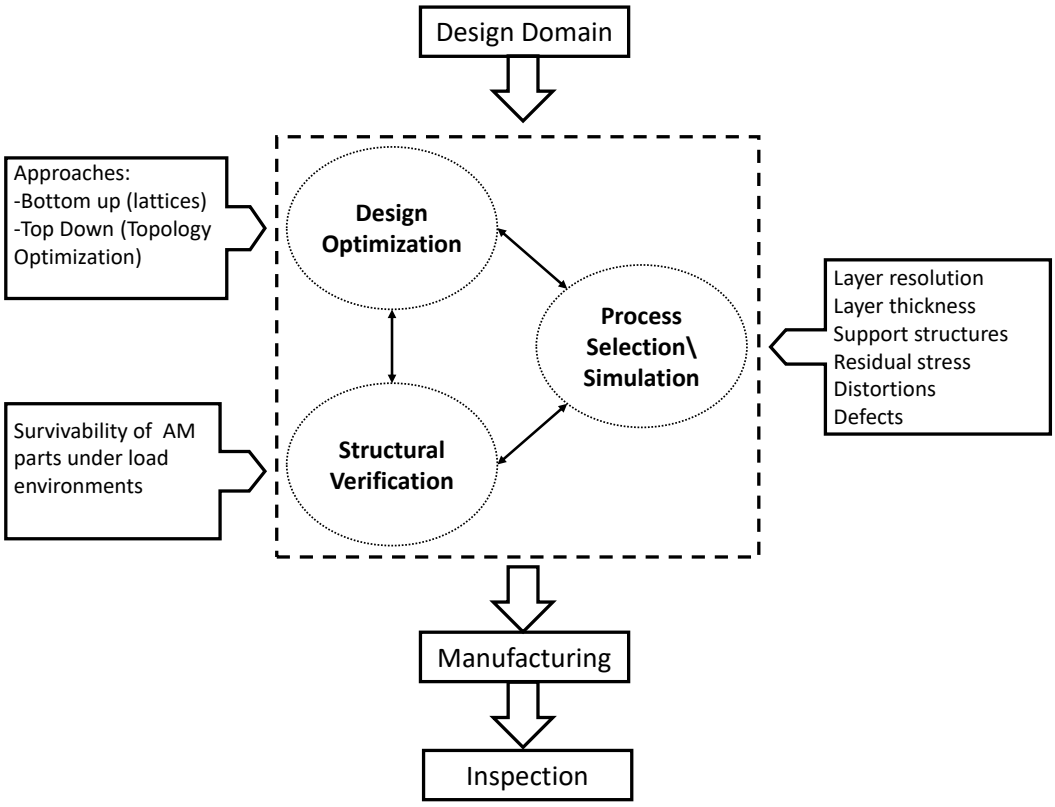

Figure 1. Overview of AM engineering cycle.

Despite all challenges and threats present in AM engineering cycles, its ability to produce lightweight structures has already been explored by the industry. For instance, the launch fees of the NEOSAT satellite costs a few tens of thousands of Euros per kilogram (An unofficial communication of P.B. Selding (Space News editor) on Twitter puts the cost at 31,000 Dollars per kilogram) and, thus, the ability to reduce weight or increase functionality becomes attractive for the aerospace industry. Nickels [15] analyzed the possible impact of AM in the referred industry, and reported several advantageous applications. For example, the development time frame of a structural bracket was reduced from six months to one using the AM technology [15], and the relation between AM and aerospace seems promising.

The goal of the present paper is to critically review AM engineering cycles in their threats, development tools and constraints in order to assess its current stage and identify its needs. The first part reviews the existing metal AM processes and, for the sake of clarity, divide them by category, referring their key characteristics and materials that can be processed. Typical defects are also listed, as well as their origin and respective inspection methods. Additionally, this article provides the reader with an overview of the processes' physics (following the authors of [16,17]) to improve the reader's understanding of typical defects and limitations. The second part of the work reviews the current design approaches, regarding their capabilities and limitations. Moreover, the currently available computational design tools are listed and the main limitations, from the manufacturing point of view, are reviewed. The third and final part reports to some of the European Space Agency (ESA) research interests and, cost-effective examples from aerospace industry are listed.

J. Manuf. Mater. Process. **2019**, *3*, 52 3 of 21

2. Additive Manufacturing

2.1. Processes Review

Metal-based Additive Manufacturing (AM) is a general concept and several technologies could be referred, including some technologies with a limited presence on the market, such as cold spray or sheet lamination. Cold spray refers to the deposition of powder material onto a substrate using pressurized gas (70 bar@1100 °C). The particles collide with the cold part forming a solid-state metallurgical bond. It is, therefore, best suited for the addition of near-net-shape features onto components, such as bosses, lugs onto shafts or coating application [18–22]. Another technology is sheet lamination, where each layer is represented by a sheet/foil. These are bonded together until a 3D shape is reached. For example, Fabrisonic commercializes machines that use this technology and bonds the foils together using ultrasonic welding. Moreover, this technology is already integrated into a hybrid solution [19]. Recently, a patent was published, where the bonding is performed using diffusion or friction welding [23].

Within the scope of this work, processes with higher relevance on the market are reviewed, being grouped in two main categories: Powder Bed Fusion (PBF) and Direct Energy Deposition (DED) [24]. In the PBF processes, layers of powder are applied and a heat source (laser or electron beam) selectively melts the applied powder. Then, the baseplate moves downwards and a new layer of powder is applied. In DED processes, the addition of material (powder or wire) is directly fed into the melt pool. Figure 2a,b shows the basic working principles involved and Table 1 compares their main characteristics.

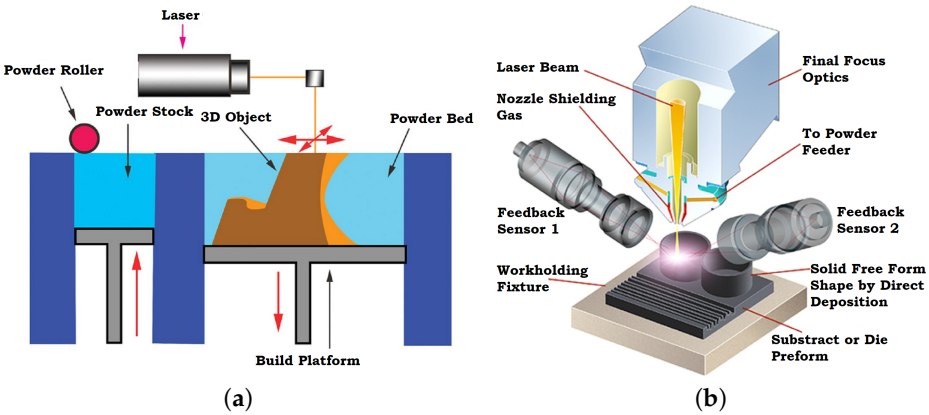

(**a**) (**b**)

Figure 2. General working principle of PBF and DED categories [25,26].

Table 1. General comparison of PBF and DED processes.

Criteria	Powder Bed Fusion (PBF)	Direct Energy Deposition (DED)
Build speed [cm^3/h]	up to 170	up to 2000
Max. build size (X; Y; Z) [mm]	(0.8; 0.4; 0.5)	(4.0; 2.0; 1.0)
Accuracy	0.05/25	0.25/25
Min. thickness [mm]	0.2	1.0
Surface quality [µm]	Ra 10	Ra 20
Design Freedom	High	Low
Applications	Rapid prototyping	Repairing parts
	High end parts	Adding features (i.e., ribs and lugs)

The values presented on this table are merely references and were based on manufacturers information and press research. Depending on the part, process and material, these values can change.

2.1.1. Powder Bead Fusion

The PBF processes takes advantage of a focused energy source that selectively melts or sinters a layer of powder. Different processes are available, as summarized in Table 2. The main energy sources

are the laser and the electron beam for Selective Laser Sintering/Melting (SLS or SLM) and Electron Beam Melting (EBM) processes, respectively. The EBM consists on high powered Scanning Electron Microscope (SEM), while SLS/SLM consists of a set of lens, mirror and galvanometer to positioning the laser beam [27].

Table 2. PBF process comparison.

Technology	Advantages	Disadvantages	Machines Companies
Shared specs	Cost effective Geometrical complexity High resolution	Powder exit points Quality powder dependent Powder quantity	Arcan (Sweden) EOS (Germany) Concept laser Cusing (Germany)
EBM	Minimal residual stress No thermal treatments Mechanical strength Malleability	Build rate Powder variety Vacuum atmosphere Surface finish Cost	MTT (Germany) Phoenix System Group (France) Renishaw (UK) Realizer (Germany) 3D Systems (USA)
SLM	Mechanical strength Surface finish	Build rate Residual stress Stress relief/HIP Malleability Inert atmosphere	Matsuura (Japan) Trumf (Germany) Voxeljet (Germany) ExOne (USA)
SLS	Build rate Foot print	Polymeric binder Thermal treatments Mechanical strength	
DMLS	Build rate	Mechanical strength Low density	

EBM, Electron Beam Melting; SLM, Selective Laser Melting; SLS, Selective Laser Sintering; DMLS, Direct Metal Laser Sintering.

EBM processes selectively melt the powder in vacuum conditions. The addition of a low-pressure helium atmosphere is used due to the risk of electrostatic discharges of the powder. This vacuum condition is almost a perfect protection against corrosion.

Currently, Ti-6Al-4V alloys are widely used in the aerospace industry due to their mechanical properties and fatigue strength [2,28]. Other possible materials are nickel-based alloys, which have excellent mechanical properties and resistance to creep and corrosion. However, these alloys are difficult to process and some are not weldable. The EBM process allows melting the metal above 1100 °C and, at these temperatures, these alloys can be successfully processed. Due to their creep resistance, these are used in high-temperature applications such as in aero-engines or power plants (e.g., inconel 625 or inconel 718 alloys). Cobalt-based alloys (e.g., vitalinum or stellite), cooper alloys, steel and stainless steel are possible materials to be processed by EBM [27]. This process does not require stress relief since the residual stresses are minimal. After the process, Hot Isostatic Pressing (HIP) is optional, since there are claims that it is possible to reach fully dense body (>99.9%) in as-built condition (without thermal post-processing) [27].

SLM process selectively melts the powder in an inert atmosphere (i.e., argon). Additionally, a few SLM machines are capable of providing pre-heating, either to the substrate plate or the entire building chamber. The most used powder with this technology is steel and other iron-based alloys (32%) [29]. Other powders are titanium and its alloys, Ni-based alloys and other metals such as aluminum, copper, magnesium, cobalt-chrome, tungsten, and gold (decreasing order of relevance) [29]. This process leads to high residual stress, with stress relief treatment being mandatory and HIP recommended. Due to the residual stress, cracking defects were identified [30]. However, thermal gradients in this process generate fine grain structures, which results in better strength limits than its cast counterparts with lower malleability [29]. However, during thermal treatment, the increased grain size has been reported [28], which leads to a decrease of strength and increase of material's malleability.

SLS process allows building parts without thermally affecting the metallic powder, since the powder contains polymeric binders, which are melted by a laser. This allows the construction of parts with great complexity and envelope. However, the process requires a furnace treatment in order to vaporize the polymeric binder and sinter the particles. At elevated temperature (below melting), the diffusion between particles occurs in order to minimize the free energy. If sufficient thermal input is provided, the densification of powder occurs, decreasing porosity with the cost of the volume shrinkage. The archived density (around 50%) is still not acceptable. Thus, an infiltration with other material or HIP process is required. This process can use different powders and, as infiltrating material, bronze or Cu-P/Ni alloys are used [31,32].

The direct metal SLS or Direct Metal Laser Sintering (DMLS) uses a mixture of low- and high-temperature melting point powders. Therefore, the laser scan is tuned to melt the powder with a lower melting point. The process requires longer times frames (and, consequently, lower building speed) when compared with SLS [33]. However, these parts can be used without furnace treatment, but in this cases strength is limited. Commercial solutions such as EOS-DMLS steel 50-V1 (contains steel, Cu-P and Ni) produce components with a relative density of 70% that can be used as inserts and small mold components [31].

2.1.2. Direct Energy Deposition

DED processes apply energy into a narrow, focused region in order to melt the substrate and simultaneously add melting material into the substrate's melting pool. Contrasting with PBF processes, DED processes melt material as it is being deposited. The material can be either powder or wire, its energy source being a laser, an electron beam or plasma (Table 3) [32].

Table 3. DED process comparison.

Technology	Advantages	Disadvantages	Machines Companies
LENS/DLF/DMD LBDM/LFF	Build rate Foot print Microstructure control Mechanical strength Repair tool Coating tool	Surface finish Geometrical complexity Resolution Controlled atmosphere Metal variety Residual stress Stress relief/HIP	Optomec (USA) InssTek (USA) Irepa Laser (France) Trumpf (Germany) Sciaky (USA) BeAM (USA)
EBAM	High build rate Foot print Microstructure control Mechanical strength Residual stress No thermal treatments	Surface finish Geometrical complexity Poor resolution Vacuum atmosphere Metal variety	
Plasma	Very high build rate Cost	Microstructure control Geometrical complexity Resolution Thermal treatments Accuracy Surface finish	Ramlab (Netherlands)

LENS, Laser Engineered Net Shaping; DLF, Direct Light Fabrication; DMD, Direct Metal Deposition; LBMD, Laser Based Metal Deposition; LFF, Laser Free Form Fabrication.

Regarding laser-based systems, several companies have been developing DED machines. These assume different names depending on the company, such as Laser Engineered Net Shaping (LENS), Directed Light Fabrication (DLF), Direct Metal Deposition (DMD), 3D Laser Cladding, Laser Generation, Laser-Based Metal Deposition (LBMD), Laser Freeform Fabrication (LFF), Laser Direct Casting, LaserCast, Laser Consolidation, LasForm and others [32]. These lasers processes are capable of processing materials such as titanium alloys (i.e., Ti-22Al-23Nb and Ti-48-2-2, TiC), steels (i.e., 10 V,

15-5 PH, 410, 416, AISI 309, Aermet 100, A2, MM 10, and CPM S7), nickel-based super alloys (i.e., CMSX-3, Haynes 188, Haynes 230, IN600, IN690, IN713, MarM247, Rene 142, and Rene N5), aluminium alloys (i.e., Al 6061 and Al 2024) and copper alloys (i.e., Cu-10%Sn and GRCop-84). In all of these cases, a controlled atmosphere is necessary (i.e., Argon), being obtained with an inert gas chamber (i.e., LENS) or by the use of shielding gas flow (i.e., 3D Laser Cladding) [34]. These technologies produce near shape parts that need to be post treated and allows great control over the resultant microstructures. Nevertheless, residual stress builds up and a stress relief is required and HIP is recommended.

Regarding DED electron beam-based systems, Electron Beam Freeform Fabrication (EBF3) was developed by NASA Langley to produce or repair parts, both terrestrially and in future space-based systems. The system uses wire as the source material instead of powder since the handling of powder in zero gravity would represent a major challenge. These electron beam DED machines are built in massive vacuum chambers. Similar to EBM, EBF3 produces ready to use parts in as-built condition. The final residual stresses are low and almost fully dense bodies are obtained. DED processes are limited in terms of geometrical freedom [32]. Regarding processable materials, these technologies can process titanium and its alloys, Inconel (IN718, IN625), tantalum, tungsten, niobium, stainless steel (300), aluminum (2319 and 4043), AISI 4340 steel, Zircalloy, and 70–30 copper–nickel and 70–30 nickel–copper alloys [35].

Regarding plasma-based systems, these are simply a gas metal arc welding machine combined with multiple axis platforms or robotic arms (e.g., Ramlab [36]), with low cost and reasonable build up speeds. However, poor control over the heat affected areas, microstructures or defects, have been the main drawbacks that have kept these approaches from wide spreading [32]. This technology requires stress relief and furnace treatments in order to improve microstructural properties and reduce defects [37].

2.1.3. Hybrid Manufacturing

The CNC technology provides advantages such as repeatability, precision and productivity with good surface finish, although being wasteful and geometrically limited, as well as having difficulty processing certain materials. On the other hand, AM technologies provide less material waste, more geometrical freedom and high buy-to-fly ratio, but it has long time cycles and poor surface finishing. To take advantage of both worlds, the technologies were combined into a single technology called Hybrid Manufacturing (HM) [38–42].

Companies such as Mastsura (Japan) and Sodick (UK) combine PBF with CNC while companies such as DMG Mori (USA), Mazzak (Japan), Reichenbacher Hamuel (Germany), and WFL (Germany) combine DED technologies with CNC. The most suitable application of these technologies is to build add-ons on existent parts or repair them. This avoids the build of a primary substructure to support the build and its post-processing, representing major gains in costs. Some of these machines can have the laser re-purposed for laser graving or cutting [43,44].

Recently, a company called Hybrid Manufacturing Technologies provides retrofitting solutions to common CNC machines with no major changes on the machine. For instance, the protective atmosphere is provided through the nozzle in the form of shielding gas flow. The solution is a compact design that includes the systems for the thermal source (laser), powder supply and protective gas supply. Furthermore, this company also provides these solutions to other companies to integrate on their new machines (partner alliances) [43,44].

2.2. Origin of Defects and Its Inspection Methods

The deposited material is melted and the shape of the melted pool is a relevant parameter. As is its solidification process. During the solidification, the first step is the nucleation. In most AM parts, the nucleation of a new phase is not required due to the presence of the previous layers, since the regrow can occur from the existent material. However, if two dissimilar materials were used, the nucleation of new phase might be required and, consequently, an energy barrier must be overcome.

This affects the final microstructure and may result in poor or non-existent inter-metallic bound. Thus, a progressive transition between the dissimilar materials is recommended.

To obtain good quality parts, there must be some remelting of the previous layer in order to remove contaminants and break oxides. Thus, a clean solid–liquid interface is provided, serving as a growth interface for the solidification process. The temperature gradient (G), the solidification rate (R) and the undercooling (ΔT) are the key parameters of the solidification process. In the presence of high ratios of G/R, the solidified microstructures tend to be planar. However, as ratio decreases, the microstructures tend to be cellular or columnar dendritic or equiaxed dendritic, as shown in Figure 3 [16].

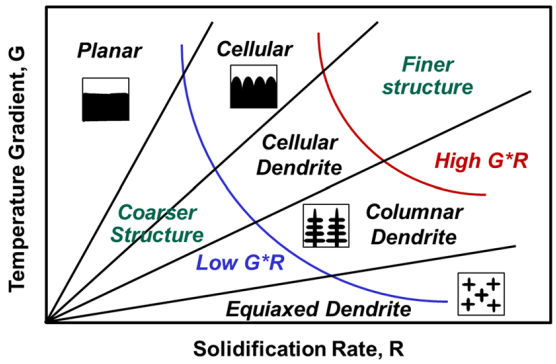

Figure 3. Effect of R and G in the solidification process [45].

In the PBF process, the fast laser scanning forms severe thermal gradients that lead planar microstructures, forming very elongated grains with a high length/depth ratio. Moreover, the grain growth direction follows the thermal gradient and, therefore, the build direction. This grain alignment with the build direction can lead to unwanted anisotropy effects present in some additively manufactured parts. However, in a DED process, the grain growth direction does not necessarily follow the build direction and has a similar length and depth. The process tends to form columnar dendritic structures due to the shape and size of the melted pool. After an AM part cools down below solidus temperature, it still needs to reach room temperature and several phase transformations can occur [16].

Any industry is cost driven and, therefore, reducing the build time of AM parts or reducing costs in feedstock materials, is wanted. However, increasing speed or decreasing quality of feedstock material increase the defects. The first cause for poor quality of AM parts is the powder quality in its shape, size distribution, surface morphology, composition and flowability (Figure 4a,b provides an example). For instance, poor flowability leads uneven layer deposition (PBF) or inconstant flow of powder (DED), which often leads to non-conform metal parts. Another source for failed parts is the incorrect reusing powder policies, where the same powder is used several times.

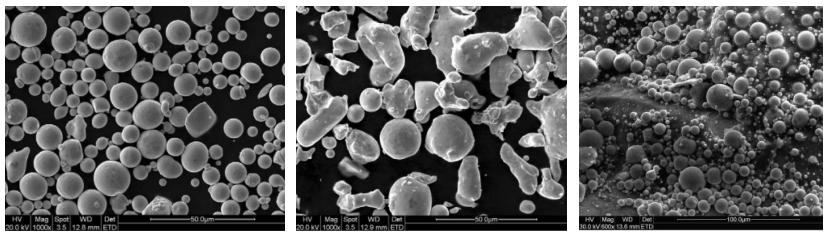

(**a**) (**b**) (**c**)

Figure 4. SEM images showing characteristic morphologies of powders produced: (**a**) using gas atomization; and (**b**) water atomization [46]. (**c**) SEM image depicts solid powders on build surface [47].

Therefore, the quality of AM raw material needs monitoring and to establish minimal quality standards in the morphology, flowability, particle size and distribution, chemical composition and allowable variation, reusing powder policies, and criteria for defect acceptance, further testing is needed [48]. Scanning Electron Microscopy (SEM) and/or X-Ray Computed Tomography (CT) can be used to monitor powder quality [16,49].

During an AM process, parameters can be maximized up to a certain limit. For instance, increasing the build speed eventually leads to instability of molten pool originating elongated pools, which break in isolated bubbles of isolated liquid (This defect is commonly called humping.). Thus, a compromise between speed and quality is often required. During metal melting, the temperature reaches elevated values. Therefore, vaporization of alloys elements can occur, since these elements are more volatile than others. However, the increase in temperature does not necessarily imply high vaporization rates. The higher temperature facilitates the vaporization. However, the size of the molten pool is also increased, increasing the stability of the pool. Combined with vaporization issues, there is the elements' segregation, where alloy elements migrate from the bulk material to grain boundaries. Therefore, the lack of micro-structural homogeneity is another defect that needs quantification. Some non-destructive methods of measurement chemical composition are X-Ray Energy Dispersive Spectroscopy (EDS) or Electron Probe MicroAnalysis (EPMA). Inductively Coupled (ICP) mass spectrometry presents a higher accuracy, but it is a destructive method [16,28].

To increase the competitiveness of the AM process, machines may operate at very high power densities and deposition rates. Sometimes the temperature of the molten pool reaches the boiling point of the alloy and a vapor cavity is formed, which improves the laser absorption. This operating mode is called the keyhole mode. Without its careful control, it can lead to defects since the keyhole mode may become unstable, leaving voids (keyhole induced porosity, as depicted in Figure 5a) due to gas entrapment.

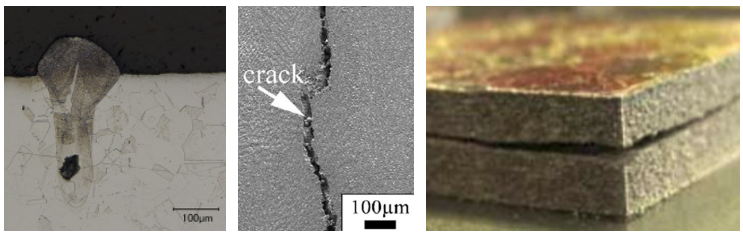

Figure 5. AM defects: (**a**) keyhole induced porosity; (**b**) cracks; and (**c**) delamination [16].

Another origin of porosity is the gas entrapment in the powder (during its production, leading to microporosity), or in lack of powder fusion (low laser absorption due to powder shape and/or morphology). There are several techniques to measure porosity such as Optical Microscopy (OM), Electron Microscopy (EM), X-Ray Computer Tomography (X-Ray CT) and Synchrotron Radiation Micro-Tomography (SRμT) [16,50–55].

Excessive surface roughness is a common defect that is unacceptable and needs expensive post-processing. The first reason for this defect is the "stair step effect". If the layer thickness is increased, the roughness is increased, and, therefore, a compromise needs to be reached. The second reason is related to process parameters. Humping effect or poor melting of powder are causes for large surface roughness, which can be measured using profilometer or analyzing the surface morphology using SEM (see Figure 4c) [16,56–58].

Cracking and delamination are other defects. The solidification will eventually suffer contraction and distortion due to thermal and inelastic strains (viscoplasticity, and creep and phase transformations). However, the previous layers already suffered the contraction process and, therefore, there is a differential contraction between layers that causes the stresses to build up. If these reach the

strength limit, cracking occurs along grain boundaries (see Figure 5b) or between layers (delamination, as depicted in Figure 5c). The element segregation allows the formation of carbides between grains. The stiffness difference between the carbides and the grains leads to stress concentrations within micro-structure that become the primary cracking site during cyclic loading. Another direct consequence of stress building up is distortion, being one of the main reasons for non-admissible final parts [16]. Thus, residual stress is a key point that needs quantification. There are techniques to measure residual stress, such as Vickers micro-indentation (indirect measure), hole drilling combined laser holography and/or strain gauges, X-ray and neutron diffraction techniques [16,59,60].

Table 4 summarizes the main possible defects of AM metal parts and possible tests to identify and quantify them [16,61,62].

Table 4. AM common defects and its inspection methods [16,61,62].

Defect	Process PBF/DED	Description	Inspection Methods
Vaporization of Alloy Elements	Both	Loss of alloy elements due to vaporization compromises mechanical strength	X-Ray EDS (NDI) EPMA (NDI) ICP mass spectrometry (DI)
Porosity and voids	Both	Quality Powder: Hollow powder (gas entrapment) Process instabilities (keyhole voids, lack of penetration, ...)	X-Ray CT (NDI) SEM (NDI)
Surface Roughness	Both	"Stair step effect", humping effect and powder poor melting	Profilometer (NDI) SEM (NDI)
Cracking	Both	Uneven contraction of deposited material builds up stress until strength limit originating fracture	Vickers micro-indentation (Indirect measure and DI) Hole drilling combined laser holography and/or strain gauges (DI) X-Ray and Neutron diffraction (NDI)
Delamination	PBF		ECT (NDI)
Distortion	Both	Residual stress leads to strains → Out of tolerance	Conventional Metrology (NDI)
Trapped Powder	PBF	Hollow Structures needs powder extraction points	CT (NDI) RT (NDI)

NDI, Non-Destructive Inspection; DI, Destructive Inspection; EDS, Energy Dispersive Spectroscopy; EPMA, Electron Probe MicroAnalysis; ICP, Inductively Coupled; CT, Computed Tomography; SEM, Scanning Electron Microscopy; ECT, Edge Current Testing; RT, Resonance Testing.

To deal with referred unwanted effects, some post treatments are usually performed. To reduce residual stress and/or reduce porosity, stress relief and/or HIP processes are performed. However, the treatments are not standard and may produce unwanted effects if not properly defined such as excessive distortion or loss of mechanical properties. Apart from thermal treatments, there is the surface quality treatment that involves machining (e.g., interfaces) and/or polishing. There are numerous types of polishing, namely: mechanical, chemical, electromechanical, vibrational or blasting. In the case of internal surfaces (difficult access), the polishing is accomplished using chemical or electrochemical or abrasive flows (suspensions of SiC, Al_2O_3, diamond, and WC particles) [63]. Finally, the quality inspections with the acceptance criteria and their standardization are needed. In fact, the certification process of AM parts in the aerospace industry is an on-going task. The European Aviation Safety Agency (EASA) and the Federal Aviation Administration (FAA) have established committees with the purpose of regulating and standardizing these new technologies [64].

2.3. AM Material Behavior

In the aerospace industry, the most used metals are titanium and aluminum alloys, stainless steel and nickel alloys. Titanium alloys, especially Ti-6Al-4V, is known for its impressive ratio of strength/mass, however, a trade-off between ductility and strength is required. On the one hand, the as-built parts tend to have higher strength but lower ductility. On the other hand, the heat-treated parts can provide more ductility at a strength cost. In some cases, these alloys show similar strength in the transverse and longitudinal directions, while, in other cases, a deviation of 7% was found, depending on the process parameters [16,65]. Furthermore, the size of the component (characteristic length) appears to be another variable. For instance, a component 1.7 mm in length showed 20% more strength and 80% less ductility when compared with a 7-mm part. The presence of large pores close to the surface was found to have a higher impact on the fatigue performance of these alloys [16,17].

AM aluminum parts are mainly produced with AlSi10Mg alloys. Their high content of silicon promotes low melting ranges, high hot tearing resistance and low shrinkage during solidification, without introducing brittleness and reducing void generation (porosity). In general, the resulting mechanical properties are better or equal to those obtained in casting processes due to the obtained fine microstructures [66], with no notable anisotropy being present [16]. However, high cycle fatigue of AlSi10Mg AM parts still requires unreasonably high factors of safety, being highly susceptible to local defects [67]. Regarding Al6061 alloys, these are widely used by industry (aerospace included) due to their weldability, corrosion resistance and suitability for critical safety applications. However, the low silicon content presence results in unacceptable levels of cracking, anisotropy and porosity, making Al6061 alloy unattractive for AM applications [66].

Austenitic stainless-steel AM parts, in as-built condition, exhibit higher strength, hardness, and anisotropy as well as lower ductility when compared with their traditionally processed counterparts. This is attributed to refined microstructure (due to rapid solidification), its structure (dendritic and cellular), higher dislocation density and residual stress (around 60–90% of yield strength). The fatigue performance of AM parts (PBF-L AISI316L) is negatively affected by the surface roughness. However, roughness reduction using machining increased the strength limit by 25% (from 200 to 250 MPa) [16].

Ni-based alloys obtained from AM require a trade-off between strength and ductility, having considerable levels of anisotropy [16,68]. Lack of fusion defects was reported to have a relevant impact in the fatigue life of AM parts in as-built condition (DED-SLM IN718), reducing its life by a factor of 2/3. On the contrary, these alloys when heat treated have shown fatigue life similar to their conventionally casted or wrought counterparts (DED-SLM IN718) [69,70] and higher creep resistance. This increase in resistance is attributed to a higher density of precipitates in their microstructure. Other Ni-based alloys, e.g., Haynes 230 (PBF-SLM), have also shown meaningful improvement of mechanical properties (yield and tensile strength) when compared to cast and wrought material. However, ductility is negatively affected due to the evident element segregation on the microstructure (cellular and dendritic structures) [71]. In short, metal-based AM parts show as good or even better mechanical properties when compared with a conventional cast or wrought parts [72].

3. AM Design Optimization

AM has the potential to reduce mass since the complexity of the part can be raised without drastically raising its cost. The AM engineering cycle requires several steps, namely design optimization, manufacturing and inspection. Recently, Walton and Moztarzadeh [73] presented a classic case study, where the design optimization cycle was performed using Topology Optimization (TO), compliance minimization was the goal and mass and stress were the constraints. Moreover, a member size limitation of 6 mm (min.) and 12 mm (max.) was used. Figure 6a presents the design domain as well as the boundary conditions, while Figure 6b represents the density maps of TO, considering a threshold of 0.25. Taking into consideration the results of TO, the part was redesigned and manufactured.

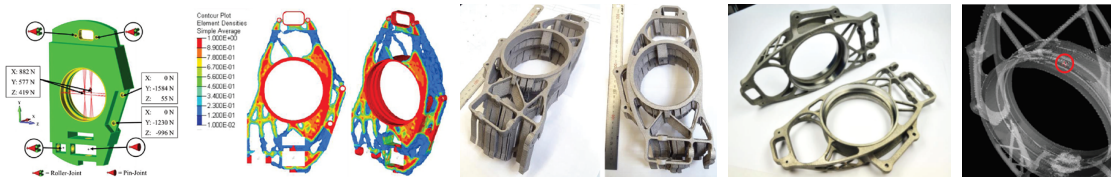

Figure 6. Engineering cycle of an AM part: (**a**) presentation of the design domain and boundary conditions; (**b**) density maps of TO, considering the threshold at 0.25; (**c**) AM part still with the support structures; (**d**) machined AM part; and (**e**) its X-Ray inspection [73].

Figure 6c depicts the AM part in its as-built condition, where the considerable amount of support structures is visible. Figure 6d depicts the AM part post-treated and Figure 6e depicts its X-Ray inspection, where an inclusion defect was found. Despite the relevant advantages of AM technologies, the reliability of the part still faces many challenges [4,74] and their success is still dependent on the minimization of certain threats and limitations.

3.1. Threats

Current design approaches are changing to take full advantage of AM technology. Particularly, to make AM economically viable, highly optimized designs are needed, representing a challenging task. Currently, three mains approaches can be indicated: bottom-up, top-down and mixed.

- The bottom-up approach is based on unit cells (lattices) that are uniformly repeated in every direction. The apparent simplicity of this approach is betrayed by its uncertainties on its analysis and the CPU cost.
- The top-down approach is based on topological optimization for both continuum and discrete domains. Nonetheless, TO provides great opportunities due to its ability to produce lightweight structures. However, this methodology sometimes produces "unfriendly" AM structures (e.g., overhangs), associated to high computational costs of optimization and analysis. Moreover, the output of these methodologies is density maps that need to be translated into geometrical forms, requiring another non-trivial step [14].
- A mixed approach can be defined, being a combination of the previous ones. Instead of a uniform distribution of the unit cells, a multiscale algorithm can be used, where the densities from the topology optimization define the level of robustness of the unit cell (e.g., diameter of truss bars) [75–77]. However, the translation of the referred densities into a final 3D model raises several computational challenges.

Current design tools (sketch based) are optimized for conventional technology (e.g., the "add hole" typical command). Thus, the edition of 3D shape using current software is complex and requires extensive training, being difficult to use and disseminate. Bottom-up approaches have some integrated software to guide the user from the beginning to the end of the design process. Software packages such as Netfabb (Autodesk), Creo 4.0 (PTC), Meshup (Uformia), and Magics (Materialise) are examples. In the same way, top-down approaches use software that combines topological optimization methods with design tools. Moreover, there are many general propose topological optimization solvers, which are summarized in Table 5 due to their extensive list.

Table 5. Overview of Topology Optimization (TO) software: commercial and educational [78]. Its developer, Finite Element Analysis (FEA) solver, analysis regimes (S—Static; E—Eigenvalues; and D—Dynamic Loading) and the existence of post-processing tools (smoothing and export) are also presented.

Commercial Software	Developer	FEA Solver	Analysis Regime	Smoothing/Export
Dreamcatcher	Autodesk	Standalone	S,E	Yes/Yes
Within Enhance	Autodesk	Standalone	S,E	Yes/Yes
Tosca	Dassault Systemes	Ansys/Abaqus /Nastran	S,E,D	Yes/Yes
ATOM	Dassault Systemes	Abaqus	S,E	Yes/Yes
Ansys		Standalone	S,E,D	Yes/Yes
Sol200	MSC	Standalone	S,E,D	Yes/Yes
Optistruct	Altair	Standalone	S,E,D	Yes/Yes
Vanderplaats Genesis	VRand	Ansys	S,E,D	Yes/Yes
Solid Thinking Inspire	Solid Thinking	Optisttruct	S,E,D	Yes/Yes
PERMAS-TOPO	Intes	Standalone	S,E,D	Yes/Yes
FEMtools Optimization	Dynamic Design Solutions	Ansys/Abaqus /Nastran	S,E,D	No/No
OPTISHAPE-TS	Quint Corporation	Ansys	S,E,D	Yes/Yes
ParetoWorks	Sciart Rethinking Design	Standalone	S	No/Yes
ProTop	CAESS	Standalone	S,E	Yes/Yes
Educational Tools				
BESO 3D	RMIT University	Abaqus	S	No/No
Topostruct	Sawapan	Standalone	S	No/No
ToPy	William Hunter	Standalone	S	No/No
TRINITAS	Linköping University	Standalone	S	No/No
TopOpt	TopOpt Research Group	Standalone	S	No/No

The structural verification of AM parts and the prediction of its failure mechanisms raise serious challenges with high-level uncertainty due to defects, anisotropy and residual stress. Moreover, other parameters (such as the surface finishing) affect the part performance. To anticipate possible issues, some companies created software for the building process simulation (also generates the necessary support structures). Thus, it is allegedly possible to predict residual stress and distortions on a part and compensate distortions on the design in order to improve final dimensional accuracy. The higher is the accuracy the less overbuild is necessary, therefore improving its economic competitiveness. Netfabb Simulation (Autodesk—former Pan computing), Simufact (MSC), Amphyon (Additive Works—Partner Alliance with Altair), Virfac (Geonx) and ExaSIM (Ansys) are examples of software packages specialized in building simulation of AM process. An alternative software solution could be FAME (Swerea), which has a general public license, but numerous limitations. In general, these software packages use multiple scales combined with other techniques in order to reduce computation time. In fact, if the simulation takes longer than the process, it will have little use.

3.2. Design Limitations

AM processes have limitations in their build time and allowable dimensions. Moreover, the cycle time of these technologies is significantly higher when compared with conventional technologies. However, this drawback can be suppressed by the opportunity of reducing material waste, increasing functionally, highly geometrical customization or reducing the difficulty to process materials (i.e., inconel or titanium). From the scalability point of view, the AM processes are limited by their nature, since the layer resolution is limited to a specific range (0.2–2.5 mm) and the scalability is also limited. On the other side, small layer thickness is also wanted, since it improves surface finish. Thus, this compromise is a recurrent problem in AM processes [14]. Additionally, its repeatability is questionable, since two identical parts on the same machine may or may not produce parts with the same structural robustness [48].

Design optimization shall be performed taking into consideration the manufacturing process and its constraints. The main constraints are the member size, cavity and support structures constraints:

- Member size constraints improve manufacturability and reduce post-processing operations, being an important and fundamental constraint.

- Cavity constraints intend to avoid enclosed voids of powder (PBF process), which can be difficult to remove in a later stage. However, cavities do not necessarily appear and their industrial relevance is limited. When they appear, their structural benefits should overcome the work of introducing a hole in the design in order to vacuum the unmelted powder.
- Overhang constraints intend to minimize (or ideally eliminate) the appearance of overhanging structures and, therefore, the need for support structures (cost reduction). Thus, it is a relevant topic and represents a strong design restriction [79].

The optimization of the build direction can (sometimes) reduce the need for support structures. The study in Ref. [80] proposes a method for searching the optimal build orientation which minimizes their use. The study in Ref. [81] proposes a TO methodology that brings the AM overhang constraints into the TO methodology, where a maximum angle of 45 degrees is considered in order to avoid support structures.

Figure 7a,b illustrates the TO results (for 2D only) without and with overhang constraints, respectively. However, this gain in eliminating support structures comes with a stiffness cost, increasing its compliance by 16% .

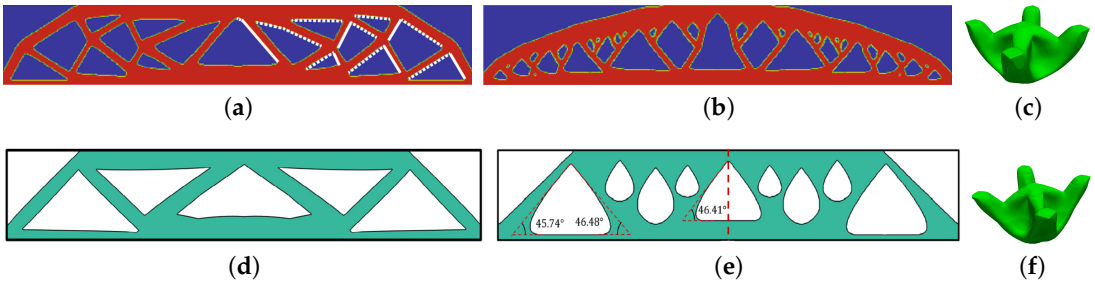

Figure 7. Comparison of TO results (**a**) without and (**b**) with overhang constraints using a simplified fabrication model [81]. TO results (**d**) without and (**e**) with overhang constraints using moving morphable components [82]. TO results (**c**) without and (**f**) with overhang constraints using convolution methodology [83].

For instance, a study in Ref. [82] proposes another method of introducing overhang constraints into the TO methodology, resulting in a different design philosophy. Figure 7d,e presents the TO results (for 2D only) without and with overhang constraints, respectively. Recently, a study in Ref. [83] suggests another method for introducing overhang constraints into the TO methodology for the 3D domain. Other studies (e.g., [84–86]) have also addressed this issue.

The application of the previous methodologies to reduce the number of support structures is pertinent since costs are reduced. However, such heavy restrictions might steer the solution away from the optimal solution. In addition, support structures might be necessary, even if the structure is self-supporting, r to prevent excessive distortion and/or cracking. In addition, excessive distortion can lead to recoater interference and, therefore, a failed build. If the top-down approach produces hollow structures, internal support structures might be required, which can be challenging to remove in a later stage. Finally, it is necessary to have exit points for the non-melted powder extraction [81,87]. In a bottom-up approach, the internal support structures can be avoided, with a careful selection of the unit cell and the print direction. However, the extraction of the unmelted powder and the smoothing of surfaces becomes a challenge. In short, a compromise between cost and performance is generally made.

J. Manuf. Mater. Process. **2019**, *3*, 52 14 of 21

4. Case Studies From Aerospace Industry

The metal AM in the Aerospace Industry will succeed if it enables overall cost, lead-time and risk reduction. For instance, this can be achieved by reducing the number of parts, joints (welds are causes for long term failures) and/or increasing the added value of the final part (increased functionality per part). Moreover, these technologies still need efforts towards its qualification and standardization [61,88,89]. Recently, the European Space Agency (ESA) has opened calls to explore these opportunities. For instance, the development of embedded thermal functions in structural parts using 3D printing, or the development of one single part integrating waveguide filter, bends, coupler and supporting structures by AM, projects that could be financed by ESA within the ITT (Invitation To Tender) (e.g., [90,91]). The material behavior and its structural response limit the widespread use of metal-based AM since they still represent challenges [92]. One of the recent projects from ESA consists in the development of supply chains, capable of producing high-end parts made of titanium, aluminum, Inconel and Invar. The mechanical characterization and post-processing (blasting, stress relief and HIP) are also included [93]. Another project consists in the development and characterization of new high strength aluminum alloys including their mechanical performance and common defects [94].

The current main space applications of metal AM is limited to a few applications. The first main application is rocket propulsion, namely components such as injectors, gas generator duct, pogo z-baffle, turbo pump inducer, flex joint, monolithic thrusters, chambers and nozzles [95,96]. Figure 8a–c illustrates a J-2X Gas Generator Duct, a Pogo Z-Baffle and a Turbopump Inducer, respectively. Gains of 70% in costs and 50% in time were reported for the Duct. In the Pogo part, gains of 64% in costs and 75% in time were disclosed. Regarding the inducer, 50% cost and 80% time reductions were declared, where the comparison term for these gains was their conventional manufacturing [96].

(**a**) (**b**) (**c**) (**d**) (**e**)

Figure 8. Cost-effective examples of additive manufactured parts: (**a**) a J-2X Gas Generator Duct; (**b**) a Pogo Z-Baffle; (**c**) a Turbopump Inducer; (**d**) a battery case; and (**e**) heat switch prototype [96].

Others applications are auxiliary structures such as thermoelastic mounts (Optic instruments need extremely stable structures, i.e., a thermal strain can misalign lenses or focal distances), wave guides filters, heat switches, structural components with embedded thermal functions (heat pipes) and components with tailored properties. On suborbital sounding rocket mission, there is a battery case (FY13), which was successfully built by AM [96], as shown in Figure 8d. For instance, an instrument prototype of thermal heat switch based on concentric titanium tubes was built by AM. The complexity of this component comes from the small gaps between tubes and the difficulties and price of processing titanium [96], as shown in Figure 8e.

On the Atlantic Bird mission (ESA 2011), a structural bracket made of titanium was built by AM (EBM) with a TRL (Technology Readiness Level) of 9 (flight model), having a mass reduction of 30% [97] (Figure 9a,c).

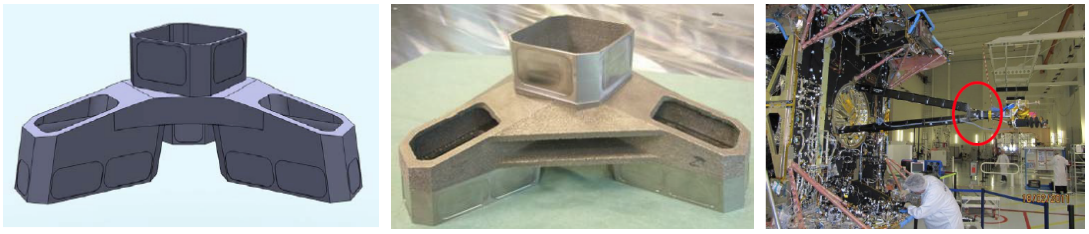

(**a**) (**b**) (**c**)

Figure 9. Flight AM part [97]: (**a**) the CAD model; (**b**) the manufactured part; and (**c**) its location the satellite.

According to T. Ghidini [95], another AM structural bracket was designed and successfully validated, where 46% mass reduction was achieved. Figure 10a,d describes the old design and the new AM design, respectively. Moreover, the number of interfaces was reduced, maintaining the structural robustness.

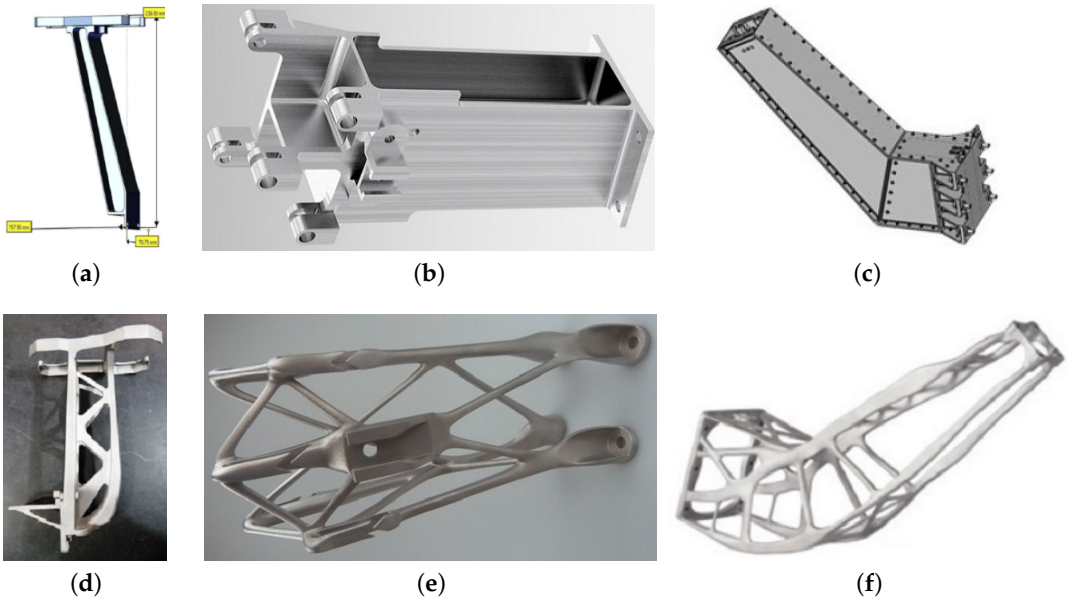

(**a**) (**b**) (**c**)

(**d**) (**e**) (**f**)

Figure 10. AM optimized structural brackets [95,98]: (**a**,**d**), (**b**,**e**) and (**c**,**f**) examples of optimized brackets from their conventional design to their AM design.

A supplementary space application of an AM bracket is given by Figure 10b,e, depicting their conventional and AM designs, respectively. Reductions of 25% in cost and 50% in weight were projected [98–100]. The antenna bracket of sentinel I weighs 1.626 kg and, thus, a potential for improvements was identified. From a partnership between RUAG and EOS, a new bracket was redesigned for AM. The final design margins of static loads, strength and stiffness were positive and a 26% mass reduction was obtained [99,100]. Figure 10c,f depicts the conventional and AM designs, respectively.

5. Conclusions

The AM market is rapidly growing and many AM machines suppliers are already available. Sometimes, the mechanical properties of the resultant parts show better properties than the brought counterparts, but its repeatability is still a challenge as is its standardization. Either raw material or process-induced, micro-structural defects are the cause for the questionable repeatability and their identification can be performed with different methods.

The AM engineering cycle has to be rethought to reach its full potential. Its stages (Design Optimization and Process Simulation) have many tools already available, but it still lacks the proper unification and maturity. Moreover, the integration of manufacturing constraints in the design methodologies is still in its infancy, although some methodologies have already been published already. Regarding the strength analysis stage, this represents a major challenge due to a number of phenomena such as anisotropy, porosity and residual stress.

In the aerospace industry, a number of cost-effective examples are available, where cost and weight reductions were verified. Project calls are being opened to finance its further development (i.e., ESA Projects), since its potential is widely accepted. Nonetheless, their field of application is restricted to complex parts (weight, materials and/or shape).

Author Contributions: Conceptualization, B.B., A.A.-C., R.A.F.V. and V.N.; methodology, B.B., A.A.-C., R.A.F.V. and V.N.; validation and formal analysis, B.B., A.A.-C., R.A.F.V. and V.N.; investigation, B.B.; writing—original draft preparation, B.B.; writing—review and editing, B.B., A.A.-C., R.A.F.V. and V.N.; project administration, A.A.-C.; funding acquisition, A.A.-C. and R.A.F.V.

Funding: This research was funded by the Portuguese Foundation for Science and Technology (FCT) under the projects CENTRO-01-0145-FEDER-029713 by UE/FEDER through the programs CENTRO 2020 and COMPETE 2020, and UID/EMS/ 00481/2013-FCT under CENTRO-01-0145-FEDER-022083. Additional funding was provided by program CENTRO 2020 and UE/FEDER through the project CENTRO-01-0247-FEDER-024039, designated as ADVANSS. Finally, the Portuguese Foundation for Science and Technology (FCT) provided additional funding via the scholarship SFRH/BD/120779/2016.

Acknowledgments: The authors gratefully acknowledge the financial support of the Portuguese Foundation for Science and Technology (FCT), program CENTRO 2020 and UE/FEDER.

Conflicts of Interest: The authors declare no conflict of interest.

References

1. Hertenberger, S. (Ed.) Market Report ID: 44670015/Global. Available online: www.maschinenmarkt.international/english/global/articles/604851/ (accessed on 18 November 2017).
2. Dutta, B.; Froes, F.H. *Additive Manufacturing of Titanium Alloys*; Butterworth-Heinemann: Oxford, UK, 2016.
3. Tao, F.; Cheng, Y.; Zhang, L.; Nee, A.Y.C. Advanced manufacturing systems: Socialization characteristics and trends. *J. Intell. Manuf.* **2017**, *28*, 1079–1094. [CrossRef]
4. Ustundag, A.; Cevikcan, E. *Industry 4.0: Managing The Digital Transformation*; Springer International Publishing: Cham, Switzerland, 2018.
5. Bremen, S.; Meiners, W.; Diatlov, A. Selective Laser Melting: A manufacturing technology for the future? *Laser Tech. J.* **2012**, *9*, 33–38. [CrossRef]
6. Murr, L.E.; Gaytan, S.M.; Ramirez, D.A.; Martinez, E.; Hernandez, J.; Amato, K.N.; Shindo, P.W.; Medina, F.R.; Wicker, R.B. Metal Fabrication by Additive Manufacturing Using Laser and Electron Beam Melting Technologies. *J. Mater. Sci. Technol.* **2012**, *28*, 1–14. [CrossRef]
7. Wikening, C.; Lohner, A. Aparatus for Producing a Three-Dimensional Object. U.S. Patent 5753274, 19 May 1998.
8. Russell, D.B.; Anderson, T.; Bredt, J.F.; Vogel, M.J.; Seymor, M.; Bornhorst, W.J.; Hatsopoulus, M.I. Aparatus for Producing a Three-Dimensional Object. U.S. Patent 6007318, 19 May 1999.
9. Batchelder, J.S.; Crump, S.S. Method for Rapid Prototyping of Solid Models. U.S. Patent 5866058, 2 February 1999.
10. Manning, G.L. End-of-Vector Laser Power Control in a Selective Laser Sintering System. U.S. Patent 08866600, 4 July 1997.
11. Meiners, W.; Wissenbach, K.; Gasser, A. Selective Laser Sintering at Melting Temperature. U.S. Patent 09319132, 10 April 1997.
12. Swanson, W.J.; Hopkins, P.E. Thin-Wall Tube Liquifier. U.S. Patent 09013388, 21 December 1998.
13. Hornick, J.; Bhushan, A. More 3D Printing Patents Are Expiring Soon: Here's a Roundup. Available online: 3dprintingindustry.com (accessed on 12 October 2018).

14. Gao, W.; Zhang, Y.; Ramanujan, D.; Ramani, K.; Chen, Y.; Williams, C.B.; Wang, C.C.; Shin, Y.C.; Zhang, S.; Zavattieri, P.D. The status, challenges, and future of additive manufacturing in engineering. *Comput. Aided Des.* **2015**, *69*, 65–89. [CrossRef]
15. Nickels, L. AM and aerospace: An ideal combination. *Met. Powder Rep.* **2015**, *70*, 300–303. [CrossRef]
16. DebRoy, T.; Wei, H.L.; Zuback, J.S.; Mukherjee, T.; Elmer, J.W.; Milewski, J.O.; Beese, A.M.; Wilson-Heid, A.; De, A.; Zhang, W. Additive manufacturing of metallic components—Process, structure and properties. *Prog. Mater. Sci.* **2018**, *92*, 112–224. [CrossRef]
17. Gorsse, S.; Hutchinson, C.; Goune, M.; Banerjee, R. Additive manufacturing of metals: A brief review of the characteristic microstructures and properties of steels, Ti-6Al-4V and high-entropy alloys. *Sci. Technol. Adv. Mater.* **2017**, *18*, 584–610. [CrossRef] [PubMed]
18. Machine Supplier Website. Available online: http://www.twi-global.com (accessed on 26 October 2017).
19. Machine Supplier Website. Available online: http://www.hermle-generativ-fertigen.de (accessed on 26 October 2017).
20. Sun, W.; Tan, A.W.; Bhowmik, A.; Marinescu, J.; Huong, Y.; Liu, E. Additive manufacturing of inconel 625 superalloy parts via high pressure cold spray. In Proceedings of the 3rd International Conference on Progress in Additive Manufacturing, Nanyang Technological University, Singapore, 14–17 May 2018.
21. Pathak, S.; Saha, G.C. Development of Sustainable Cold Spray Coatings and 3D Additive Manufacturing Components for Repair/Manufacturing Applications: A Critical Review. *Coatings* **2017**, *7*, 122. [CrossRef]
22. Wang, X.; Feng, F.; Klecka, M.A.; Mordasky, M.D.; Garofano, J.K.; El-Wardany, T.; Nardi, A.; Champagne, V.K. Characterization and modeling of the bonding process in cold spray additive manufacturing. *Addit. Manuf.* **2015**, *8*, 149–162. [CrossRef]
23. Wu, L. Method and System for Additive Manufacturing of Complex Metal Part by Sheet Lamination. U.S. Patent 0207924 A1, 26 July 2018.
24. Tofail, S.A.; Koumoulos, E.P.; Bandyopadhyay, A.; Bose, S.; O'Donoghue, L.; Charitidis, C. Additive manufacturing: Scientific and technological challenges, market uptake and opportunities. *Mater. Today* **2018**, *21*, 22–37.

    [CrossRef]
25. Machine Supplier Website. Available online: http://www.3dprintingkorea.co.kr/default.asp (accessed on 17 December 2018).
26. Dutta, B.; Froes, F.S. The Additive Manufacturing (AM) of titanium alloys. *Met. Powder Rep.* **2017**, *72*, 96–106. [CrossRef]
27. Körner, C. Additive manufacturing of metallic components by selective electron beam melting—A review. *Int. Mater. Rev.* **2016**, *61*, 361–377. [CrossRef]
28. Sames, W.J.; List, F.A.; Pannala, S.; Dehoff, R.R.; Babu, S.S. The metallurgy and processing science of metal additive manufacturing. *Int. Mater. Rev.* **2016**, *61*, 315–360. [CrossRef]
29. Yap, C.Y.; Chua, C.K.; Dong, Z.L.; Liu, Z.H.; Zhang, D.Q.; Loh, L.E.; Sing, S.L. Review of selective laser melting: Materials and applications. *Appl. Phys. Rev.* **2015**, *2*, 041101. [CrossRef]
30. Zhang, B.; Li, Y.; Bai, Q. Defect Formation Mechanisms in Selective Laser Melting: A Review. *Chin. J. Mech. Eng.* **2017**, *30*, 515–527. [CrossRef]
31. Kruth, J.; Wang, X.; Laoui, T.; Froyen, L. Lasers and materials in selective laser sintering. *Assem. Autom.* **2003**, *23*, 357–371. [CrossRef]
32. Gibson, I.; Rosen, D.; Stucker, B. *Additive Manufacturing Technologies*; Springer: New York, NY, USA, 2015; pp. 107–145.
33. Bunnell, D.E.; Das, S.; Bourell, D.L.; Beaman, J.B.; Marcus, H.L. Fundamentals of Liquid Phase Sintering During Selective Laser Sintering. *Assem. Autom.* **2003**, *24*, 440–447.
34. Shamsaei, N.; Yadollahi, A.; Bian, L.; Thompson, S.M. An overview of Direct Laser Deposition for additive manufacturing; Part II: Mechanical behavior, process parameter optimization and control. *Addit. Manuf.* **2015**, *8*, 12–35. [CrossRef]
35. Machine Supplier Website. Available online: http://www.sciaky.com (accessed on 26 October 2017).
36. Service Supplier Website. Available online: http://www.ramlab.com (accessed on 26 October 2017).

37. Szost, B.A.; Terzi, S.; Martina, F.; Boisselier, D.; Prytuliak, A.; Pirling, T.; Hofmann, M.; Jarvis, D.J. A comparative study of additive manufacturing techniques: Residual stress and microstructural analysis of CLAD and WAAM printed Ti–6Al–4V components. *Mater. Des.* **2016**, *89*, 559–567. [CrossRef]
38. Flynn, J.M.; Shokrani, A.; Newman, S.T.; Dhokia, V. Hybrid additive and subtractive machine tools—Research and industrial developments. *Int. J. Mach. Tools Manuf.* **2016**, *101*, 79–101. [CrossRef]
39. Du, W.; Bai, Q.; Zhang, B. A Novel Method for Additive/Subtractive Hybrid Manufacturing of Metallic Parts. *Procedia Manuf.* **2016**, *5*, 1018–1030. [CrossRef]
40. Manogharan, G.; Wysk, R.A.; Harrysson, O.L. Additive Manufacturing—Integrated Hybrid Manufacturing and Subtractive Processes: Economic Model and Analysis. *Int. J. Comput. Integr. Manuf.* **2015**, *29*, 473–488. [CrossRef]
41. Yamazaki, T. Development of A Hybrid Multi-tasking Machine Tool: Integration of Additive Manufacturing Technology with CNC Machining. *Procedia CIRP* **2016**, *42*, 81–86. [CrossRef]
42. Merklein, M.; Junker, D.; Schaub, A.; Neubauer, F. Hybrid Additive Manufacturing Technologies—An Analysis Regarding Potentials and Applications. *Phys. Procedia* **2016**, *83*, 549–559. [CrossRef]
43. Machine Supplier Website. Available online: http://www.hybridmanutech.com/ (accessed on 26 October 2017).
44. Jones, J.B. *Hybrid CNC + Additive: Two Heads Are Better Than One*; Wohlers Talk: SME's RAPID; Wohlers: Long Beach, CA, USA, 2015.
45. Lee, Y.; Nordin, M.; Babu, S.S.; Farson, D.F. Effect of Fluid Convection on Dendrite Arm Spacing in Laser Deposition. *Metall. Mater. Trans. B* **2014**, *45*, 1520–1529. [CrossRef]
46. Li, R.; Shi, Y.; Wang, Z.; Wang, L.; Liu, J.; Jiang, W. Densification behavior of gas and water atomized 316L stainless steel powder during selective laser melting. *Appl. Surf. Sci.* **2010**, *256*, 4350–4356. [CrossRef]
47. Gu, D.; Shen, Y. Balling phenomena in direct laser sintering of stainless steel powder: Metallurgical mechanisms and control methods. *Mater. Des.* **2009**, *30*, 2903–2910. [CrossRef]
48. Addispace. *Diagonosis and Study of Oportunities of Metallic Additive Manufacturing on SUDOE Aerospatial Sector*; Technical Report for Sudoe and Interreg: Santander, Spain, December 2016.
49. Hadadzadeh, A.; Baxter, C.; Amirkhiz, B.S.; Mohammadi, M. Strengthening mechanisms in direct metal laser sintered AlSi10Mg: Comparison between virgin and recycled powders. *Addit. Manuf.* **2018**, *23*, 108–120. [CrossRef]
50. Du Plessis, A.; le Roux, S.G. Standardized X-ray tomography testing of additively manufactured parts: A round robin test. *Addit. Manuf.* **2018**, *24*, 125–136. [CrossRef]
51. Townsend, A.; Racasan, R.; Leach, R.; Senin, N.; Thompson, A.; Ramsey, A.; Bate, D.; Woolliams, P.; Brown, S.; Blunt, L. An interlaboratory comparison of X-ray computed tomography measurement for texture and dimensional characterisation of additively manufactured parts. *Addit. Manuf.* **2018**, *23*, 422–432. [CrossRef]
52. Wits, W.W.; Carmignato, S.; Zanini, F.; Vaneker, T.H. Porosity testing methods for the quality assessment of selective laser melted parts. *CIRP Ann.* **2016**, *65*, 201–204. [CrossRef]
53. Fieres, J.; Schumann, P.; Reinhart, C. Predicting failure in additively manufactured parts using X-ray computed tomography and simulation. *Procedia Eng.* **2018**, *213*, 69–78. [CrossRef]
54. Gong, H.; Rafi, K.; Gu, H.; Starr, T.; Stucker, B. Analysis of defect generation in Ti–6Al–4V parts made using powder bed fusion additive manufacturing processes. *Addit. Manuf.* **2014**, *1–4*, 87–98. [CrossRef]
55. Aboulkhair, N.T.; Everitt, N.M.; Ashcroft, I.; Tuck, C. Reducing porosity in AlSi10Mg parts processed by selective laser melting. *Addit. Manuf.* **2014**, *1–4*, 77–86. [CrossRef]
56. Chen, Z.; Wu, X.; Tomus, D.; Davies, C.H. Surface roughness of Selective Laser Melted Ti-6Al-4V alloy components. *Addit. Manuf.* **2018**, *21*, 91–103. [CrossRef]
57. Tian, Y.; Tomus, D.; Rometsch, P.; Wu, X. Influences of processing parameters on surface roughness of Hastelloy X produced by selective laser melting. *Addit. Manuf.* **2017**, *13*, 103–112. [CrossRef]
58. Safdar, A.; He, H.; Wei, L.; Snis, A.; de Paz, L.E.C. Effect of process parameters settings and thickness on surface roughness of EBM produced Ti-6Al-4V. *Rapid Prototyp. J.* **2012**, *18*, 401–408. [CrossRef]
59. Robinson, J.; Ashton, I.; Fox, P.; Jones, E.; Sutcliffe, C. Determination of the effect of scan strategy on residual stress in laser powder bed fusion additive manufacturing. *Addit. Manuf.* **2018**, *23*, 13–24. [CrossRef]

60. Salmi, A.; Atzeni, E.; Iuliano, L.; Galati, M. Experimental Analysis of Residual Stresses on AlSi10Mg Parts Produced by Means of Selective Laser Melting (SLM). *Procedia CIRP* **2017**, *62*, 458–463. [CrossRef]
61. Seifi, M.; Gorelik, M.; Waller, J.; Hrabe, N.; Shamsaei, N.; Daniewicz, S.; Lewandowski, J.J. Progress Towards Metal Additive Manufacturing Standardization to Support Qualification and Certification. *JOM* **2017**, *69*, 439–455. [CrossRef]
62. Teng, C.; Pal, D.; Gong, H.; Zeng, K.; Briggs, K.; Patil, N.; Stucker, B. A review of defect modeling in laser material processing. *Addit. Manuf.* **2017**, *14*, 137–147. [CrossRef]
63. Choi, H.; Byun, J.M.; Lee, W.; Bang, S.R.; Kim, Y.D. Research Trend of Additive Manufacturing Technology—A = B + C + D + E, add Innovative Concept to Current Additive Manufacturing Technology: Four Conceptual Factors for Building Additive Manufacturing Technology. *J. Korean Powder Metall. Inst.* **2016**, *23*, 149–169. [CrossRef]
64. Joshi, S.C.; Sheikh, A.A. 3D printing in aerospace and its long-term sustainability. *Virtual Phys. Prototyp.* **2015**, *10*, 175–185. [CrossRef]
65. Baufeld, B.; Brandl, E.; van der Biest, O. Wire based additive layer manufacturing: Comparison of microstructure and mechanical properties of Ti–6Al–4V components fabricated by laser-beam deposition and shaped metal deposition. *J. Mater. Process. Technol.* **2011**, *211*, 1146–1158. [CrossRef]
66. Roberts, C.E.; Bourell, D.; Watt, T.; Cohen, J. A Novel Processing Approach for Additive Manufacturing of Commercial Aluminum Alloys. *Phys. Procedia* **2016**, *83*, 909–917. [CrossRef]
67. Romano, S.; Bruckner-Foit, A.; Brandao, A.; Gumpinger, J.; Ghidini, T.; Beretta, S. Fatigue properties of AlSi10Mg obtained by additive manufacturing: Defect-based modelling and prediction of fatigue strength. *Eng. Fract. Mech.* **2018**, *187*, 165–189. [CrossRef]
68. Kelly, S.M. *Volume 1: Development and Measurement Analysis of Design Data for Laser Powder Bed Fusion Additive Manufacturing of Nickel Alloy 625*; Deliverable under Cooperative Agreement No. 70NANB12H26. EWI Technical Report; National Institute of Standards and Technology, United States Department of Commerce: Gaithersburg, MD, USA, 2014.
69. Johnson, A.S.; Shuai, S.; Shamsaei, N.; Thompson, S.M.; Bian, L. Fatigue behaviour and failure mechanisms of direct laser deposited inconel 718. In Proceedings of the Solid Freeform Fabrication Symposium—An Additive Manufacturing Conference: University of Texas in Austin, Austin, TX, USA, 8–10 August 2016; pp. 499–511.
70. Amsterdam, E.; Kool, G.A. High Cycle Fatigue of Laser Beam Deposited Ti-6Al-4V and Inconel 718. In *ICAF 2009, Bridging the Gap between Theory and Operational Practice*; Springer: Dordrecht, The Netherlands, 2009; pp. 1261–1274.
71. Bauer, T.; Dawson, K.; Spierings, A.B.; Wegener, K. *Microstructure and Mechanical Characterisation of SLM Processed Haynes ® 230 ®*; Technical Report; Laboratory for Freeform Fabrication, University of Texas: Austin, TX, USA, 2011.
72. Murr, L. Metallurgy of additive manufacturing: Examples from electron beam melting. *Addit. Manuf.* **2015**, *5*, 40–53. [CrossRef]
73. Walton, D.; Moztarzadeh, H. Design and Development of an Additive Manufactured Component by Topology Optimisation. *Procedia CIRP* **2017**, *60*, 205–210. [CrossRef]
74. Uriondo, A.; Esperon-Miguez, M.; Perinpanayagam, S. The present and future of additive manufacturing in the aerospace sector: A review of important aspects. *Proc. Inst. Mech. Eng. Part G J. Aerosp. Eng.* **2015**, *229*, 2132–2147.

    [CrossRef]
75. Liu, C.; Du, Z.; Zhang, W.; Zhu, Y.; Guo, X. Additive Manufacturing-Oriented Design of Graded Lattice Structures Through Explicit Topology Optimization. *J. Appl. Mech.* **2017**, *84*, 081008.

    [CrossRef]
76. Brackett, D.; Ashcroft, I.; Hague, R. Topology Optimization for Additive Manufacturing. Available online: https://sffsymposium.engr.utexas.edu/Manuscripts/2011/2011-27-Brackett.pdf (accessed on 25 June 2019).
77. Maskery, I.; Aboulkhair, N.; Aremu, A.; Tuck, C.; Ashcroft, I.; Wildman, R.; Hague, R. A mechanical property evaluation of graded density Al-Si10-Mg lattice structures manufactured by selective laser melting. *Mater. Sci. Eng. A* **2016**, *670*, 264–274. [CrossRef]

78. Ferguson, I.; Frecker, M.; Simpson, T.W.; Dickman, C.J. Topology Optimization Software for Additive Manufacturing: A Review of Current Capabilities and a Real-World Example. In *Volume 2A: 42nd Design Automation Conference*; ASME: Charlotte, NC, USA, 2016.
79. Clausen, A. Topology Optimization for Additive Manufacturing. Ph.D. Thesis, DTU Mechanical Engineering, Technical University of Denmark, Lyngby, Denmark, 2016.
80. Das, P.; Chandran, R.; Samant, R.; Anand, S. Optimum Part Build Orientation in Additive Manufacturing for Minimizing Part Errors and Support Structures. *Procedia Manuf.* **2015**, *1*, 343–354. [CrossRef]
81. Gaynor, A.T.; Guest, J.K. Topology optimization considering overhang constraints: Eliminating sacrificial support material in additive manufacturing through design. *Struct. Multidiscip. Optim.* **2016**, *54*, 1157–1172. [CrossRef]
82. Guo, X.; Zhou, J.; Zhang, W.; Du, Z.; Liu, C.; Liu, Y. Self-supporting structure design in additive manufacturing through explicit topology optimization. *Comput. Methods Appl. Mech. Eng.* **2017**, *323*, 27–63. [CrossRef]
83. Zhao, D.; Li, M.; Liu, Y. Self-supporting Topology Optimization for Additive Manufacturing. *CoRR* **2017**, arXiv:1708.07364.
84. Allaire, G.; Dapogny, C.; Estevez, R.; Faure, A.; Michailidis, G. Structural optimization under overhang constraints imposed by additive manufacturing technologies. *J. Comput. Phys.* **2017**, *351*, 295–328. [CrossRef]
85. Mirzendehdel, A.M.; Suresh, K. Support structure constrained topology optimization for additive manufacturing. *Comput. Aided Des.* **2016**, *81*, 1–13. [CrossRef]
86. Langelaar, M. Topology optimization of 3D self-supporting structures for additive manufacturing. *Addit. Manuf.* **2016**, *12*, 60–70. [CrossRef]
87. Gaynor, A.T. Topology Optimization Algorithms for Additive Manufacturing. Ph.D. Thesis, The Johns Hopkins University, Baltimore, MD, USA, 2015.
88. Frazier, W.E. Metal Additive Manufacturing: A Review. *J. Mater. Eng. Perform.* **2014**, *23*, 1917–1928. [CrossRef]
89. Seifi, M.; Salem, A.; Beuth, J.; Harrysson, O.; Lewandowski, J.J. Overview of Materials Qualification Needs for Metal Additive Manufacturing. *JOM* **2016**, *68*, 747–764. [CrossRef]
90. ESA Open Invitation to Tender AO9085. Development of Embedded Thermal Functions in Structural Parts Using 3D Printing; Available online: http://www2.rosa.ro/index.php/en/esa/oferte-furnizori/2318-development-of-embedded-thermal-functions-in-structural-parts-using-3d-printing (accessed on 25 June 2019).
91. ESA Open Invitation to Tender AO9112. Development of One Single Part Integrating Waveguide Filter, Bends, Coupler, Supporting Structures by Additive Manufacturing; Available online: http://www2.rosa.ro/index.php/en/esa/oferte-furnizori/2378-development-of-one-single-part-integrating-waveguide-filter-bends-coupler-supporting-structures-by-additive-manufacturing (accessed on 25 June 2019).
92. Energetics Incorporated. *Measurement Science Roadmap for Metal-Based Additive Manufacturing: Workshop Summary Report*; Technical Report; NIST: Maryland, DC, USA, 2013.
93. ESA Open Invitation to Tender AO9094. Advanced Aluminium Alloys Tailored for Additive Manufacturing Space Applications, Targeting High End Structural Spacecraft Parts; Available online: http://www2.rosa.ro/index.php/en/esa/oferte-furnizori/2359-advanced-aluminum-alloys-tailored-for-additive-manufacturing-space-applications-targeting-high-end-structural-spacecraft-parts (accessed on 25 June 2019).
94. ESA Open Invitation to Tender AO 9032. Additive Manufacturing Powder Material Supply Chain: Verification and Validation. Available online: http://www2.rosa.ro/index.php/en/esa/oferte-furnizori/2337-additive-manufacturing-powder-material-supply-chain-verification-and-validation (accessed on 25 June 2019).
95. Ghidini, T. *An Overview of Current AM Activities at the European Space Agency: 3D Printing Additive Manufacturing—Industrial Applications*; 3D Printing & Additive Manufacturing; Industrial Applications Global Summit: London, UK, 2013.
96. Werkheiser, N. *Overview of NASA Initiatives in 3D Printing and Additive Manufacturing*; DoD Maintenance Symposium: Birmingham, UK, 2014.

97. Ghidini, T. *European Space Agency Perspective on Additive Manufacturing (AM): 3D Printing Additive Manufacturing—Industrial Applications*; 3D Printing & Additive Manufacturing; Industrial Applications Global Summit: London, UK, 2013.
98. Oerlikon. RUAG Deepens Cooperation With Oerlikon to Achieve Serial Production of 3D Printed Components for Space. Available online: additivemanufacturing.com (accessed on 12 October 2018).
99. Bromberger, M. Technology Symbiosis Additive Manufacturing & Topology Optimization. In *Additive Manufacturing Design & Engineering Symposium*; Altair Engineering, Inc.: Troy, MI, USA, 2014.
100. Aerospace: RUAG—Additive Manufacturing of Satellite Components. Available online: www.eos.info (accessed on 11 October 2018).

Chapter 3

Material characterization

3.1 Experimental testing

Designing structures for the aerospace industry involves numerous phases, such as design optimization or structural verification. However, in either phase, accurate constitutive data is crucial for their success. Therefore, an experimental testing campaign of Ti6Al4V alloy was performed and the main results are provided in the original article, which is provided in the current section and entitled "Experimental mechanical characterization of SLM samples via a comparative study" [P2]. In the referred study, different suppliers are compared in terms of the resultant materials processed via SLM. In a preliminary analysis, the samples' mechanical performance from different suppliers can be arguably similar. However, when advanced testing is performed, some fundamental and critical differences may arise at its microscopic level.

Experimental mechanical characterization of Ti6Al4V SLM samples via a comparative study

B. Barroqueiro[a,b], I. Bola[b], A. Santos[b], A. Andrade-Campos[a], R.A.F. Valente[a], I. Duarte[a], S.C. Pinto[a], V. Infante[c], D.F.O. Braga[c], T. Bento[c]

[a] *Department of Mechanical Engineering, Centre for Mechanical Technology & Automation (TEMA), University of Aveiro, 3810-193 Aveiro, Portugal.*
[b] *Active Space Technologies, Actividades Aeroespaciais S.A., Parque Industrial de Taveiro, Lote12, 3045-508 Coimbra, Portugal*
[c] *IDMEC, Instituto Superior Técnico, Universidade de Lisboa, Av. Rovisco Pais, 1, 1049-001, Lisboa, Portugal*

Abstract

Selective Laser Melting (SLM) allows the low-cost construction of highly customized parts. However, the understanding of their mechanical behavior still represents a challenge. In the scope of this work, an experimental testing of SLM Ti6Al4V samples is presented using homogeneous macroscopic testing (tensile, compression, density, hardness, and fatigue) and microscopic testing for defects detection using X-ray microcomputed tomography (μCT) scan. For that, the sample's manufacturing was subcontracted to different suppliers to allow their comparative analysis in terms of their mechanical performance. From a macroscopic point of view, the samples' mechanical performance from different suppliers can be arguably similar. However, if advanced testing is performed (*e.g.* fatigue testing and μCT technique), some fundamental and critical differences may arise at its microscopic level.

Keywords: Selective laser melting; Ti6Al4V; Mechanical Testing; Fatigue; X-ray microcomputed tomography.

1. Introduction

Ti6Al4V alloy, processed via Selective Laser Melting (SLM), has attracted relevant interest in both academia and industry. Despite the ongoing challenges [1], nowadays the SLM fabrication of Ti6Al4V parts has reached some level of maturity and, therefore, several companies started to provide it as a service (*e.g.* Renishaw, Materialise, 3D-Alchemy...). However, it is worth noting that SLM can process other materials such as different steels, aluminum or nickel alloys, and other materials [2]. The Ti6Al4V alloy, processed via SLM, provides high strength (1100-1300 MPa) at a cost of ductility (<8%). This lack of ductility

*Corresponding author
Email address: bjfb@ua.pt (B. Barroqueiro)

is commonly attributed to the resultant microstructures, which tend to be fully martensitic (α') due to the high cooling rates occurring during SLM ($> 10^6$K/s). These martensitic structures are brittle, being responsible for the observed low ductility. In order to tackle this issue, post SLM heat treatments are typically performed to decompose α' (hcp) in the α (ccc) and β (fcc) phases. The resultant improvement in ductility is significant however, with a relevant loss of strength (<1000 MPa) [3–6].

In the scope of this work, samples of Ti6Al4V alloy are analyzed, being processed via SLM. However, many studies have been published on the subject. For instance, some works such as [3, 7–12] are focused in the process parameters and its physics to have a better understanding of the occurring phenomena with the ultimate goal of improving the process parameterization. For instance, Shipley *et al.* [8] reviews the influence of the process parameters on the material. An increase in the powder bed temperature (as process parameter) improves the material ductility and reduces residual stresses without losing strength. Increasing downtime between layers may also lead to reduced residual stresses. Moreover, the layer thickness can also increase ductility but it comes with a cost of strength and an increase in porosity. A detailed overview of process physics and its defects is presented in [1] and a critical succinct overview can be seen in [2].

Other studies such as [13–25] are focused on the fundamental mechanical properties such as strength limits or elastic properties. For instance, Chen *et al.* [13] studied the anisotropic responses in terms of hardness and electrochemical resistance of the SLM Ti-6Al-4V samples. In contrast, Facchini *et al.* [14] studied the change in the mechanical properties with special emphasis on ductility when processed with different SLM process parameterization.

Alternatively, other studies such as [26–34] are more interested in the performance of SLM Ti6Al4V samples when subjected to repeated loading. For Instance, Kasperovicha and Hausmann [26] study the fatigue resistance and ductility of TiAl6V4 processed by SLM and compares it to the wrought TiAl6V4. In contrast, Nicoletto [29] focused his research on the anisotropic high cycle fatigue behavior of Ti6Al4V obtained by SLM.

Despite all optimization already performed in the SLM fabrication of Ti-6Al-4V samples, after any SLM manufacturing job, stress relief heat treatment is still mandatory [2]. Therefore, some studies, such as [35–38], study the impact of post-heat treatments on the final mechanical properties. For example, Frkan *et al.* [38] studied the fatigue performance of SLM Ti6Al4V alloy after different stress relief heat treatments and reported a slight increase of fatigue life, when stress relief temperature is increased from 740°C to 900°C (likely due to the increase of ductility from 13% to 18%). In contrast, Longhitano *et al.* [39] analyzed the changes in the sample's SLM microstructures when subjected to different heat treatments and its consequent influence in the corrosion behavior in the anodizing process.

Any engineer that wants to build a highly customized part can take advantage of Additive Layer Manufacturing (ALM) namely SLM. However, SLM machines are expensive and most companies do not own their machines directly. Thus, engineers that need to take advantage of ALM are forced to subcontract the manufacturing of the part. Moreover, and consequently, the control over the manufacturing process is limited. Thus, the experience of the suppliers in SLM productions and the reliability of their SLM machine are important threats, which affect the reliability of the mechanical behavior of SLM Ti6Al4V material

(*e.g.* level of defects). Therefore, a better understanding of the mechanical behavior of SLM Ti6Al4V components is needed by the industry. However, the comparison of the structural performance between different suppliers has not received much attention from academia. Thus, the goal of this study is to compare three distinct suppliers with three distinct SLM machines in terms of mechanical performance (tensile, compression, hardness, density, and fatigue testing) and defects as a function of the manufacturing direction.

2. Experimental

Tensile testing

Tensile testing was performed on flat dog-bone type E-3 (see Figure 1(a)) according to the standard DIN50125 [40]. Additionally, a linear deformation rate of 0.75 mm/s was selected. Regarding deformation measurement, an optical Digital Image Correlation (DIC) full-field method was used. The optical system was calibrated according to the parameters recommended by the supplier [41]. A full description of the system (*e.g.* camera model, focal distance and subset size) is described in detail by Aquino *et al.* [42] using the 3D algorithm and an acquisition rate of 1 Hz. The average of the major and minor strains are considered for all subsequent calculations.

Compression testing

The compression testing specimens are cylinders with 25 mm of height and 13 mm of diameter, and its dimensions were defined by ASTM E9 [43]. Additionally, a linear deformation rate of 0.05 mm/s was defined. Regarding deformation measurement, a clip gauge Instron 1225 was used.

Fatigue testing

The fatigue testing specimens are the cylindrical bog-bones (see Figure 1(b)) and its dimensions were defined according to the recommendations of ASTM E466 [44]. Testing was conducted on constant amplitude loading at a frequency of 17 Hz and a stress ratio $R = 0.1$.

Density testing

The density testing specimens are parallelepiped of 3x3x12 mm^3 and the density measurements were performed according to ASTM B311 [45], which is based on the principle of Archimedes.

Hardness testing

The hardness testing specimens are parallelepiped of 12x12x3 mm^3 and the Shimadzu micro Vickers hardness tester HMV-2000 was used with a force of 0.5 kg and a holding time of 5 s.

CT scan

In order to search for closed porosity in the specimens, μCT scans were performed on the density specimens using Bruker SkyScan 1275 and its main parameters are defined in Table 1.

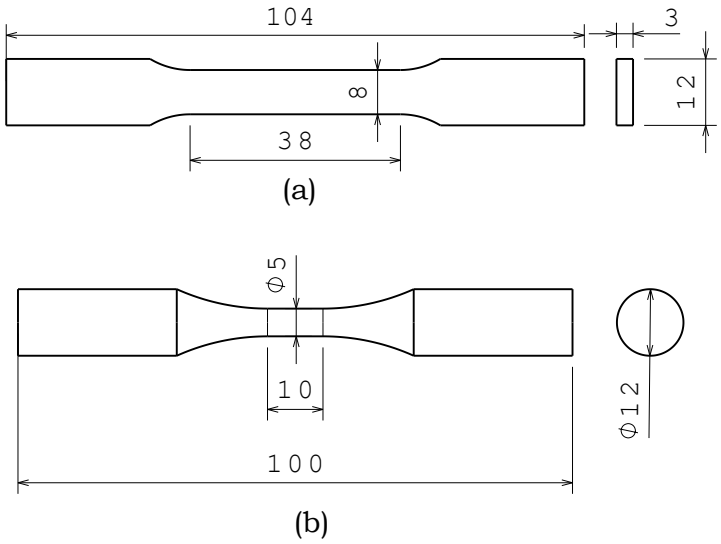

Figure 1: Specimen's main dimensions for (a) tensile and (b) fatigue tests. All dimensions are mm.

Specimen's manufacturing

Three distinct suppliers were subcontracted for the specimen's manufacturing using the EOS M290, Trumpf 3000, and Renishaw AM 500 S machines, respectively. For the specimen's production, Ti6Al4V powder was requested with an average size of 30 μm. The service was defined as fine construction for the best mechanical performance and the used process parameters were considered confidential by the suppliers. After SLM fabrication, the specimens were cleaned (removing the excess powder) and subjected to stress relief. In the end, the specimens underwent a sandblasting and machining process.

Considering a cartesian reference `X` (gas flow direction), `Y` and `Z` (build direction), the specimens were printed in three distinct directions 0, 45 and 90 according to the following vectors <1,0,0>, <1,0,1> and <0,0,1>, respectively.

3. Results and discussion

After the specimen's SLM manufacturing, stress relief, sand-blasting, and cut-off from the base plate, some warping was detected in relation to the original design and, therefore, extra thickness was necessary in order to ensure that the original dimensions were possible to meet after machining. Taking as reference the tensile test specimen, an extra thickness of 0.3 mm, 0.9 mm, and 0.2 mm for the orientations of 0°, 45° and 90°, respectively, were necessary. In contrast, the fatigue specimens required even higher thickness. The fatigue specimens needed a radial increase of 2.8 mm, 1.4 mm, and 1.1 mm for the orientations of 0°, 45°, and 90°, respectively. The layout of the specimens on the base plate during their SLM fabrication is shown in Figure 2. The largest warping of tensile specimens occurred at 45° orientation due to poor choice on the support structures generation. A small buckling of the support structures is visible on the referred figure, indicating the need for additional structures to minimize their deformation. The remaining orientations exhibited an acceptable deformation. In contrast, the warping on fatigue specimens is far more challenging

Table 1: Overview of μCT scan main parameters.

System Setup		Reconstruction	
Scanner	SkyScan1275	Reconstruction Program	NRecon
Instrument S/N	17G15048	Program Version	Version: 1.7.3.1
Software Version	1.0.16	Reconstruction engine	GPUReconServer
Embedded Controller Version	3.5	Engine version	Version: 1.7.3
Source Type	HAMAMATSU_L11871_20	Reconstruction from batch	No
Camera Type	DEXELA_1512A	Postalignment Applied	1
Camera Pixel Size (μm)	75.0	Postalignment	-13.50
Camera binning	1x1	First Section	197
Image Rotation	0.42300	Last Section	1302
Optical Axis (line)	742	Section to Section Step	1
Object to Source (mm)	21.164	Sections Count	1106
Camera to Source (mm)	286.0	Result File Type	BMP
Source Voltage (kV)	100	Result File Header Length (bytes)	1134
Source Current (μA)	100	Result Image Width (pixels)	1944
Image Pixel Size (μm)	6.000902	Result Image Height (pixels)	1944
Scaled Image Pixel Size (μm)	6.000902	Pixel Size (um)	6.00090
Depth (bits)	16	Reconstruction Angular Range (deg)	360.00
Reference Intensity	58000	Use 180+	OFF
Exposure (ms)	260	Angular Step (deg)	0.2000
Rotation Step (deg)	0.200	Smoothing	0
Use 360 Rotation	YES	Ring Artifact Correction	15
Scanning position	22.000 mm	Draw Scales	ON
Frame Averaging	ON (10)	Object Bigger than FOV	OFF
Random Movement	OFF (30)	Reconstruction from ROI	OFF
Flat Field Correction	ON	Filter cutoff relative to Nyquist frequency	100
FF updating interval	360	Filter type	0
Filter	Cu 1mm	Filter type description	Hamming (Alpha)
Gantry direction	CC	Under sampling factor	1
Rotation Direction	CC	Threshold for defect pixel mask (%)	0
Scanning Start Angle	0.000	Beam Hardening Correction (%)	5
Type of Detector Motion	STEP AND SHOOT	CS Static Rotation (deg)	0.00
Scanning Trajectory	ROUND	CS Static Rotation Total(deg)	0.00
Number Of Horizontal Offset Positions	1	Minimum for CS to Image Conversion	0.000000
Suggested HU - Calibration	180000	Maximum for CS to Image Conversion	0.045000
Maximum vertical TS	5.0	HU Calibration	OFF
		BMP LUT	0
		Cone-beam Angle Horiz.(deg)	30.816811
		Cone-beam Angle Vert.(deg)	24.088736
		Pseudo-parallel projection calculated	1

due to the large difference in radius of the main sections, where all orientations exhibited important deformations with particular relevance in the 0° orientation.

Regarding the μCT scan, Figure 3 provides an overview of the results of the three suppliers. The μCT images are shown in gray-scale maps since the defect's boundary is not clearly defined due to high pixel size (6 μm). Thus, the process of image binarization

Figure 2: Layout of the specimens on base plate after sand blasting

(transformation to a black and white mapping) is highly sensitive to the threshold parameter. Therefore, the authors believe it is more appropriate to present the results in grayscale. Nonetheless, the largest presented defects should be around 70 µm, which seems appropriated since the average powder size of 30 µm was used by the suppliers. Regarding supplier

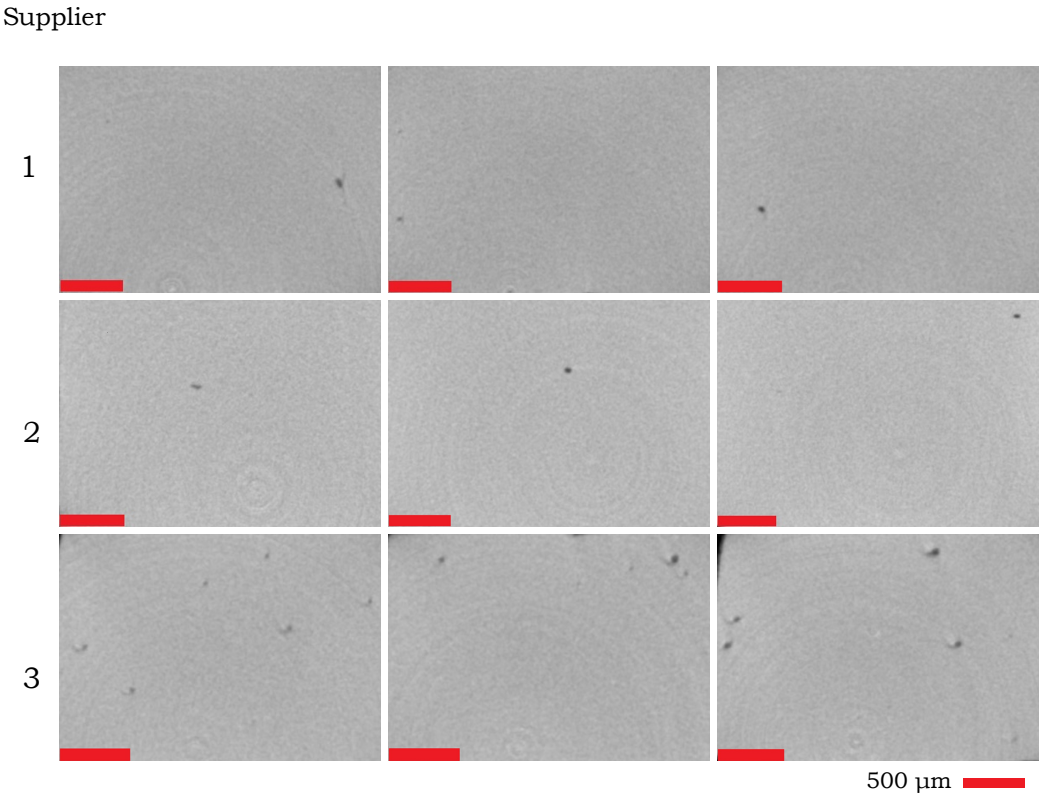

Figure 3: Comparative overview of common defects in different suppliers using µCT images.

1, defects across the one thousand sections of the µCT scan are rare and the majority of frames do not have visible defects. However, micro-porosity similar to pixel size cannot be detected using the available laboratory conditions. For instance, porosity originated from the poor quality of metal powder (*e.g.* hollow powder due to gas entrapment during powder production) cannot be detected. Regarding supplier 2, defects are more frequent and in a few sections, isolated defects were detected. In contrast, the samples from supplier 3 exhibited considerably more defects and, more importantly, within the same section, several defects were detected as shown in Figure 3.

Regarding tensile properties, a comparison between different suppliers and different manufacturing orientations is provided in Table 2. Concerning elastic anisotropy, some differences are visible in the Young modulus (E) and Poisson ratio (ν), but their relevance is limited. Regarding plastic anisotropy, it seems that 0° orientations result in the lowest strength limits and the 45° orientation results in the highest strength limit. Nonetheless, all the strength limits comply with ASTM F2924 standard [46], which imposes a minimum 0.2% flow stress ($\sigma_{0.2\%}$) and ultimate stress (σ_{u}) of 825 MPa and 895 MPa, respectively. Moreover, these specimens show better static properties than the brought counterparts. For

Table 2: Tensile properties comparison between different suppliers and different manufacturing orientations.

Supplier	Properties	0°		45°		90°	
		Value	Error	Value	Error	Value	Error
1	E [GPa]	114.8	0.4	114.5	0.5	116.8	0.5
	v [-]	0.305	0.002	0.313	0.001	0.315	0.001
	$\sigma_{0.2\%}$ [MPa]	967	5	985	9	978	2
	σ_u [MPa]	1038	6	1051	4	1037	2
	ε_f [MPa]	0.124	0.005	0.140	0.005	0.14	0.02
	Hardness [HV]	377	5	384	4	372	13
2	E [GPa]	113	2	116.0	0.2	117.1	0.2
	v [-]	0.319	0.003	0.307	0.002	0.318	0.004
	$\sigma_{0.2\%}$ [MPa]	1027	35	1107	2	1085	7
	σ_u [MPa]	1120	23	1156	3	1170	2
	ε_f [MPa]	0.067	0.005	0.060	0.008	0.08	0.01
	Hardness [HV]	416	9	398	7	399	11
3	E [GPa]	118.4	0.5	117.2	0.8	118.6	0.3
	v [-]	0.311	0.001	0.311	0.004	0.312	0.002
	$\sigma_{0.2\%}$ [MPa]	1088	7	1124	21	1090	23
	σ_u [MPa]	1154	10	1180	16	1159	18
	ε_f [MPa]	0.093	0.006	0.095	0.005	0.09	0.01
	Hardness [HV]	383	6	394	4	398	6

instance, the ultimate strength of an annealed plate is around 900 MPa [47]. Regarding the fracture strain (ε_f), the supplier 1 material complies with the imposed inferior limit of 10% (ASTM F2924 standard [46]) and the remaining ones failed to achieve it. Still, regarding supplier 1, the engineering stress-strain curves are plotted in Figure 4, being visible a high dispersion of results with particular emphasis in 90° manufacturing orientation. In contrast, the 45° orientation provides the most consistent results. As already referred,

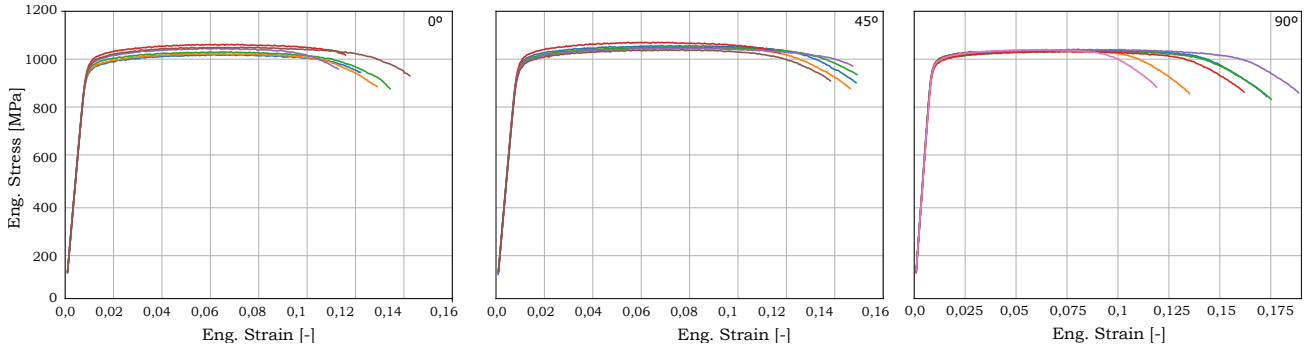

Figure 4: Overview of the engineering stress strain curves of supplier 1.

supplier 1 has the highest values of fracture strain and a stress relief of 800ºC/4H was applied. The supplier 2 has the lowest values of fracture strain and a stress relief of 700ºC/2H was applied. The supplier 3 material has the intermediate values (almost compliant with referred standard) applied a stress relief of 730ºC/2H. Across the suppliers' different metal powders,

SLM machines and SLM parameterizations were used but the results suggest a connection between the heat input heat treatments and the ductility, being in line with the literature [3]. Moreover, the loss of strength to gain ductility is also visible between supplier 1 and the remaining ones.

Regarding hardness (HV), typically there is a linear correlation between the hardness and the ultimate strength [48]. However, in the scope of this work, the referred linear correlation was not observed. It seems that more specimens and more tests would be needed or, perhaps, the underlying micro-porosity is influencing the hardness results.

Regarding compression, a single test per supplier was performed to get an estimate of the compression strength of Ti6Al4V alloy. The resultant compressive stresses at maximum compressive load are 2049 MPa (at 37.3% strain), 1846 MPa (at 27.3% strain), and 2048 MPa (at 38.9% strain) for the suppliers 1, 2 and 3 materials, respectively, in terms of nominal stresses in the 90° orientation. From an engineering point of view, nominal stresses are definitely useful. However, in order to make an accurate comparison between tension and compression stresses, these should be compared in terms of true stresses. Table 3 compares the tension and compression true stress values at maximum load for all suppliers. Since only one test per supplier was performed, its statistical representativeness is limited. Nonetheless, it is counter-intuited that supplier 3 material, which had a larger amount of defects in the selected sample, has the lowest difference in terms of tension and compression true stresses.

Table 3: Comparison between tensile tests and compression tests via true stresses at maximum load.

Supplier	True tension stress [MPa]	True compression stress [MPa]
1	1149±17	1285
2	1244±10	1342
3	1242±10	1251

Regarding fatigue performance, Figure 5 describes the fatigue testing results per supplier, being clear the dispersion of the results resultant from the mechanical behavior of the SLM samples. For instance, the results from supplier 2 material for a given stress level have points near low cycle fatigue up to high cycle fatigue. Nonetheless, supplier 1 material achieves the highest fatigue strength. In contrast, the supplier 2 material achieves the lowest fatigue strengths. Nonetheless, in a mean perceptive, supplier 1 material has the highest fatigue strength, likely, due to the lowest presence of defects. In contrast, the supplier 2 material shows high dispersion in the results which seems to be related with (i) the arbitrary presence of defects and (ii) lack of ductility. Furthermore, the lack of ductility of the referred material is similar to the ductility obtained in as-built condition, suggesting that insufficient heat input was applied during heat treatment. Additionally, it is worth noting the 90° orientation specimens were particularly affected in terms of fatigue strength while not visible on tensile tests. Finally, material from supplier 3 consistently exhibits low fatigue strength likely due to the regular presence of defects. In short, a correlation between the presence of defects and their fatigue strength was observed as expected.

Regarding porosity, density measurements were made. The density results per material

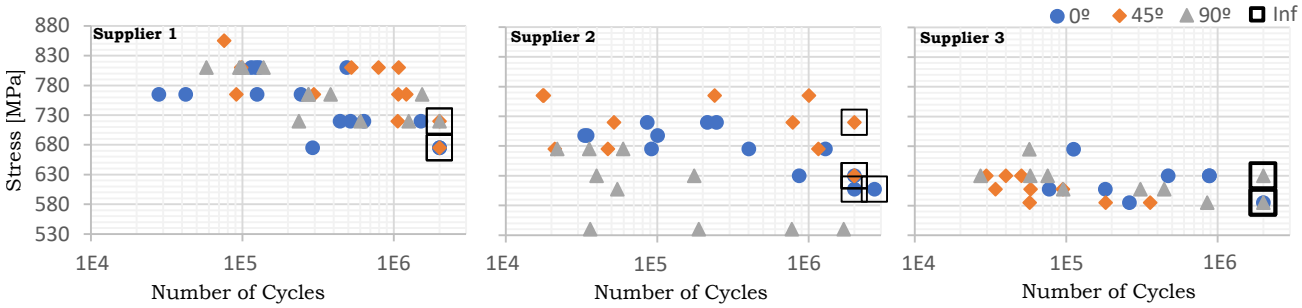

Figure 5: Comparative overview of fatigue results.

are 4.43±0.02 g/cm^3, 4.48±0.02 g/cm^3 and 4.47±0.02 g/cm^3 for suppliers 1, 2 and 3, respectively. The initial goal associated with these measurements was the calculation of the porosity. However, the observed porosity has a very low volume percentage and, thus, finding an accurate reference value for each supplier material proved to be a challenge. In contrast, the μCT scan would be able to provide more exact values about porosity if there were no pixel size limitations (already referred). Thus, the resultant values are highly dependent on the analyst. Nonetheless, the resulting porosity across different supplier materials is well below 1%.

4. Concluding remarks

An experimental testing campaign of Ti6Al4V alloy using SLM specimens has been presented using different suppliers and different manufacturing orientations. Moreover, each supplier uses a distinct machine from different machine constructors. Furthermore, both macroscopic and microscopic testing was used in order to contribute to a deeper understanding of the mechanical behavior of the referred alloy.

These samples show better static properties than the brought counterparts. Moreover, the elastic anisotropy has limited relevance. However, the plastic anisotropy has higher relevance and the repeatability of SLM samples still represents a challenge. In a preliminary analysis, the performance of the specimens from different suppliers would show similar tensile properties if identical heat treatments were applied, since these have a relevant impact on the compromise between strength and ductility. When comparing the mechanical performance of SLM specimens from different suppliers, some fundamental and critical differences may arise, if more advanced testing is performed such as μCT scan or fatigue testing.

Acknowledgements

The authors gratefully acknowledge the financial support of the Portuguese Foundation for Science and Technology (FCT) under the projects: (i) CENTRO-01-0145-FEDER-029713 by UE/FEDER through the programs CENTRO 2020, COMPETE 2020, (ii) UID/EMS/00481/2013-FCT under CENTRO-01-0145-FEDER-022083 and (iii) UIDB/50022/2020 through the program IDMEC under LAETA. Financial support of program CENTRO 2020 and UE/FEDER is also acknowledged through the project CENTRO-01-0247-FEDER-024039,

designated as ADVANSS. B. Barroqueiro also acknowledges the financial support by the FCT through the scholarship SFRH/BD/120779/2016.

Additionally, the authors acknowledge all the technical recommendations from OHB Systems at Oberpfaffenhofen. Finally, the authors acknowledge the kindness and support of Professor Matej Vesenjak from the University of Maribor for performing the compression tests in these difficult times.

Contributions

B. Barroqueiro: Conceptualization, Methodology, Investigation (Tensile testing), Software, Formal analysis, Validation, Writing - original draft, Writing - review & editing. I. Bola: Conceptualization, Methodology, Validation, Writing - review & editing. A. Santos: Conceptualization, Methodology, Resources, Validation, Writing - review & editing, Project administration. A. Andrade-Campos: Writing - review & editing, Project administration, Funding acquisition. R.A.F. Valente: Writing - review & editing. I. Duarte: Investigation (Hardness and compression testing, and μCT scan), Writing - review & editing. S. Pinto: Investigation (Hardness and compression testing, and μCT scan), Writing - review & editing. V. Infante: Investigation (Fatigue testing), Writing - review & editing. D.F.O. Braga: Investigation (Fatigue testing), Writing - review & editing. T. Bento: Investigation (Fatigue testing).

References

[1] T. DebRoy, H. L. Wei, J. S. Zuback, T. Mukherjee, J. W. Elmer, J. O. Milewski, A. M. Beese, A. Wilson-Heid, A. De, W. Zhang, Additive manufacturing of metallic components – Process, structure and properties, Progress in Materials Science 92 (2018) 112–224.

[2] B. Barroqueiro, A. Andrade-Campos, R. A. F. Valente, V. Neto, Metal additive manufacturing cycle in aerospace industry: A comprehensive review, Journal of Manufacturing and Materials Processing 3 (3) (2019).

[3] A. Zafari, M. R. Barati, K. Xia, Controlling martensitic decomposition during selective laser melting to achieve best ductility in high strength Ti-6Al-4V, Materials Science and Engineering A 744 (2019) 445–455.

[4] S. Liu, Y. C. Shin, Additive manufacturing of Ti6Al4V alloy: A review, Materials and Design 164 (2019) 107552.

[5] M. J. Donachie, Titanium: A Technical Guide, ASM, 2000.

[6] J. J. Lewandowski, M. Seifi, Metal Additive Manufacturing: A Review of Mechanical Properties, Annual Review of Materials Research 46 (1) (2016) 151–186.

[7] B. Song, S. Dong, B. Zhang, H. Liao, C. Coddet, Effects of processing parameters on microstructure and mechanical property of selective laser melted Ti6Al4V, Materials and Design 35 (2012) 120–125.

[8] H. Shipley, D. McDonnell, M. Culleton, R. Coull, R. Lupoi, G. O'Donnell, D. Trimble, Optimisation of process parameters to address fundamental challenges during selective laser melting of Ti-6Al-4V: A review, International Journal of Machine Tools and Manufacture 128 (September 2017) (2018) 1–20.

[9] M. Bisht, N. Ray, F. Verbist, S. Coeck, Correlation of selective laser melting-melt pool events with the tensile properties of Ti-6Al-4V ELI processed by laser powder bed fusion, Additive Manufacturing 22 (January) (2018) 302–306.

[10] Z. Zhao, J. Chen, H. Tan, G. Zhang, X. Lin, W. Huang, Achieving superior ductility for laser solid formed extra low interstitial Ti-6Al-4V titanium alloy through equiaxial alpha microstructure, Scripta Materialia 146 (2018) 187–191.

[11] W. Xu, S. Sun, J. Elambasseril, Q. Liu, M. Brandt, M. Qian, Ti-6Al-4V Additively Manufactured by Selective Laser Melting with Superior Mechanical Properties, JOM 67 (3) (2015) 668–673.
[12] H. Gong, K. Rafi, H. Gu, T. Starr, B. Stucker, Analysis of defect generation in ti–6al–4v parts made using powder bed fusion additive manufacturing processes, Additive Manufacturing 1-4 (2014) 87 – 98.
[13] L. Y. Chen, J. C. Huang, C. H. Lin, C. T. Pan, S. Y. Chen, T. L. Yang, D. Y. Lin, H. K. Lin, J. S. Jang, Anisotropic response of Ti-6Al-4V alloy fabricated by 3D printing selective laser melting, Materials Science and Engineering A 682 (October 2016) (2017) 389–395.
[14] L. Facchini, E. Magalini, P. Robotti, A. Molinari, S. Höges, K. Wissenbach, Ductility of a Ti-6Al-4V alloy produced by selective laser melting of prealloyed powders, Rapid Prototyping Journal 16 (6) (2010) 450–459.
[15] V. K. Balla, S. Martinez, B. T. Rogoza, C. Livingston, D. Venkateswaran, S. Bose, A. Bandyopadhyay, Quasi-static torsional deformation behavior of porous Ti6Al4V alloy, Materials Science and Engineering C 31 (5) (2011) 945–949.
[16] N. Biswas, J. L. Ding, V. K. Balla, D. P. Field, A. Bandyopadhyay, Deformation and fracture behavior of laser processed dense and porous Ti6Al4V alloy under static and dynamic loading, Materials Science and Engineering A 549 (2012) 213–221.
[17] D. A. Hollander, M. Von Walter, T. Wirtz, R. Sellei, B. Schmidt-Rohlfing, O. Paar, H. J. Erli, Structural, mechanical and in vitro characterization of individually structured Ti-6Al-4V produced by direct laser forming, Biomaterials 27 (7) (2006) 955–963.
[18] A. Mertens, S. Reginster, H. Paydas, Q. Contrepois, T. Dormal, O. Lemaire, J. Lecomte-Beckers, Mechanical properties of alloy Ti-6Al-4V and of stainless steel 316L processed by selective laser melting: Influence of out-of-equilibrium microstructures, Powder Metallurgy 57 (3) (2014) 184–189.
[19] C. Qiu, N. J. Adkins, M. M. Attallah, Microstructure and tensile properties of selectively laser-melted and of HIPed laser-melted Ti-6Al-4V, Materials Science and Engineering A 578 (2013) 230–239.
[20] H. K. Rafi, N. V. Karthik, H. Gong, T. L. Starr, B. E. Stucker, Microstructures and mechanical properties of Ti6Al4V parts fabricated by selective laser melting and electron beam melting, Journal of Materials Engineering and Performance 22 (12) (2013) 3872–3883.
[21] M. Simonelli, Y. Y. Tse, C. Tuck, Effect of the build orientation on the mechanical properties and fracture modes of SLM Ti-6Al-4V, Materials Science and Engineering A 616 (2014) 1–11.
[22] T. Vilaro, C. Colin, J. D. Bartout, As-fabricated and heat-treated microstructures of the Ti-6Al-4V alloy processed by selective laser melting, Metallurgical and Materials Transactions A: Physical Metallurgy and Materials Science 42 (10) (2011) 3190–3199.
[23] S. Q. Wu, Y. J. Lu, Y. L. Gan, T. T. Huang, C. Q. Zhao, J. J. Lin, S. Guo, J. X. Lin, Microstructural evolution and microhardness of a selective-laser-melted Ti-6Al-4V alloy after post heat treatments, Journal of Alloys and Compounds 672 (2016) 643–652.
[24] B. Wysocki, P. Maj, R. Sitek, J. Buhagiar, K. J. Kurzydłowski, W. Świeszkowski, Laser and electron beam additive manufacturing methods of fabricating titanium bone implants, Applied Sciences (Switzerland) 7 (7) (2017) 1–20.
[25] J. Yang, H. Yu, Z. Wang, X. Zeng, Effect of crystallographic orientation on mechanical anisotropy of selective laser melted Ti-6Al-4V alloy, Materials Characterization 127 (2017) 137–145.
[26] G. Kasperovich, J. Hausmann, Improvement of fatigue resistance and ductility of TiAl6V4 processed by selective laser melting, Journal of Materials Processing Technology 220 (2015) 202–214.
[27] S. Leuders, M. Thöne, A. Riemer, T. Niendorf, T. Tröster, H. A. Richard, H. J. Maier, On the mechanical behaviour of titanium alloy TiAl6V4 manufactured by selective laser melting: Fatigue resistance and crack growth performance, International Journal of Fatigue 48 (2013) 300–307.
[28] B. Van Hooreweder, D. Moens, R. Boonen, J. P. Kruth, P. Sas, Analysis of fracture toughness and crack propagation of Ti6Al4V produced by selective laser melting, Advanced Engineering Materials 14 (1-2) (2012) 92–97.
[29] G. Nicoletto, Anisotropic high cycle fatigue behavior of Ti–6Al–4V obtained by powder bed laser fusion, International Journal of Fatigue 94 (2017) 255–262.
[30] E. Wycisk, A. Solbach, S. Siddique, D. Herzog, F. Walther, C. Emmelmann, Effects of defects in laser

additive manufactured Ti-6Al-4V on fatigue properties, Physics Procedia 56 (C) (2014) 371–378.
[31] A. J. Sterling, B. Torries, N. Shamsaei, S. M. Thompson, D. W. Seely, Fatigue behavior and failure mechanisms of direct laser deposited ti–6al–4v, Materials Science and Engineering: A 655 (2016) 100 – 112.
[32] K. S. Chan, M. Koike, R. L. Mason, T. Okabe, Fatigue life of titanium alloys fabricated by additive layer manufacturing techniques for dental implants, Metallurgical and Materials Transactions A 44 (2013) 1543–1940.
[33] M. Kahlin, H. Ansell, J. Moverare, Fatigue behaviour of notched additive manufactured ti6al4v with as-built surfaces, International Journal of Fatigue 101 (2017) 51 – 60.
[34] S. Razavi, F. Berto, Fatigue strength of notched specimens made of ti-6al-4v produced by selected laser melting technique, Procedia Structural Integrity 13 (2018) 74 – 78.
[35] B. Vrancken, L. Thijs, J. P. Kruth, J. Van Humbeeck, Heat treatment of Ti6Al4V produced by Selective Laser Melting: Microstructure and mechanical properties, Journal of Alloys and Compounds 541 (2012) 177–185.
[36] M. Benedetti, E. Torresani, M. Leoni, V. Fontanari, M. Bandini, C. Pederzolli, C. Potrich, The effect of post-sintering treatments on the fatigue and biological behavior of Ti-6Al-4V ELI parts made by selective laser melting, Journal of the Mechanical Behavior of Biomedical Materials 71 (February) (2017) 295–306.
[37] X. Yan, S. Yin, C. Chen, C. Huang, R. Bolot, R. Lupoi, M. Kuang, W. Ma, C. Coddet, H. Liao, M. Liu, Effect of heat treatment on the phase transformation and mechanical properties of Ti6Al4V fabricated by selective laser melting, Journal of Alloys and Compounds 764 (2018) 1056–1071.
[38] M. Frkan, R. Konecna, G. Nicoletto, L. Kunz, Microstructure and fatigue performance of SLM-fabricated Ti6Al4V alloy after different stress-relief heat treatments, Transportation Research Procedia 40 (2019) 24–29.
[39] G. A. Longhitano, M. A. Arenas, A. Conde, M. A. Larosa, A. L. Jardini, C. A. de Carvalho Zavaglia, J. J. Damborenea, Heat treatments effects on functionalization and corrosion behavior of ti-6al-4v eli alloy made by additive manufacturing, Journal of Alloys and Compounds 765 (2018) 961 – 968.
[40] DIN 50125, Testing of metallic materials - tensile test pieces, Standard ICS 77.040.10, Deutsches Institut für Normung (Jully 2009).
[41] GOM GMBH, ARAMIS v6.1 User Manual software (2009).
[42] J. Aquino, A. G. Andrade-Campos, J. M. P. Martins, S. Thuillier, Design of heterogeneous mechanical tests: Numerical methodology and experimental validation, Strain 55 (4) (2019) e12313.
[43] ASTM E466, Standard test methods of compression testing of metallic materials at room temperature, Standard, American Society for Testing and Materials (2000).
[44] ASTM E466, Standard practice for conducting force controlled constant amplitude axial fatigue tests of metallic materials, Standard, American Society for Testing and Materials (2002).
[45] ASTM B311-17, Standard test method for density of powder metallurgy (pm) materials containing less than two percent porosity, Standard, American Society for Testing and Materials (2017).
[46] ASTM F2924-14, Standard Specification for Additive Manufacturing Titanium-6 Aluminum-4 Vanadium with Powder Bed Fusion, Standard, American Society for Testing and Materials (2014).
[47] R. C. Rice, J. L. Jackson, J. Bakuckas, S. Thompson, Metallic Materials Properties Development and Standardization (MMPDS), Office of Aviation Research Washington D.C. (2003).
[48] J. S. Keist, T. A. Palmer, Development of strength-hardness relationships in additively manufactured titanium alloys, Materials Science and Engineering: A 693 (2017) 214 – 224.

3.2 Heterogeneous specimens

After testing tens of specimens and spending dozens of thousand euros, the amount of information retrieved is still far from a full characterization. Different building directions also need testing as well as different tests (*e.g.* shear tests). However, the cost and time of such a campaign make it unviable for many projects. In order to reduce costs and time, each test should provide more information and the heterogeneous strain maps may play an important role. Thus, in this section, an article, entitled "Design of mechanical heterogeneous specimens using topology optimization", is presented, which proposes an innovative TO algorithm capable of designing heterogeneous specimens indirectly [P3].

International Journal of Mechanical Sciences 181 (2020) 105764

Contents lists available at ScienceDirect

International Journal of Mechanical Sciences

journal homepage: www.elsevier.com/locate/ijmecsci

Design of mechanical heterogeneous specimens using topology optimization

B. Barroqueiro[a,b,*], A. Andrade-Campos[a], João Dias-de-Oliveira[a], R.A.F. Valente[a]

[a] Department of Mechanical Engineering, Centre for Mechanical Technology & Automation (TEMA), University of Aveiro, Aveiro 3810-193, Portugal
[b] Active Space Technologies, Actividades Aeroespaciais S.A., Parque Industrial de Taveiro, Lote12, Coimbra 3045-508, Portugal

ARTICLE INFO

Keywords:
Topology optimization
Heterogeneous specimen
Specimen design
Tensile loading

ABSTRACT

Nowadays, the development and design of new parts require an increasing knowledge of the materials' behaviour. Additionally, for the current sophisticated numerical modeling tools, accurate material characterization is critical for the correct calibration of their constitutive models. The constitutive behaviour of a material can be characterized via macroscopic mechanical tests. However, the full material characterization is expensive due to a large number of required tests. Therefore, there is a need to reduce the number of tests by increasing (quantitatively and qualitatively) the information available on a single test. To this end, heterogeneous strain field specimens can provide an answer. In the scope of this work, an innovative numerical methodology to design heterogeneous specimens using Topology Optimization (TO) is presented, together with its formulation and implementation. Numerous designs are presented and assessed through a performance indicator that evaluates the uniformity of the equivalent stress maps and the presence of various stress states (tension, compression and shear) in the specimen. Finally, the most adequate design is redrawn, analyzed and evaluated in an elastoplasticity framework. Validation of the test is also made by comparison.

1. Introduction

To decrease associated delays and costs, mechanical design of parts/processes tends nowadays to be a virtual process using numerical simulation and optimization. The reduction of the development lead-time and the provision of robust solutions with highly improved quality is one of the major objectives of the automotive and aircraft industry, and numerical solutions are opportunities for these goals. However, the quality of simulation results is directly linked to the quality of the input data, particularly on the choice of an appropriate constitutive law to the accurate calibration of its parameters. Therefore, the characterization of materials has received increasing attention due to the need for precise input data to computational analysis software. A simulation software (e.g. FEM/FEA code) uses complex material constitutive models and its success reproducing the real behaviour is largely dependent on the accuracy of their calibration [1,2].

In general, the macroscopic mechanical material characterization is made using standard tests. However, the homogeneous stress-strain fields generated in these relatively simple tests do not resemble the complex stress and strain fields which occur in many metal forming operations [3] or even in complex parts' in-service operation, such as automotive or aerospace structures. Since plastic deformation is strain path-dependent, the validity of phenomenological models is limited to situations comparable to the range of experiments on which these are based. Therefore, the material behaviour obtained from standard tests and described by phenomenological models, is, at best, an approximation that in many cases does not allow a reliable simulation of complex forming processes.

Additionally, a large set of tests would be required for a full material characterization using standard homogeneous tests, resulting in time and material costly procedures. As an example, using titanium additive manufactured material, a tensile specimens are quoted as more than $200 each. For a full structural assessment, including defects, anisotropy or lack of repeatability, print direction dependence [4–6], more than 30 tests are required.

The representation of the mechanical behaviour of materials through complex/sophisticated constitutive models required for the use of simulation software presents two major challenges/difficulties: (i) the iden-

* Corresponding author at: Department of Mechanical Engineering, Centre for Mechanical Technology & Automation (TEMA), University of Aveiro, 3810-193 Aveiro, Portugal.
E-mail address: bjfb@ua.pt (B. Barroqueiro).

https://doi.org/10.1016/j.ijmecsci.2020.105764
Received 10 February 2020; Received in revised form 5 May 2020; Accepted 8 May 2020
Available online 12 May 2020

tification of a large number of parameters, and (ii) the quality, amount of information and number of performed experiments.

A very recent alternative to circumvent the limitations of standardized testing is the use of experiments that induce heterogeneous strain states in the specimen, which can be measured through full-field experimental techniques such as Digital Image Correlation (DIC) [7–11], and later processed with a suitable full-field inverse technique such as the Finite-Element Model Updating (FEMU) Method [12,13] and the Virtual Fields Method (VFM) [14–17]. An overview of most of these identification techniques is provided by Avril et al. [18].

Merely obtaining heterogeneous strain fields from an experiment is not sufficient to ensure accurate identification of the needed material parameters. Unless these are strongly activated (*i.e.*, have a strong influence on the measured kinematic fields), they cannot be uniquely ascertained using an inverse scheme [19,20]. To ensure such activation, optimization of the geometry of the specimen and loading profiles should be performed. This approach directly affects the well-posedness of the inverse problem and is an active area of research. In general, refinement of the experiment is done to ensure strain and strain-rate heterogeneity and thus ensuring activation of all material parameters.

In the last couple of years, some works have been presented to design a specimen geometry that can improve the parameter identification process [21–27]. One approach is to directly use the identification process itself to verify which specimen geometry leads to accurate results [28]. Although this can lead to improvements in the specimen geometry, it still requires a high trial-and-error effort. Another approach involves the definition of a function/criterion that evaluates the richness of the strain field in the specimen, leading to a profile with large heterogeneity and a maximum number of strain states [22,23]. Although the results of both approaches improve the identification procedure and the material characterization in a wide range of strain states, there is still room for improvement.

The first limitation that must be overcome is related to the shape optimization procedure and its geometry definition. The use of a specimen profile mathematically defined by a NURBS parametrization (or other curve definition) always limits the design solutions. For instance, a solution involving a specimen with a hole can be attractive; however, this solution cannot be found unless the initial shape already considers this specific profile. This test can be developed through the design of a new specimen and boundary conditions [23]. However, the development of new tests using new boundary conditions requires the development and building of a whole new experimental apparatus, including new testing machines [29,30]. In spite of the large design freedom [23], the large costs would constrain its wide use. For instance, the use of Universal Testing Machines (UTM) that provide standard grips with tension/compression uniaxial loading, is a constraint for a wide acceptation and use of the test by the material and mechanical engineering community, as well as for standardization. Therefore, a new test must be developed by designing new specimens.

However, the classical trial-and-error design procedure is not effective and the solutions are limited by the definition of the design boundary. Here, a Topology Optimization (TO) approach is suggested. The design of a specimen for elastoplasticity by TO is surely innovative and can lead to solutions with multiple holes, impossible to achieve with a shape optimization approach. The design procedure should maximize the number of strain-states and the richness of strain fields [3]. Some very little attempts were made to design specimens using topology optimization [24]. However, their success is still very limited and large challenges are still open [31].

This paper presents a new specimen design methodology using a computational topology optimization algorithm and a mechanical technology criterion. In the scope of this work, the specimen designs are limited to plane stress and tensile loading conditions. Firstly, this work introduces a computational algorithm (both formulation and implementation) capable of generating several designs and provides an indicator to estimate their performance. Secondly, the most adequate design is redrawn, analyzed, evaluated in an elastoplasticity framework, and validated.

2. Designing heterogeneous specimens

Within this work, the ideal heterogeneous specimen subjected to tensile loading would have the same fraction of the material in the three considered stress states: tension, shear and compression. Moreover, the equivalent stress (*e.g.* von Mises stress) along the specimen would remain constant, when loaded, ensuring a maximum range of deformation. Considering the previous hypothesis, assuming plane stress condition and double symmetry, the idealized problem can be described in Fig. 1.

The constants n_{elx} and n_{ely} correspond to half of the length and height of the specimen, respectively. Additionally, the constants k_{out} and k_{in} represents springs that were introduced in output and input locations, respectively, in order to improve the numerical stability of the problem. Finally, L and r represent the element size and the radius of the minimum member size constraint (later defined), respectively. In the current geometry, the design domain (Fig. 1) is mostly dominated by tension. In order to introduce other stress states, some portions of the material shall be removed. In theory, a function could be defined in order to impose some level of stress state heterogeneity, but the non-linearity of stress constraints led to poor or nonexistent numerical stability. Therefore, an indirect method of imposing stress states heterogeneity was developed and consists of creating heterogeneity in displacement fields using an extended and repurposed synthesis of compliant mechanisms theory. Nonetheless, the validity of the referred indirect method is limited to the conceptual problem of Fig. 1. In order to introduce the referred displacement heterogeneity, the ratio between the displacements u_{out} and u_{in} is either minimized or maximized (see Fig. 1). In both scenarios, the algorithm tries to keep the point u_{in} movement close to zero. In contrast, the algorithm tries to move the point u_{out} downwards (negative) if a minimization scenario is considered or tries to move the point u_{out} upwards (positive) if a maximization scenario is considered. In either scenario, the u_{in} imposes minimum compliance in the solution. In fact, if a unitary force is considered, the sensitivity of this term in the chain rule differentiation is equal to the well-known TO compliance problem [32]. In contrast, the term u_{out} controls how the specimen deforms. In a minimization scenario, the referred term is negative and therefore the specimen contracts, while in a maximization scenario, the term u_{out} is positive and therefore the specimen expands. Considering that, in both cases, the material has to undergo the three stress states (tension, shear and compression), the goal is to find most suitable problem parameters, namely: ratio between length and width; the remaining volume fraction; the deformation type (contraction or expansion); or the location output displacement (*e.g.* location 1 or 2 of Fig. 1, but any other location could be easily defined) that leads to the most heterogeneous mechanical specimen. Within the scope of this work, these four parameters are parametrically analyzed in order to find the most promising candidates.

2.1. Numerical methodology for heterogeneous displacement optimization

2.1.1. Problem formulation

The well-known Solid Isotropic Material with Penalization (SIMP) [33] is used, where the optimal material distribution, $\mathbf{x}$, across the design domain, Ω, is the goal. Thus, the classic problem of mechanisms synthesis of linearly quasi-static loaded structures can be mathematically extended to the following form:

$$\min/\max \quad T(\mathbf{x}) = \frac{u_{\text{out}}(\mathbf{x})}{u_{\text{in}}(\mathbf{x})}, \tag{1}$$

subjected to:

$$\mathbf{K}(\rho)\mathbf{U} = \mathbf{F},$$

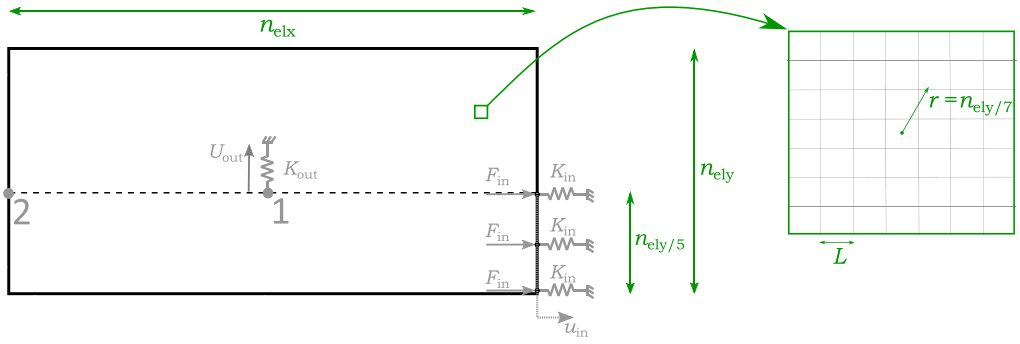

Fig. 1. Conceptual problem for designing heterogeneous specimens subjected to tensile loading conditions. The left and bottom edges of figure have symmetry conditions and the right edge has unitary forces applied to its nodes.

$$\sum_{e\in\Omega} \frac{V_e \rho_e(\mathbf{x})}{V_\Omega} = V_f, \quad e \in \Omega \quad \text{and}$$

$$0 < x_e < 1, \tag{2}$$

where **U**, **F** and **K** are the global displacements, forces and stiffness matrices, respectively. Furthermore, **x** represents the design densities, which becomes physical densities (ρ) after filtering. Additionally, V_f and V_Ω stands for volume fraction (constraint) and volume of the domain, respectively. The term u_{in} is the mean horizontal displacement of nodes on Neumann boundary condition (F_{in} - force applied by the UTM grip). In contrast, the term u_{out} is the vertical displacement of the output node (locations 1 or 2). In the scope of this work, the location of u_{out} was limited to the middle of the specimen (on the dashed line of Fig. 1). Since, the goal of topology optimization is to find the optimal distribution of material (or void) in the design domain, the placement of u_{out} should be done in a way not to limit the search universe. Therefore, the location of u_{out} should not be near to the design domain boundary (upper and right edges of Fig. 1).

Regarding the element stiffness matrix, K_e, becomes:

$$\mathbf{K}_e = \left(\rho_{min} + \rho_e^\eta\right)\mathbf{K}_e^0, \tag{3}$$

where $\mathbf{K}_e^0$ is the stiffness matrix of the solid element, and η is the penalty parameter [32].

2.1.2. Minimum member size

In order to ensure the existence of a solution, to impose a minimum feature size and avoid problems such as the formation of checkerboard patterns, a filtering operation is recommended. The linear density filter (*e.g.* [34,35]) can be formulated as:

$$\rho_e = \sum_{k\in\mathbf{N}} w_{ek} x_k, \tag{4}$$

where **N** defines the filtering neighborhood, composed by the elements k [36]. Thus, $\mathbf{N}_e = \{e : \ d(e,k) \le r\}$, where $d(e, k)$ is the distance between the centroids of elements e and k. Considering conic weights, w_{ek} becomes:

$$w_{ek} = \begin{cases} \frac{r - d(e,k)}{\sum_{l\in\mathbf{N}} r - d(e,l)} & , \quad k \in \mathbf{N}_e \\ 0 & , \quad k \notin \mathbf{N}_e. \end{cases} \tag{5}$$

Within the scope of this work, an extension of density filter is used. Initially proposed by Wang et al. [37], this filter uses the Heaviside function, formulated as:

$$\rho_e = \frac{\tanh(\beta\varphi) + \tanh(\beta(\mu_e - \varphi))}{\tanh(\beta\varphi) + \tanh(\beta(1-\varphi))} \quad \text{and} \tag{6}$$

$$\mu_e = \sum_{k\in\mathbf{N}} w_{ek} x_k, \tag{7}$$

where φ is set 0.5. Additionally, β controls the "aggressiveness" of the Heaviside function [38].

2.1.3. Sensitivity analysis

The derivative of the constraint function is straightforward [32,39,40]. However, the derivative of the objective function in order to the independent variable, **x**, is computed using the chain rule as:

$$\frac{\partial T}{\partial \mathbf{x}} = \frac{\partial T}{\partial \boldsymbol{\rho}} \frac{\partial \boldsymbol{\rho}}{\partial \mathbf{x}}. \tag{8}$$

The first term is given by:

$$\frac{\partial T}{\partial \boldsymbol{\rho}} = (-1)^\psi \frac{\frac{\partial u_{in}}{\partial \boldsymbol{\rho}} u_{out} - \frac{\partial u_{out}}{\partial \boldsymbol{\rho}} u_{in}}{u_{in}^2}, \tag{9}$$

where

$$\frac{\partial u_{in}}{\partial \rho_e} = -\eta \rho_e^{\eta-1} \boldsymbol{\lambda}_e^T \mathbf{k}_e^0 \mathbf{u}_e \quad \text{and} \tag{10}$$

$$\frac{\partial u_{out}}{\partial \rho_e} = -\eta \rho_e^{\eta-1} \boldsymbol{\gamma}_e^T \mathbf{k}_e^0 \mathbf{u}_e. \tag{11}$$

The ψ constant is 1 in the minimization scenario and 2 in the maximization scenario. The variables $\mathbf{u}_e$ and $\mathbf{k}_e^0$ are displacements and stiffness matrix, respectively, associated with element, e. Finally, the second term is computed using the chain rule as:

$$\frac{\partial \boldsymbol{\rho}}{\partial \mathbf{x}} = \frac{\partial \boldsymbol{\rho}}{\partial \boldsymbol{\mu}} \frac{\partial \boldsymbol{\mu}}{\partial \mathbf{x}} = \sum_{k\in\mathbf{N}} w_{ek} \frac{\beta\left(\operatorname{sech}(\beta(\mu_k(\mathbf{x}) - \varphi)\right)^2}{\tanh(\beta\varphi) + \tanh(\beta(1-\varphi))}. \tag{12}$$

The multipliers $\boldsymbol{\lambda}$ and $\boldsymbol{\gamma}$ require the resolution of the adjoint problems, which can be obtained via

$$\mathbf{K}(\boldsymbol{\rho})\boldsymbol{\lambda} = -\mathbf{G}_{out} \quad \text{and} \tag{13}$$

$$\mathbf{K}(\boldsymbol{\rho})\boldsymbol{\gamma} = \mathbf{G}_{in}. \tag{14}$$

The load vector $\mathbf{G}_{out}$ is a vector with the value of one at the output DOF and zeros in the remaining DOFs. For the load vector $\mathbf{G}_{in}$, the rational is identical. However, if an unit force is chosen, the multiplier $\boldsymbol{\gamma}$ is equal to **u**. Thus, this optimization requires the resolution of system of equations with two load vectors (**F** and $\mathbf{G}_{out}$).

2.2. Design evaluation

The previously described methodology presents a procedure to generate a material distribution in the defined design domain, which contains a heterogeneous displacement field. However, as already referred, the ideal heterogeneous specimen would have the same portion of the

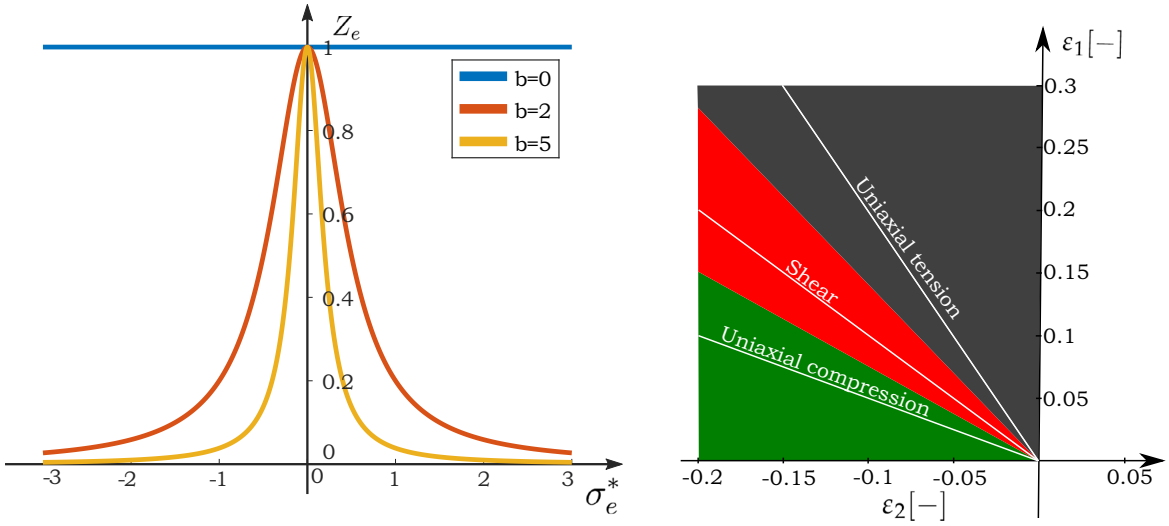

Fig. 2. (a) von Mises stress penalization function and (b) stress state identification via principal strains.

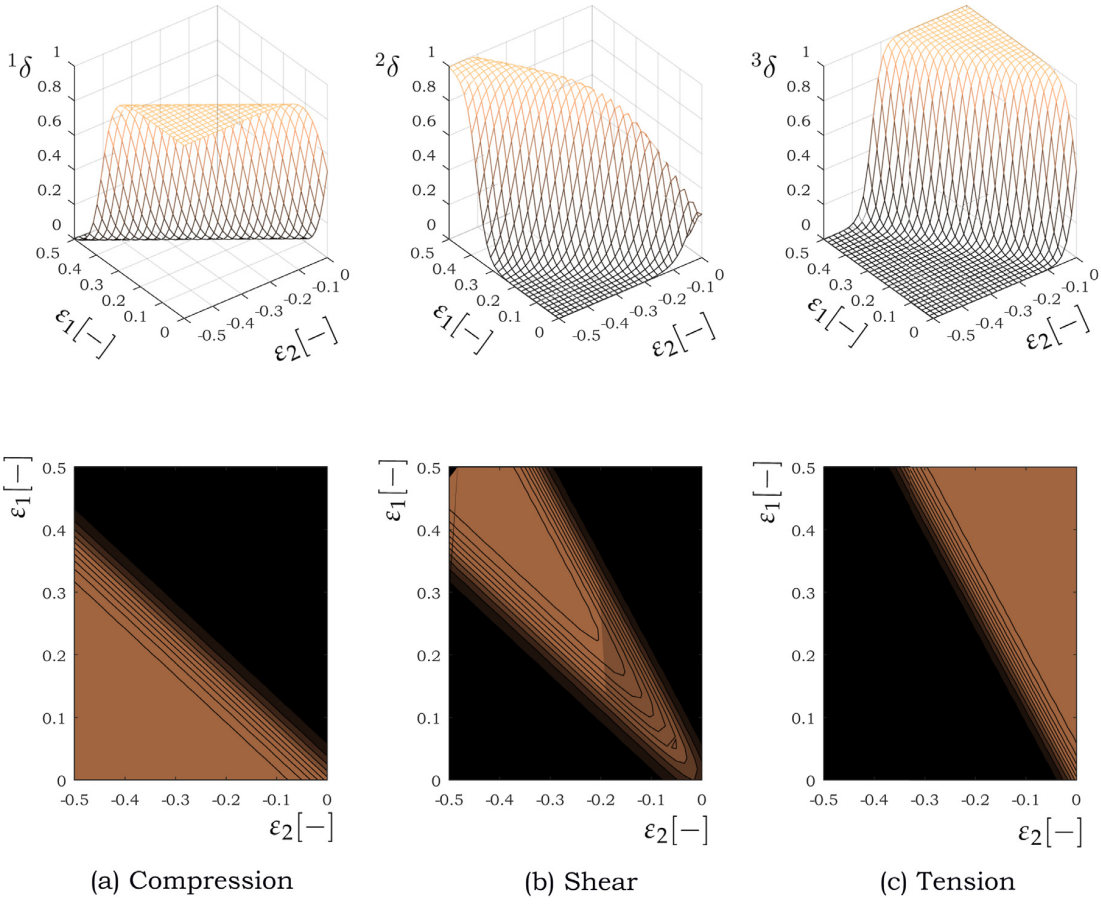

Fig. 3. Graphical representation of the operator ${}^s\delta_e$.

material in different stress states (tension, shear and compression) without stress concentrations or unstressed material. Thus, the heterogeneous displacement field condition does not directly enforce an ideal specimen and, in fact, the true optimum might be missed, being the main drawback of the presented methodology. Thus, a performance indicator is needed with several designs being computed and compared.

An effort towards the encapsulation of all the previous assumptions has been made, being mathematically described as:

$$id = \prod_{s=1}^{3} \left[\frac{3}{\sum_{e=1}^{n} \rho_e} \sum_{e=1}^{n} \left({}^s\delta_e Z_e \rho_e \right) \right], \tag{15}$$

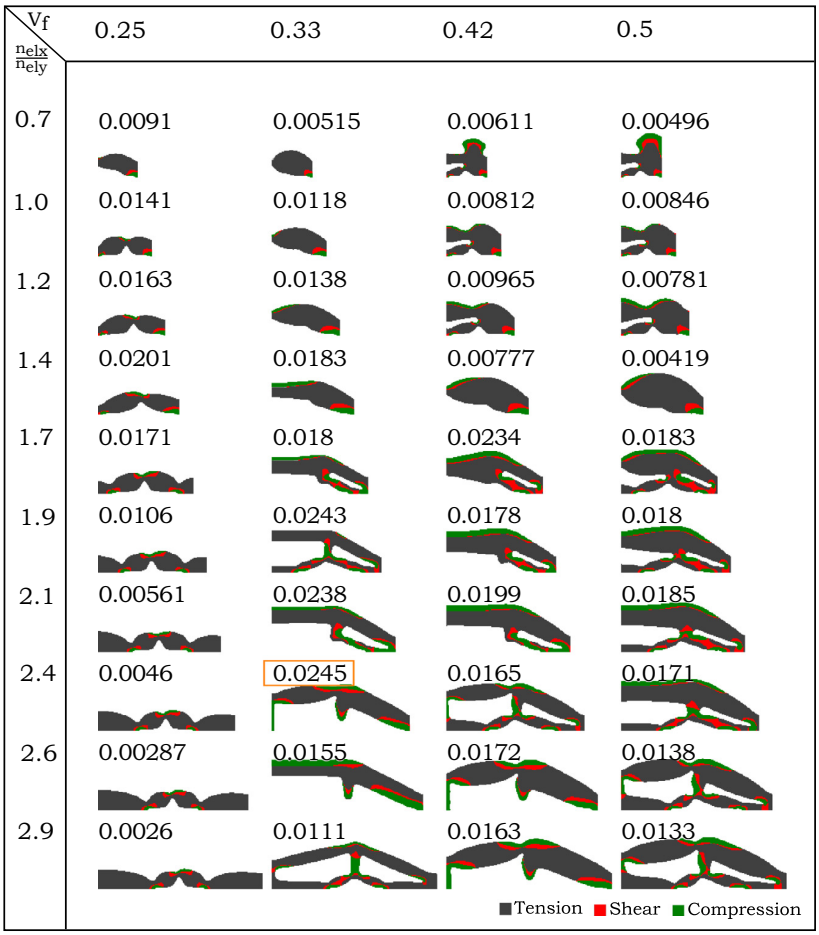

Fig. 4. Heterogeneous displacement optimization results for tensile specimens using double symmetry (1/4 of the specimen), location 1 and contraction deformation type for various aspect ratios and volume fractions indicated on the figure. Above each solution, the performance indicator is also represented.

where s denotes indexes, which are defined in Eq. (18). In short, s equals to indexes 1, 2 or 3, indicating compression, shear and tension, respectively. The term Z_e penalizes solutions with stress concentrations and non-stressed material, being formulated as

$$Z_e = \frac{1}{1 + \left(b\sigma_e^*\right)^2}. \tag{16}$$

The constant b controls the "aggressiveness" of the referred penalization function as described in Fig. 2(a). The term σ_e^* is given by

$$\sigma_e^* = \frac{\sigma_e^{\mathrm{VM}} - \bar{\sigma}^{\mathrm{VM}}}{\bar{\sigma}^{\mathrm{VM}}} \tag{17}$$

where the superscript VM indicates the von Mises Stress and $\bar{\sigma}^{\mathrm{VM}}$ represents the mean stress. The operator ${}^s\delta_e$ filters the elements correspondent to the s stress state. In order to identify the referred stress state of each element, the principal strains are used (see Fig. 2(b)). The stress states relationships were retrieved from the bibliography [23]. Regarding traction, the relation of $\varepsilon_e^{11} = -2\varepsilon_e^{22}$ was used. Regarding shear, the relation of $\varepsilon_e^{11} = -\varepsilon_e^{22}$ was used. Regarding compression, the relation of $\varepsilon_e^{11} = -0.5\varepsilon_e^{22}$ was used. Nevertheless, the same methodology could be used using different principal strain ratios relationships or different assumptions (small/large strains, volume conservation, etc.).

The operator $({}^s\delta_e)$ takes approximately the value of one if the element is in the s stress state and zero otherwise. This is achieved via a 2D generalization of the smooth Heaviside function, being formulated as

$${}^s\delta_e = \begin{cases} \frac{1}{2}\left(1 - \tanh\left(\beta\left(\varepsilon_e^{11} + 0.75\varepsilon_e^{22}\right)\right)\right), & s = 1 \\ \frac{1}{4}\left(1 + \tanh\left(\beta\left(\varepsilon_e^{11} + 0.75\varepsilon_e^{22}\right)\right)\right)\left(1 - \tanh\left(\beta\left(\varepsilon_e^{11} + 1.5\varepsilon_e^{22}\right)\right)\right), & s = 2. \\ \frac{1}{2}\left(1 + \tanh\left(\beta\left(\varepsilon_e^{11} + 1.5\varepsilon_e^{22}\right)\right)\right), & s = 3 \end{cases} \tag{18}$$

In order to facilitate the reader's interpretation of the operator, a graphical representation is provided in Fig. 3, with a 3D representation as well as its projection (2D) in the principal strain plane.

Regarding the finite element analysis, it is worth pointing out some considerations. About the strain tensor, it is computed in matrix form via

$$\boldsymbol{\varepsilon}_e = \mathbf{B}_e \mathbf{u}_e, \tag{19}$$

where $\mathbf{B}_e$ is the derivatives of shape functions for a 2D bilinear plane stress element. Finally, the stress tensor is computed in matrix form via

$$\boldsymbol{\sigma}_e = \rho_e^{\eta} \mathbf{D}_e \boldsymbol{\varepsilon}_e, \tag{20}$$

where $\mathbf{D}$ is constitutive relation defined by Hooke's law. Although this design methodology here presented uses elastic behavior as the material model, it can be extended and the results extrapolated to elastoplasticity. In fact, a comparison between an elastic and an elastoplastic material models is shown later, and the differences between the assumptions are small. Moreover, the inclusion of the plasticity phenomena significantly raises the computational cost of the optimization process. In the scope of this work, the goal is the discovery of solid initial designs using TO,

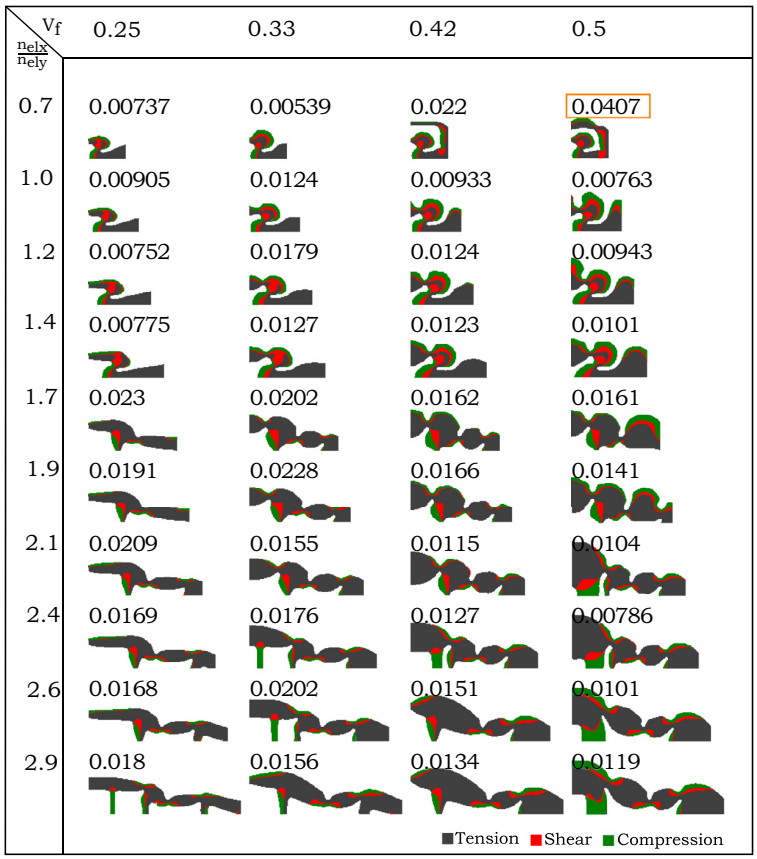

Fig. 5. Heterogeneous displacement optimization results for tensile specimens using double symmetry (1/4 of the specimen), location 1 and expansion deformation type for various aspect ratios and volume fractions indicated on the figure. Above each solution, the performance indicator is also represented.

Table 1
Algorithm structure for generating heterogeneous specimens designs.

1. Define the four initial characteristics of the specimen:
(a) deformation type: contraction (min) or expansion (max);
(b) location of the output displacement (*e.g.* location 1 or 2 from Fig. 1);
(c) aspect ratio of design domain (n_{elx}/n_{ely});
(d) volume fraction (V_f);
2. Begin the design conceptualization:
(a) Build and save neighborhood, $\mathbf{N}_e$, for an efficient filtering operation;
(b) Initialize design domain, $\mathbf{x}$;
(c) Compute physical densities, ρ, using Eqs. (7) and (6);
(d) Optimization loop:
i. solve the structural problem ($\mathbf{K}(\rho)[\mathbf{U}, \lambda] = [\mathbf{F}, \mathbf{G}_{out}]$);
ii. compute sensitivity $\partial T/\partial \rho$ based on physical densities (Eq. (9));
iii. perform filtering operation in order to obtain final sensitivities using Eq. (12);
iv. calculate new $\mathbf{x}$ using an optimizer (*e.g.* MMA)
v. compute physical densities, ρ, using Eqs. (7) and (6);
vi. return to sub-step (i) or break the loop if solution converged.
(e) eliminate any remaining intermediate physical densities (ρ);
(f) solve the structural problem ($\mathbf{K}(\rho)\mathbf{U} = \mathbf{F}$) with η set to 1 (non-penalized) and without the springs K_{in} and K_{out};
(g) compute performance indicator and store the solution;
(h) repeat the process with different initial parameters in order to obtain multiple designs.

which then subsequently require an additional step of optimization in order to obtain the final geometry. The second optimization step can be done by means of a trial-and-error approach or using more systematic methodology (*e.g.* shape optimization). The approach here is to use elasticity in the first step with TO, and add plasticity in the second step.

2.3. Implementation

The program structure closely follows the algorithm described in the Table 1. The TO problem is solved with the gradient-based Method of Moving Asymptotes (MMA) [41], using the default parameters unless otherwise specified. The parameters β, η, b and φ are set to 20, 3, 3 and 0.5, respectively [32,42].

2.4. Methodology overview

The presented methodology requires two steps. The first step is the application of the presented topology optimization algorithm that generates many geometries with heterogenous displacements fields, which have some level of richness in terms of stress states. The u_{out} term forces the displacement field to be highly non-uniform, while the term u_{in} forces the geometry to have some level of stiffness. The algorithm

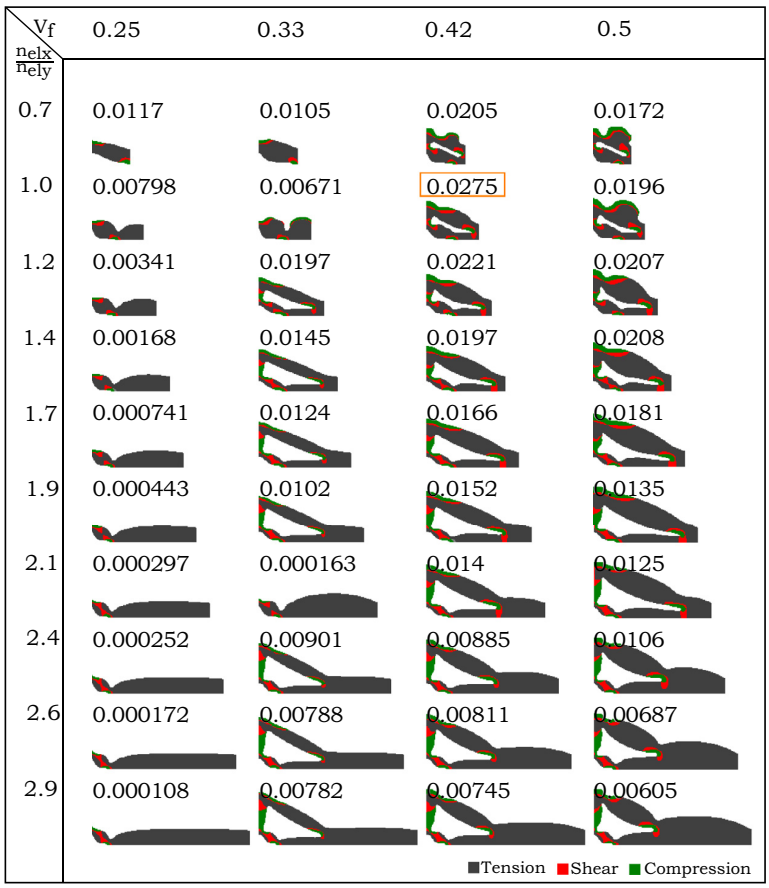

Fig. 6. Heterogeneous displacement optimization results for tensile specimens using double symmetry (1/4 of the specimen), location 2 and contraction deformation type for various aspect ratios and volume fractions indicated on the figure. Above each solution, the performance indicator is also represented.

has its foundations on mechanism's theory, which allow the computation of a particular material distribution that generates the predefined displacement output when provided with an input force. Knowing that stress/strain states are a consequence of displacement fields, it was found that specific stress/strain fields could be generated by controlling displacement fields. In topology optimization, using compliance mechanism objective functions, it is possible to find geometries (material distributions) that contain highly heterogenous displacement fields when subjected to tensile loading. Thus, the idea is the generation of large set of geometries using different initial conditions (type of deformation; location of the output displacement; aspect ratio of design domain; remaining volume fraction of design domain). The second step analyses the performance of the previous set of geometries using the performance indicator, which evaluates the specimens in terms of richness of stress states and uniformity of equivalent stress levels.

The reader might argue that the presented performance indicator could replace the current objective function of the TO algorithm (possibly with some compliance constraint) in order to avoid this multi-step methodology and directly search for the optimal design. However, in practice, the non-linearity of performance indicator led to numerical instabilities and, despite the on going research efforts, no single step methodology was found yet. In short, the one-step methodology remains an open topic for future work.

3. Results and discussion

Figs. 4 and 5 describe the results for the heterogeneous displacement optimization for specimens subjected to tensile loading using location 1 for contraction and expansion deformation types, respectively. Several analyses are presented for different aspect ratios (0.7, 1.0, 1.2, 1.4, 1.7, 1.9, 2.1, 2.4, 2.6 and 2.9) and different volume fractions (0.25, 0.33, 0.42 and 0.5). In a similar way, Figs. 6 and 7 describe the results for the heterogeneous displacement optimization for specimens subjected to tensile loading using location 2 for contraction and expansion deformation types. The same number of analyses are presented for the same aspect ratios and volume fractions. It worth noting that all specimens have a gripping area, which is contained in the non-design domain and, thus, not shown on Figs. 4–7. Moreover, the referred gripping area is similar to Fig. 10(a).

The main results are described in Fig. 8 in order to facilitate the parametric analysis of the deformation type and location of the output node as function of the aspect ratio and the volume fraction. It is worth noting that the size of the circles are proportional to the value of the performance indicator, allowing their comparison. After the analysis of the previous results, it is difficult to establish any trends with respect to aspect ratio and volume fraction, being largely depend on the initial parameters.

Regarding location and deformation type, the designs with highest performance indicator from Figs. 4–7 are drastically different from a geometrical point of view, but the magnitude of performance indicators (0.0245, 0.0407, 0.0275, 0.0511) are similar. The design of Fig. 7 [1.0;0.42] has the highest performance indicator but the strain deformation field leads to a very premature rupture and, therefore, the design was abandoned. The design of Fig. 5 [1.0;0.5] has the second highest performance indicator but the thickness required to avoid buckling was high and the design was therefore abandoned. Finally, the design of Fig. 6 [1.0;0.42] was selected (third design with the highest indicator), since it has reasonably long strain deformation filed in the elastoplastic regime. Additionally, Fig. 9 describes the convergence curve for the proposed specimen.

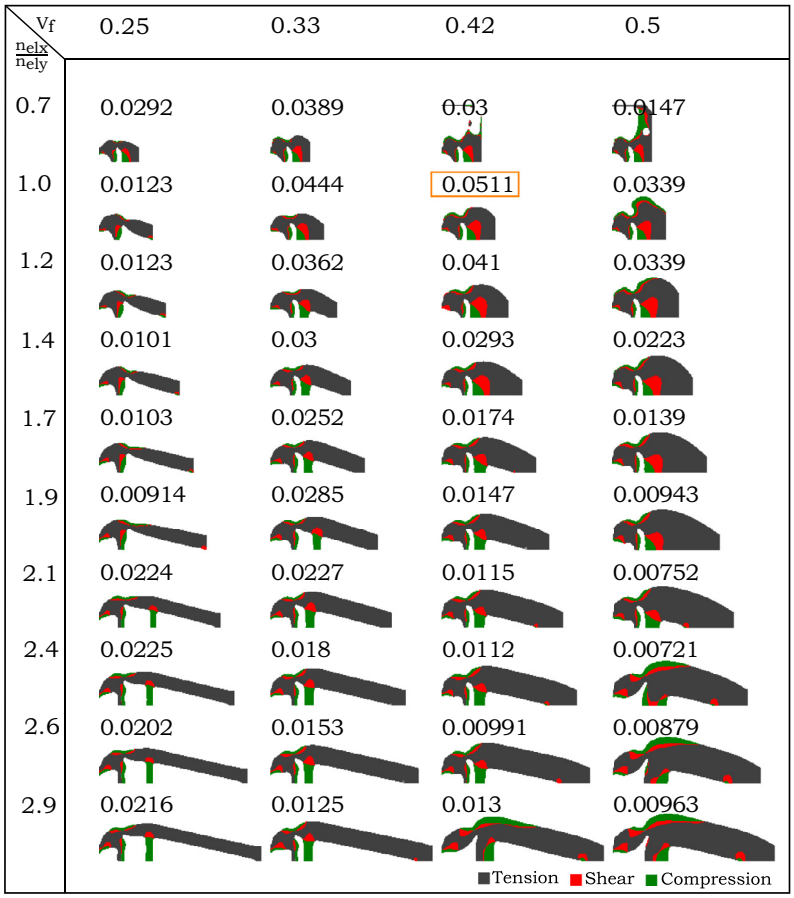

Fig. 7. Heterogeneous displacement optimization results for tensile specimens using double symmetry (1/4 of the specimen), location 2 and expansion deformation type for various aspect ratios and volume fractions indicated on the figure. Above each solution, the performance indicator is also represented.

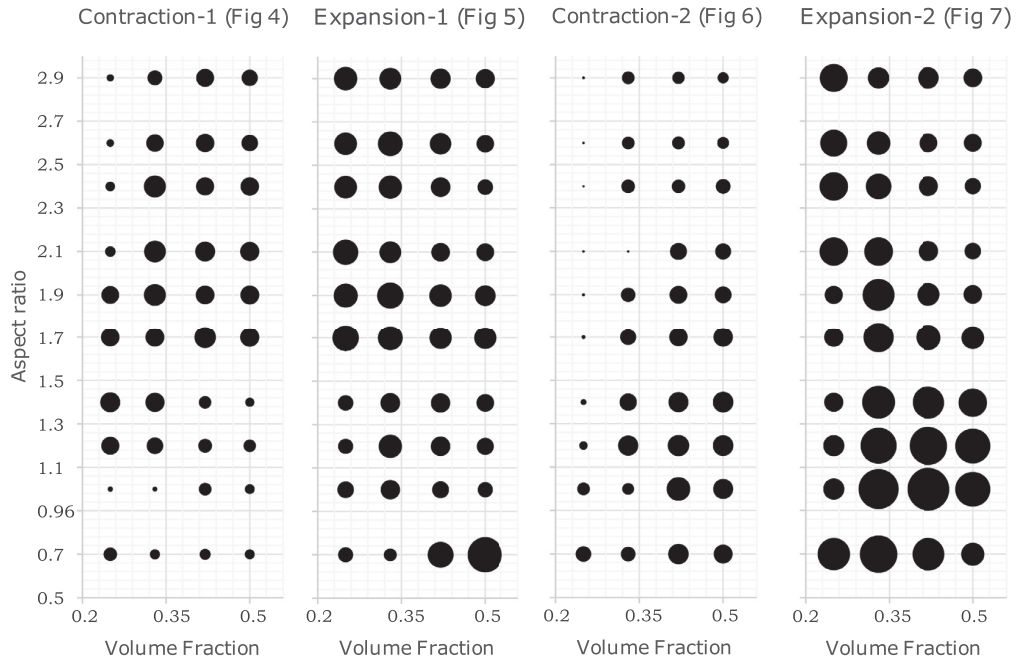

Fig. 8. Overall comparison of the performance indicators.

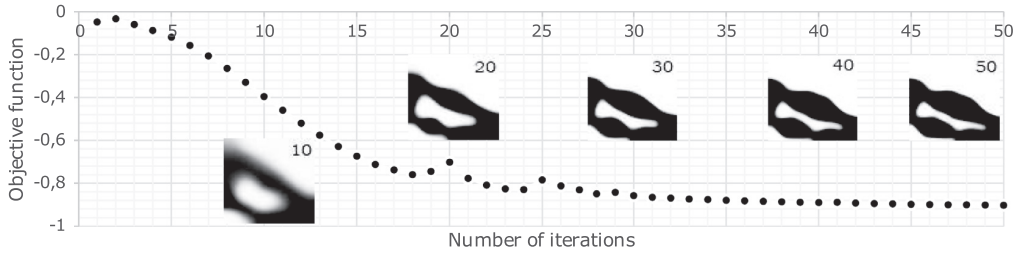

Fig. 9. Convergence curve of the proposed specimen.

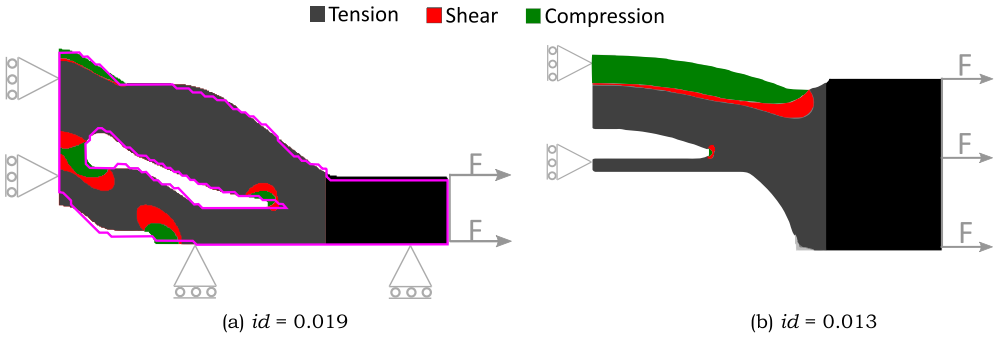

Fig. 10. Comparison of the proposed design (quarter symmetry) with a reference solution (half symmetry) in terms of design stress states (color maps) and performance indicator. The pink line indicates the design boundary before the redesign.

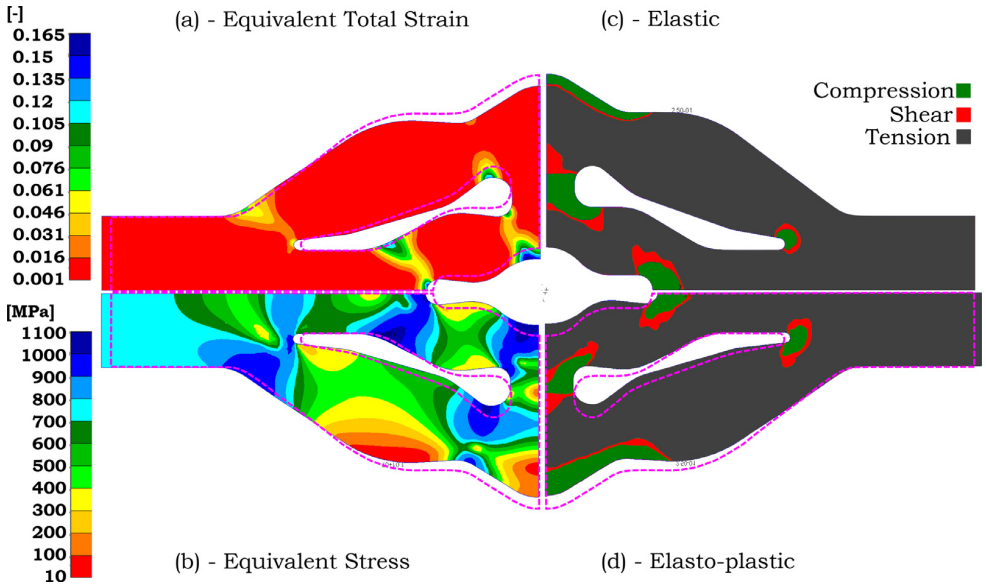

Fig. 11. Final validation of proposed specimen: (a) equivalent total strain and (b) equivalent stress at the final increment, including plasticity. Both (a) and (b) plot contours on the deformed specimen shape, while the dashed pink line indicates the original, undeformed shape. (c) presents the stress states along the specimen in the first increment, before plasticity, while (d) maps the stress states along the specimen in the last increment, already in the plastic regime.

Regarding the transition between optimization results and the final geometry, at least two approaches are possible: (i) shape optimization or (ii) manual redesign. However, neither of referred approaches are trivial. On the one hand, the shape optimization is complex as demonstrated in previous works [21–23]. On the other hand, manual redesign based on empirical knowledge, is labor intensive. However, in this work, manual redesign was used, since the shape optimization methodology was considered out of scope. During the manual redesign, some small changes were introduced in order to expand the elastoplastic regime with a cost of performance indicator (0.0275 to 0.019) as described in the Fig. 10(a).

The referred sub-figure describes the proposed redesigned specimen in terms of stress states (tension, shear, and compression) and the overlapped pink line indicates the initial design (Fig. 6 [1.0;0.42]). The gripping areas (marked in black) are not considered in the performance indicator calculation and its low value is related to the high stress amplitude and low presence of the shear stress state within the specimens. In Fig. 10(b), a reference design proposed by Jones et al. [43] is pre-

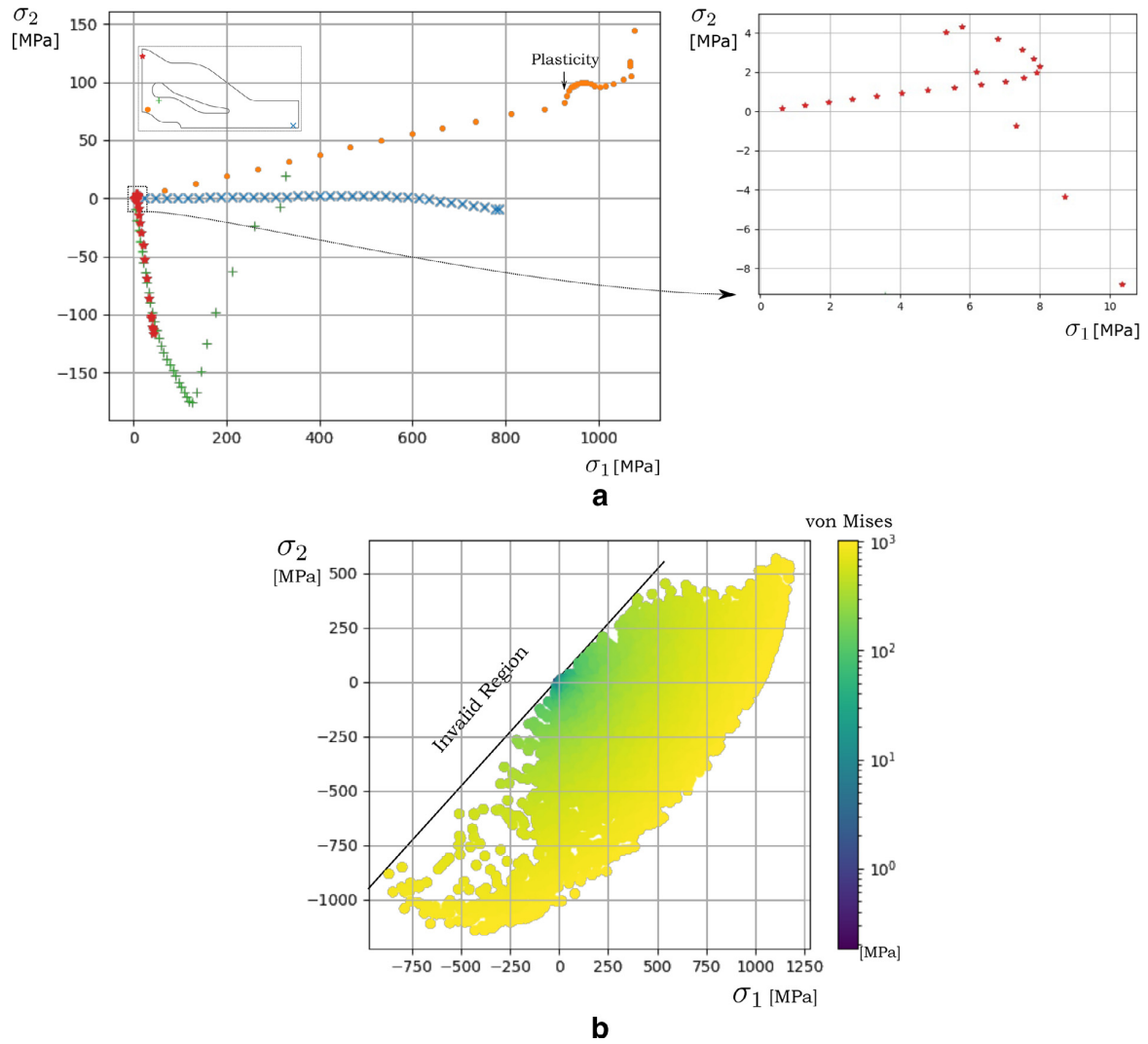

Fig. 12. (a) stress paths of some elements with high non-linearity and (b) von Mises stress representation (color bar) in the principal plane.

sented for comparison purposes, having a lower performance indicator when compared with the proposed solution. As a validation step, the proposed specimen is also analyzed with FEA program [44], using a 3D shell formulation in a classic elastoplastic analysis (von Mises criteria is also used). An elastoplastic material model of the Ti6Al4V titanium alloy was used, being available in [45] with the strain rate of 0.1 mm/s. Moreover, a minimum thickness of 4 mm was determined in order to avoid buckling before plastic rupture. Additionally, the total length of the proposed specimen is 290 mm. The main results as described in Fig. 11.

The Fig. 11(a) and (b) indicate the equivalent strain and von Mises stress maps at the final increment in the elastoplastic analysis. The deformed shapes, overlapped in Fig. 11(a) and (b), are shown in true scale, thus, the reader can visualize the levels of displacements occurring when the specimen is subjected to 81.6 kN. Fig. 11(c) describes the stress states across the specimen at the initial increment (without plasticity), while the Fig. 11(d) describes the stress states across the specimen at the final increment (with plasticity). Ideally, the stress state maps of Figs. 10(a) and 11(c) would be similar, but some differences are also visible due to plane stress approximation. It is worth noting that the optimization procedure used a 2D plane stress formulation while the final validation used a 3D shell formulation. Nevertheless, the plane stress approach allows a quick and straightforward optimization algorithm.

Comparing the design of Fig. 11(c) and (d), stress states maps without and with plasticity do not change significantly, meaning the initial purpose of heterogeneous stress states is not significantly deteriorated when the specimen enters the non-linear regime. In fact, the majority of the elements follows a linear strain path. However, there are a few elements that change stress state during the elongation process and consequently their path becomes non-linear. Moreover, elements that undergo large plastic strain also suffer changes in the path.

Examples for all the previous observations are described in Fig. 12(a). The element marked with green symbol + starts in compression states and, at some point in the elongation process, the element progressively changes its stress state to tension. In contrast, the element marked with magenta symbol * suffers the opposite process (tension to compression). Additionally, it is worth noting that both elements do not enter in the plastic regime. The element marked with orange symbol · remains in the tension state but suffers high plastic strain (near rupture initiation point), being the cause for the non-linearity in stress path. Finally, the element marked with cyan × is the reference point, suffering neither change in stress state nor plasticity.

The richness of stress states in a heterogeneous specimen is undoubtedly important. However, if the stress or strain distribution along the specimen differs by orders of magnitude, experimental methods used during the specimen's elongation will not be able to capture the large range of strains simultaneously. Thus, the Fig. 12(b) presents the von Mises stress distribution on the principal plane, where all increments were plotted in the referred figure. On the one hand, the von Mises yield surface is not fully filled. One the other hand, the filled regions of the von Mises yield surface are interestingly well within an order of magnitude, being an important indicator that the proposed specimen might be well suited for experimental testing.

The strain levels of the proposed heterogeneous specimen when subjected to tensile loading, is shorter than classic homogeneous test specimens, *i.e.* around 7 mm for the presented Ti6Al4V specimen (about 2.5% of the specimen total length). In contrast, in classical homogeneous testing, 5.5% of total length would be a more representative number. Moreover, the stress state heterogeneity, unfortunately, leads to stress concentrations. Thus, the methodology user is forced to sacrifice some strain range in order to gain richness in terms of stress states. The reader can argue that the strain range is small, but it is a direct consequence of the stress concentrations and, most importantly, the chosen material (Ti6Al4V alloy due to the scope of the funding project). The referred titanium alloy has low hardening capability and the plastic regime is small. Therefore, the areas of proposed specimen that suffers plastic strains, are small.

4. Concluding remarks

A systematic methodology for designing heterogeneous specimens has been presented. The methodology's formulation has its foundations on mechanisms synthesis theory, which was extended and repurposed to design heterogeneous specimens with success. Moreover, the methodology allows a straightforward and simple implementation, which is described in a step-by-step manner. Furthermore, an indicator to estimate their performance was developed and presented. It is able to capture the stress states' richness of the specimen and penalizes solutions with stress concentrations or unstressed material.

Several results are shown and many more can be generated using the presented methodology and given different initial conditions. The proposed design, when subject to a tensile loading, is seen to be capable of providing an interesting diversity of stress states and, therefore, the encouragement to proceed with a mechanical experimental testing campaign for future works.

Declaration of Competing Interest

The authors declare that they have no known competing financial interests or personal relationships that could have appeared to influence the work reported in this paper.

CRediT authorship contribution statement

B. Barroqueiro: Conceptualization, Methodology, Software, Validation, Formal analysis, Investigation, Writing - original draft, Writing - review & editing. **A. Andrade-Campos:** Conceptualization, Methodology, Writing - review & editing, Project administration, Funding acquisition. **João Dias-de-Oliveira:** Methodology, Writing - review & editing. **R.A.F. Valente:** Writing - review & editing.

Acknowledgements

The authors gratefully acknowledge the financial support of the Portuguese Foundation for Science and Technology (FCT) under the projects CENTRO-01-0145-FEDER-029713 by UE/FEDER through the programs CENTRO 2020 and COMPETE 2020, and UID/EMS/00481/2013-FCT under CENTRO-01-0145-FEDER-022083. Financial support of program CENTRO 2020 and UE/FEDER is acknowledged through the project CENTRO-01-0247-FEDER-024039, designated as ADVANSS. The Authors also acknowledge the help of Krister Svanberg for providing Matlab code. B. Barroqueiro also acknowledges the financial support by the FCT through the scholarship SFRH/BD/120779/2016.

References

[1] Lin J, Liu Y, Dean TA. A review on damage mechanisms, models and calibration methods under various deformation conditions. Int J Damage Mech 2005;14(4):299–319.
[2] Aretz H, Hopperstad OS, Lademo OG. Yield function calibration for orthotropic sheet metals based on uniaxial and plane strain tensile tests. J Mater Process Technol 2007;186(1):221–35.
[3] Souto N, Thuillier S, Andrade-Campos A. Design of an indicator to characterize and classify mechanical tests for sheet metals. Int J Mech Sci 2015;101–102:252–71.
[4] DebRoy T, Wei HL, Zuback JS, Mukherjee T, Elmer JW, Milewski JO, et al. Additive manufacturing of metallic components – process, structure and properties. Prog Mater Sci 2018;92:112–224.
[5] Gorelik M. Additive manufacturing in the context of structural integrity. Int J Fatigue 2017;94:168–77.
[6] Lewandowski JJ, Seifi M. Metal additive manufacturing: a review of mechanical properties. Annu Rev Mater Res 2016;46(1):151–86.
[7] Pierron F. Test design for identification from full-field measurements: a concise review. In: Baldi A, Kramer SLB, Pierron F, Considine J, Bossuyt S, Hoefnagels J, editors. Residual stress, thermomechanics & infrared imaging and inverse problems, volume 6. Springer International Publishing; 2020. p. 105–10.
[8] Hild F, Roux S. Comparison of local and global approaches to digital image correlation. Exp Mech 2012;52(9):1503–19.
[9] Pierré J-E, Passieux J-C, Périé JN. Finite element stereo digital image correlation: Framework and mechanical regularization. Exp Mech 2017;57(3):443–56.
[10] Chemisky Y, Meraghni F, Bourgeois N, Cornell S, Echchorfi R, Patoor E. Analysis of the deformation paths and thermomechanical parameter identification of a shape memory alloy using digital image correlation over heterogeneous tests. Int J Mech Sci 2015;96–97:13–24.
[11] Wang Y, Lava P, Coppieters S, De Strycker M, Houtte PV, Debruyne D. Investigation of the uncertainty of DIC under heterogeneous strain states with numerical tests. Strain 2012;48(6):453–62.
[12] Teughels A, Roeck GD. Damage detection and parameter identification by finite element model updating. Revue Européenne de Génie Civil 2005;9(1-2):109–58.
[13] Wu J, Li Q. Structural parameter identification and damage detection for a steel structure using a two-stage finite element model updating method. J Constr Steel Res 2006;62(3):231–9.
[14] Martins J, Andrade-Campos A, Thuillier S. Calibration of anisotropic plasticity models using a biaxial test and the virtual fields method. Int J Solids Struct 2019;172–173:21–37.
[15] Lattanzi A, Barlat F, Pierron F, Marek A, Rossi M. Inverse identification strategies for the characterization of transformation-based anisotropic plasticity models with the non-linear vfm. Int J Mech Sci 2020;173:105422.
[16] Kim J-H, Barlat F, Pierron F, Lee MG. Determination of anisotropic plastic constitutive parameters using the virtual fields method. Exp Mech 2014;54.
[17] Rahmani B, Ghossein E, Villemure I, Levesque M. In-situ mechanical properties identification of 3d particulate composites using the virtual fields method. Int J Solids Struct 2014;51(18):3076–86.
[18] Avril S, Bonnet M, Bretelle A-S, Grédiac M, Hild F, Ienny P, et al. Overview of identification methods of mechanical parameters based on full-field measurements. Exp Mech 2008;48(4):381.
[19] Martins J, Andrade-Campos A, Thuillier S. Calibration of anisotropic plasticity models using a biaxial test and the virtual fields method. Int J Solids Struct 2019;172–173:21–37.
[20] Jones E, Carroll J, Karlson K, Kramer S, Lehoucq R, Reu P, et al. Parameter covariance and non-uniqueness in material model calibration using the virtual fields method. Comput Mater Sci 2018;152:268–90.
[21] Aquino J, Andrade-Campos AG, Martins JMP, Thuillier S. Design of heterogeneous mechanical tests: numerical methodology and experimental validation. Strain 2019;55(4). E12313
[22] Souto N, Andrade-Campos A, Thuillier S. Mechanical design of a heterogeneous test for material parameters identification. Int J Mater Form 2017;10(3):353–67.
[23] Souto N, Andrade-Campos A, Thuillier S. A numerical methodology to design heterogeneous mechanical tests. Int J Mech Sci 2016;107:264–76.
[24] Almeida F, Barroqueiro B, Oliveira JD-d, Andrade-Campos A. On the development of a heterogeneous mechanical test specimen using topology optimization. Procedia Manufacturing 2020;47:816–23. 23rd International Conference on Material Forming.
[25] Belhabib S, Haddadi H, Gaspérini M, Vacher P. Heterogeneous tensile test on elastoplastic metallic sheets: comparison between FEM simulations and full-field strain measurements. Int J Mech Sci 2008;50(1):14–21.
[26] Prates P, Oliveira M, Fernandes J. A new strategy for the simultaneous identification of constitutive laws parameters of metal sheets using a single test. Comput Mater Sci 2014;85:102–20.
[27] Haddadi H, Belhabib S. Improving the characterization of a hardening law using digital image correlation over an enhanced heterogeneous tensile test. Int J Mech Sci 2012;62(1):47–56.

[28] Rossi M, Badaloni M, Lava P, Debruyne D, Pierron F. A procedure for specimen optimization applied to material testing in plasticity with the virtual fields method. In: AIP Conference proceedings, 1769; 2016. p. 200016.
[29] Pottier T, Vacher P, Toussaint F, Louche H, Coudert T. Out-of-plane testing procedure for inverse identification purpose: application in sheet metal plasticity. Exp Mech 2012;52(7):951–63.
[30] Zhang S, Léotoing L, Guines D, Thuillier S. Potential of the cross biaxial test for anisotropy characterization based on heterogeneous strain field. Exp Mech 2015;55(5):817–35.
[31] Pierron F. Test design for identification from full-field measurements: a concise review. In: Conference proceedings of the society for experimental mechanics series; 2019.
[32] Bendsøe MP, Sigmund OO. Topology optimization: theory, methods, and applications. Springer; 2004.
[33] Bendsøe MP. Optimal shape design as a material distribution problem. Struct Optim 1989;1(4):193–202.
[34] Bruns TE, Tortorelli DA. Topology optimization of non-linear elastic structures and compliant mechanisms. Comput Methods Appl MechEng 2001;190(26):3443–59.
[35] Bourdin B. Filters in topology optimization. Int J Numer MethodsEng 2001;50(9):2143–58.
[36] Svanberg K, Svärd H. Density filters for topology optimization based on the pythagorean means. Struct Multidiscip Optim 2013;48(11).
[37] Wang F, Lazarov BS, Sigmund O. On projection methods, convergence and robust formulations in topology optimization. Struct Multidiscip Optim 2011;43(6):767–84.
[38] Langelaar M. An additive manufacturing filter for topology optimization of print-ready designs. Struct Multidiscip Optim 2017:871–83.
[39] Andreassen E, Clausen A, Schevenels M, Lazarov BS, Sigmund O. Efficient topology optimization in matlab using 88 lines of code. Struct Multidiscip Optim 2011;43(1):1–16.
[40] Sigmund O. A 99 line topology optimization code written in matlab. Struct Multidiscip Optim 2001;21(2):120–7.
[41] Svanberg K. The method of moving asymptotes–a new method for structural optimization. Int J Numer MethodsEng 1987;24(2):359–73.
[42] Barroqueiro B, Andrade-Campos A, Valente RAF. Designing self supported SLM structures via topology optimization. J Manuf Mater Process 2019;3(3).
[43] Jones EMC, Karlson KN, Reu PL. Investigation of assumptions and approximations in the virtual fields method for a viscoplastic material model. Strain 2019;55(4). E12309
[44] MSC software. 2017. MSC Nastran 2017.1: Nonlinear User's Guide SOL 400.
[45] Wojtaszek M, Sleboda TJ, Czulak A, Weber G, Hufenbach WA. Quasi-static and dynamic tensile properties of Ti-6Al-4V alloy. Arch Metall Mater; 2013.

Chapter 4

Designing ALM Structures for the aerospace industry

Designing ALM structures for the space industry is challenging since the tight requirements of the space industry are merged with the limitations of ALM processes. The widespread of ALM processes in the referred industry is limited by the lack of reliability in the structural verification stage. Under a perspective of spacecraft subsystems structural analysis, these structures are usually validated with the following analysis/load types [1, 2]:

- Minimum stiffness (normal modes analysis): the subsystems must have minimum stiffness, meaning that its first mode of resonance must be above a given limit to avoid dynamic coupling with primary structures.
- Static Loads (static analysis): these are generated by constant or slowly changing forces in time such as engine chugging.
- Thermal Loads (static analysis): these are generated by thermal gradients formed in structure and/or mismatch of material's Coefficient of Thermal Expansion (CTE). For instance, a heating stage of an aluminum bracket on a titanium plate can present a relevant stress state, since aluminum undergoes three/four times higher thermal expansion than titanium.
- Low-frequency loads (sine analysis or frequency response analysis): these correspond to "predictable" dynamic excitations in a typical range of 0-100Hz using deterministic models. Fluid slosh in tanks is an example.
- High-frequency random vibration loads (random analysis): these are characterized by their chaotic behavior in a typical range of 20-2000Hz using stochastic models. These are transmitted from the launch vehicle to the payload at the launch vehicle interfaces.
- Shock loads (transient analysis or response spectrum analysis or frequency response analysis [conservative – assumes full amplification during a shock]): these are chaotic loads that are typically concentrated above 500Hz and measured in a range of 100-10000 Hz. Pyrotechnic events are an example of shock loads.

The detailed study of the required methods to analyze each load type is beyond the scope of this work. Instead, the standard practices of the industry were considered, and these rely on commercial FEA programs.

4.1 Engineering cycle and a case study application

AM has the potential to revolutionize the way products are developed. However, the engineering cycle needs to be rethought. Thus, in this section, two industrial articles are presented. The main

goal of the first article is the systematization of AM engineering cycle in its various phases namely: (i) TO, (ii) smoothing and part edition, (iii) structural verification, (iv) process simulation and (iv) manufacturing, where a possible approach for each phase is discussed. Then, the preliminary results of a case study are presented [C1]. The second article presents the final results of the previous case study for all phases [C2].

II International Conference on Simulation for Additive Manufacturing - Sim-AM 2019
F. Auricchio, E. Rank, P. Steinmann, S. Kollmannsberger and S. Morganti (Eds)

DESIGNING ADDITIVELY MANUFACTURED PARTS VIA TOPOLOGY OPTIMIZATION - A SPACE INDUSTRY CASE STUDY

B. Barroqueiro[1,2,*], A. Andrade-Campos[1] and R.A.F. Valente[1]

[1] Department of Mechanical Engineering, Centre for Mechanical Technology & Automation, University of Aveiro, 3810-193 Aveiro, Portugal.

[2] Active Space Technologies, Actividades Aeroespaciais S.A., Parque Industrial de Taveiro, Lote12, 3045-508 Coimbra, Portugal.

[*] Corresponding Author: B. Barroqueiro (bjfb@ua.pt)

Key words: Topology Optimization; Additive Manufacturing; Case Study; Space Industry;

Abstract. Additive Manufacturing (AM) allows unprecedented design freedom, which can be explored by the Topology Optimization (TO) algorithm. Their interplay allows a new engineering cycle with the potential to design and manufacture disruptive concepts. Thus, a systematic methodology for designing AM parts is presented, being the main goal of this study. The methodology is subdivided into several phases, each phase contains several tasks. Moreover, the data flow between phases is considered and solutions are provided. Finally, the methodology is applied to a space case study and preliminary results of the AM engineering cycle (TO, part design and structural analysis) are depicted.

1 INTRODUCTION

"Additive Manufacturing (AM) is a process of joining bulk raw materials to make parts from 3D model data, usually layer upon layer, as opposed to subtractive manufacturing and formative methodologies. It is an inherent part of the parts development or production process. It is used to manufacture prototypes and production parts" [1]. Moreover, this process provides great geometrical freedom and the tools to explore the referred freedom are needed. The search-optimal material layout can be performed by Topology Optimization (TO) and its interplay with AM has proven to be advantageous [2]. In the space industry, there are successful examples, where the interplay of TO and AM allow the reduction of the number of parts, assembling operations, mass and, therefore, cost (*e.g.* [3, 4]). Beyond that, the new technology opens a new dimension of design solutions by overcoming the restrictions of conventional manufacturing processes. The adopted engineering cycle consists in topology optimization (*e.g.* MSC Nastran® tool for an initial design), manual CAD[1] construction (*e.g.* CATIA V5®), structural analysis and production (process preparation and manufacturing). However, manual CAD reconstruction is ineffective. In the one hand, TO commonly produces complex geometries that are labour intensive to reproduce in CAD software. On the other hand, the TO design can be simplified in

[1]Computer Aided Design

order to allow a rapid CAD model construction with a performance cost. Thus, in this work, the presented methodology proposes an alternative methodology to the manual CAD model construction, which allows for a quicker engineering cycle. Moreover, this paper proposes a systematic methodology of a complete engineering cycle for space AM part. Furthermore, a space case study is presented, where the topology optimization, part design and structural analysis are presented and discussed. Finally, the main goal of this article is the methodology systematization for designing AM parts. Therefore, this work can provide valuable guidance for new engineers working in this field.

2 Methodologies

The complete engineering cycle of AM structures involves numerous steps. Figure 1 depicts the whole process of designing structures within framework subsystems structures of the space industry. For the sake of clarity, the process is illustrated as a linear flow, but iterative work between steps is expected to originate a non-linear flow.

2.1 Topology optimization

Topology optimization is a type of structural optimization that seeks the optimum material layout [5]. Within the scope of this work, solver 200 from MSC Software [6] was used to perform the Topology Optimization (TO) analysis, considering compliance minimization with a volume constraint. The referred solver uses the well known Solid Isotropic Material with Penalization (SIMP) method and the process starts with initial domain definition [6, 7]. Within the scope of this work, the domain is meshed using isoparametric `HEX8` elements. The mesher is available on a Patran utility named *Regular Cube Mesher 2*. After application of the boundary conditions, objective, constraint and design/non-design domains definition, the optimization cycle can start. After convergence, the resultant material distribution would ideally be a binary distribution (void or solid material) across the design domain. However, the SIMP model uses a continuous function and some intermediate densities may remain after convergence. These intermediate densities have to become either void (zero) or solid (one) and, thus, the user has to define the threshold. At the end, all solid elements become the optimized topology. Using the referred topology, the skin elements are extracted using the utility named *Skin Solid Elements*. Then, the resultant `QUAD` elements are broken into `TRIA` elements and the surface STL mesh is exported using the export STL utility.

2.2 Smoothing and Part Edition

The smoothing operation can be done within Patran® with limited options. Within the scope of this work, the Netfabb® from Autodesk® is used to perform all the smoothing, remeshing and repair operations [**?**]. The translation between the surface STL mesh to a volume `TET` mesh is not possible in Netfabb neither in Patran. The free software named GMSH [8], is used to make the referred translation, being a straightforward procedure[2]. A Nastran input file is a GMSH output, which can be imported in Patran.

[2]GMSH list of instructions: File>Merge>*.STL; Geometry>Add>Volume; Mesh>3D; File>Export>*.bdf

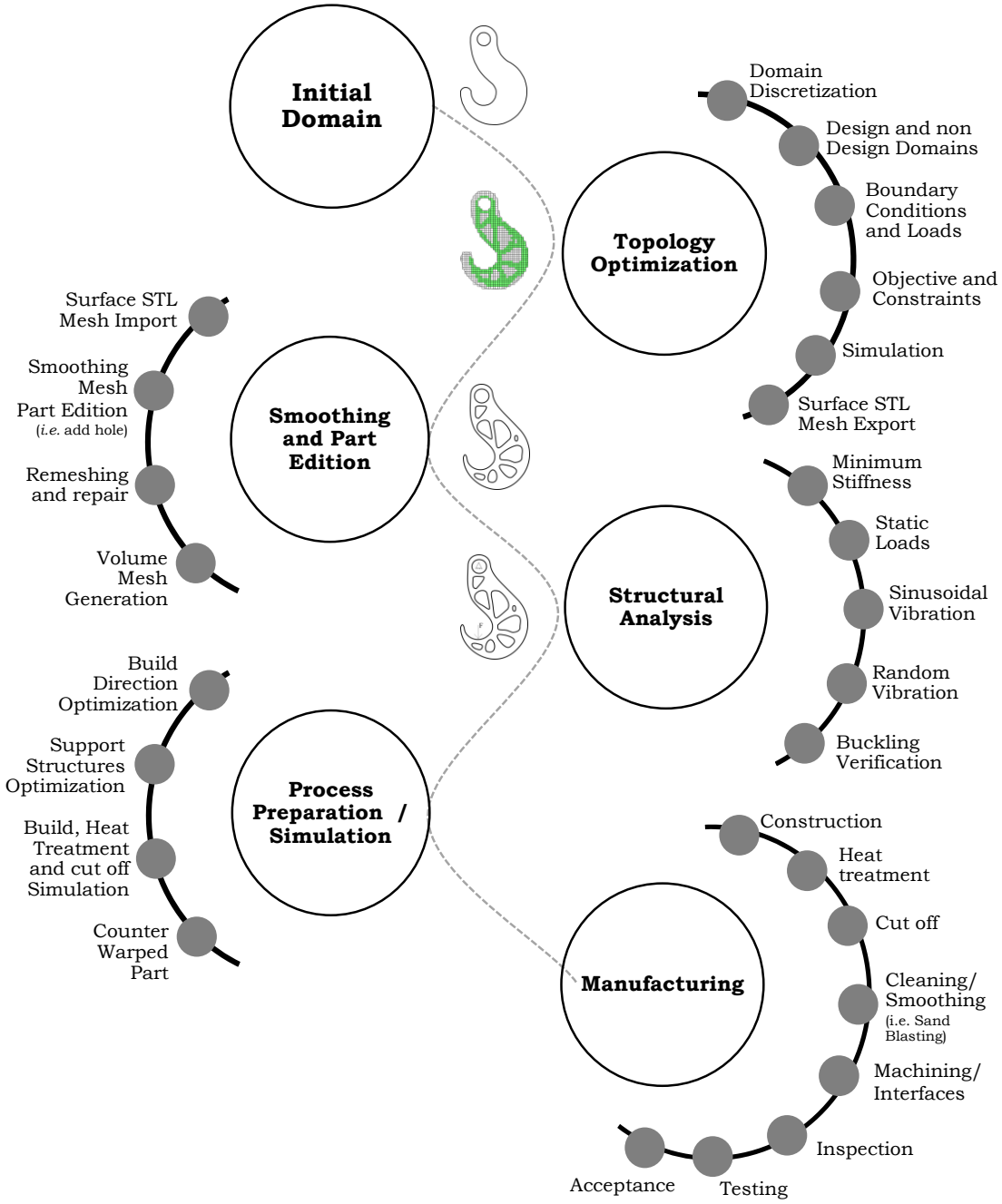

Figure 1: Engineering cycle of AM structures for the space industry.

2.3 Structural Analysis

In the space industry, the structural analysis involves at least static loads, minimum stiffness and sinusoidal/random vibration loads. Due to the typical slenderness of the designs, buckling verification is also performed. The static loads are analysed with MSC Nastran solver 101 using inertial loads [9]. The minimum stiffness requirement is verified using the MSC Nastran

solver 103 (normal modes analysis) [10], where the first eigenvalue should be above a defined limit. The sinusoidal vibration analysis is verified using the MSC Nastran modal solver 111 (Lanczos solver: frequency response) [10], considering modal damping. The random vibration is a two-step analysis. First, the frequency response analysis is performed for sinusoidal loading conditions at a sequence of frequencies. Typically, these loads are chosen to be unit loads. Thus, the output response works as a transfer function. The second step uses the referred function in order to compute the amplified random response. A quality factor of 400, a 3σ analysis and a log-log integration are considered. Additionally, the load levels are quantified in terms of Power Spectral Densities (G^2/Hz) [10]. Finally, the buckling verification is performed with MSC Nastran solver 105 using equivalent inertial loads derived the most severe load case [9].

2.4 Process Preparation and Simulation

The process preparation can be performed with some software such as Netfabb® [**?**]. The first step is the optimization of the build direction, where several orientations are considered and classified in terms of different criteria (*e.g.* ratio between area and volume of support structures and/or height and volume of the build). The second step is the support structures generation, which can be generated by different available algorithms. Finally, the simulation of the build layer by layer can be also simulated in order to predict residual stress, distortions and some defects such as support structures failure or recoater interference or hot/cold spots. For instance, the Simulation Utility for Netfabb can be allegedly used to make such predictions [11]. Moreover, the software also performs the stress relief (viscoplastic analysis) and part response to the cut-off from the base. This integrated procedure allows the prediction of the part total distortion and excessive distortion on the part may lead to failure of dimensional tolerances. Thus, the process simulation can be used to apply a negative distortion on the part in order to minimize distortions and overbuild.

2.5 Manufacturing

The manufacturing stage shall start with the slicing operation of the prepared part and the G-Code generation, which can be performed in Netfabb, for example. After construction, the part shall be stress relieved, in order to decrease residual stress. Then, the part can be cut off from the baseplate and the cleaning/smoothing process (*e.g.* sandblasting) can be performed. The interfaces with tight tolerances are typically machined. Regarding quality control, the non-destructive inspection campaign can take advantage of methods such as computed tomography, eddy current testing, infrared thermography, neutron diffraction and ultrasonic testing [12]. Finally, the testing campaign involves static, sinusoidal and random testing, where the structure shall survive without deterioration. The deterioration detection can be performed with a low-intensity sinusoidal vibration sweep before and after each vibration test. If the response curve of the low-intensity sine sweeps (before and after each vibration test) are identical, no major structural deterioration will occur. The success criteria can be defined by a maximum shift of 5% and 20% for frequency and amplitude, respectively [13].

3 Case Study

The structure responsible for supporting the lens for a space instrument is analysed, named as Large Lens Mount (LLM). Titanium alloy (TI6Al4V) shall be its manufacturing material and I/F to its supporting structure is composed of six bolted connections. This use case was derived from a use case of OHB Sytems at Oberpfaffenhofen.

3.1 Topology Optimization and Smoothing

The design domain was discretised with linear isoparametric `HEX8` elements and the transition between the solid elements and the bolted connection centre point is modelled with rigid connection (RBE2). The connection between the lens (reduced to a point element) and the solid elements are modelled with RBE3, where the master nodes of volume mesh connects to a slave node on the len's CoG location (see Sub-figure 2(a)). The RBE2 element was not used, because it adds stiffness to the model. In fact, the interface region of the lens would become rigid and the TO algorithm would take advantage of the referred fact, leaving the interface poorly reinforced or the user would add to include it in the non-design domain (defeating the propose of the TO algorithm). Regarding loading conditions, the acceleration levels were replaced by an equivalent force on the len's node. Finally, the TO was performed and its objective function consists in the compliance minimization of the LLM structure, when loaded in directions X, Y and Z (weighted sum of three static load cases).

Sub-figures 2(b), 2(d), 2(f) and 2(h) describe the TO results for the volume constraints of 40%, 20%, 10% and 5%, respectively. Sub-figures 2(c), 2(e), 2(g) and 2(i) show the resultant smooth surface mesh after smoothing in Netfabb. Preliminary analysis on the designs of Sub-figures 2(c) and 2(e) revealed a design overestimation for the considered loading conditions. On the other hand, a visual inspection of the design of the Sub-figure 2(i) indicates high level of risk from the manufacturing point of view. For instance, the removal of referred support structures could lead to fracture of the thin members of the referred part. Therefore, the design of the Sub-figure 2(g) was selected and it weights 0.628 kg, which is compliant with the mass requirement. In order to facilitate the previous assessment, the model of the Sub-figures 2(g) and 2(i) were prototyped in PLA for part visualization proposes only. The Figure 3 illustrates the referred prototypes.

3.2 Structural Analysis

The design domain, Sub-figure 2(g), was discretised with isoparametric `TET10` quadratic elements [9] and the transition between the solid elements and the bolted connection center point is modelled with a rigid connection (RBE2). The connection between the lens and the volume mesh is modelled as RBE2 and the lens is modelled as a lumped mass (see Sub-figure 4(a)). In contrast with the TO analysis, the structural analysis uses RBE2, since the lens adds some stiffness and the main goal is a correct distribution of stress maps.

Table 1 lists the first ten eigenvalues of the LLM with its modal effective mass fraction for the translation (`TX`, `TY`, `TZ`) and rotational (`RX`, `RY`, `RZ`) degrees of freedom. . Within the scope of this work, only the first three modes are in excitation range and, thus, only these are

considered in analysis of the LLM. It should be noted the relevant level of coupling between the first three modes, meaning that an excitation in a given axis is likely to activate all modes in excitation range. The sine vibration excitation range (up to 100 Hz with 47 G in plane and 36 G out of plane) are far from the first eigenvalue (1461.9 Hz) and, thus, the sinusoidal vibrational analysis should be approximated to a static analysis since no relevant dynamic amplification is foreseen. The random vibration is likely to activate the first three modes and, thus, their dynamic amplification should be estimated. The direct responses for the X, Y and Z directions are shown in Sub-figures 5(a) and 5(b), considering the lens node as the monitoring point and quality factor of 400. As expected, all three modes appear in the excitation directions and their magnitude is directly related to their modal effective mass fraction.

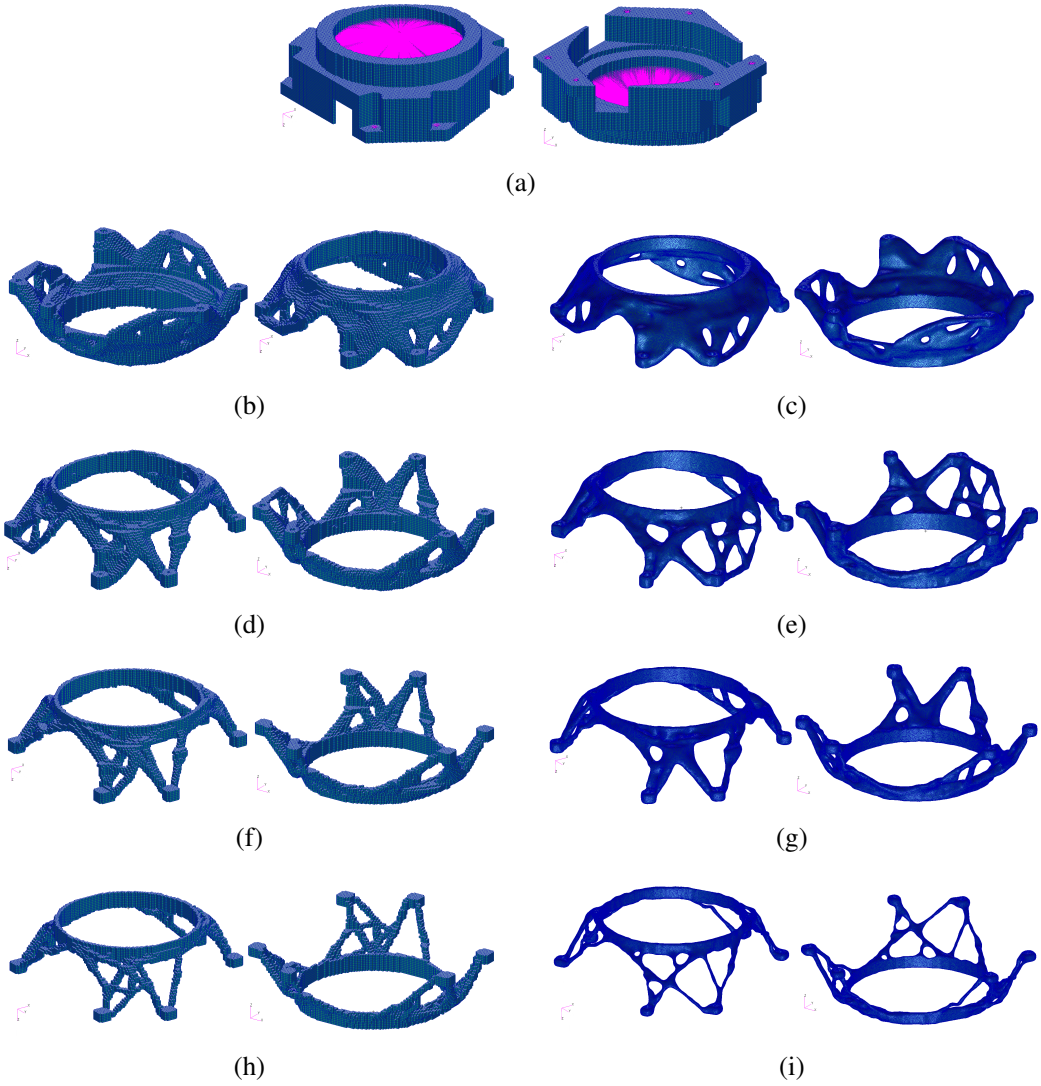

Figure 2: Discretisation of design domain in Sub-figure (a). Sub-figures (b), (d), (f) and (h) are topology optimisation results for 40%, 20%, 10% and 5% of volume fractions, respectively. Sub-figures (c), (e), (g) and (i) depicts the smooth surface meshes of the respective volume fractions.

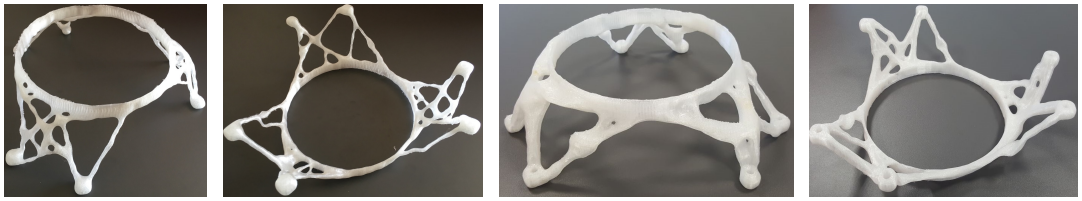

(a) (b) (c) (d)

Figure 3: The LLM physical model printed in a dummy material (PLA). Sub-figures (a) and (b) are the design resultant from 5% of volume constraint, while Sub-figures (c) and (d) are the design resultant from 10% of volume constraint.

Table 1: List of the first ten eigenvalues of the LLM with its modal effective mass fraction for the translation.

Mode	Frequency (Hz)	TX	TY	TZ	RX	RY	RZ
1	1461.9	0.134	0.762	0.034	0.036	0.038	0.615
2	1580.0	0.757	0.152	0.014	0.014	0.009	0.178
3	1913.3	0.039	0.018	0.731	0.640	0.650	0.045
4	3142.8	0.003	0.003	0.018	0.036	0.010	0.001
5	3303.0	0.008	0.005	0.000	0.000	0.013	0.013
6	3447.1	0.000	0.006	0.003	0.000	0.001	0.001
7	3920.5	0.003	0.000	0.006	0.016	0.008	0.000
8	4173.8	0.002	0.001	0.002	0.030	0.000	0.001
9	4401.5	0.000	0.000	0.003	0.001	0.001	0.059
10	4641.9	0.001	0.001	0.039	0.002	0.009	0.008

Sub-figures 4(b), 4(d) and 4(f) depicts modal shapes of the first three eigenvalues values of the LLM. While, Sub-figures 4(c), 4(e) and 4(g) describe the static stress levels (von Mises) from the sinusoidal vibration loads and Sub-figures 4(h), 4(j) and 4(l) depict the Root Mean Square (RMS) of the stress levels (von Mises) from the random vibration loads. Due to the slenderness of the structure, buckling analysis are also presented and its inputs loads were derived from random vibration analysis. Each load case of the random vibration analysis originates a buckling load case, where the indirect and direct responses are used to compute equivalent quasi-static accelerations. The buckling stability factor is presented in Sub-figures 4(i), 4(k) and 4(m).

The minimum stiffness requirement is reached with the first eigenvalue at 1461.9 Hz when compared with 400 Hz requirement. The geometrical stability (buckling) has a relevant positive margin. The stability factor (MSC Nastran result output) should be superior to one, otherwise, the solver is predicting failure. The current design of LLM has a stability factor of 2560.9 ([3]).

Regarding strength margins, the yield stress of the Ti6Al4V should be at least 825 MPa [14] and the maximum stress levels expected from the analysis is 40 MPa, leaving the margin for further optimization (in theory). However, due to manufacturing risk, the compliance minimization with a lower volume fraction constraint (see Sub-figure 2(i)) is not used.

[3]If the factor was dangerously closer to one, a knock-down factor analysis needed to be performed due to analysis uncertainty.

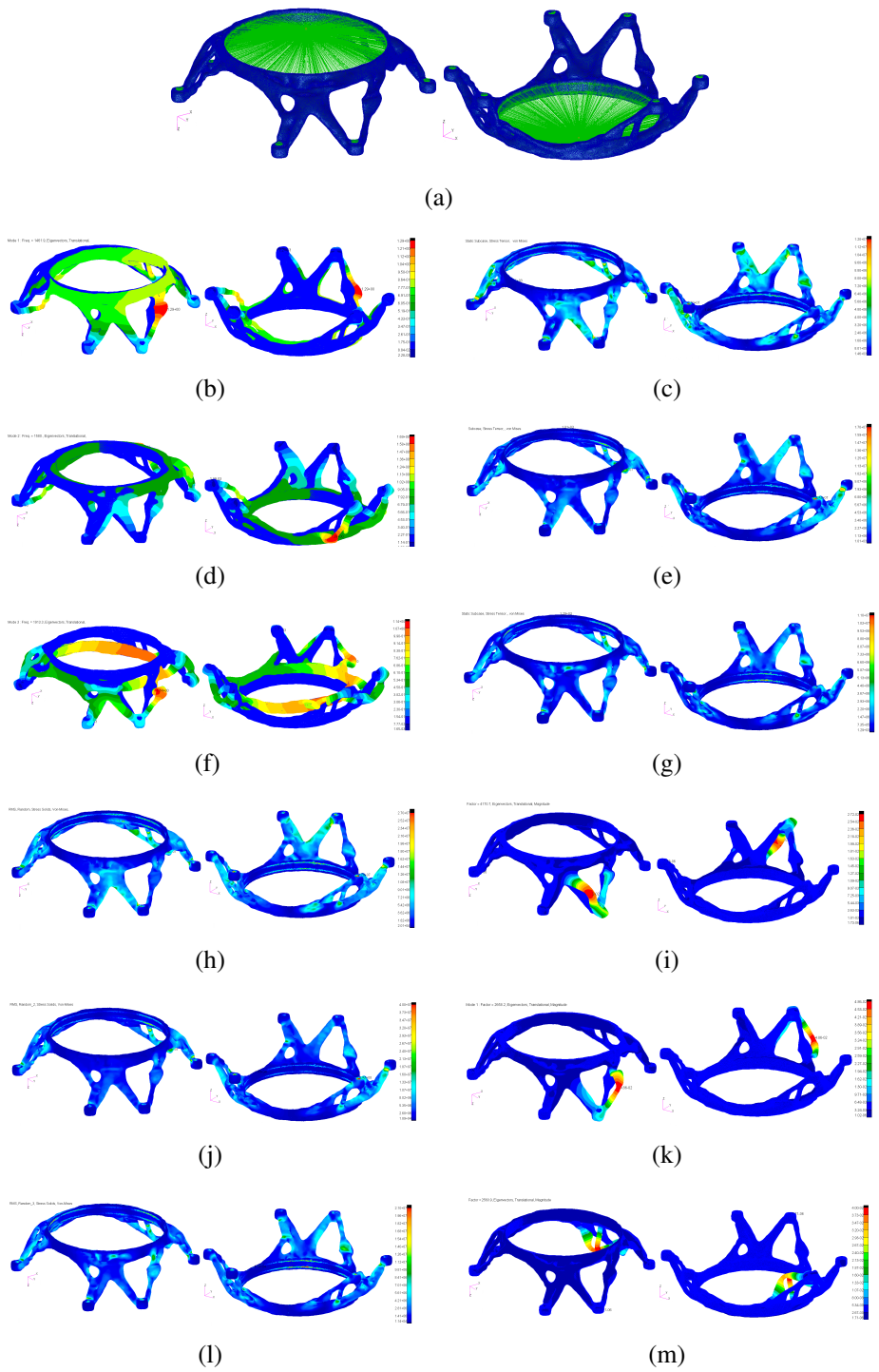

Figure 4: (a) FE modal analysis of the optimized LLM. Sub-figures (b), (d) and (f) are the modal shapes of first three eigenvalues. (c), (e) and (g) are the static von Mises stress maps when loaded in direction X, Y and Z, respectively. Sub-figures (h), (j) and (l) are the von Mises RMS values of the random vibration when exited in X, Y and Z directions, respectively. Sub-figures (i), (k) and (m) are the first buckling mode when loaded in directions X, Y and Z, respectively. All stress maps are in Pa.

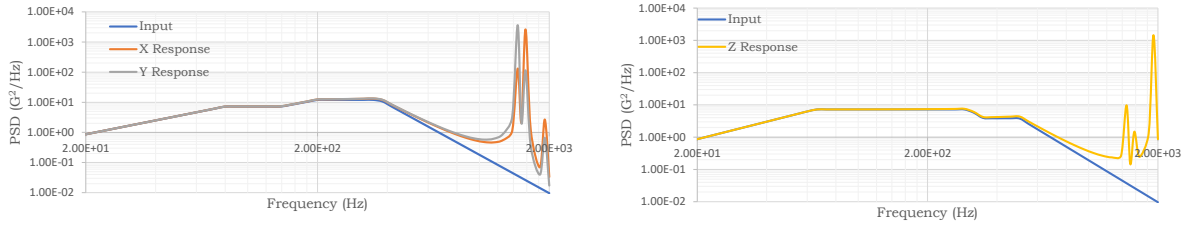

(a) (b)

Figure 5: Random vibration responses. Sub-figures (a) and (b) are the in plane response and out of plane response, respectively.

4 Concluding remarks

A systematic methodology for designing AM parts is conceptually presented in a step-by-step manner. Issues of communication between different softwares were considered and a solution was provided. Finally, the presented methodology is applied to a case study and some encouraging preliminary results of the topology optimization, part design (smoothing and part edition) and structural analysis stages are shown. The resultant design, compliant with the mass constraint, shows good behaviour in terms of stress and stiffness considering structural requirements only.

5 Future Work

In the short term, the engineering cycle of the LLM needs to be concluded. At this point, the engineering cycle of LLM considered structural requirements only. However, the work environment of an optomechanical part requires additional load cases and requirements. For instance, mechanical loading due to I/F tolerances and thermo-elastic loading due to the mismatch of thermal expansion coefficients. Finally, the process preparation and manufacturing campaign stages need to be also concluded. Moreover, the presented methodology is still in development and some key aspects are still missing. For instance, Ti6Al4V constitutive data (anisotropy, porosity and strength data) is missing, which shall be obtained from the ongoing experimental testing campaign. Additionally, fatigue testing campaign will be also performed in order to evaluate the probability of failure during launch. Finally, AM manufacturing constraints need to be added to the TO algorithm, namely the overhang constraints.

Acknowledgements

The authors gratefully acknowledge the financial support of the Portuguese Foundation for Science and Technology (FCT) under the projects CENTRO-01-0145-FEDER-029713 by UE/FEDER through the programs CENTRO 2020 and COMPETE 2020, and UID/EMS/ 00481/2013-FCT under CENTRO-01-0145-FEDER-022083. Financial support of program CENTRO 2020 and UE/FEDER is acknowledged through the project CENTRO-01-0247-FEDER-024039, designated as ADVANSS. B. Barroqueiro also acknowledges the financial support by the FCT through the scholarship SFRH/BD/120779/2016. The authors also acknowledge all the technical recommendations and revision cycles from OHB Systems at Oberpfaffenhofen.

References

[1] ISO International Standard. Additive manufacturing General principles Part 3: Main characteristics and corresponding test methods, 2014.

[2] Anders Clausen. *Topology Optimization for Additive Manufacturing*. PhD thesis, DTU Mechanical Engineering, Technical University of Denmark, 2016.

[3] Sebastian Kébreau, Dr. Patricia Cambrésy, André Dröse, Vincent Gröne, Kai Schimanski, and Freerk Syassen. Maturation of additive manufacturing for implementation into ariane secondary structures: Overview and status of "alm iscar". In *14th European Conference on Spacecraft Structures, Materials And Environmental Testing*.

[4] Gilles Pommatau, Florence Montredon, Antoine Carlino, Marion Salvi, Emmanuel Kot, Florence Clement, and Stephane Abed. Engineering design cycle for an additive layer manufactured secondary structure, from concept to final validation. In *Thales Alenia Space Comunication*.

[5] Aremu A, Ashcroft I, Hague R, Wildman R, and Tuck C. Suitability of SIMP and BESO Topology Optimization Algorithms for Additive Manufacture. *Wolfson School of Mechanical and Manufacuring Engineering*, 2010.

[6] MSC Software. MSC Nastran 2017.1: Design Sensitivity and Optimization User Guide, .

[7] M. P. Bendsøe. Optimal shape design as a material distribution problem. *Structural Optimization*, 1(4):193–202, dec 1989.

[8] C. Geuzaine and J.-F. Remacle. Gmsh: a three-dimensional finite element mesh generator with built-in pre- and post-processing facilities. *International Journal for Numerical Methods in Engineering*, 79(11):1309–1331, 2009.

[9] MSC Software. MSC Nastran 2017.1: Linear Static Analysis User Guide, .

[10] MSC Software. MSC Nastran 2017.1: Dynamic Analysis User Guide, .

[11] Michael Gouge and Pan Michaleris, editors. *Thermo-Mechanical Modeling of Additive Manufacturing*. Elsevier, 2018.

[12] ASTM International, West Conshohocken. ASTM WK47031: New Guide for Nondestructive Testing of Additive Manufactured Metal Parts Used in Aerospace Applications, 2014.

[13] ECSS E ST 10 03C. Space engineering: Testing, 2012.

[14] ASTM International, West Conshohocken. ASTM F3001-14, Standard Specification for Additive Manufacturing Titanium-6 Aluminum-4 Vanadium ELI (Extra Low Interstitial) with Powder Bed Fusion, 2014.

16th European Conference on Spacecraft Structures, Materials and Environmental Testing

Development of ALM Technology for Space Structures. An Opto-mechanical case study.

B. Barroqueiro [1,2], I. Bola [1], A. Santos [1], A. Andrade-Campos[2], R.A.F Valente [2], M. Thiel[3], S. Senese[3], T. Sedlmaier[3], A. Widhammer[3]

[1] Active Space Technologies, Aerospace Activities S.A., Parque Industrial de Taveiro, Portugal.
[2] Department of Mechanical Engineering, Centre for Mechanical Technology & Automation (TEMA), University of Aveiro, 3810-193 Aveiro, Portugal.
[3] OHB System AG, Manfred-Fuchs-Str. 1, D-82234 Weßling, Germany

Theme: Additive layer manufacturing

Keywords: Topology Optimization; Selective Laser Melting; Process Simulation; Structural Dynamics; Manufacturing; Vibrational Testing; Thermal Cycling.

Abstract:

Additive Layer Manufacturing (ALM), in particular Selective Laser Melting (SLM), allows unprecedented design freedom, which can be explored by the Topology Optimization (TO) algorithm. Their interplay allows a new engineering cycle with the potential to design and manufacture disruptive concepts. In this work, the full engineering cycle is presented and briefly discussed, including the following stages: (i) Topology Optimization, (ii) part edition (non-trivial transition between TO and smooth design), (iii) structural analysis (*e.g.* stiffness, static and vibrational), (iv) process simulation (*e.g.* designing support structures), (v) manufacturing (*e.g.* part construction, machining interfaces…) and (vi) testing (vibrational and thermal cycling). Furthermore, the referred engineering cycle is applied to an opto--mechanical case study, where the challenging opto-mechanical functional requirements are merged with ALM technology limitations. The resultant set requirements pose an interesting case study, being the main topic of this study. Some results of this case study are presented and some strategies to tackle some hard-won requirements are discussed.

Introduction

The metal Additive Layer Manufacturing (ALM) market has been growing at double-digit rates in the past few years. The industry increasing interest in the ALM technology is characterized by its higher level of maturity shifting from earlier prototypes to final high-quality functional structures [1]. In particular, the Aerospace industry has shown great interest in the ALM technology and ALM has proven to be advantageous in several cases due to higher geometrical freedom, greater waste reduction, and superior functionality integration [2]. The unprecedented design freedom can also pose a threat to itself since any structure needs to be designed and optimized for ALM in order to be economically competitive. Thus, the current engineering cycle needs to be rethought in order to take full advantage of the referred technology. In the scope of this work, a possible engineering cycle is conceptually introduced [3] and each stage is briefly discussed. Additionally, the presented methodology is applied to an opto-mechanical case study, where the functional requirements are merged with ALM technology limitations, resulting in a challenging optimization problem. Finally, the main results obtained from the referred optimization procedure are presented and briefly discussed.

16th European Conference on Spacecraft Structures, Materials and Environmental Testing

ALM Engineering Cycle for Space Industry

The ALM engineering cycle is briefly described in Figure 1. It involves many stages such as (i) Topology Optimization, (ii) smoothing and part edition (transition between TO and smooth design), (iii) structural analysis (*e.g.* stiffness, static and vibrational), (iv) process simulation (*e.g.* designing support structures), (v) manufacturing (*e.g.* part construction, machining interfaces…) and (vi) testing (vibrational and thermal cycling).

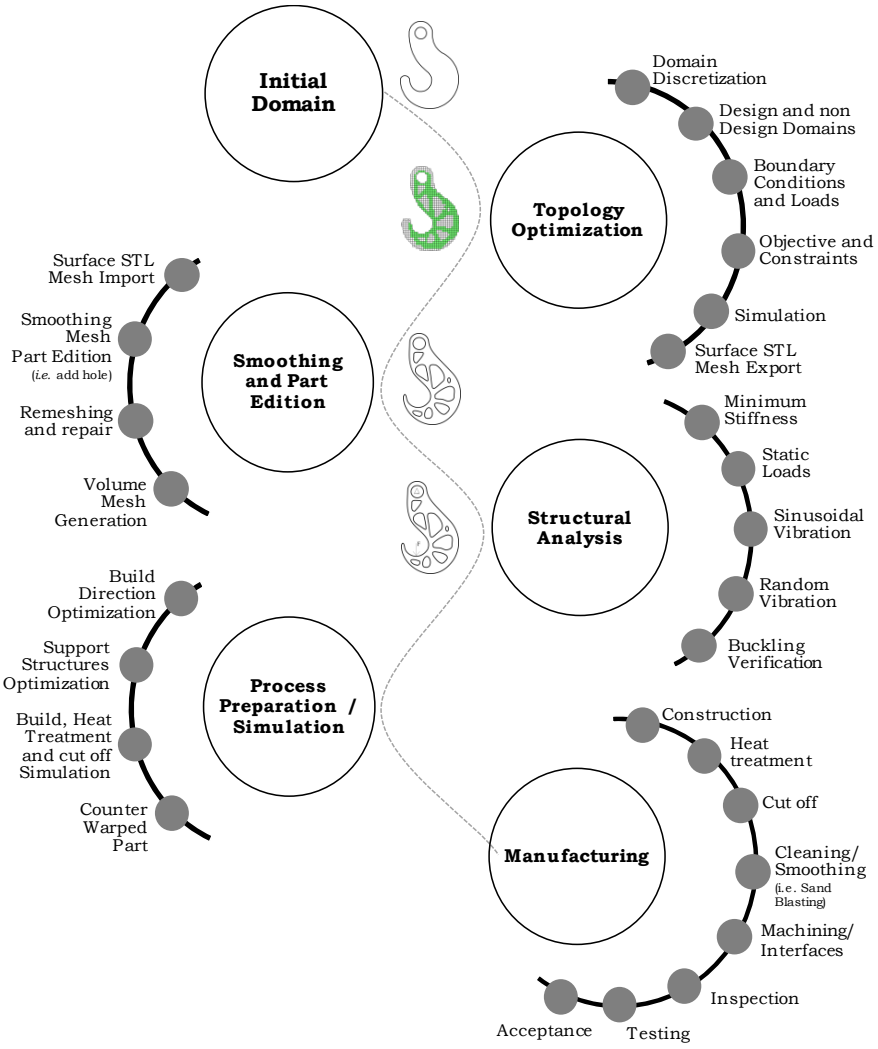

Figure 1: Main stages of the ALM engineering cycle [3].

In the scope of this work, TO optimizations were performed using commercial codes (MSC Nastran® and/or Ansys®) in order to generate solid initial designs, which resulted from different modeling hypothesis. On the one hand, TO can provide efficient mass distributions across the design domain. On the other hand, the transition between TO and a final smooth geometry raises some issues. The referred transition can either be labor intensive with high control over the final geometry (manual reconstruction on existing CAD platforms *e.g.* CATIA®) or reduced labor with poor control of the final geometry (Laplacian smoothing such as the used in Netfabb®). In the scope of structural verification,

structures for space applications should withstand to some loading environments such as static loads and/or vibration, which are verified using a commercial FEA program (*e.g.* MSC Nastran®). Regarding process preparation and simulation, there is the need to increase the chance of success of every build in order to reduce tryouts and, therefore, costs. Thus, computer simulation may provide some insight into the problems that can arise during fabrication. In the scope of this work, Simufact® is used to optimize the build direction and predict the final part distortion. These distortions are predicted using the Inherent Strain (IS) method in a macroscopic part scale simulation using a precomputed inherent strain vector available at the software database considering the machine model, Selective Laser Melting (SLM) process and Ti6Al4V alloy. The IS method allows a quick simulation of the layer by layer part fabrication but lacks accuracy. In contrast, the inclusion of the mesoscale (hatch pattern simulation) and microscale (melting pool dynamics) could increase the accuracy of the results, but the computational costs may become prohibitive for some applications [4], [5]. Concerning the part fabrication and its heat treatment, these phases are subcontracted and consequent phases such as machining, inspection, and testing are once again performed in house. The apparent simplicity of these last phases is betrayed by the typical slenderness of these structures, being discussed later in greater detail.

Opto-mechanical Case study

OHB performed a complete review of in-house past space projects, with a focus on structural and opto--mechanical assemblies, in order to establish case studies that might be able to largely explore the high design freedom provided by Additive Layer Manufacturing (ALM). One of the OHB established case studies is named Large Lens Mount (LLM) assembly, which is studied in the scope of this work. Its development was performed within the ADVANSS project, which intends to improve the AST's internal capabilities in metallic ALM of specialized components for space applications over two main areas: secondary and tertiary structures [6]. The Large Lens Mount (LLM) Assembly is a subassembly within a 4-Lens System, developed for the EUCLID mission. Within ADVANSS, the LLM assembly is redesigned considering the ALM engineering cycle [6]. The LLM redesign process involves several topology optimizations considering different modeling approaches and/or software. In the TO stage, the lens of LLM is reduced to a point and equivalent forces are applied instead of its mass and quasi-static accelerations levels. The zero-displacement condition is applied to the location of bolted joints. The design of Subfigure 1(a) was obtained considering simple symmetry (half of the model) while for Subfigure 1(b) cyclic symmetry (1/3 of the model) was considered. Both simulations took advantage of the commercial FEA code MSC Nastran®. The design of Subfigure 1(c) also considered cyclic symmetry (1/3 of the model) and was obtained using the commercial FEA code Ansys®. Taking into account specific optical requirements associated with isostaticity and simplicity, the design of Subfigure 1(c) was selected and its transition to the final smooth geometry was performed via Laplacian smoothing (see Subfigure 1(a)) and manual reconstruction (see Subfigure 1(b)). The reader might argue that the results showed in Subfigure 3(a) had no use since the structure was manually reconstructed. However, its quick nature allows running preliminary structural analysis to have a first estimate on its viability, including potential volume fraction reductions. The final design requires several additional details, which were incorporated in the design such as (i) lugs (to support the lens dummy), (ii) a plane surface (machining reference), and (iii) measurement bores (facilitates the final dimensional control).

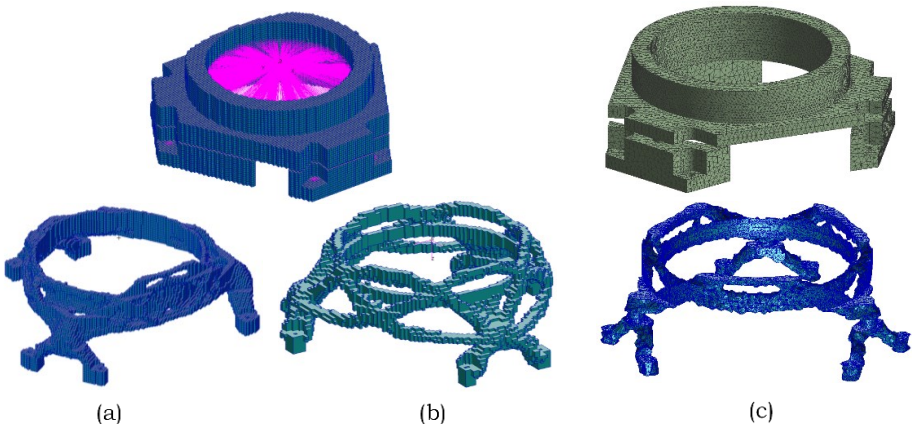

Figure 2: Topology optimization results in a compliance optimization problem considering 20% of final volume fraction. Results in (a) and (b) were obtained using MSC Nastran® while (c) used Ansys®. The upper subfigures describe the design volume, while the lower subfigures describe the TO final results.

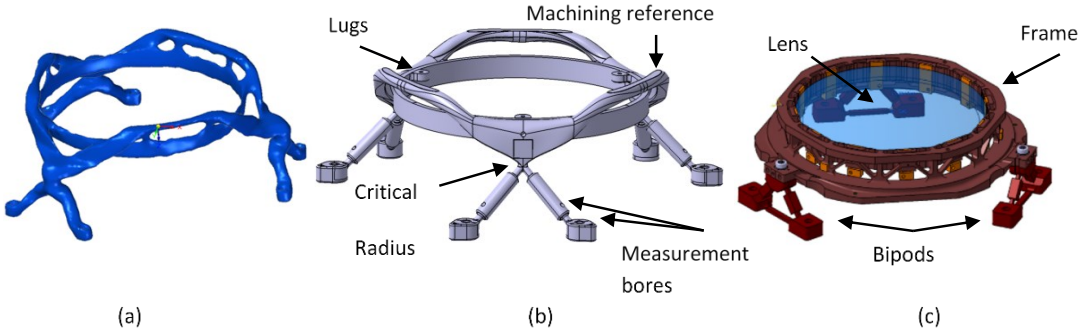

Figure 3: (a) smoothen geometry obtained via Laplacian smoothing, (b) interpretation and manual reconstrued design in CAD platform and (c) conventional design for reference purposes only [6].

In order to increase the knowledge of the part's thermomechanical behavior during the layer by layer fabrication, numerical simulation of the process was performed using Simufact®. Subfigure 4(a) presents the prediction of total displacements at the end of fabrication, considering the four most promising orientations. After fabrication, the stress relief and cut-off from baseplate are also simulated, and, in the end, the final distortion of the part, as well as its residual stresses, are presented in subfigures 4(b) and 4(c), respectively. Regarding Simufact®, several macroscale simulations were performed, including baseplate unclamping, heat treatment and cut off of support structures. The obtained results (summarized in Figure 4) are useful in a qualitative manner since general trends of deformations are captured. The first orientation was considered preferably since it provides low distortion at the interface with the baseplate, which is particularly important for the case study in analysis.

Regarding structural verification, several requirements are considered such as (i) geometric stability (plastic rupture before buckling), (ii) performance, (iii) minimum stiffness and (iv) survivability of the LLM without degradation in several load environments, namely sinusoidal and random vibration, thermoelastic loading and mechanical interfaces mismatch.

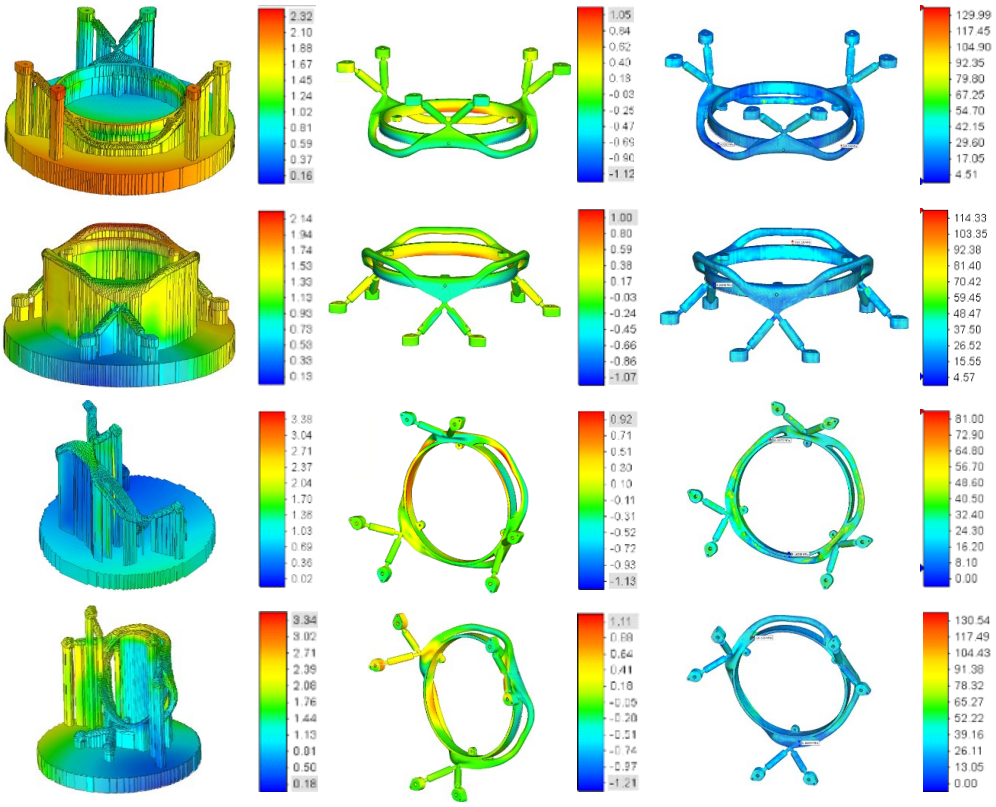

(a) Displacement [mm] (b) Surface Deviation [mm] (c) Equivalent Stress [MPa]

Figure 4: (a) displacement magnitudes after manufacturing, (b) final distortions magnitudes on LLM after manufacturing sequence and (c) its residual stresses in the form of equivalent stresses.

Figure 5(b) describes the Finite Element Model (FEM) used for the structural verification of LLM (see CAD model in Figure 5(a)). Regarding the LLM lens, the real ceramic convex shape was replaced by an approximate shape (dummy) made of Ti6Al4V alloy. The design of the dummy is representative of the real lens in terms of mass, center of gravity, and inertia within a 5% margin of error. It is worth noting that the red part is manufactured with the cutting excess of the blue part (see Figure 5a)). Moreover, it should be highlighted that the LLM lens dummy was manufactured by conventional manufacturing processes since its purpose is to aid the LLM testing. The model uses linear tet4 elements to discretize all parts and the connections are modeled using rigid connections and springs. Finally, all numerical analysis was performed using MSC NASTRAN® 2019.

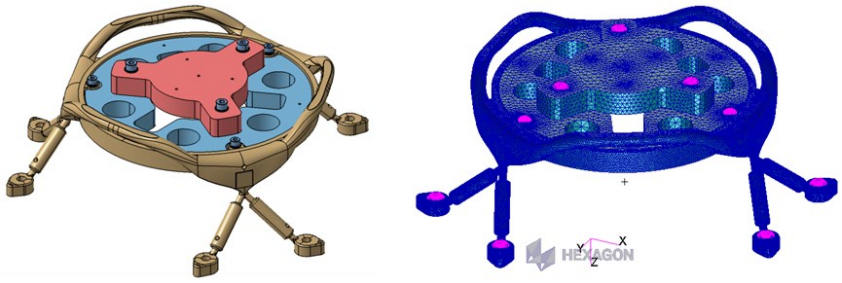

(a) (b)

Figure 5: Overview of (a) CAD design model of LLM and (b) FEM used for the structural verification of LLM.

Regarding geometric stability, a linear buckling analysis was performed using the highest load environment. Figure 6 shows the first buckling and its load factor, being well above one.

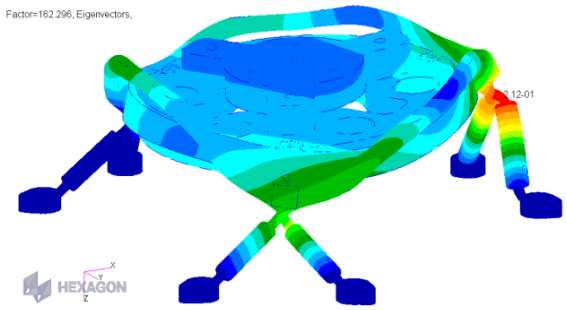

Figure 6: Shape of the first buckling mode of LLM and its load factor of 162.

Regarding the performance requirement, the LLM operates at low temperature, and the thermal deformation (contraction) resultant from the cooling process between the assembling temperature and the operating temperature, can misalign the lens focal point. Thus, the present design, when subjected to the referred cooling process, should not move the lens in the in-plane directions due to its cyclic symmetry. Regarding the volumetric contraction in the out of the plane direction, the used strategy to compensate this deformation is related to the mismatch between the LLM material (Ti6Al4V alloy) and the base plate material (stainless steel duplex 1.4462). The referred steel suffers higher contractions in the cooling process when compared with Ti6Al4V alloy, meaning that the elastic bipods are elastically deformed inwards. The referred inwards displacement generates up awards displacement on the lens and thus compensates for the displacement generated by the volumetric contraction of the cooling process. In theory, the proposed engineering solution should promote small-displacement (less than 20 µm) of the lens when LLM enters its operating temperature. However, some threats might generate higher displacements on the LLM's lens such as non-perfect cyclic symmetry of design (deviations from manufacturing), thermal expansion coefficients of the materials (*i.e.* mean values from the literature were used) and non-symmetric residual stress distributions due to laser patterns.

Regarding minimum stiffness, the requirement recommends the first eigenfrequency above 400 Hz, which is achieved by the current design according to the normal mode's analysis (see Figure 7 for the shape and frequency of the first and second mode).

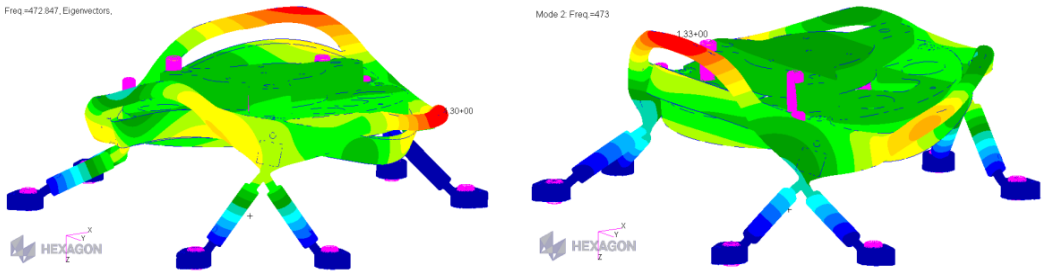

(a) (b)

Figure 7: Shape of the (a) first and (b) second resonance modes of the LLM at a frequency of 473 Hz.

Regarding the numerical analysis of mechanical interfaces mismatch between LLM and its baseplate due to manufacturing accuracy, its analysis is not straightforward. Since there are 6 points at the interface between LLM and its base plate, some of the points can be non-coincident with the interface plane and, when bolted, these may deform towards the referred plane. Within the manufacturing tolerance considered at the interface under analysis, a search for the most severe load case is performed. In the scope of this work, the metric used to quantify the most severe load case was the sum of the forces' magnitudes at the 6 bolted connections. This metric was chosen instead of stresses on the LLM since local stress concentrations with limited relevance could mislead the automatized search. The process modeling approximation consists of finding a set of 6 translations (one for each bolted connection) that generates the highest metric. Initially, the innovative global search algorithm (Endres *et al.* 2018 [7]) was used without success due to the high number of design variables (inverse problem). In the end, the search was performed using the Monte Carlo method using more than 1000 iterations.

Regarding the survivability of the LLM, the most demanding load cases are the quasi-static (47 g's in the in-plane direction and 36 g's in the out of plane applied simultaneously in all axes) and thermoelastic loads (cooling process). In both load cases, the mechanical interfaces mismatch is overlapped in the previous loads employing prescribed displacements at the LLM interfaces with base plate. Figure 8 presents both load cases in terms of equivalent stresses. Comparing the LLM stress state with the minimum strength values imposed by the standard [8], it can be concluded that the threat of LLM failure due to lack of strength is limited from a FEA perspective.

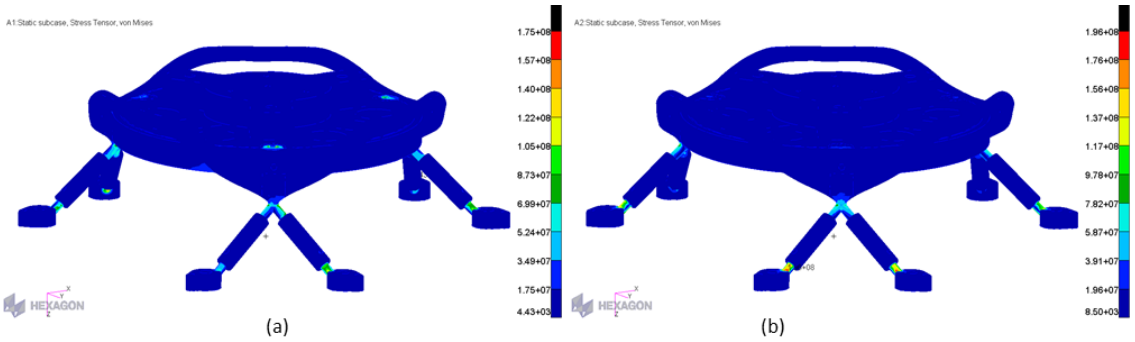

Figure 8: Equivalent stress distribution in the LLM in two load cases: (a) overlap of quasi-static loads with interface mismatch and (b) overlap of thermoelastic loads with interfaces mismatch.

Regarding the process preparation and manufacturing of LLM, these tasks were subcontracted to 2 suppliers. The LLM manufactured by the first supplier was unsuccessful. Due to the build chamber size limitation, the LLM was manufactured using an orientation similar to the third orientation of Figure 4, leading to high distortions on the bipods and non-admissible final part. In contrast, the second supplier was able to manufacture the LLM using the first orientation showed in Figure 4, leading to low distortions on the bipods and an admissible final part. Figure 9 shows the previously described manufacturing orientations. Moreover, as shown in the referred figure, additional samples were manufactured in the same build job of the LLM. The referred samples include a powder container (hollow pyramid with unmelted powder inside for future reference) and specimens for further mechanical testing. Concerning the post-processing of LLM, tasks such as heat treatment, cut off from the base plate, and cleaning, were performed by the supplier. Regarding interfaces' machining of LLM,

it raised some challenges due to the tight tolerances of the project. The tolerances, defined for the interface between LLM and the baseplate, require its machining as well as for the interface between LLM and the lens lugs as described in Figure 10(a). Due to bipods vibration during machining, auxiliary structures were manufactured in order to minimize vibration. The bipods were glued to an auxiliary structure and after machining, the glue was chemically removed. Regarding inspection, the initial LLM dimensional control was successful.

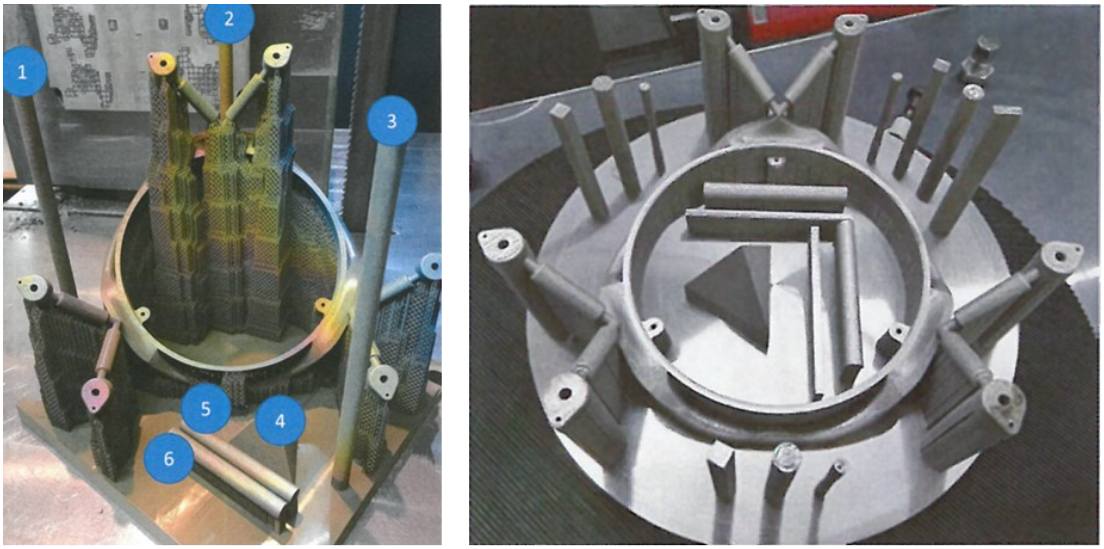

(a) (b)

Figure 9: Overview of suppliers manufacturing orientations: (a) first supplier and (b) second supplier.

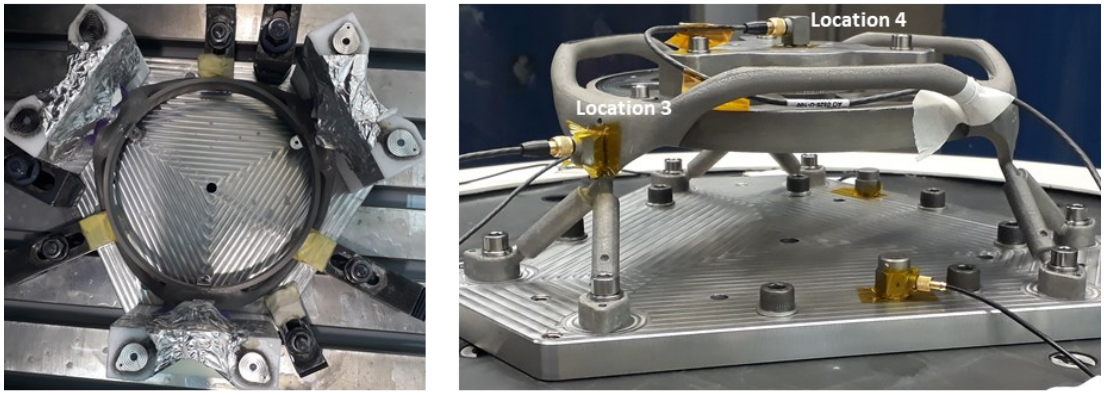

(a) (b)

Figure 10: (a) machining setup with auxiliary structures; (b) vibrational testing setup with accelerometers locations.

Regarding testing, LLM suffered a vibrational testing campaign, namely sinusoidal and random vibration. For instance, Figure 11 illustrates the Direct Responses (DR) of LLM under random vibration for locations 3 (L3) and 4 (L4) in all axis (X, Y, and Z), being denominated with suffix Exp (experimental). Moreover, the random vibration predictions of the FE model of the LLM are also overlapped in the referred figure in order to demonstrate its accuracy, being denominated with suffix Num (numerical).

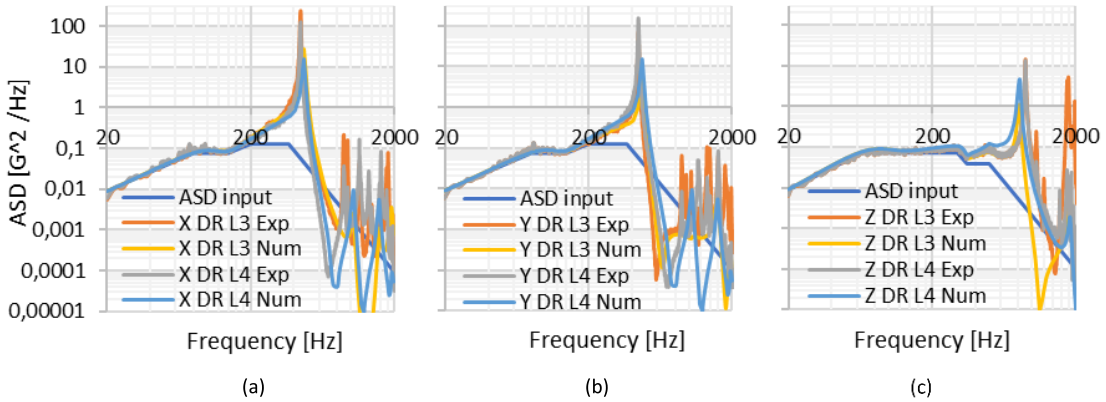

Figure 11: Overview of LLM DR under random vibration for locations 3 (L3) and 4 (L4) in all axis (X - (a); Y - (b); Z - (c)).

Comparing the experimental and numerical eigenfrequencies, the FEA of LLM overpredicts the frequencies in the in-plane directions (X, Y). In contrast, the FEA of LLM underpredicts the frequencies out of the plane direction. Taking as reference the first eigenmode associated with each axis, the error between experimental and numerical results is 5.5%, 6.4% and 11.1% for axis X, Y and Z, respectively. Still concerning Figure 11, the vertical error between the experimental and numerical responses is high due to a poor choice of the model's damping. During the dynamic analysis of the LLM, a quality factor of 10 was used, but a more accurate estimate would be 60.

Before and after each structural test, a low sine sweep is performed. In the case of LLM damage during its testing, the overlap of low sine sweep curves (before and after each test) will show some shift in frequency and/or acceleration. During the vibrational testing campaign of LLM, the sine test in Z direction exhibited a shift in frequency of 2.8% and 4.1 % for the locations 3 and 4, respectively, as described in Figure 12. Regarding the remaining tests, no relevant shift was observed. According to the ESA standard ECSS-E-ST-10-03C [9], the maximum recommended shift in terms of frequency is 5% and/or 20% in accelerations. Thus, the LLM shift in the sine test is acceptable according to the referred standard. However, the authors pursued the shift's origin and it was related to loosening of bolted joints during vibration. In order to address the issue, a small amount of glue was added to the bolt fillets in all the bolted connections and the sine test in Z was repeated. Thus, the shift was no longer observed.

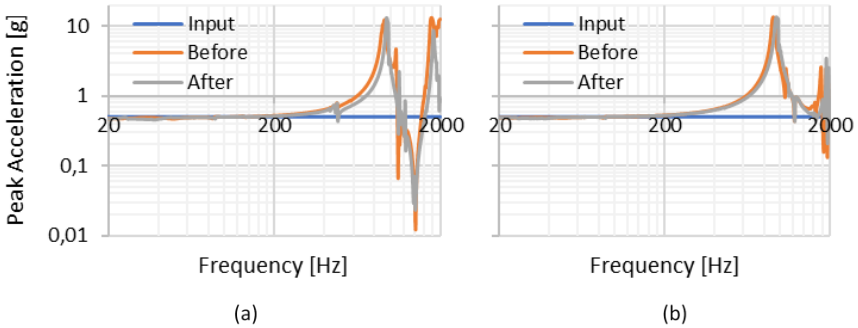

Figure 12: Overlap of the low sine sweep before and after the sine test in the Z direction for location 3 and 4.

Conclusions and Final Remarks

A systematic methodology for designing AM parts is conceptually presented in a step-by-step manner. Furthermore, the ALM engineering cycle is applied to an opto-mechanical case study, where the challenging opto-mechanical functional requirements are merged with ALM technology limitations. The resultant set requirements posed an interesting case study, where many unforeseen issues during the referred cycle had to be addressed. Despite the challenges, some encouraging results are presented for various phases of the ALM engineering cycle. The resultant design is compliant with all tested requirements.

Future work

The LLM's testing campaign is near the end. Currently, the Thermal Vacuum Chamber (TVAC) testing is being performed and its goal is to evaluate the impact of the cooling process (previously described) in the structural performance of LLM.

Contributions

B. Barroqueiro: Conceptualization, Methodology, Validation, Investigation, Writing - original draft, Writing - review & editing. I. Bola: Conceptualization, Methodology, Software, Validation, Formal analysis, Investigation, Writing - review & editing. A. Santos: Conceptualization, Methodology, Validation, Writing - review & editing, Project administration. A. Andrade-Campos: Writing - review & editing, Project administration, Funding acquisition. R.A.F. Valente: Writing - review & editing. M. Thiel: Conceptualization, Methodology, Validation. M. Senese: Validation, Writing - review & editing. T. Sedlmaier: Conceptualization, Methodology, Validation, Writing - review & editing. A. Widhammer: Conceptualization, Methodology, Validation, Writing - review & editing.

Acknowledgments

The authors gratefully acknowledge the financial support of the Portuguese Foundation for Science and Technology (FCT) under the projects CENTRO-01-0145-FEDER-029713 by UE/FEDER through the programs CENTRO 2020 and COMPETE 2020, and UID/EMS/ 00481/2013-FCT under CENTRO-01-0145-FEDER-022083. Financial support of program CENTRO 2020 and UE/FEDER is acknowledged through the project CENTRO-01-0247-FEDER-024039, designated as ADVANSS. B. Barroqueiro also acknowledges the financial support by the FCT through the scholarship SFRH/BD/120779/2016.

References

[1] G. Costabile, M. Fera, F. Fruggiero, A. Lambiase, and D. Pham, "Cost models of additive manufacturing: A literature review," *Int. J. Ind. Eng. Comput.*, pp. 263–283, 2017, doi: 10.5267/j.ijiec.2016.9.001.

[2] L. Nickels, "AM and aerospace: An ideal combination," *Met. Powder Rep.*, vol. 70, no. 6, pp. 300–303, 2015.

[3] B. Barroqueiro, A. Andrade-Campos, and R. A. F. Valente, "Designing additively manufactured parts via topology optimization – a space industry case," *Proc. II Int. Conf. Simul. Addit. Manuf. - Sim-AM*, pp. 1–10, 2019.

[4] M. Bugatti and Q. Semeraro, "Limitations of the inherent strain method in simulating powder bed fusion processes," *Addit. Manuf.*, vol. 23, no. May, pp. 329–346, 2018.

[5] N. Keller and V. Ploshikhin, “New method for fast predictions of residual stress and distortion of AM parts,” in *Mathematical Modelling of Weld Phenomena12*, 2014.

[6] M. Thiel *et al.*, “OHB initiatives in development of additive manufacturing technology for opto-mechanical and mechatronic space systems,” in *Proceedings of the International Astronautical Congress, IAC*, 2018, vol. 2018-Octob, no. October, pp. 1–5.

[7] S. C. Endres, C. Sandrock, and W. W. Focke, “A simplicial homology algorithm for Lipschitz optimisation,” *J. Glob. Optim.*, vol. 72, no. 2, pp. 181–217, 2018.

[8] ASTM F2924-14, “Standard Specification for Additive Manufacturing Titanium-6 Aluminum-4 Vanadium with Powder Bed Fusion,” 2014.

[9] ECSS-E-ST-10-03C, “Space Engineering: Testing.” ESA Requirements and Standards Division, 2012.

4.2 Topology Optimization (TO) with ALM Constraints

The "marriage" between TO and ALM has been seen as an advantageous interconnection, which can be improved if ALM constraints are incorporated in the TO algorithm. Therefore, in this section, an original article, entitled "Designing Self Supported SLM Structures via Topology Optimization", is presented, which studies the design limitations of SLM (as an ALM process) and possible approaches to overcome them. Moreover, the study presents a topology optimization algorithm capable of including the main limitations of SLM namely the minimum member size and the overhang angle limitation [P4]. The goal of this article (and consequently the section) is to provide a robust computational methodology capable of providing initial solid designs, which are validated using different reference geometries (cantilever and MBB), different material penalization models (SIMP or RAMP) and different FEM approximations (plane stress and 3D). Finally, a 3D application is shown using interactive models. However, it is worth noting that the models' interactivity is lost when the original article was embedded in the present document. Alternatively, a copy of these models is provided in Appendix C.

Journal of
Manufacturing and Materials Processing

MDPI

Article

Designing Self Supported SLM Structures via Topology Optimization

B. Barroqueiro [1,2,*], A. Andrade-Campos [1] and R. A. F. Valente [1]

[1] Department of Mechanical Engineering, Centre for Mechanical Technology & Automation, University of Aveiro, 3810-193 Aveiro, Portugal
[2] Active Space Technologies, Actividades Aeroespaciais S.A., Parque Industrial de Taveiro, Lote 12, 3045-508 Coimbra, Portugal
* Correspondence: bjfb@ua.pt

Received: 27 June 2019; Accepted: 6 August 2019; Published: 8 August 2019

Abstract: The potential of Additive Manufacturing (AM) is high, with a whole new set of manufactured parts with unseen complexity being offered. However, the process has limitations, and for the sake of economic competitiveness, these should also be considered. Therefore, a computational methodology, capable of including the referenced limitations and providing initial solid designs for Selective Laser Melting (SLM) is the subject of the present work. The combination of Topology Optimization (TO) with the simplified fabrication model is the selected methodology. Its formulation, implementation, and integration on the classic TO algorithm is briefly discussed, being capable of addressing the minimum feature size and the overhang constraint limitations. Moreover, the performance and numerical stability of the methodology is evaluated, and numerical variables, such as the accuracy of structural equilibrium equations and the material interpolation model, are considered. A comparative study between these variables is presented. The paper then proposes an enhanced version of the selected methodology, with a better convergence towards a discrete solution.

Keywords: AM limitations; topology optimization; overhang constraints

1. Introduction

Metal Additive Manufacturing (AM), in particular Selective Laser Melting (SLM) and Electron Beam Melting (EBM), is at the forefront of the advanced manufacturing technologies [1]. These consist of the manufacturing of the 3D model layer by layer, allowing a great design freedom. On the other hand, Topology Optimization (TO) is a type of structural optimization that seeks the optimum material layout [2] and thus provides the means for intelligently exploring this freedom. In this way, the interconnection between AM and TO has proven to be advantageous [3]. Moreover, Figure 1 illustrates their interplay, as well as their main steps and key advantages.

J. Manuf. Mater. Process. **2019**, *3*, 68 2 of 20

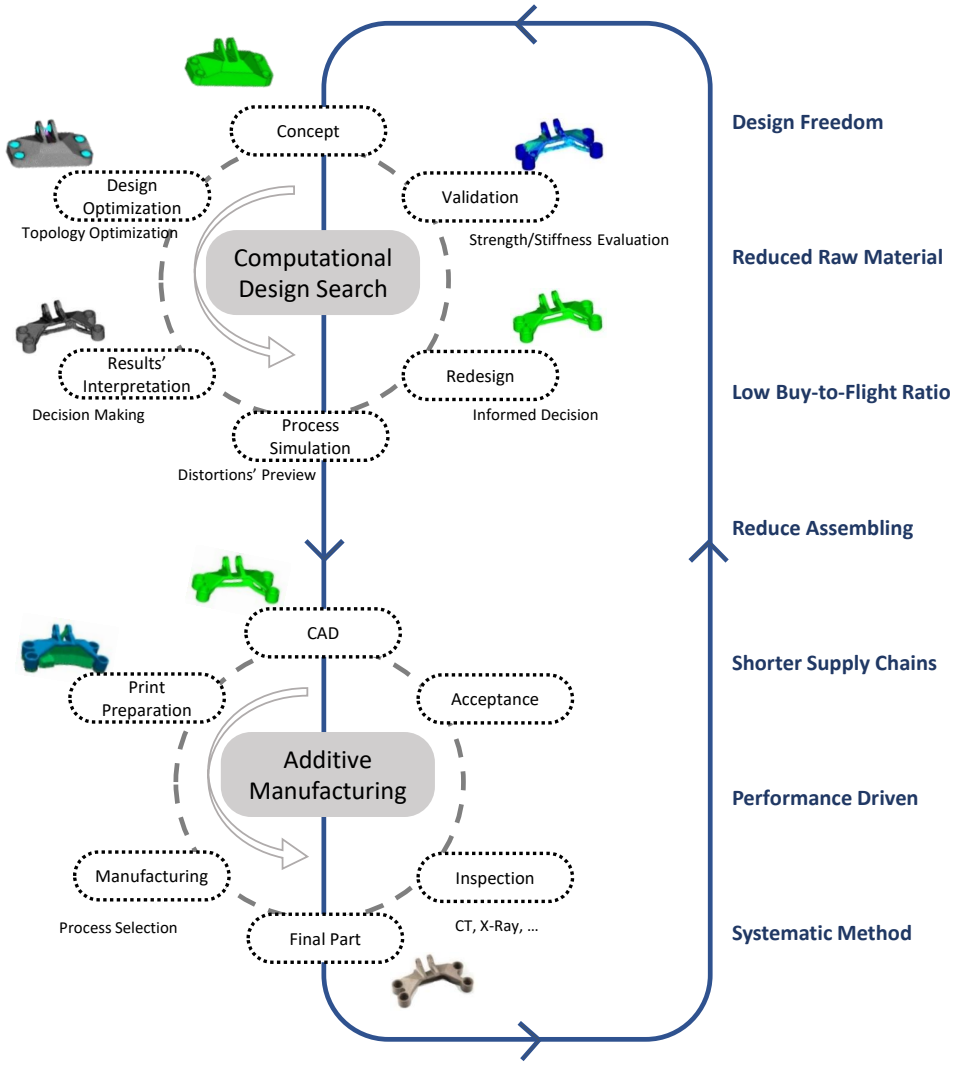

Figure 1. The interplay between additive manufacturing and topology optimization (bracket's figures extracted from Komi [4]).

The current market trends indicate that clients are increasingly demanding mass customization instead of mass production, and therefore, industry needs to adapt in order to be successful. Therefore, effective and flexible processes are needed in order to reduce the time to market and the development cycles [5]. Moreover, engineers and designers are encouraged to reduce geometric complexity, since there is a direct link between costs and part complexity. Within this context, Additive Manufacturing (AM) is seen as a disruptive technology [6,7] with the potential to overcome a number of limitations of traditional processes. These advantages can be grouped into:

- shape complexity: it is possible to take advantage of great geometrical freedom in order to reduce several parts in an assembly and/or using design optimization methodologies (TO), which opens a new world of customization possibilities [8–10];
- material complexity: multi-material parts can be built [11–13]; non-weldable materials can be joined [14]; coatings can be applied [15,16]; and surface finishing can be performed (polishing) [17];
- hierarchical complexity: multi-scale structures can be designed and fabricated using a geometric mesostructure in order to provide information to the part-scale macrostructure (i.e., lattices with negative or zero or positive coefficients of thermal expansion) [9,18,19];

J. Manuf. Mater. Process. **2019**, *3*, 68 3 of 20

- operational simplicity: AM allows for simpler supply chains and, therefore, shorter lead-times, lower inventories (less expensive storage), and no tooling (i.e., molds) [9,10,20].

According to Nickels [21], the aerospace industry can greatly benefit from AM technologies, with several advantageous applications being reported. For instance, the development time frame of a component (i.e., structural brackets) can be reduced from six months to just one using AM technologies, since the part is produced directly from 3D without tooling. Another driver for the aerospace industry is the highly-expensive storage of rarely-used spare parts all around the world. Due to its operational simplicity, the alternative is using the AM technology to produce the spare parts on site and just in time.

However, the unclear part is its limitations as reported by Weller et al. [10] and Kelly [22]; there are several AM limitations, namely: build size, reproducibility, surface finishing, low build rate, skilled and experienced labor, standardization, and lack of design tools and guidelines to exploit the technology fully. Thus, the article's goal is a computational methodology capable of providing initial solid designs for metal AM, in particular SLM. Moreover, process limitations can also be accounted for in the referenced methodology. Therefore, the study presents its limitations in a succinct manner, as well as the main methodologies to overcome the referenced limitations. In this way, the rationale behind the present methodology is available, as well as the other alternatives, each one with its advantages and disadvantages. Then, the paper presents the selected methodology in a succinct manner, which is based on the TO filter and fabrication model in order to impose a minimum member size and an overhang constraint, respectively. The methodology presentation includes a succinct problem formulation, the computational algorithm structure and implementation, the performance evaluation, and an industrial application. Regarding performance evaluation, two well-known problems are considered: cantilever and MBB. During the TO of the referenced problems, variables such as: (i) the material interpolation model, (ii) the precision of structural equilibrium (approximated structural equilibrium versus a full precision industry solver), and (iii) the existence of a simplified fabrication model are considered in order to evaluate their impact in the convergence of TO, as well as their industrial applicability. After this study, an improved version of the simplified fabrication model is presented, showing a greater ability to converge to discrete solutions.

2. Current State of AM Limitations and Its Design Approaches

Powder bed fusion processes, in particular SLM, provide a cost-effective and time-efficient way of producing highly-customized low-volume parts [23]. While AM seems to have unlimited potential, it does not have unlimited applicability [24]. In fact, the design stage shall be meticulously carried out in order to take full advantage of AM. Thus, Design for Additive Manufacturing (DfAM) is an important research topic. Studies such as Thomas [25], Vayre et al. [26,27], Adam and Zimmer [28], Klahn et al. [29], Kranz et al. [30], Lemu and Gebisa [31], and Sossou et al. [32] focused on stabilizing design rules for AM, which are crucial for achieving competitive and successful parts.

The current limitations of the AM processes can be grouped into non-directional and directional constraints. Non-directional constraints are the minimum feature size and cavities, while directional constraints can be seen as warping, anisotropy, and overhangs [3]. In a nutshell, these are:

- The minimum feature size is important in order to guarantee the manufacturability: for instance, the SLM processes cannot print walls with less than 0.4 mm [25];
- Regarding cavities, the design shall ensure that all cavities have exit points for the non-melted powder. For simple cavities, one exit can be sufficient, but more complex geometries require more than one exit point. On the other hand, the use of these cavities can avoid issues such as material accumulation or a large volume of solid material [30];
- Regarding warping, its occurrence is related to the local melting and non-uniform cooling, which causes the referenced effect. Strains such as thermal, creep, and phase transformations are the causes of residual stresses [14]. In order to avoid warping, support structures can be used [3];

- Regarding anisotropy, AM can create parts that often exhibit anisotropy between the in-plane and out-of-plane directions. This issue is a direct consequence of the layer-wise construction, but the origin of this phenomenon is related to the resultant microstructures, being explained in detail in DebRoy et al. [14].
- Concerning the overhang constraints, their construction at zero degrees is not advisable, since the molten pool would simply sink into the powder. Even, if a support structure is used, the resultant geometry will be inaccurate with poor surface quality [25]. Thus, this constraint shall be considered. The solution can either be the use of chamfers and/or optimizing the build direction in order to maximize the overhang angles. A 45° angle is usually indicated as an acceptable threshold [25].

The intelligent search for a design that seeks the optimal material distribution (i.e., minimum compliance) and accounts for the previous constraints poses a greater challenge. Studies such as Joshi and Sheikh [33], Reddy K. et al. [34], Mirzendehdel and Suresh [35], Walton and Moztarzadeh [36], Allaire et al. [37], and Guo et al. [38] indicated that TO may provide the answer. Moreover, this method can include in its formulation some of the previous constraints and, thus, provide a solid initial design. The inclusion of AM constraints in the formulation of the TO algorithm has received some attention from the scientific community, namely the overhang constraints. In TO algorithms, the minimum feature size can be controlled by the radius of the filtering operation [3]. These are largely studied and reviewed in works such as Sigmund [39], Svanberg and Svärd [40], where extensive studies on the existing filters are available. On the other hand, imposing the overhang constraints on the topology optimization poses a greater problem, due to the implicit high non-linearity. Currently, there are several approaches to tackle the overhang constraint. These are:

- Modifying the design in order to limit the overhang to a certain limit. Since this approach is a post-processing technique, the resulting geometries have their ratio mass and stiffness compromised. For further details, consult Leary et al. [41];
- Using two scale calculations: a discrete scale where the overhang constraints are enforced and a continuous scale that uses the information from the discrete scale in order to produce self-supporting structures [42]. Alternative to the use of two macroscales (discrete and continuous) is the use of a mesoscale and a macroscale, where the mesoscale is defined by a Representative Unit Cell (RUC) and the macroscale uses the information of the homogenized mesoscale [43–45]. Thus, the RUC can be chosen to be self-supporting, but some manufacturing restrictions arise, namely minimum dimensions and extraction of non-melted powder;
- Using local constraints, being a simple and effective implementation. However, local constraints are expensive to compute and not very well suited for large-scale problems [46];
- Using edge detection algorithms to control the overhang angles [47–49]. The suppression method of intermediate densities in Qian [47] and Mezzadri et al. [49] uses an additional constraint, while the work in Garaigordobil and Ansola [48] used a Heaviside projection;
- Using simplified fabrication models, which stand for a low computational cost operation. Moreover, this does not require additional constraints to the optimization problems. Currently, there are two main AM fabrication models, one based on min-max operators [50–52], the other being based on area occupation and Heaviside projections [53–56], which can provide self-supporting designs.

In short, the last approach is considered the way forward, due to its computational cost and its simple integration on existent TO codes. Their drawback is related to the impossibility of parallel computing since the simplified fabrication model imposes that the algorithm must proceed in a layer-wise manner. In a preliminary analysis, this limitation can be seen as prohibitive. However, after a deep analysis, the relevance of this limitation becomes rather limited, if the implementation is properly structured. Thus, these fabrication models can be subdivided into three main steps. The first step corresponds to the supporting region search, which is computationally expensive, but can be

fully parallelized. The second and third steps correspond to sensitivities and densities scanning in a layer-wise manner in order to impose the overhang constraint. These steps are not parallelizable. However, their computational cost is marginal when compared with the structural equilibrium required by TO. In the current implementation, the difference is several orders of magnitude. The simplified fabrication model based on Heaviside projections requires high Heaviside penalization, making it highly susceptible to local minima. Moreover, if low Heaviside penalization is used, the algorithm converges to the classic solutions and uses intermediate densities to support it, defeating its purpose. The model based on min-max operators [50,51], which has already gained commercial applicability [52], exhibits good convergence properties and is less susceptible to be trapped in local minima. Therefore, the authors defend a preference for the last referenced approach due to its numerical performance. Therefore, the next section presents the topology optimization algorithm in order to explain the integration fabrication model in the referenced algorithm.

3. Topology Optimization

3.1. Standard Algorithm

3.1.1. Problem Formulation

Topology Optimization (TO) is a type of structural optimization that seeks the optimum material layout [2]. There are numerous methods to perform TO with a compressive list being available in Rozvany and Lewiński [57] and Deaton et al. [58]. Within the present work, density methods were used, namely the well-known Solid Isotropic Material with Penalization (SIMP) [59,60] and the Rational Approximation of Material Properties (RAMP) [61]. Both approaches seek the optimal material distribution, $\mathbf{x}$, across the design domain, Ω, in order to minimize compliance (for example). Thus, the classic TO problem of compliance minimization of a quasi-static loaded structure can be mathematically formulated as:

$$\min \quad f(\mathbf{x}) = \mathbf{U}^{\mathrm{T}}\mathbf{K}(\mathbf{x})\mathbf{U}, \tag{1}$$

subjected to:

$$\begin{gathered} \mathbf{K}(\mathbf{x})\mathbf{U} = \mathbf{F}, \\ \sum_{e\in\Omega} \frac{V_e \boldsymbol{\rho}_e(\mathbf{x})}{V_\Omega} = V_f, \quad e \in \Omega \quad \text{and} \\ 0 < \mathbf{x}_e < 1, \end{gathered} \tag{2}$$

where $\mathbf{U}$, $\mathbf{F}$, and $\mathbf{K}$ are the global displacements, forces, and stiffness matrices, respectively. Furthermore, $\mathbf{x}$ represents the design densities, which become physical densities ($\boldsymbol{\rho}$) after filtering. Additionally, V_f, V_e, and V_Ω stand for the volume fraction (constraint), the volume of the element, and the domain, respectively. Using the SIMP approach, the element stiffness matrix, $\mathbf{K}_e$, becomes:

$$\mathbf{K}_e = \left(\rho_{\min} + \boldsymbol{\rho}_e^{\eta}\right)\mathbf{K}_e^0, \tag{3}$$

where $\mathbf{K}_e^0$ is the stiffness matrix of the solid element, $\rho_{\min}$ is a small constant to avoid an ill-conditioned system of equations, and η is the penalty parameter. Alternatively, using RAMP, the element stiffness matrix, $\mathbf{K}_e$, becomes:

$$\mathbf{K}_e = \left(\rho_{\min} + \frac{\boldsymbol{\rho}_e}{1+\eta(1-\boldsymbol{\rho}_e)}\right)\mathbf{K}_e^0, \tag{4}$$

where $\mathbf{K}_e^0$ is the stiffness matrix of the solid element multiplied by $1/(1+\rho_{\min})$ [55] and η is again the penalty parameter.

3.1.2. Minimum Member Size

In order to ensure the existence of a solution, to impose a minimum member size and avoid problems such as the formation of checkerboard patterns, a filtering operation is recommended. The linear density filter (e.g., Bruns and Tortorelli [62], Bourdin [63]) can be formulated as:

$$\boldsymbol{\rho}_e = \sum_{k \in N} w_{ek} \mathbf{x}_k, \tag{5}$$

where N defines the filtering neighborhood, composed by a set of elements, k [40]. Thus, $N_e = \{e : d(e,k) \leq r\}$, where $d(e,k)$ is the distance between the centroids of elements e and k. Considering conic weights, w_{ek} becomes:

$$w_{ek} = \begin{cases} \frac{r - d(e,k)}{\sum_{l \in N} r - d(e,l)} & , \quad k \in N_e \\ 0 & , \quad k \notin N_e. \end{cases} \tag{6}$$

Within the scope of this work, an extension of the density filter is used. Initially proposed by [64], this filter uses the Heaviside function, formulated as:

$$\boldsymbol{\rho}_e = \frac{\tanh(\beta\varphi) + \tanh(\beta(\boldsymbol{\mu}_e - \varphi)}{\tanh(\beta\varphi) + \tanh(\beta(1 - \varphi))} \quad \text{and} \tag{7}$$

$$\boldsymbol{\mu}_e = \sum_{k \in N} w_{ek} \mathbf{x}_k, \tag{8}$$

where φ is set to 0.5. Additionally, β controls the "aggressiveness" of the Heaviside function [50].

3.1.3. Sensitivity Analysis

The derivatives of the objective function and constraint function for the independent variable, $\mathbf{x}$, are computed using the chain rule as:

$$\frac{\partial f}{\partial \mathbf{x}} = \frac{\partial f}{\partial \boldsymbol{\rho}} \frac{\partial \boldsymbol{\rho}}{\partial \mathbf{x}}. \tag{9}$$

Using SIMP, the first term is given by:

$$\frac{\partial f}{\partial \boldsymbol{\rho}} = -\eta \boldsymbol{\rho}_e^{\eta - 1} \mathbf{u}_e{}^{\mathrm{T}} \mathbf{k}_e^0 \mathbf{u}_e, \tag{10}$$

where $\mathbf{u}_e$ and $\mathbf{k}_e^0$ are displacements and the stiffness matrix, respectively, associated with element e. Alternately, using RAMP, the first term is given by:

$$\frac{\partial f}{\partial \boldsymbol{\rho}} = -\frac{\eta + 1}{(\eta(\boldsymbol{\rho}_e - 1) - 1)^2} \mathbf{u}_e{}^{\mathrm{T}} \mathbf{k}_e^0 \mathbf{u}_e. \tag{11}$$

Finally, the second term is computed using the chain rule as:

$$\frac{\partial \boldsymbol{\rho}}{\partial \mathbf{x}} = \frac{\partial \boldsymbol{\rho}}{\partial \boldsymbol{\mu}} \frac{\partial \boldsymbol{\mu}}{\partial \mathbf{x}} = \sum_{k \in N} w_{ek} \frac{\beta \left(\operatorname{sech}(\beta(\boldsymbol{\mu}_k(\mathbf{x}) - \varphi)\right)^2}{\tanh(\beta\varphi) + \tanh(\beta(1 - \varphi))}. \tag{12}$$

3.2. Simplified Fabrication Model

3.2.1. Integration in TO

This section briefly presents a methodology that allows the control of overhang angles (simplified fabrication model), as well as its integration in the classic topology optimization algorithm, being

based on min-max operators [50,51]. This algorithm proceeds in a layer-wise manner, mimicking the actual AM process. Thus, the algorithm starts on the first layer (that would be printed) up to the last layer. During this process, the densities of layer i cannot be higher than the maximum of the densities in the support region defined in layer $i-1$. For the 2D case, the support region, $S(i,j)$, is defined according to Figure 2. It is worth noting that if a regular mesh (squares) is used, then an implicit overhang constraint of 45° is imposed, the extension to 3D being straightforward [51].

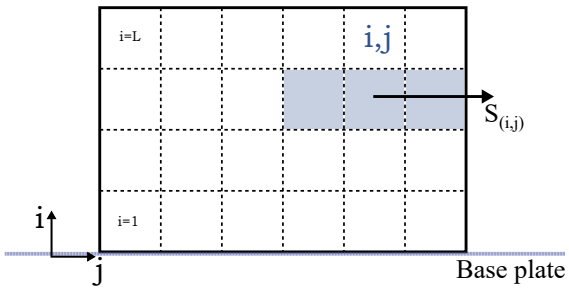

Figure 2. Definition of support region, $S(i,j)$, for the element (i,j) [50].

Thus, the smooth approximation of this constraint is formulated as:

$$\xi_{(i,j)} = \text{smin}(\rho_{(i,j)}, \Xi_{(i,j)}) = \frac{1}{2}\left(\rho_{(i,j)} + \Xi_{(i,j)} - \left(\left(\rho_{(i,j)} - \Xi_{(i,j)}\right)^2 + \epsilon\right)^{\frac{1}{2}} + \sqrt{\epsilon}\right), \tag{13}$$

$$\Xi_{(i,j)} = \text{smax}\left(\xi_{(i-1,j-1)}, \xi_{(i-1,j)}, \xi_{(i-1,j+1)}\right) = \left(\xi^P_{(i-1,j-1)} + \xi^P_{(i-1,j)} + \xi^P_{(i-1,j+1)}\right)^{\frac{1}{Q}} \tag{14}$$

$$\text{with} \quad Q = P + \frac{\log(n_S)}{\log(\rho_0)}, \quad \xi_{(1,j)} = \rho_{(1,j)} \quad \text{and} \quad 1 < i \leq L, \tag{15}$$

where P, ρ_0, and ϵ are constants, n_S is the size of the region S (meaning three in 2D), and L is the number of layers. The new density, ξ, is called the printed density. These densities result from the application of the previous equations to the physical densities. Since every ξ_i is dependent of all ξ_{i-1}, the calculation of the print densities shall proceed in a layer-wise manner, starting with the first layer up to the last. On the first layer, printed densities are equal to the physical densities. On the second layer, printed densities from the previous layer are used to compute *smax* (maximum density of region S), and then, *smin* is computed using the physical density of the current layer and the maximum from the previous layer (minimum between both). For the third layer and the remaining ones, the process is repeated.

Regarding the evaluation of the objective function, the printed densities are the ones that should be used, meaning that in Equation (3) or (4), the term $\boldsymbol{\rho}$ is replaced by $\boldsymbol{\xi}$.

3.2.2. Sensitivity Analysis

The sensitivity analysis of the standard topology optimization requires some changes. The chain rule differentiation (Equation (9)) requires an additional term, becoming:

$$\frac{\partial f}{\partial \mathbf{x}} = \frac{\partial f}{\partial \boldsymbol{\xi}} \frac{\partial \boldsymbol{\xi}}{\partial \boldsymbol{\rho}} \frac{\partial \boldsymbol{\rho}}{\partial \mathbf{x}}. \tag{16}$$

the term $\partial f / \partial \boldsymbol{\xi}$ corresponds to:

$$\frac{\partial f}{\partial \xi_e} = -\eta \xi_e^{\eta-1} \mathbf{u}_e^T \mathbf{k}_e^0 \mathbf{u}^e \quad \text{or} \tag{17}$$

$$\frac{\partial f}{\partial \xi_e} = -\frac{\eta+1}{(\eta(\xi_e - 1) - 1)^2} \mathbf{u}_e^T \mathbf{k}_e^0 \mathbf{u}^e, \tag{18}$$

using SIMP or RAMP, respectively. The term $\partial\boldsymbol{\rho}/\partial\mathbf{x}$ is already defined by Equation (12). The term $\partial\boldsymbol{\xi}/\partial\boldsymbol{\rho}$ is the referenced additional term. This term is computed via an adjoint formulation (in addition to the adjoint formulation of TO), with its full formulation being shown in [50,51]. Briefly and given the sensitivities $\partial f/\partial\boldsymbol{\xi}$, the present procedure modifies them in order to compute $\partial f/\partial\boldsymbol{\rho}$. Thus, the procedure can be formulated as follows:

$$\frac{\partial f}{\partial \boldsymbol{\rho}_i} = \boldsymbol{\lambda}_i^{\mathrm{T}} \frac{\partial \mathrm{smin}_i}{\partial \boldsymbol{\rho}_i} \quad \text{and} \tag{19}$$

$$\boldsymbol{\lambda}_i^{\mathrm{T}} = \begin{cases} \frac{\partial f}{\partial \tilde{\boldsymbol{\xi}}_i} + \boldsymbol{\lambda}_{i+1}^{\mathrm{T}} \frac{\partial \mathrm{smin}_{i+1}}{\partial \boldsymbol{\xi}_i} & \text{for } 1 \leq i < L \\ \\ \frac{\partial f}{\partial \tilde{\boldsymbol{\xi}}_i} & \text{for } i = L \end{cases}, \tag{20}$$

where i stands for the layer index and $i+1$ stands for the layer above, and therefore, each multiplier depends on the layer above. The algorithm modifies the existent sensitivities in the reversed print direction, meaning that the algorithm starts on the last layer until the first. The remaining derivatives are computed as:

$$\frac{\partial \mathrm{smin}}{\partial \boldsymbol{\rho}} = \frac{1}{2}\left(1 - (\boldsymbol{\rho}_i - \boldsymbol{\Xi}_i)\left((\boldsymbol{\rho}_i - \boldsymbol{\Xi}_i)^2 + \epsilon\right)^{-\frac{1}{2}}\right), \tag{21}$$

$$\frac{\partial \mathrm{smin}}{\partial \boldsymbol{\xi}} = \frac{\partial \mathrm{smin}}{\partial \boldsymbol{\Xi}} \frac{\partial \boldsymbol{\Xi}}{\partial \boldsymbol{\xi}}, \tag{22}$$

$$\frac{\partial \mathrm{smin}}{\partial \boldsymbol{\Xi}} = \frac{1}{2}\left(1 + (\boldsymbol{\rho}_i - \boldsymbol{\Xi}_i)\left((\boldsymbol{\rho}_i - \boldsymbol{\Xi}_i)^2 + \epsilon\right)^{-\frac{1}{2}}\right) \quad \text{and} \tag{23}$$

$$\frac{\partial \boldsymbol{\Xi}_k}{\partial \boldsymbol{\xi}_i} = \frac{P}{Q} \boldsymbol{\xi}_i^{P-1} \left(\sum_{k \in S} \boldsymbol{\xi}_k^P\right)^{\frac{1}{Q}}. \tag{24}$$

3.2.3. Modified Fabrication Model

Following the work of [50], the study points out that the *smax* operator has numerical problems. Initially, the study proposed the use of the P max function as the *smax* operator, but it suffered from severe overestimation, and then, the P-Q max function was proposed to tackle the referenced issue. However, the proposed solution solved the problem partially, since the operator can still accumulate relevant errors. Thus, this issue motivated the search for another smooth max function that would reduce the referenced errors. The function denominated as *softmax* [65] can be an interesting alternative, since this function does not produce overshoot. This function can be expressed as:

$$\mathrm{smax}(\boldsymbol{\xi}_i) = \boldsymbol{\Xi}(\boldsymbol{\xi}_i) = \frac{\sum_{i \in S} \boldsymbol{\xi}_i \mathrm{e}^{P\boldsymbol{\xi}_i}}{\sum_{i \in S} \mathrm{e}^{P\boldsymbol{\xi}_i}}, \tag{25}$$

where $P > 0$, and its gradient is expressed as:

$$\frac{\partial \boldsymbol{\Xi}_k}{\partial \boldsymbol{\xi}_i} = \frac{\mathrm{e}^{P\boldsymbol{\xi}_i}}{\sum_{k \in S} \mathrm{e}^{P\boldsymbol{\xi}_k}} \left[1 + P\left(\boldsymbol{\xi}_i - \boldsymbol{\Xi}\right)\right]. \tag{26}$$

Thus, this function can be used as the new *smax* operator instead of the P-Q max function. In order to quantify the precision increase of the new *smax* operator, several support regions $\left(\boldsymbol{\xi}_{(i-1,j-1)}, \boldsymbol{\xi}_{(i-1,j)}, \boldsymbol{\xi}_{(i-1,j+1)}\right)$ were generated randomly, and their maximum was computed using the P-Q max and the *softmax* functions. Considering a "large number" of random support regions, the P-Q max function (for $P = 40$) provides a maximum absolute error (difference between real maximum and maximum smooth approximation) about 0.02, and around 7% of the support regions still get overestimated (these values may vary for different random number generators). The reader may

consider that an absolute error of 0.02 has limited relevance; however, it should be highlighted that this algorithm proceeds in a layer-wise manner. Thus, as the number of layers increases, the referenced absolute error can propagate in a relevant way, crippling the ability of the algorithm to converge towards a discrete solution. On the other hand, the *softmax* operator fully addresses the referenced issues. Regarding overestimation, the new operator provides no overestimation, allowing a precise computation of the smax operator and a more effective convergence to a discrete solution. In fact, for the same level of P, the absolute error of the *smax* operator is reduced by a factor of 1.5 in unfavorable situations up to 2.4 in more favorable situations. In the scope of work, a P value of 40 was considered, being an effective compromise between precision and problem non-linearity. The value of P can be raised, but no relevant practical advantage was observed; however, the increase of the referenced constant increases the problem non-linearity, negatively affecting the numerical stability of the problem.

3.2.4. Algorithm Structure

The integration of the simplified fabrication model in the TO algorithm results in a procedure with numerous steps. Thus, a simplified flowchart of the optimization algorithm is shown in Algorithm 1.

Algorithm 1 Topology optimization algorithm structure with the fabrication model.

1. Build and save the neighborhood, N_e, for an efficient filtering operation;
2. Build and save the support region, S_e, for an efficient application of the fabrication model;
3. Initialize the design domain, $\mathbf{x}$;
4. Compute the physical densities, $\boldsymbol{\rho}$, using Equations (7) and (8);
5. Compute the print densities, $\boldsymbol{\xi}$. In the layer-wise loop following print direction, apply Equations (13) and (14);
6. Optimization loop:
   (a) solve the structural problem ($\mathbf{K}(\boldsymbol{\xi})\mathbf{U} = \mathbf{F}$), using the element stiffness matrix given by Equation (3) or Equation (4), where $\boldsymbol{\rho}$ shall be replaced by $\boldsymbol{\xi}$;
   (b) compute sensitivity $\partial f/\partial \boldsymbol{\xi}$ based on print densities (Equation (17) or Equation (18));
   (c) update sensitivities using the sensitivity information of the fabrication model. In a layer-wise loop following the reversed print direction, apply Equations (19) and (20) in order to update them;
   (d) perform the filtering operation in order to obtain the final sensitivities using Equation (12).
   (e) calculate new $\mathbf{x}$ using an optimizer
   (f) compute physical densities, $\boldsymbol{\rho}$, using Equations (7) and (8);
   (g) Compute print densities, $\boldsymbol{\xi}$. In a layer-wise loop following the print direction, apply Equations (13) and (14)
   (h) return to Sub-step (a) or break the loop if the solution has converged

3.3. Implementation

This implementation is aligned with the architecture proposed in [66]. The quality of the resultant solutions (ideally void (zero) and solid (one)) was evaluated using an indicator denominated as a measure of non-discreteness, M_{nd}. This indicator can be evaluated as [39]:

$$M_{nd} = \sum_{e=1}^{n} 4.0\xi_e(1.0 - \xi_e)/n, \tag{27}$$

where zero means that the design is fully discrete (there are no intermediate densities) and one means that the design is full of intermediates densities (for $V_f = 0.5$). The optimization problem was solved with the gradient-based Method of Moving Asymptotes (MMA) [67], using the default

parameters unless otherwise specified. The parameter η was set to three using SIMP and six using RAMP. Additionally, the parameter V_f was set to 0.5. Regarding Heaviside filtering, the filtering radius was set to four units; the parameter β was set to two and then doubled at Iterations 100, 150, 200, and 250; and finally, the parameter φ was set to 0.5. Regarding fabrication models, the parameters P, ρ_0, and ϵ were set to 40, 0.5, and 1×10^{-4}, respectively, following Langelaar [50]. Unless otherwise specified, the build direction of fabrication was considered to be from bottom to top (upwards).

4. Examples

In order to increase manufacturability, in particular SLM, the initial designs resulting from the presented methodology always considered a minimum member size constraint imposed by TO filter. Unless otherwise stated, the filter radius was set to three elements in width. The overhang constraint may or may not be considered. If considered, the model is denominated as restricted. If not considered, the model is denominated as unrestricted.

4.1. Comparative Study

This section presents the topology optimization results of two well-known problems. The first problem, a cantilever structure, is depicted in Figure 3a, which is discretized by a regular quadrilateral mesh of 160 $\times$ 100 elements. The second problem, MBB, is depicted in Figure 3b, discretized by a regular quadrilateral mesh of 240 $\times$ 80 elements using symmetry conditions. Both problems consider unitary forces in the depicted direction.

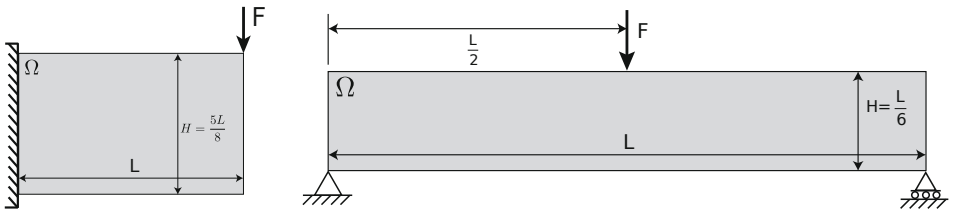

a - Cantiliver **b** - MBB beam

Figure 3. Benchmark problems' definition [55,68].

Figure 4 presents a compilation of the results of the cantilever problem at Iterations 20, 90, 150, and 300. Each subfigure contains two similar analyses, the difference being on the structural equilibrium evaluation. The simulation on the left used MSC Nastran code with a full integration rule to perform the structural equilibrium, while the analysis on the right used an approximated FE model presented in Andreassen et al. [66] and Sigmund [69]. Figure 5 presents a compilation of the results of the MBB problem at Iterations 20, 90, 150, and 300. Similar to the previous problem, each left subfigure used MSC Nastran to evaluate the structural equilibrium, while each right half used an approximated FE model presented in Andreassen et al. [66] and Sigmund [69].

Table 1 presents the final results at Iteration 300 of the cantilever and MBB problems, where it is possible to compare different variables such as FE model precision, the material interpolation models (SIMP or RAMP), and solution performance without (unrestricted) and with (restricted) the severe restriction of the simplified fabrication model.

After a close analysis of Figures 4 and 5, as well as Table 1, it becomes clear that the precision of the structural equilibrium had limited relevance even with such highly non-linear operators such as the fabrication model in a general perspective. However, Figure 4o is an exception, because a problematic member appeared (gray) with approximated structural equilibrium and not with MSC Nastran. Regarding filtering, the material interpolation model influenced the minimum member size solution. The RAMP model produced solutions with a larger minimum member size, but the final solutions were in accordance with the published results [66,69]. Moreover, the RAMP model allowed

material to grow out of the void, while SIMP did not. However, the numerical stability of SIMP combined with the topological "morphing" capabilities [56] makes the decision of the best material interpolation model somehow unclear. In the scope of this work, the SIMP model was used in the subsequent analysis since it is an industry standard.

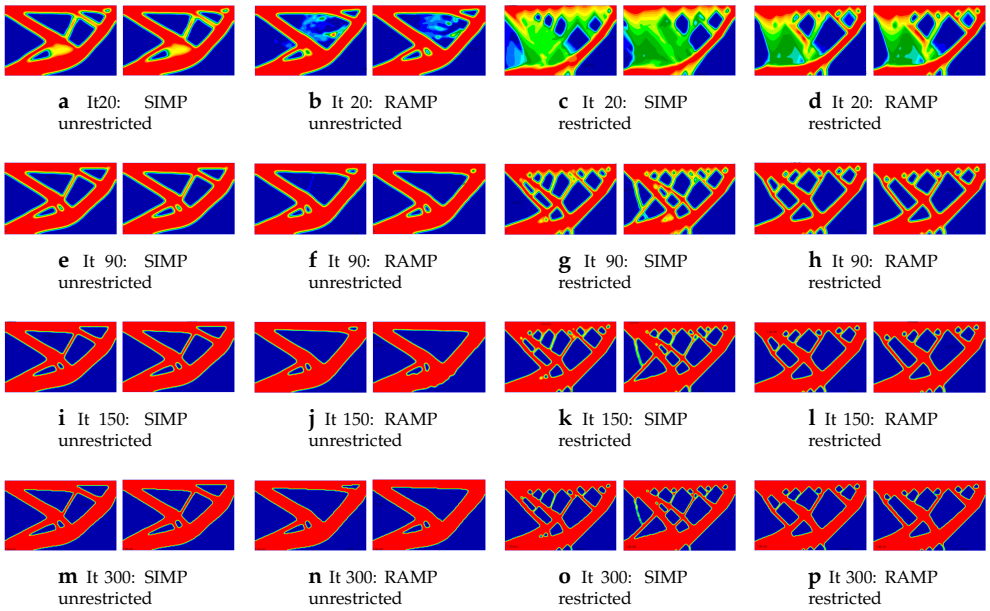

Figure 4. Topology optimization of the cantilever problem at Iterations 20, 90, 150, and 300. In each subfigure, the left image uses the full precision structural equilibrium, and the right image uses approximate structural equilibrium. SIMP, Solid Isotropic Material with Penalization; RAMP, Rational Approximation of Material Properties.

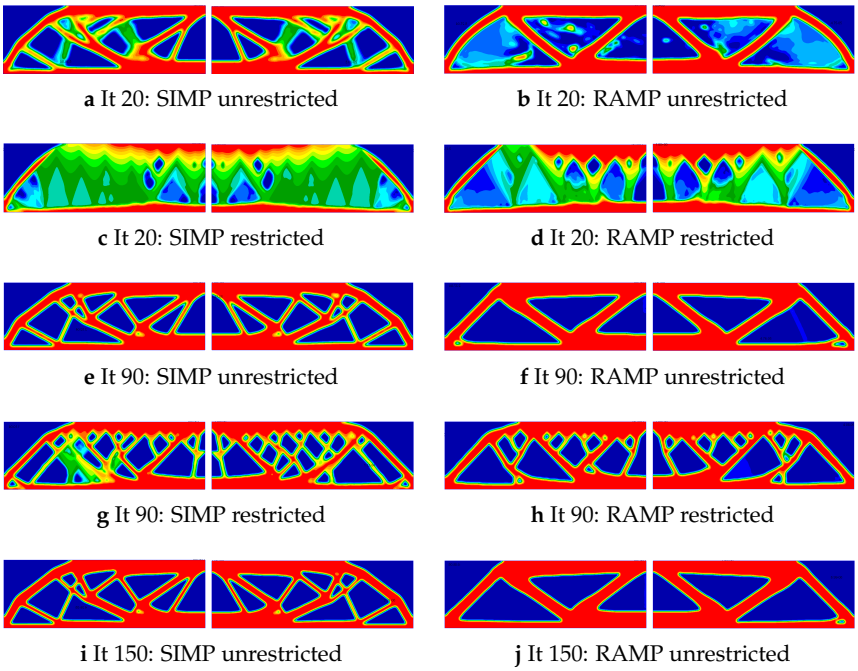

Figure 5. *Cont.*

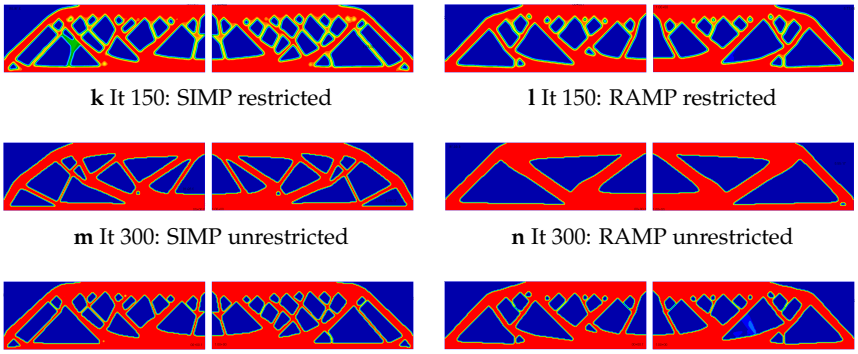

k It 150: SIMP restricted **l** It 150: RAMP restricted

m It 300: SIMP unrestricted **n** It 300: RAMP unrestricted

o It 300: SIMP restricted **p** It 300: RAMP restricted

Figure 5. Topology optimization of the MBB problem at Iterations 20, 90, 150, and 300. In each subfigure, the left image uses full precision structural equilibrium, and the right image uses approximate structural equilibrium.

Table 1. Overview of the topology optimization of the cantilever and MBB problems at Iteration 300 in terms of Compliance (C) and the measure of non-discreteness level (M_{nd}).

	SIMP				**RAMP**			
	MSC Nastran		**Aprox Model**		**MSC Nastran**		**Aprox Model**	
	C	***M_{nd}*** (%)	***C***	***M_{nd}*** (%)	***C***	***M_{nd}*** (%)	***C***	***M_{nd}*** (%)
Cantilever Problem								
Unrestricted	1.0	0.7	1.004	0.8	1.012	0.8	1.015	0.5
Restricted	1.058	0.6	1.051	1.0	1.066	0.8	1.038	0.1
MBB Problem								
Unrestricted	1.0	1.0	1.0	1.0	1.037	0.9	1.037	0.5
Restricted	1.049	0.4	1.049	0.7	1.054	1.0	1.055	1.4

Figure 6a,c shows the convergence curves of the cantilever and MBB problems using the original and modified (*softmax*) simplified fabrication models. The results consider the SIMP model and the approximated structural equilibrium. Moreover, a solution without the fabrication model is also included for reference purposes. The non-linearity of the referenced model with Heaviside filtering led to numerical instability in the initial iterations. At this point, the evaluation of the convergence properties resulting from the original and modified smooth max functions was required, and the initial instability made it less clear. Thus, this issue can be tackled by reducing the init parameter, s_0 (from [67]), to 0.05 [70], making the convergence slower in the initial iterations, but perfectly smooth. The overall convergence with original and modified smooth max functions remained similar, and an overview of the final iteration can be seen in Table 2. In these two problems, the modified version led to a marginal increase in compliance when compared to the original. On the other hand, Figure 6b,d depicts the evolution of the measure of non-discreteness M_{nd}. The modified filter showed a greater ability to converge to discrete solutions as depicted in Figure 7. This ability should be related to a more precise computation of the smax operator. The final values of M_{nd} are given in Table 2.

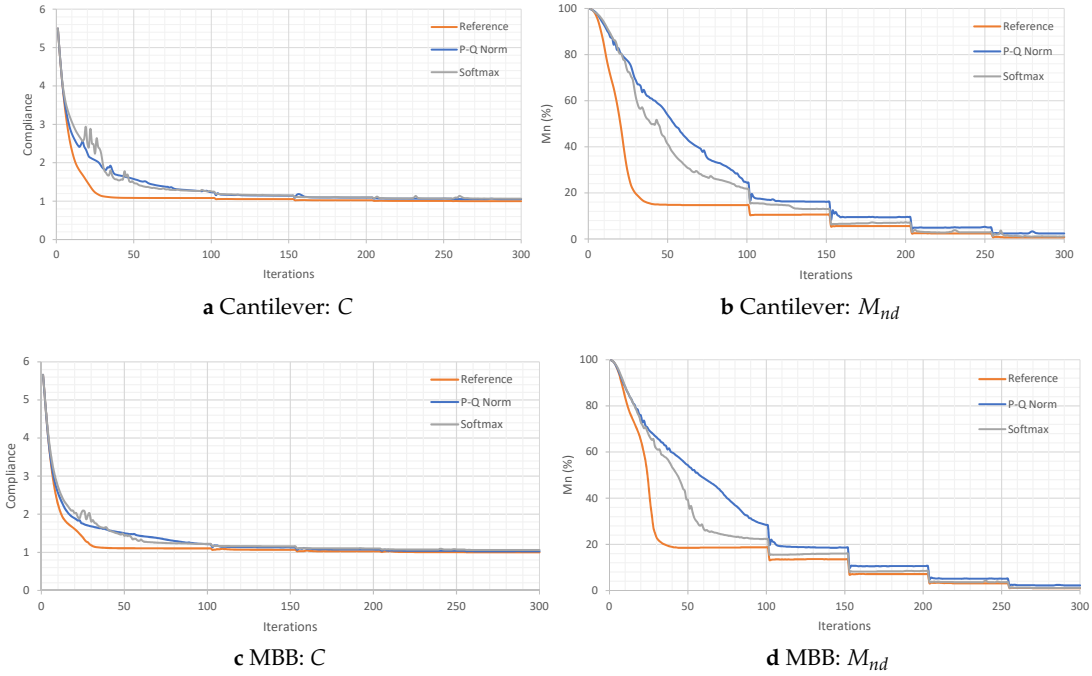

a Cantilever: C **b** Cantilever: M_{nd}

c MBB: C **d** MBB: M_{nd}

Figure 6. Comparison of the cantilever and MBB problems' topology optimization with the original and modified fabrication models.

Table 2. Overview of the cantilever and MBB problems' topology optimization with the original and modified fabrication models.

	Reference		**P-Q Norm**		**Softmax**	
	C	M_{nd}	C	M_{nd}	C	M_{nd}
Cantilever Problem	1.000	0.7	1.052	2.4	1.066	1.1
MBB Problem	1.000	1.0	1.028	2.2	1.061	1.1

The cantilever and MBB topology optimization problems presented in Figures 4 and 5 (SIMP restricted) are similar to the ones shown in Figure 7. The difference between them is the referenced change on the s_0 parameter of the MMA. Both simulations converged to self-supporting designs; however, different designs were observed, corresponding to different minima solutions.

In short, the proposed modified fabrication model addressed the issues identified by Langelaar [51] such as the performance of smax, the high level of intermediate densities, and the problematic grey scale member. The proposed new smax operator provided smaller error, no overestimation, and no additional parameter, and thus, the filter showed better ability to use fewer intermediate densities. For instance, on the cantilever and MBB problems at Iteration 100, the use of the new operator led to a reduction of the intermediate densities by 11% and 23%, respectively (consult Figure 6b,d). Regarding the problematic grey scale member, it should be related to the precision of structural equilibrium and not with fabrication model.

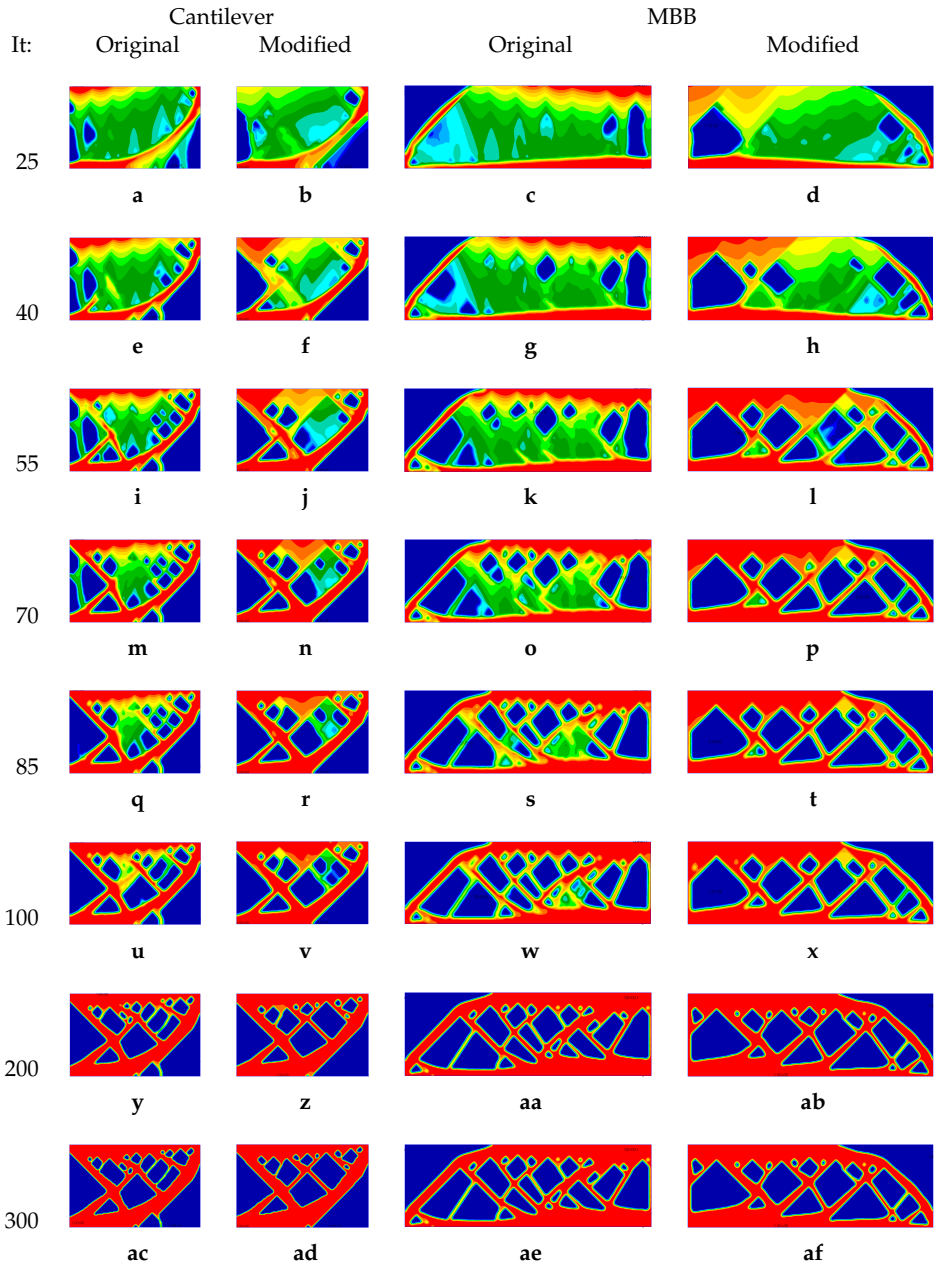

Figure 7. Comparison of the topology optimization problem of MBB using the original and modified version of the fabrication model.

5. A 3D Case Study

The section presents the TO results of the Sentinel-1 Antenna Support Bracket (approximated dimensions were used, since the real ones were not available). Figure 8 presents the available design domain, as well as boundary conditions. As depicted in the figure, the zero-displacement condition was applied to the four corners of the bracket, while the force was at its tip. The TO load case consisted of three subcases: (i) unitary force in the `X` direction, (ii) unitary force in the `Y` direction, and (iii) unitary force in the `Z` direction. Taking into consideration the maximum characteristic length of the part of 250 mm, a minimum member size constraint of 4.5 mm was considered (approximately a radius of three elements), as well as the overhang constraint. Moreover, a supporting region of five elements was used. Figures 9 and 10 present interactive models of the obtained material distribution

considering $V_f = 0.3$. In the design of Figure 9, the printing direction was aligned to the Z axis shown in Figure 8, and the faces of the design domain at Z were considered to be supported by support structures that connected the part to the base plate. The bottom oblique face (all the way to its tip) respected the overhang constraint; however, some support structures on its tip (at least) are recommended in order to avoid excessive thermo-mechanical warping. In the design of Figure 10, the printing direction was aligned to the X axis shown in Figure 8, and the faces of the design domain at X were considered to be supported by support structures that connected the part to the base plate. Some support structures on its tip (at least) are also recommended (for the same reasons) in order to avoid excessive thermo-mechanical warping.

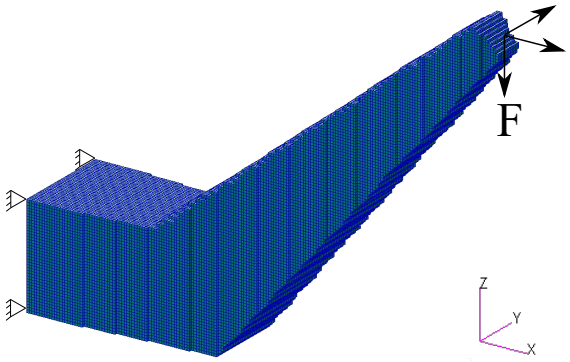

Figure 8. Topology Optimization (TO) design volume and boundary conditions.

The presented results showed that the algorithm was able to produce a self-supporting design in the 3D domain, as well. Moreover, the self-supporting design of Figure 9 had a similar compliance level when compared with the unrestricted solution. In fact, the restricted design suffered a marginal increase in compliance of 2%. On the other hand, the self-supporting design of Figure 10 led to an important increase in compliance (23%) when compared with the unrestricted solution.

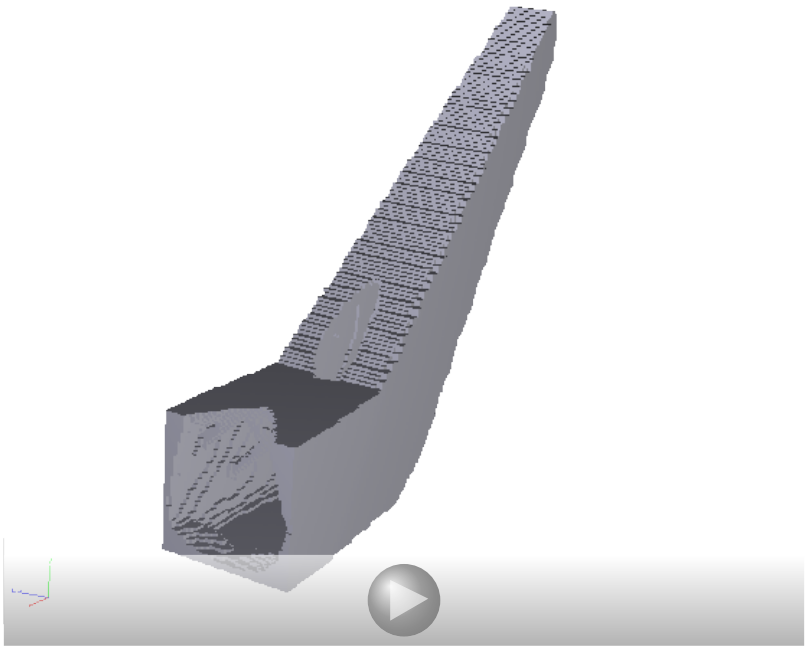

Figure 9. TO result considering the Z axis as the printing direction.

From a manufacturing and post-processing point of view, the major advantage of considering the overhang constraint was related to the reduction of support structures. In fact, the design can change significantly in order to become self-supporting and avoid the use of support structures. This advantage comes with a cost of compliance and computational time. On the other hand, internal support structures represent costs in terms of raw material, building time, and post-processing (i.e., cutting and machining). Moreover, their removal can pose a major challenge if they are internal to the design volume due to access and/or the risk of rupture of thin structural members during cutting and machining operations.

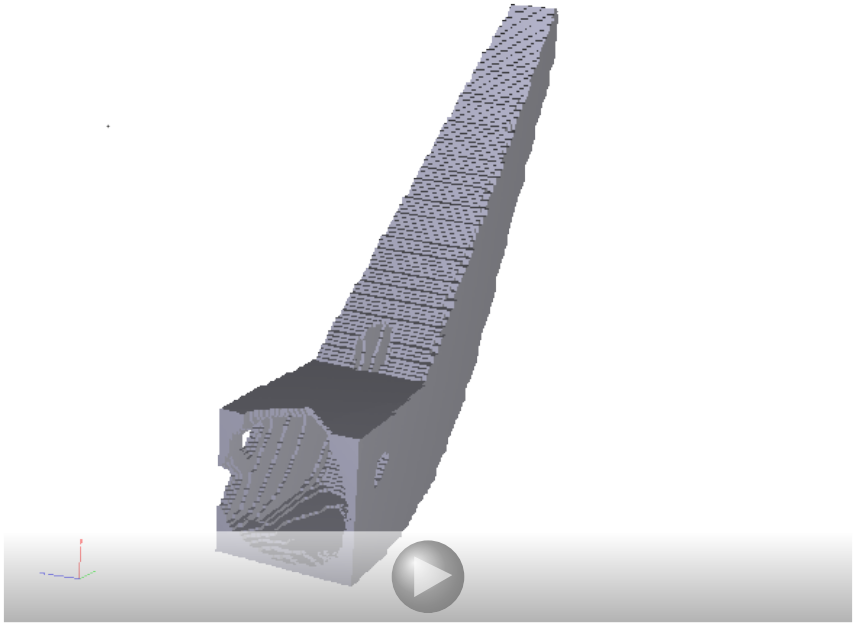

Figure 10. TO result considering the `X` axis as the printing direction.

6. Concluding Remarks

This study presented a computational methodology capable of providing initial solid designs for metal AM, and its performance was evaluated via a comparative study. The final methodology showed an improved capability of converging towards a discrete solution, having considerable relevance. In fact, a solution with a high level of intermediate densities has little practical use. However, the modified fabrication model was able to provide solutions with higher compliance when compared to the original. On the other hand, the compliance difference had limited relevance due to the small difference.

The initial self-supporting designs provided by the presented methodology allowed controlling the minimum member size and the overhang features in a closed computational environment, which was performance driven. Moreover, the resultant designs took advantage of the freedom provided by SLM, and TO played an important role in the search for optimal material distribution. Moreover, the referenced distribution can reduce the need for support structures.

Author Contributions: Conceptualization, B.B. and A.A.-C.; methodology, B.B. and A.A.-C.; software, B.B.; validation and formal analysis, B.B.; investigation, B.B.; writing, original draft preparation, B.B.; writing, review and editing, B.B., A.A.-C., and R.A.F.V.; project administration, A.A.-C.; funding acquisition, A.A.-C.

Funding: This research was funded by the Portuguese Foundation for Science and Technology (FCT) under the projects CENTRO-01-0145-FEDER-029713 by UE/FEDER through the programs CENTRO 2020 and COMPETE 2020 and UID/EMS/ 00481/2013-FCT under CENTRO-01-0145-FEDER-022083. Additional funding was provided by program CENTRO 2020 and UE/FEDER through the project CENTRO-01-0247-FEDER-024039, designated as

ADVANSS. Finally, the Portuguese Foundation for Science and Technology (FCT) provided additional funding via the scholarship SFRH/BD/120779/2016.

Acknowledgments: The authors gratefully acknowledge the financial support of the Portuguese Foundation for Science and Technology (FCT), program CENTRO 2020, and UE/FEDER. The authors also acknowledge the help of Krister Svanberg for providing MATLAB code, which was important for a successful Python implementation, and Matthijs Langelaar for providing article clarifications.

Conflicts of Interest: The authors declare no conflict of interest.

References

1. Murr, L.E.; Gaytan, S.M.; Ramirez, D.A.; Martinez, E.; Hernandez, J.; Amato, K.N.; Shindo, P.W.; Medina, F.R.; Wicker, R.B. Metal Fabrication by Additive Manufacturing Using Laser and Electron Beam Melting Technologies. *J. Mater. Sci. Technol.* **2012**, *28*, 1–14. [CrossRef]
2. Aremu A.; Ashcroft I.; Hague R.; Wildman R.; Tuck C. *Suitability of SIMP and BESO Topology Optimization Algorithms for Additive Manufacture*; Wolfson School of Mechanical and Manufacuring Engineering: Loughborough, UK, 2010.
3. Clausen, A. Topology Optimization for Additive Manufacturing. Ph.D. Thesis, DTU Mechanical Engineering, Technical University of Denmark, Kongens Lyngby, Denmark, 2016.
4. Komi, E. *Topology Optimized in Design for Additive Manufacturing*; AM-Teknologista uutta Liiketoimintaa, Report of VTT Technical Research Centre; VTT: Helsinki, Finland, 2014.
5. Matt, D.T.; Rauch, E.; Dallasega, P. Trends towards Distributed Manufacturing Systems and Modern Forms for their Design. *Procedia CIRP* **2015**, *33*, 185–190. [CrossRef]
6. Attaran, M. Additive manufacturing: The most promising technology to alter the supply chain and logistics. *J. Serv. Sci. Manag.* **2017**, *10*, 189–206. [CrossRef]
7. Attaran, M. The rise of 3-D printing: The advantages of additive manufacturing over traditional manufacturing. *Bus. Horiz.* **2017**, *60*, 677–688. [CrossRef]
8. Fera, M.; Fruggiero, F.; Lambiase, A.; Macchiaroli, R. State of the art of additive manufacturing: Review for tolerances, mechanical resistance and production costs. *Cogent Eng.* **2016**, *3*, 1261503. [CrossRef]
9. Rosen, D.W. Computer-Aided Design for Additive Manufacturing of Cellular Structures. *Comput.-Aided Des. Appl.* **2007**, *4*, 585–594. [CrossRef]
10. Weller, C.; Kleer, R.; Piller, F.T. Economic implications of 3D printing: Market structure models in light of additive manufacturing revisited. *Int. J. Prod. Econ.* **2015**, *164*, 43–56. [CrossRef]
11. Anstaett, C.; Schafnitzel, M.; Seidel, C.; Reinhart, G. Laser-based Powder Bed Fusion of 3D-Multi-Material-Parts of Copper-Chrome-Zirconia and Tool Steel. In Proceedings of the European Powder Metallurgy Association Proceedings, Milan, Italy, 1–5 October 2017.
12. Bobbio, L.D.; Otis, R.A.; Borgonia, J.P.; Dillon, R.P.; Shapiro, A.A.; Liu, Z.K.; Beese, A.M. Additive manufacturing of a functionally graded material from Ti-6Al-4V to Invar: Experimental characterization and thermodynamic calculations. *Acta Mater.* **2017**, *127*, 133–142. [CrossRef]
13. Kotoban, D.; Aramov, A.; Tarasova, T. Possibility of Multi-material Laser Cladding Fabrication of Nickel Alloy and Stainless Steel. *Phys. Procedia* **2016**, *83*, 634–646. [CrossRef]
14. DebRoy, T.; Wei, H.L.; Zuback, J.S.; Mukherjee, T.; Elmer, J.W.; Milewski, J.O.; Beese, A.M.; Wilson-Heid, A.; De, A.; Zhang, W. Additive manufacturing of metallic components—Process, structure and properties. *Prog. Mater. Sci.* **2018**, *92*, 112–224. [CrossRef]
15. Balla, V.K.; Xue, W.; Bose, S.; Bandyopadhyay, A. Laser-assisted Zr/ZrO_2 coating on Ti for load-bearing implants. *Acta Biomater.* **2009**, *5*, 2800–2809. [CrossRef] [PubMed]
16. Zhang, Y.; Sahasrabudhe, H.; Bandyopadhyay, A. Additive manufacturing of Ti-Si-N ceramic coatings on titanium. *Appl. Surf. Sci.* **2015**, *346*, 428–437. [CrossRef]
17. Fang, Z.; Lu, L.; Chen, L.; Guan, Y. Laser Polishing of Additive Manufactured Superalloy. *Procedia CIRP* **2018**, *71*, 150–154.
18. Ai, L.; Gao, X.L. Metamaterials with negative Poisson's ratio and non-positive thermal expansion. *Compos. Struct.* **2017**, *162*, 70–84. [CrossRef]
19. Wei, K.; Peng, Y.; Wang, K.; Duan, S.; Yang, X.; Wen, W. Three dimensional lightweight lattice structures with large positive, zero and negative thermal expansion. *Compos. Struct.* **2018**, *188*, 287–296. [CrossRef]

20. Holmström, J.; Partanen, J.; Tuomi, J.; Walter, M. Rapid manufacturing in the spare parts supply chain: Alternative approaches to capacity deployment. *J. Manuf. Technol. Manag.* **2010**, *21*, 687–697. [CrossRef]
21. Nickels, L. AM and aerospace: An ideal combination. *Met. Powder Rep.* **2015**, *70*, 300–303. [CrossRef]
22. Kelly, S.M. *Volume 1: Development and Measurement Analysis of Design Data for Laser Powder Bed Fusion Additive Manufacturing of Nickel Alloy 625*; Technical Report; EWI: Columbus, OH, USA, 2014.
23. Huang, Y.; Leu, M.C.; Arbor, A. Additive Manufacturing: Current State , Future Potential, Gaps and Needs, and Recommendations. *ASME J. Manuf. Sci. Eng.* **2015**, *137*, 1087-1357. [CrossRef]
24. Thompson, M.K.; Moroni, G.; Vaneker, T.; Fadel, G.; Campbell, R.I.; Gibson, I.; Bernard, A.; Schulz, J.; Graf, P.; Ahuja, B.; et al. Manufacturing Technology Design for Additive Manufacturing: Trends, opportunities, considerations and constraints. *CIRP Ann.* **2016**, *65*, 737–760. [CrossRef]
25. Thomas, D. The Development of Design Rules for Selective Laser Melting the Development of Design Rules for Selective Laser Melting. Ph.D. Thesis, University of Wales Institute, Cardiff, UK, 2009.
26. Vayre, B.; Vignat, F.; Villeneuve, F. Designing for Additive Manufacturing. *Procedia CIRP* **2012**, *3*, 632–637. [CrossRef]
27. Vayre, B.; Vignat, F.; Villeneuve, F. Identification on some design key parameters for additive manufacturing: Application on Electron Beam Melting. *Procedia CIRP* **2013**, *7*, 264–269. [CrossRef]
28. Adam, G.A.O.; Zimmer, D. CIRP Journal of Manufacturing Science and Technology Design for Additive Manufacturing—Element transitions and aggregated structures. *CIRP J. Manuf. Sci. Technol.* **2014**, *7*, 20–28. [CrossRef]
29. Klahn, C.; Leutenecker, B.; Meboldt, M. Design Strategies for the Process of Additive Manufacturing. *Procedia CIRP* **2015**, *36*, 230–235. [CrossRef]
30. Kranz, J.; Herzog, D.; Emmelmann, C.; Kranz, J.; Herzog, D. Design guidelines for laser additive manufacturing of lightweight structures in TiAl6V4. *J. Laser Appl.* **2016**, *27*, S14001. [CrossRef]
31. Lemu, H.G.; Gebisa, A.W. Design for manufacturing to design for Additive Manufacturing: Analysis of implications for design optimality and product sustainability. *Procedia Manuf.* **2017**, *13*, 724–731.
32. Sossou, G.; Demoly, F.; Montavon, G.; Gomes, S. Journal of Computational Design and Engineering An additive manufacturing oriented design approach to mechanical assemblies. *J. Comput. Des. Eng.* **2018**, *5*, 3–18.
33. Joshi, S.C.; Sheikh, A.A. 3D printing in aerospace and its long-term sustainability. *Virtual Phys. Prototyp.* **2015**, *10*, 175–185. [CrossRef]
34. Reddy K., S.N.; Ferguson, I.; Frecker, M.; Simpson, T.W.; Dickman, C.J. Topology Optimization Software for Additive Manufacturing: A Review of Current Capabilities and a Real-World Example. In Proceedings of the ASME 2016 International Design Engineering Technical Conferences and Computers and Information in Engineering Conference, Charlotte, NC, USA, 21–24 August 2016.
35. Mirzendehdel, A.M.; Suresh, K. Support structure constrained topology optimization for additive manufacturing. *Comput.-Aided Des.* **2016**, *81*, 1–13. [CrossRef]
36. Walton, D.; Moztarzadeh, H. Design and Development of an Additive Manufactured Component by Topology Optimisation. *Procedia CIRP* **2017**, *60*, 205–210. [CrossRef]
37. Allaire, G.; Dapogny, C.; Estevez, R.; Faure, A.; Michailidis, G. Structural optimization under overhang constraints imposed by additive manufacturing technologies. *J. Comput. Phys.* **2017**, *351*, 295–328. [CrossRef]
38. Guo, X.; Zhou, J.; Zhang, W.; Du, Z.; Liu, C.; Liu, Y. Self-supporting structure design in additive manufacturing through explicit topology optimization. *Comput. Methods Appl. Mech. Eng.* **2017**, *323*, 27–63. [CrossRef]
39. Sigmund, O. Morphology-based black and white filters for topology optimization. *Struct. Multidiscip. Optim.* **2007**, *33*, 401–424. [CrossRef]
40. Svanberg, K.; Svärd, H. Density filters for topology optimization based on the Pythagorean means. *Struct. Multidiscip. Optim.* **2013**, *48*, 859–875. [CrossRef]
41. Leary, M.; Merli, L.; Torti, F.; Mazur, M.; Brandt, M. Optimal topology for additive manufacture: A method for enabling additive manufacture of support-free optimal structures. *Mater. Des.* **2014**, *63*, 678–690. [CrossRef]
42. Mass, Y.; Amir, O. Topology optimization for additive manufacturing: Accounting for overhang limitations using a virtual skeleton. *Addit. Manuf.* **2017**, *18*, 58–73. [CrossRef]

43. Liu, C.; Du, Z.; Zhang, W.; Zhu, Y.; Guo, X. Additive Manufacturing-Oriented Design of Graded Lattice Structures Through Explicit Topology Optimization. *J. Appl. Mech.* **2017**, *84*, 081008-81020. [CrossRef]
44. Brackett, D.; Ashcroft, I.; Hague, R. *Topology Optimization for Additive Manufacturing*; Wolfson School of Mechanical and Manufacturing Engineering, Loughborough University: Loughborough, UK, 2011.
45. Maskery, I.; Aboulkhair, N.; Aremu, A.; Tuck, C.; Ashcroft, I.; Wildman, R.; Hague, R. A mechanical property evaluation of graded density Al-Si10-Mg lattice structures manufactured by selective laser melting. *Mater. Sci. Eng. A* **2016**, *670*, 264–274. [CrossRef]
46. Zhao, D.; Li, M.; Liu, Y. Self-supporting Topology Optimization for Additive Manufacturing. *arXiv* **2017**, arXiv:1708.07364.
47. Qian, X. Undercut and overhang angle control in topology optimization: A density gradient based integral approach. *Int. J. Numer. Methods Eng.* **2016**, *111*, 247–272. [CrossRef]
48. Garaigordobil, A.; Ansola, R. A new overhang constraint for topology optimization of self-supporting structures in additive manufacturing. *Struct. Multidiscip. Optim.* **2018**, *58*, 2003–2017. [CrossRef]
49. Mezzadri, F.; Bouriakov, V.; Qian, X. Topology optimization of self-supporting support structures for additive manufacturing. *Addit. Manuf.* **2018**, *21*, 666–682. [CrossRef]
50. Langelaar, M. An additive manufacturing filter for topology optimization of print-ready designs. *Struct. Multidiscip. Optim.* **2017**, *55*, 871–883. [CrossRef]
51. Langelaar, M. Topology optimization of 3D self-supporting structures for additive manufacturing. *Addit. Manuf.* **2016**, *12*, 60–70. [CrossRef]
52. Hoffarth, M.; Gerzen, N.; Pedersen, C. ALM Overhang Constraint in Topology Optimization for Industrial Applications. In Proceedings of the 12th World Congress on Structural and Multidisciplinary Optimisation, Braunschweig, Germany, 5–9 June 2017.
53. Gaynor, A.T.; Meisel, N.A.; Williams, C.B.; Guest, J.K. Topology Optimization for Additive Manufacturing: Considering Maximum Overhang Constraint. In Proceedings of the 15th AIAA/ISSMO Multidisciplinary Analysis and Optimization Conference, Atlanta, GA, USA, 16–20 June 2014.
54. Gaynor, A.T. Topology Optimization Algorithms for Additive Manufacturing. Ph.D. Thesis, The Johns Hopkins University, Baltimore, MD, USA, 2015.
55. Gaynor, A.T.; Guest, J.K. Topology optimization considering overhang constraints: Eliminating sacrificial support material in additive manufacturing through design. *Struct. Multidiscip. Optim.* **2016**, *54*, 1157–1172. [CrossRef]
56. Johnson, T.E.; Gaynor, A.T. Three-dimensional projection-based topology optimization for prescribed-angle self-supporting additively manufactured structures. *Addit. Manuf.* **2018**, *24*, 667–686. [CrossRef]
57. Rozvany, G.I.N.; Lewiński, T. *Topology Optimization in Structural and Continuum Mechanics*; Springer: Vienna, Italy, 2014.
58. Deaton, J.D.; Grandhi, R.V.; Deaton, J.D.; Grandhi, R.V. A survey of structural and multidisciplinary continuum topology optimization: Post 2000. *Struct. Multidiscip. Optim.* **2014**, *49*, 1–38. [CrossRef]
59. Bendsøe, M.P. Optimal shape design as a material distribution problem. *Struct. Optim.* **1989**, *1*, 193–202. [CrossRef]
60. Bendsøe, M.P.; Sigmund, O.O. *Topology Optimization: Theory, Methods, and Applications*; Springer: Berlin/Heidelberg, Germany, 2004.
61. Stolpe, M.; Svanberg, K. An Interpolation Model for Minimum Compliance Topology Optimization. *Struct. Multidiscip. Optim.* **2001**, *22*, 116–124. [CrossRef]
62. Bruns, T.E.; Tortorelli, D.A. Topology optimization of non-linear elastic structures and compliant mechanisms. *Comput. Methods Appl. Mech. Eng.* **2001**, *190*, 3443–3459. [CrossRef]
63. Bourdin, B. Filters in topology optimization. *Int. J. Numer. Methods Eng.* **2001**, *50*, 2143–2158. [CrossRef]
64. Wang, F.; Lazarov, B.S.; Sigmund, O. On projection methods, convergence and robust formulations in topology optimization. *Struct. Multidiscip. Optim.* **2011**, *43*, 767–784. [CrossRef]
65. Lange, M.; Zuhlke, D.; Holz, O.; Villmann, T. Applications of lp-Norms and their Smooth Approximations for Gradient Based Learning Vector Quantization. In Proceedings of the ESANN 2014 Proceedings, European Symposium on Artificial Neural Networks, Computational Intelligence and Machine Learning, Bruges, Belgium, 23–25 April 2014.
66. Andreassen, E.; Clausen, A.; Schevenels, M.; Lazarov, B.S.; Sigmund, O. Efficient topology optimization in MATLAB using 88 lines of code. *Struct. Multidiscip. Optim.* **2011**, *43*, 1–16. [CrossRef]

67. Svanberg, K. The method of moving asymptotes—a new method for structural optimization. *Int. J. Numer. Methods Eng.* **1987**, *24*, 359–373. [CrossRef]
68. Rozvany, G.I.N. Exact analytical solutions for some popular benchmark problems in topology optimization. *Struct. Optim.* **1998**, *15*, 42–48. [CrossRef]
69. Sigmund, O. A 99 line topology optimization code written in Matlab. *Struct. Multidiscip. Optim.* **2001**, *21*, 120–127. [CrossRef]
70. Guest, J.K.; Asadpoure, A.; Ha, S.H. Eliminating beta-continuation from Heaviside projection and density filter algorithms. *Struct. Multidiscip. Optim.* **2011**, *44*, 443–453. [CrossRef]

4.3 Laplacian smoothing as the bridge tool between TO and ALM

The transition between TO and a final smooth geometry is non-trivial and can be tackled in different ways. A possible approach uses Laplacian smoothing as the bridging tool due to its simplicity. This Laplacian approach is the scope of the present section, which is composed of an original research article entitled "Bridging between topology optimization and additive manufacturing via Laplacian smoothing". The referred study presents and evaluates an innovative algorithm, named "mutable diffusion", and compares it with the standard algorithms. Given the scope of this work, the performance evaluation uses three TO optimized parts from an aerospace industry case study with different design considerations (without and with overhang angle constraint in two distinct directions) [P5]. All the resultant geometries are shown as interactive models, that allows the reader a close inspection of resultant geometries. However, it is worth noting that the models' interactivity is lost when the original article was embedded in the present document. Alternatively, a copy of these models is provided in Appendix C.

Bridging between topology optimization and additive manufacturing via Laplacian smoothing

B. Barroqueiro*
Department of Mechanical Engineering, Centre for Mechanical Technology & Automation (TEMA),
University of Aveiro, Portugal.
Active Space Technologies, Actividades Aeroespaciais S.A., Parque Industrial de Taveiro, Portugal

A. Andrade-Campos

Department of Mechanical Engineering, Centre for Mechanical Technology & Automation (TEMA),
University of Aveiro, Portugal.

J. Dias-de-Oliveira

Department of Mechanical Engineering, Centre for Mechanical Technology & Automation (TEMA),
University of Aveiro, Portugal.

R.A.F. Valente

Department of Mechanical Engineering, Centre for Mechanical Technology & Automation (TEMA),
University of Aveiro, Portugal.

ABSTRACT

The potential of Additive Layer Manufacturing (ALM) is high, with a whole new set of manufacturable parts with unseen complexity being offered. Moreover, the combination of Topology Optimization (TO) with ALM has been seen as an advantageous combination. However, the transition between TO and ALM is a non-trivial step that requires a robust methodology. Thus, the purpose of this work is to evaluate the capabilities of adopting a commonly used methodology, named as Laplacian smoothing, as the bridging tool between TO and ALM. Several algorithms are presented and compared in terms of efficiency and performance. Most importantly, a different concept of Laplacian smoothing is presented as well as a set of metrics to evaluate the performance of the algorithms, with the advantages and disadvantages of each algorithm being discussed. In the end, the proposed mutable diffusion Laplacian algorithm is presented and exhibits less volume shrinkage and shows better preservation of some geometrical features such as thin members and edges. Moreover, a new volume constraint is presented, decreasing the resulting structural changes in the presented geometry and improving its final mesh quality.

1 Introduction

Additive Layer Manufacturing (ALM) consists in the manufacturing of 3D models layer by layer, allowing greater design freedom. In contrast, Topology Optimization (TO) represents a type of structural optimization that seeks the optimum material layout [1], thus providing the means to fully explore this freedom coming from ALM. The interplay between TO and ALM is, therefore, advantageous, defining rules of Design for Additive Manufacturing (DfAM) that allow the reduction of the number of parts involved, assembling operations, mass and, therefore, costs (*e.g.* [2–4]). Designing a part for ALM involves many steps, briefly shown in the flowchart of Figure 1, for the particular case of the space industry. The process is illustrated as a linear flow, for the sake of clarity, but iterative work between steps is expected and can easily originate

*Corresponding author: bjfb@ua.pt

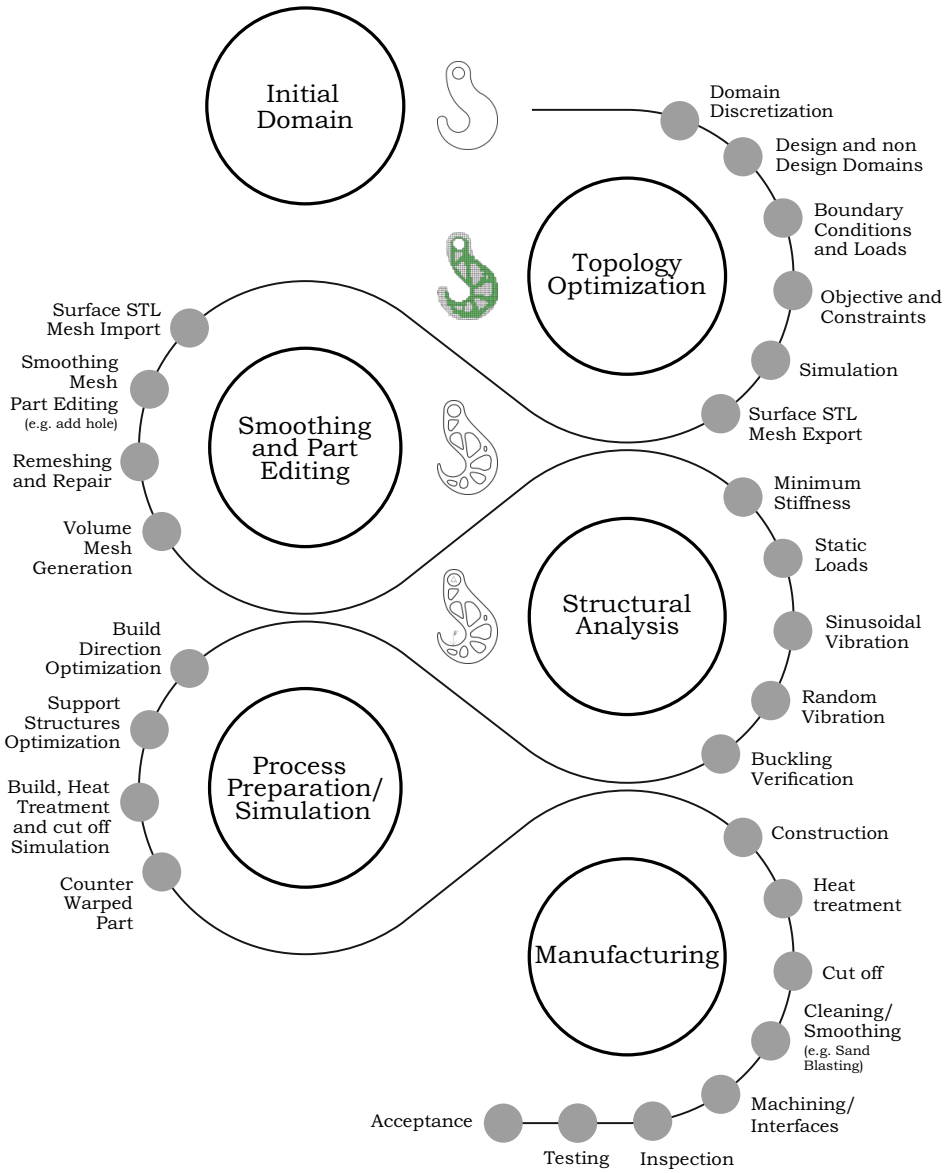

Figure 1: Engineering cycle of ALM structures for the space industry.

a recursive workflow. The engineering cycle shown in Figure 1 starts with TO followed by part smoothing, structural verification, process preparation and, finally, manufacturing. Regarding the smoothing stage of these optimized topologies, the achievement of a ready to print geometry is a non-trivial step and represents the scope of the present work.

The complexity of this step is related to the high irregularity generally present in optimized topologies and due to their discrete nature. Consequently, its conversion into a continuous, smooth and rigorous geometry is needed, and some approaches have been proposed in the literature. For instance, Kébreau *et al.* [5], and Pommatau *et al.* [6] have proposed the manual reconstruction of the optimized topologies using CAD platforms (e.g. Catia®). Alternatively, Zegard and Paulino [7] presented the use of the isosurfaces resultant from density maps of TO results, in order to provide a print-ready design. Vogiatzis *et al.* [8] and Maute *et al.* [9] have proposed the use of boundary information of the level set method in the TO, in order to generate the surface mesh of the part. Another approach consists in the application of geometry processing techniques in order to smooth the geometry. In the scope of geometry processing, there are several types of algorithms [10] such as Laplacian smoothing [11, 12], mean curvature flow [13, 14], spectral smoothing [15, 16] and feature preserving algorithms [17–19]. For instance, mean curvature and feature preserving algorithms produce remarkable results in the field of mesh denoising. However, in the scope of this work, the goal is to remove the high irregularities present in topology optimized geometries. After some research, the authors developed a preference over Laplacian smoothing algorithms, due to their performance and numerical robustness. Moreover, the Laplacian algorithms are capable of removing the referred

irregularities as demonstrated in [20, 21]. Thus, the Laplacian smoothing algorithms can be adopted to perform the bridge between TO and the smooth print-ready design. Despite being available in several commercial solutions (*i.e.* Ansys Workbench®, Hypermesh®, MSC Patran®, Netfabb®, *etc.*) due to industry needs, there is still a need in the literature for a comprehensive study regarding the performance of distinct smoothing methodologies when acting as a bridging tool between TO and ALM.

Therefore, the goal of this study is to evaluate the performance of several Laplacian smoothing methodologies when acting as bridging tools. After this benchmarking and comparative analysis, an improved Laplacian methodology is proposed, exhibiting less volume shrinkage and showing better preservation of some geometrical features such as thin members and edges. Moreover, a new volume constraint is introduced, producing less structural changes in the part and improving the final mesh quality of the presented geometry. Additionally, its performance is evaluated against the classic methodologies using several metrics. Furthermore, a convergence metric is proposed in order to provide an automatic stop criterion. Finally, the impact of this smoothing operation on a given part printability is presented and discussed.

2 Methodology

Within the scope of this work, the presented geometries are obtained using the TO methodology described in [22]. However, this approach discretizes the domain using a regular cube mesher with non-matching boundaries, due to higher simplicity and computational efficiency. These advantages are related to the implementation of the ALM fabrication model, which corresponds to a numerical algorithm that emulates the actual process in order to impose the overhang constraint [22, 23]. Additionally, the meshing technique allows the computational cost reduction in the structural analysis since all elements are identical. However, this mesher introduces a stair-case effect on the resultant optimized topologies, which needs to be removed by the smoothing methodology. Therefore, in the following sections, different Laplacian smoothing methodologies are presented, and their performance is evaluated using different metrics.

2.1 Laplacian smoothing formulation

In the scope of this work, $\mathbf{\Gamma}$ denotes a surface mesh, where $\mathbf{X}$, $\mathbf{E}$ and $\mathbf{F}$ represents its vertices coordinates, edges and faces connectivity, respectively. Additionally, $\mathbf{N}$ and $\mathbf{M}$ denote the first ring of neighbor vertices and neighbor faces, respectively. Finally, $\boldsymbol{\eta}$ denotes the face normal and the $\bar{\boldsymbol{\eta}}$ is the vertex normal orientation, which is an average orientation of neighbor faces, given by

$$\bar{\boldsymbol{\eta}}_i = \frac{1}{\left\| \sum_f \boldsymbol{\eta}_f \right\|} \sum_f \boldsymbol{\eta}_f, \quad \forall f \in \mathbf{M_i} \tag{1}$$

Mesh smoothing can be archived via a diffusion process, being mathematically formulated as

$$\frac{\partial \mathbf{X}}{\partial t} = \lambda_0 \mathbf{L}\mathbf{X}, \tag{2}$$

where t denotes time. The parameter λ_0 is the diffusion constant and $\mathbf{L}$ is the Laplacian operator that performs the vertex averaging. This operator can be defined in its simplest form by

$$\mathbf{L} = \mathbf{I} + \mathbf{K}, \tag{3}$$

$$K_{ij} = \frac{1}{\sum_j w_{ij}} \begin{cases} w_{ij}, & \text{if } j \in \mathbf{N}_i \\ 0, & \text{else} \end{cases}, \tag{4}$$

where $\mathbf{I}$ is identity matrix and w_{ij} are the weights. Constant weights are considered in Equation 4 since all elements are identical, but different weighting functions can be used (*e.g.* distance to neighbors). In order to perform the mesh smoothing, the application of the smoothing principle can be achieved in different ways.

2.1.1 Explicit classic Laplacian

The simplest way to set up a smoothing methodology is by integrating the diffusion equation (Equation 2) in time using an iterative forward Euler scheme. Thus, the resultant equation becomes

$$\mathbf{X}^k = (\mathbf{I} + \lambda \mathbf{L})\, \mathbf{X}^{k-1}, \tag{5}$$

where the constant λ corresponds to $\lambda_0 \Delta t$ if a unitary time step is considered. Moreover, k and $k-1$ correspond to the current and previous iterations, respectively. However, the constant λ must be less than one for a numerically stable process [24].

2.1.2 Implicit classic Laplacian

Another possible scheme to perform a smoothing process, is to admit that derivative should be evaluated at iteration k and, therefore, the integration becomes

$$(\mathbf{I} - \lambda \mathbf{L})\, \mathbf{X}^k = \mathbf{X}^{k-1}, \tag{6}$$

being a linear dependent system of equations and, thus, the constant λ can be larger than one [24].

2.1.3 Taubin Laplacian

The classic Laplacian smoothing is commonly used for its simplicity. However, the part volume shrinkage is a common issue. In order to tackle this issue, a second order operator $\mathbf{L}$ has been proposed [25]. Thus, the new vertex updating scheme is

$$\mathbf{X}^k = (\mathbf{I} - \lambda \mathbf{L})\, (\mathbf{I} - \mu \mathbf{L})\, \mathbf{X}^{k-1}, \tag{7}$$

corresponding to a band-pass filter. The term λ should be positive (> 0), and μ should be within the interval $\mu < -\lambda < 0$. In practice, this filter is implemented in two passes of the Laplacian filter. The first pass induces shrinkage, while the second step recovers the previous shrinkage. For a given λ, the μ constant can be estimated by

$$k_{\mathrm{pb}} = \frac{1}{\lambda} + \frac{1}{\mu}, \tag{8}$$

where k_{pb} is typically set to 0.1 [26].

2.1.4 Humphrey Laplacian

The basic principle of the Humphrey algorithm can be explained in two passes. The first pass modifies the existing mesh using the classic Laplacian and the second pass pushes the vertices back to the location of the previous iteration and/or to the original locations. The algorithm can be rearranged in the form

$$\mathbf{X}^k = (\Upsilon_0 \mathbf{I} + \Upsilon_1 \mathbf{K})\, \mathbf{X}^{k_0} + \left(\Upsilon_2 \mathbf{I} + \Upsilon_3 \mathbf{K} + \Upsilon_4 \mathbf{K}^2\right) \mathbf{X}^{k-1}, \tag{9}$$

where

$$\Upsilon_l = \begin{cases} \alpha\beta, & \text{if } l = 0 \\ \alpha(1-\beta), & \text{if } l = 1 \\ (1-\alpha)\beta, & \text{if } l = 2 \\ \alpha\beta - \alpha - 2\beta + 2, & \text{if } l = 3 \\ \beta - 1, & \text{if } l = 4 \end{cases}, \tag{10}$$

with subscript k_0 corresponding to the initial iteration before smoothing. The constant α controls the weight of the original locations, while β controls the weight of the previous location. For instance, if $\beta = 1$ there is no smoothing ($\mathbf{X}^k = \mathbf{X}^{k-1}$), or if $\alpha = 0$, the original location of vertices ($\mathbf{X}^{k_0}$) are not considered [27].

2.1.5 A new smoothing algorithm: mutable diffusion Laplacian

The smoothing algorithm, proposed in this work, shares some similarities with the explicit Laplacian algorithm. The distinctive characteristic of the algorithm is related to its diffusion value, which becomes mesh dependent. The main idea of this method is simple: the vertex close the original coordinates gets higher diffusion, while the vertex furthest from the original coordinates gets a lower diffusion, and the average diffusion is the algorithm input. Therefore, the numerical procedure can be mathematically defined as

$$\mathbf{X}^k = \left(\mathbf{I} + [\hat{\boldsymbol{\lambda}} \; ... \; \hat{\boldsymbol{\lambda}}] \circ \mathbf{L}\right)\mathbf{X}^{k-1}, \tag{11}$$

where $\hat{\boldsymbol{\lambda}}$ is formulated by

$$\hat{\boldsymbol{\lambda}} = \min\left(1, \lambda\frac{\mathbf{u}}{\bar{u}}\right) \quad \text{and} \tag{12}$$

$$\mathbf{u} = \frac{\mathbf{1}}{\left|\bar{\boldsymbol{\eta}} \cdot \left(\mathbf{X}^k - \mathbf{X}^{k_0}\right)\right| + \epsilon}. \tag{13}$$

The term ϵ has a small value to avoid division by zero, the $\mathbf{1}$ is a vector of ones with the size equal to the number of vertices ($S_{\mathbf{X}}$) and the operator "$\cdot$" denotes an inner product for all vectors stored in a row wise manner. Moreover, the Equation 13 corresponds to a Hadamard division of two vectors. Regarding Equation 11, the vector $\hat{\boldsymbol{\lambda}}$ is repeated $S_{\mathbf{X}}$ times in order to form a square matrix. Then, the referred matrix and the Laplacian operator ($\mathbf{L}$) suffer a Hadamard product, which is denoted by "$\circ$".

The physical meaning of equation 12 and 13 is to compute the vector between the current vertex coordinates and its original coordinates, and project it on its normal. The inverse of the computed distance is normalized by its average and used to rescale the diffusion value λ. A projected distance is proposed rather than a simple Euclidean distance since the Euclidean distance would penalize vertices tangential drifting. In some fields of research [17], this aspect would be positive, but within the scope of this work, drifting is wanted since it usually improves mesh quality. The "min" operator of Equation 12 is required, due to the stability limit of the explicit algorithm. Although an implicit approach could be seen as a more effective implementation (avoiding the use of "min" operator), the elements of $\hat{\boldsymbol{\lambda}}$ can differ in several orders of magnitudes, making the linear dependent system of equations ill-conditioned. Therefore, the computational cost of tackling this issue makes the approach ineffective. However, the combination of the explicit approach with the "min" operator has an additional side-effect related to a decrease of the average diffusion as the iterative process converges, in particular, if a large value of λ is used.

2.2 Volume Constraint

Volume shrinkage during Laplacian smoothing is a well-known issue. However, the passband Laplacian or Humphrey Laplacian can minimize this issue if the empirical constants are finely tuned. On the other hand, the classic Laplacian (either explicit or implicit) or the proposed mutable diffusion Laplacian requires some sort of constraint in order to minimize volume shrinkage. Within the scope of this work, two volume constraints are presented.

2.2.1 Volume constraint A

The first constraint corresponds to vertex rescaling [24], being formulated as

$$\mathbf{X}^k = \mathbf{X}^k\left(\frac{V^{k_0}}{V^k}\right)^{\frac{1}{3}}, \tag{14}$$

where the parameter V is the volume delimited by the mesh $\mathbf{M}$ at the superscript iteration.

2.2.2 Volume constraint B

The second volume constraint, proposed in this work, uses the vertex normals to compute a mesh dilation in order to compensate for the shrinkage. Thus, the constraint can be formulated as

$$\mathbf{X}^k = \mathbf{X}^k + \bar{\boldsymbol{\eta}}\frac{\partial \oplus}{\partial V}(V^{k_0} - V^k), \tag{15}$$

where $\oplus$ corresponds to the linear dilation parameter. This parameter indicates the magnitude of vertices translation oriented according to its normal.

2.3 Evaluation Metrics

In order to avoid large volume shrinkage during smoothing, the use of small values of the diffusion constant is advised. However, the number of required iterations also increases and discovering the ideal number of iterations becomes an issue. On the one hand, a reduced number of iterations can lead to unsmooth solutions. On the other hand, a large number of iterations can lead to over-smoothing. Within the scope of this work, the Authors propose a metric for convergence evaluation given by

$$\kappa = \frac{1}{S_{\mathbf{X}}} \sum_{i \in \mathbf{X}} \max \left(\bar{\boldsymbol{\eta}}_i \cdot \boldsymbol{\eta}_f \right), \ \forall f \in \mathbf{M}_i. \tag{16}$$

A deviation of κ lower than 0.01% is considered as the convergence stop criterion (unless otherwise stated). Thus, it assumes that the solution is already stabilized in terms of shape. Additionally, a high value of κ indicates that the geometry contains many flat areas (group of neighboring triangular faces with the same orientation) and a κ equal to one would mean that the geometry under smoothing is just a portion of a plane.

In this work, there are the reference and the smooth designs. On the one hand, the user wants to remove all the irregularly of the reference design. On the other hand, the user disapproves the loss of structural performance and/or printability. Thus, the metrics used to evaluate the smooth design and the process efficiency are: (i) number of iterations to converge (It); (ii) computational time; (iii) Volume of the Bounding Box (VBB); (iv) part inertia (IX, IY and IZ for axis OX, OY and OZ, respectively); (v) compliance variation (CX, CY and CZ for axis OX, OY and OZ, respectively) when compared with reference design; and (vi) the mesh quality of the smooth design (mean aspect ratio and mean skew angle[1]).

2.4 Implementation

The presented Laplacian smoothing algorithms have been implemented in Python 3.7 and the code is merged in a high-level module entitled Trimesh. Its source code is available on Github [28] and the regular user can access it via Conda environment [29], for instance. The main advantage of this environment is related to the sharp learning curve, being particularly interesting to quickly test new algorithm concepts. Auxiliary codes to import the skin of 3D FE models are available, as well as tools to generate volume mesh (for structural analysis) after smoothing via Gmsh SDK [30].

3 Results

Several smoothing results from different meshed parts are presented in this section. The smoothing algorithms are referred as follows: (i) ELA: Explicit Laplacian with volume constraint A; (ii) ILA: Implicit Laplacian with volume constraint A; (iii) ELB: Explicit Laplacian with volume constraint B; (iv) ILB: Implicit Laplacian with volume constraint B; (v) TL: Taubin Laplacian; (vi) HL: Humphrey Laplacian; and (vii) MDLB: Mutable Diffusion Laplacian with volume constraint B. If no volume constraint is used, the letters A or B are dropped.

3.1 Efficiency and volume shrinkage in Laplacian smoothing for standard solids

Laplacian smoothing is known to produce volume shrinkage and the proposed MDL smoothing is no exception. Nevertheless, the comparison of its performance against the classic algorithm is an important source of information to understand its behavior. Table 1 provides a comparison between the EL and the MDL in terms of convergence, efficiency and volume shrinkage for primitive solids (cube, sphere and cone). The characteristic length of the solids is unitary, being meshed with an element size of 0.05 and 0.025 for meshes A and B, respectively.

[1] Corresponds to the smallest angle in a triangular element.

Table 1: Comparison of the EL and MDL in terms of convergence efficiency and volume shrinkage.

Solids	Laplacian	Mesh					
		A			B		
		N^{er} iterations	Volume shrinkage	Time ratio	N^{er} iterations	Volume shrinkage	Time ratio
Sphere	EL	14	0.49%	0.14	20	0.18%	0.074
	MDL	34	0.62%	0.75	36	0.20%	1.12
Cube	EL	28	2.08%	0.28	31	0.61%	0.12
	MDL	39	1.32%	0.86	45	0.45%	1.40
Cone	EL	21	1.64%	0.21	25	0.53%	0.093
	MDL	33	1.00%	0.726	45	0.44%	1.40

Table 2: Smoothing algorithms results in different solids and mesh refinement.

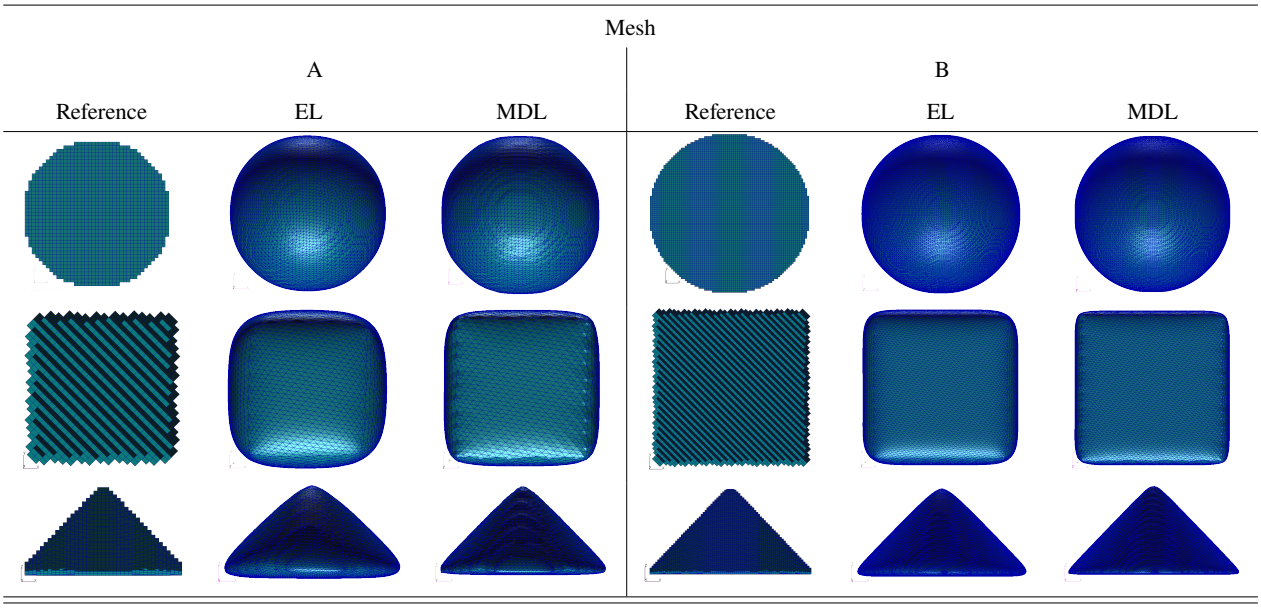

From Tables 1 and 2, it can be seen that the mutable diffusion Laplacian smoothing shows less volume shrinkage for prismatic solids (cube and cone). Depending on the mesh and shape, the reduction of volume shrinkage can vary between 20% to 50%. In spherical solids, it produces higher volume shrinkage, but the sphericity is maintained and, thus, a volume constraint can fully address this issue. In contrast, the additional volume shrinkage produced by the explicit Laplacian leads to rounding of the edges of the cube, which cannot be tackled by a volume constraint. In short, the mutable diffusion Laplacian algorithm provides designs with higher robustness. The main drawback of this algorithm is the number of iterations required to converge. Moreover, the computational cost per iteration also increases due to the need of vertex normals. Additionally, Table 2 provides a comparison of computation time of each smoothing operation (Time ratio). It should be highlighted that the referred time is dimensionless since it was divided by the computation of time of laplacian operator $\mathbf{L}$.

3.2 Smoothing TO designs

The aim of this section is to evaluate the performance/effectiveness of the smoothing algorithms (ELA, ILA, ELB, TL, HL and MDLB) in removing the staircase effect present on optimized topologies. The previously enumerated smoothing algorithms are applied to three designs resultant from the same design domain with different constraints. The first design does not have an overhang constraint (T0). The second design has an overhang constraint and the print direction is given by axis OZ (T1), while the third design has also an overhang constraint, but the printing direction is given by OX-axis (T2). The

Reference row of Table 3 provides an interactive 3D model of T0, T1 and T2 designs[2].

Table 3: Interactive 3D models of the reference and the smooth designs.

	TO	T1	T2
Reference	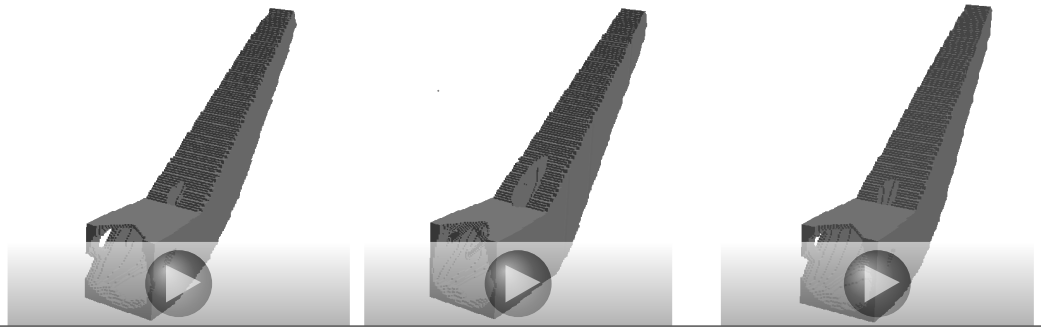		
ELA			
TL	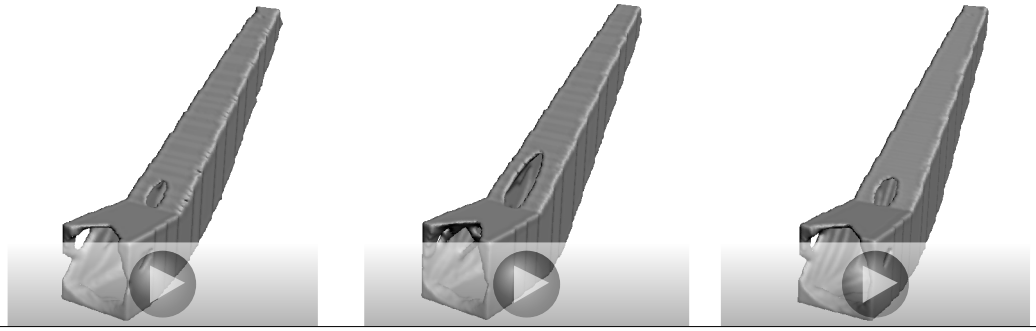		
MDLB			

Figure 2 describes the first 100 iterations of smoothing algorithms previously enumerated in terms of convergence, VBB, inertia, aspect ratio and skew angle on the T0, T1 and T2 topologies. However, the algorithms converge earlier than one hundred iterations as shown in Figure 2. It should be highlighted that the convergence criteria of Equation 16 is used. Figure 3 compares the converged solution of each smoothing algorithm in the three reference topologies in terms of It, VBB, I X, I Y, I Z, C X, C Y, C Z and mesh quality (aspect ratio and skew angle). For the same diffusion value (0.5), the explicit or implicit

[2]Adobe Acrobat is recommended for visualization of these interactive models and, with right click, an option for full screen visualization is available.

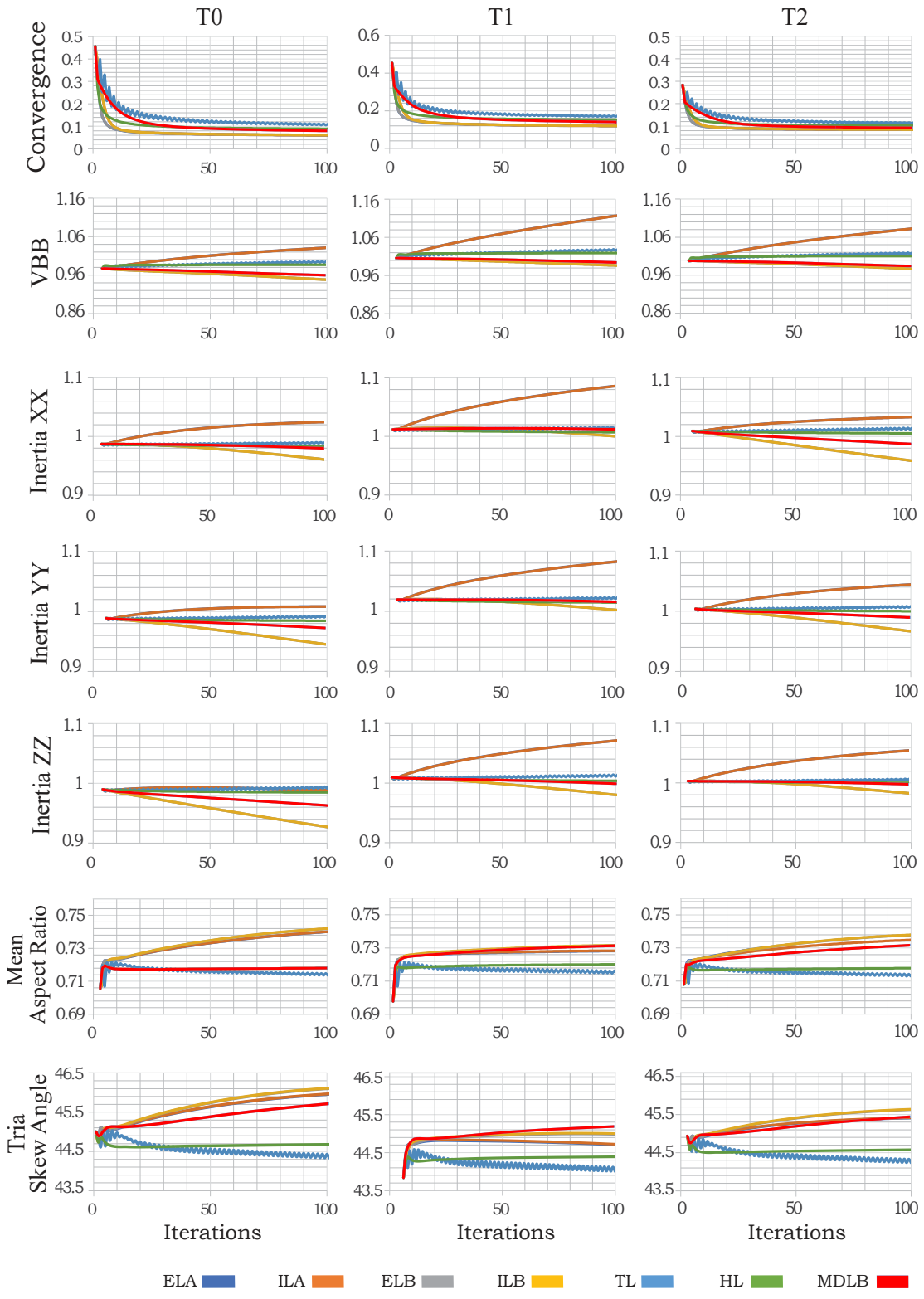

Figure 2: Comparison of the time evolution of different smoothing algorithms in term convergence, VBB, inertia, aspect ratio and skew angles.

time integration does not provide relevant differences in the selected metrics. In contrast, the volume constraint produces relevant differences. More important, but not visible on the chosen metrics, is that the volume constraint A promotes element

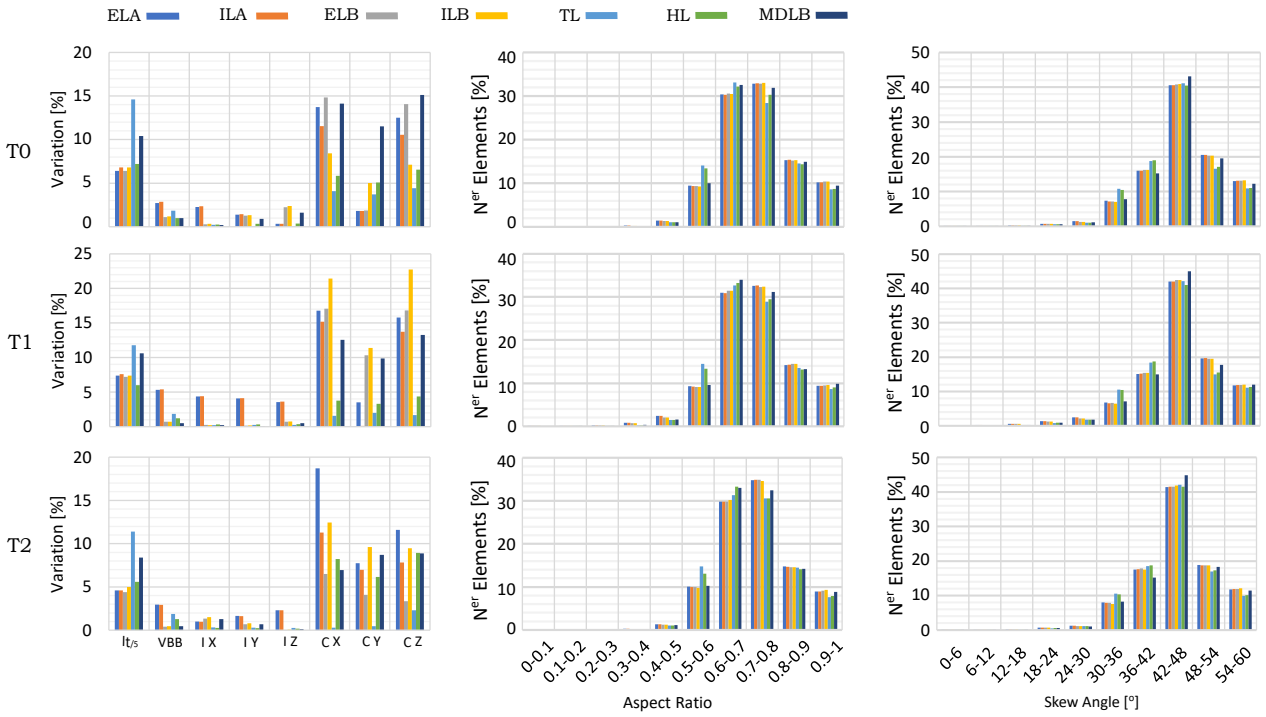

Figure 3: Comparison of the smoothing algorithms converged solution.

collapse. Regarding VBB, the volume constraint A produces stretching of the part, leading to an unwanted VBB increase in time. Although the volume constraint B produces shrinkage, the volume variation is considerably smaller in the tested topologies. Regarding inertia, the volume constraint A produces higher variations in a mean perspective. Taking into account the load case used in the topology optimizations responsible for the topologies T0, T1 and T2, the compliance before and after smoothing is compared for OX (C X), OY (C Y) and OZ (C Z) axis. Despite not being possible to identify a clear trend, a deviation of 10-20% can be expected.

In a naked-eye analysis, designs produced by ELA, ILA, ELB and ILB are similar, and therefore it is difficult to objectively evaluate any differences. Thus, without the metrics, no relevant conclusions can be stated. In the same manner, the designs produced by TL and HL are also similar. Therefore, Table 3 enumerates the designs for produced ELA, TL and MDLB for the reference designs TO, T1, T2 only.

The classic Laplacian algorithms (ELA, ILA, ELB and ILB) can remove the stair-case effect present in the topology optimized design. However, in some situations these may produce unwanted over-smoothing. For instance, the design T1 processed by ELA algorithm is an example of over-smoothing, which can be visualized in Table 3 as an interactive 3D model (or in the static Figure 4). On the other hand, the designs produced by TL or HL show high surface irregularity, being less capable of removing the stair effect of the optimized topology. Finally, the MDLB designs provide an intermediate solution

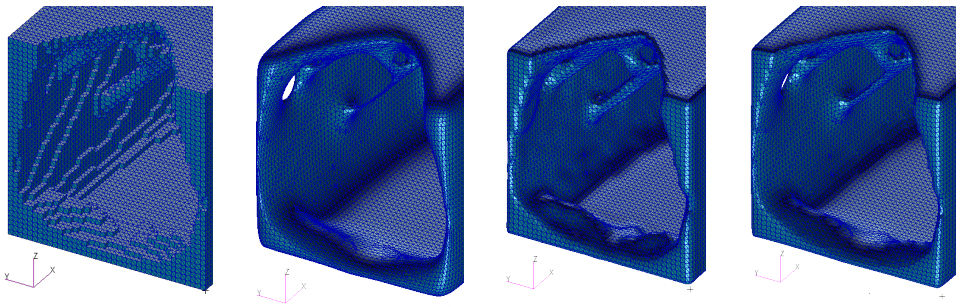

(a) Ref (b) ELA (c) TL (d) MDLB

Figure 4: Results of the smoothing algorithms for topology T1, highlighting over smoothing of a structural member.

that is capable of partially removing the stair-case effect and providing less over-smoothing. However, this algorithm requires more iterations to converge, which is depicted in Figure 3.

Regarding computational cost, the cost per iteration of ELA, ILA, ELB, ILB, TL, HL and MDLB represents 0.122, 0.811, 0.311, 0.989, 0.004, 0.011 and 0.322 of the **L** operator's computational cost, respectively, considering a 280000 faces mesh. As expected, the implicit algorithms require higher computational cost and the TL algorithm has the lowest computational cost per iteration, but a higher number of iterations is required. Regarding MDLB, its computational cost is identical to ELB, meaning the computation of the mutable diffusion vector $\hat{\boldsymbol{\lambda}}$ has limited relevance in practical terms. Regarding volume constraints, the volume constraint B has a higher computational cost, due to the computation of vertex normals. In large meshes, this can increase the computational cost to prohibitive levels, but the methodology of constraint B does not require normals update at every iteration. The methodology only requires vertex normals computation at the end of the first iteration, and therefore the subsequent iterations can be performed without updating the vertex normals. The cost of this simplification is related to a decrease of mesh quality of the MDLB smooth designs.

3.2.1 Printability

Although, the designs T1 and T2 are optimized to be self-supporting, smoothing operations produces areas with critical overhang angles that may need support structures. In order to produce self-supporting substructures, the constrained TO algorithm uses sharp edges which are partially rounded by the Laplacian algorithms. Figure 5 describes a conceptual example of the phenomena under discussion [21]. Taking as reference the solutions produced by the algorithm MDLB,

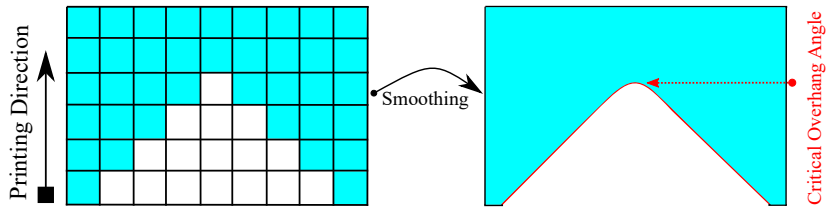

Figure 5: Effect of the smoothing algorithm in the optimized topologies with overhang constraint [21].

Figure 6 compares the volume of support structures required without (T0) and with (T1, T2) the overhang constraint for the two distinct printing directions. The criteria for the support structures generation are the typical values available on Netfabb® 2019, considering a selective laser melting process. The smooth design of T1 was initially optimized to be self-supporting.

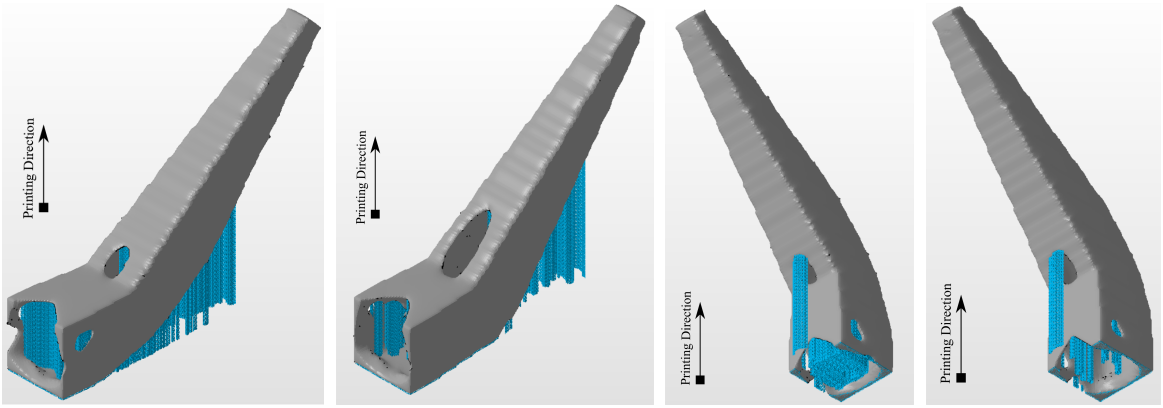

(a) T0 (b) T1 (c) T0 (d) T2

Figure 6: Comparison of the volume of support structures without (T0) and with (T1, T2) the overhang constraint for the two distinct printing directions.

However, the resultant smooth design still requires support structures as shown in Figure 6(b), due to the smoothing operation. Additionally, the smooth design of T2, which is shown in Figure 6(d), follows the same rationale. Nonetheless, for the same printing direction, the use of the overhang constraint greatly reduces (not eliminate) the need for support structures. Table 4

provides a comparison of the needed volume of support structures without (T0) and with (T1, T2) the overhang constraint for the two distinct printing directions.

Table 4: Comparison of the volume of the support structures.

	Volume of support structures		
	Direction 1	Direction 2	Reduction [%]
T0	7.2	3.9	45.8
T1/T2	3.3	1	69.7
Reduction [%]	54.2	74.4	

Even if the overhang constraint is considered, the printing direction can affect the residual volume of support structures. Nonetheless, other variables can be considered in the choice of optimal printing direction, such as height of the build or maximization of parts per build, or simply the available footprint of the machine.

4 Conclusions

The bridging between ”topology optimized” and ”print-ready” designs requires some non-trivial tasks. In this work, several Laplacian algorithms were presented and compared in terms of efficiency and performance. The concept of mutable diffusion (instead of constant value) was proposed and exhibits a promising behavior in terms of structural indicators. Furthermore, the MDL produces less volume shrinkage and shows better preservation of some geometrical features such as thin members and edges. Moreover, the presented volume constraint B, when compared with A, introduces less structural changes in the part and improves the final mesh quality. The algorithm can partially remove the stair-case effect present on optimized topologies without producing over-smoothing and thinning of some structural members.

Regarding volume constraints, the volume constraint A proved to have poor performance and low numerical robustness due to promoting element collapse of the mesh. Moreover, it produces unwanted stretching of the part over time. The volume constraint B proved to have higher performance and numerical robustness since it does not promote element collapse of the mesh and produces smaller changes in VBB.

Concerning the printability of a part, this is negatively affected by the smoothing operation. However, the designs that consider the overhang constraint considerably uses fewer supporting structures when compared with designs that do not consider overhang constraint.

Acknowledgements

The authors gratefully acknowledge the financial support of the Portuguese Foundation for Science and Technology (FCT) under the projects CENTRO-01-0145-FEDER-029713 by UE/FEDER through the programs CENTRO 2020 and COMPETE 2020, and UID/EMS/ 00481/2013-FCT under CENTRO-01-0145-FEDER-022083. Financial support of program CENTRO 2020 and UE/FEDER is acknowledged through the project CENTRO-01-0247-FEDER-024039, designated as ADVANSS. B. Barroqueiro also acknowledges the financial support by the FCT through the scholarship SFRH/BD/120779/2016.

References

[1] Aremu, A., Ashcroft, I., Hague, R., Wildman, R., and Tuck, C., 2010. “Suitability of SIMP and BESO Topology Optimization Algorithms for Additive Manufacture”. *Wolfson School of Mechanical and Manufacuring Engineering*.

[2] Barroqueiro, B., Andrade-Campos, A., Valente, R. A. F., and Neto, V., 2019. “Metal additive manufacturing cycle in aerospace industry: A comprehensive review”. *Journal of Manufacturing and Materials Processing,* **3**(52).

[3] Rosen, D. W., Seepersad, C., Simpson, T. W., and Williams, C. B., 2015. “Special issue: Design for additive manufacturing: A paradigm shift in design, fabrication, and qualification”. *Journal of Mechanical Design, ASME,* **137**, pp. 110301–110302.

[4] Schmelzle, J., Kline, E. V., Dickman, C. J., Reutzel, E. W., and Simpson, T. W., 2015. “(re)designing for part consolidation: Understanding the challenges of metal additive manufacturing”. *Journal of Mechanical Design,* **137**, pp. 111404–111416.

[5] Kébreau, S., Cambrésy, D. P., Dröse, A., Gröne, V., Schimanski, K., and Syassen, F., 2016. "Maturation of additive manufacturing for implementation into ariane secondary structures: Overview and status of "alm iscar"". In 14th European Conference on Spacecraft Structures, Materials And Environmental Testing.

[6] Pommatau, G., Montredon, F., Carlino, A., Salvi, M., Kot, E., Clement, F., and Abed, S., 2016. "Engineering design cycle for an additive layer manufactured secondary structure, from concept to final validation". In Thales Alenia Space Comunication.

[7] Zegard, T., and Paulino, G. H., 2016. "Bridging topology optimization and additive manufacturing". *Structural and Multidisciplinary Optimization,* **53**(1), Jan, pp. 175–192.

[8] Vogiatzis, P., Chen, S., and Zhou, C., 2017. "An open source framework for integrated additive manufacturing and level-set-based topology optimization". *Journal of Computing and Information Science in Engineering,* **17**, pp. 41012–41022.

[9] Maute, K., Tkachuk, A., Wu, J., Jerry Qi, H., Ding, Z., and Dunn, M. L., 2015. "Level set topology optimization of printed active composites". *Journal of Mechanical Design, ASME,* **137**, pp. 111402–111415.

[10] Bærentzen, J., Gravesen, J., Anton, F., and Aanæs, H., 2012. *Guide to Computational Geometry Processing: Foundations, Algorithms, and Methods*. Springer.

[11] Vartziotis, D., and Himpel, B., 2014. Laplacian smoothing revisited.

[12] Liu, T., Chen, M., Song, Y., Li, H., and Lu, B., 2017. "Quality improvement of surface triangular mesh using a modified laplacian smoothing". *PLoS One,* **12**(9), pp. 1–16.

[13] Ohtake, Y., Belyaev, A., and Bogaevski, I., 2001. "Mesh regularization and adaptive smoothing". *Computer-Aided Design,* **33**(11), pp. 789 – 800.

[14] Duarte, M. E., and Sacht, L., 2017. "Mean curvature flow and applications". In 30th Conference on Graphics, Patterns and Images SIBGRAPI 2017, pp. 1–4.

[15] Vallet, B., and Lévy, B., 2008. "Spectral geometry processing with manifold harmonics". *Computer Graphics Forum,* **27**(2), pp. 251–260.

[16] Zhang, H., Van Kaick, O., and Dyer, R., 2010. "Spectral mesh processing". *Computer Graphics Forum,* **29**(6), pp. 1865–1894.

[17] Fleishman, S., Drori, I., and Cohen-Or, D., 2003. "Bilateral mesh denoising". *ACM Trans. Graph.,* **22**(3), July, pp. 950–953.

[18] Wei, M., Shen, W., Qin, J., Wu, J., Wong, T.-T., and Heng, P.-A., 2013. "Feature-preserving optimization for noisy mesh using joint bilateral filter and constrained laplacian smoothing". *Optics and Lasers in Engineering,* **51**(11), pp. 1223 – 1234.

[19] Li, T., Liu, W., Liu, H., Wang, J., and Liu, L., 2019. "Feature-convinced mesh denoising". *Graphical Models,* **101**, pp. 17 – 26.

[20] Dede, E. M., Joshi, S. N., and Zhou, F., 2015. "Topology optimization, additive layer manufacturing, and experimental testing of an air-cooled heat sink". *Journal of Mechanical Design, ASME,* **137**, pp. 111403–110312.

[21] Hoffarth, M., Gerzen, N., and Pedersen, C., 2017. "ALM Overhang Constraint in Topology Optimization for Industrial Applications".

[22] Barroqueiro, B., Andrade-Campos, A., and Valente, R. A. F., 2019. "Designing self supported slm structures via topology optimization". *Journal of Manufacturing and Materials Processing,* **3**(3).

[23] Langelaar, M., 2017. "An additive manufacturing filter for topology optimization of print-ready designs". *Structural and Multidisciplinary Optimization*, pp. 871–883.

[24] Desbrun, M., Meyer, M., Schröder, P., and Barr, A. H., 1999. "Implicit fairing of irregular meshes using diffusion and curvature flow". In Proceedings of the 26th Annual Conference on Computer Graphics and Interactive Techniques, SIGGRAPH '99, ACM Press/Addison-Wesley Publishing Co., pp. 317–324.

[25] Taubin, G., 1995. "A signal processing approach to fair surface design". In Proceedings of the 22Nd Annual Conference on Computer Graphics and Interactive Techniques, SIGGRAPH '95, ACM, pp. 351–358.

[26] Taubin, G., 2000. "Geometric Signal Processing on Polygonal Meshes". In Eurographics 2000 - STARs, Eurographics Association.

[27] Vollmer, J., Mencl, R., and Müller, H., 1999. "Improved laplacian smoothing of noisy surface meshes". *Computer Graphics Forum,* **18**(3), pp. 131–138.

[28] Haggerty, M. D., Version 2.37.27, 2019. Trimesh. Computer Software avaialable in `https://github.com/mikedh/trimesh`.

[29] Continuum Analytics, Version 4.7.5, 2019. Conda. OS-agnostic, system-level binary package and environment manager avaialable in `https://conda.io`.

[30] Geuzaine, C., and Remacle, J.-F., 2009. "Gmsh: a three-dimensional finite element mesh generator with built-in pre- and post-processing facilities". *International Journal for Numerical Methods in Engineering,* **79**(11), pp. 1309–1331.

Chapter 5

Final remarks

5.1 Conclusions

Additive Manufacturing (AM) is growing more rapidly than ever and has the potential to revolutionize the way products are designed and manufactured. With some patents expiring, AM machines suppliers are emerging (*e.g.* Adira - This Portuguese company is entering the market) and many others are already available. In the space industry, several cost-effective examples are available, where cost and weight reductions were verified. Project calls are being opened to finance its further development (*e.g.* ESA Projects), since its potential is widely accepted. Nonetheless, their field of application is restricted to complex parts (weight, materials and/or shape).

Regarding structural robustness, the resultant mechanical properties of Ti6Al4V show better static properties than the brought counterparts, but its repeatability is still a challenge as well as its standardization. Either raw material or process-induced, micro-structural defects are the cause of the questionable repeatability (high results dispersion in the fatigue behavior). Thus, more experimental testing is needed. Regarding the macroscopic properties of referred material, its characterization using classic methods is expensive and time-consuming. Thus, a methodology for designing heterogeneous specimens has been presented with some success as well as a smooth indicator to estimate their performance. The referred indicator can capture the stress states' richness of the specimen and penalizes solutions with stress concentrations or unstressed material.

The ALM engineering cycle must be rethought to reach its full potential and despite the existence of many tools, there is still a lack of proper unification and maturity. Moreover, the integration of manufacturing constraints in the design methodologies is still in its infancy. In the scope of this work, a computational methodology capable of providing initial solid designs for metal ALM is presented, and its performance was evaluated via a comparative study. Moreover, the presented methodology allows some control over the final designs in terms of minimum member size and overhang features in a closed computational environment.

The bridging between "topology optimized" and "print-ready" designs requires some non-trivial tasks. In this work, several Laplacian algorithms were presented and compared in terms of efficiency and performance. The new concept of mutable diffusion is introduced, exhibiting a promising behavior in terms of structural indicators. The algorithm can partially remove the stair-case effect present on optimized topologies without producing over-smoothing and thinning of some structural members. Moreover, a new volume constraint is also proposed, which exhibits less deterioration of structural indicators and mesh quality. Concerning the printability of a part, the smoothing operation may have a negative effect on the TO self-supporting topology. However, an important reduction in the volume of supporting structures has been observed in the presented case study.

Regarding industrial contributions, the opto-mechanical case study (LLM) is an example, where the functional requirements supersede some of the ALM design limitations. In fact, the design driver were functional requirements and the fabrication limitations had to be mitigated by other means (*e.g.*

optimizing print directions and support structures). Despite the optimization of the print direction, the persistent overhang features exhibited poor surface finish and had to be post-processed. Moreover, excessive deformation was also detected and had to be mitigated using over-thickness, which was machined afterward. In fact, due to the slenderness of the structure, the machining operation raised several problems, which led to the development of an auxiliary structure that ensured a stress-free clamping of LLM (avoid spring back after machining).

In short, the presented work made some relevant contributions across the engineering cycle of ALM namely at the mechanical Ti6Al4V characterization, topology optimization, and Laplacian smoothing. Moreover, a new methodology and heterogeneous specimen are proposed as an alternative, providing richer stress states and, consequently, a more valuable mechanical test.

5.2 Open source contribution

In this work, improvements for the ALM engineering cycle are proposed and new algorithms are presented. In order to contribute to the scientific community, the resultant python codes were rewritten, optimized and integrated into a greater open-source software module entitled "Trimesh" [3], which which has the goal of providing a fully-featured and well-tested library for easy manipulation and analysis of triangular surface meshes.

The software contribution added some important features to the referred module, such as: (i) TO capability with minimum member size and overhang angle constraints and (ii) Laplacian smoothing algorithms, which includes classic Laplacian (both explicit and implicit integration), Taubin, Humphrey and mutable diffusion algorithms. It is worth noting that the added functionality is self-contained, all minor tasks such as (i) importing geometry files for the definition of design domain or (ii) mesh generation or (iii) transition between surface and volume mesh or (iv) 3D node picking for boundary conditions definition are available [C3, C5].

Regarding the implementation, the software contribution is written in Python and, thus, provides high readability for the user. The TO algorithm uses a regular cube approach with precomputed stiffness matrices for a more efficient assembling and solving. Furthermore, it provides average computations suitable for large meshes since optimized c-libraries such as Numpy and Scipy were used. Regarding result's visualization, the algorithm uses an OpenGl framework, which allows large mesh visualization and manipulation. For further details consult Barroqueiro *et al.* [C3] and the source code is available on Github [3].

5.3 Future Work

Considering the work presented, future developments may be outlined. According to the presented work, the engineering cycle of ALM structures for aerospace structures was systematized and, more important, relevant contributions were made. However, these contributions can be further developed. Regarding mechanical characterization, more macroscopic testing is certainly needed but it may be insufficient. Microscopic testing may provide more information regarding the dispersion of the results. Due to time and economic reasons, heterogeneous specimens are proposed in order to increase the level of information per test. However, the presented methodology is still in its "infancy" and could undergo improvements. In an ideal scenario, the performance indicator would be included in the objective function in order to perform an effective search of the ideal geometry. However, the non-linearity of the problem has proven to be too high and, despite the efforts, the process has no numerical stability, being unable to converge to a solution so far.

Regarding topology optimization, the minimum member and overhang angles are already included in the presented methodology. However, additional constraints can be added, such as maximum member size (avoiding large differences in thickness improves its ALM fabrication) or no cavities formation (avoiding extraction holes for unmelted powder). An additional constraint that has the

potential to improve the ALM designs, is related to the process' physics. Depending on the process parameterization and the geometry to be fabricated, the amount of heat input to the part can be highly uneven and, therefore, some areas can suffer excessive heating (vaporization issues named hot spots) or insufficient heating (unmelted powder named cold spots). Thus, the inclusion of this information as an additional constraint to TO methodology would be very attractive, but it is a challenging problem due to computational costs. An inexpensive way of modeling the ALM fabrication needs to be developed in order to provide qualitative information (no need for exact quantification) regarding the formation of hot and cold spots.

Regarding Laplacian smoothing, the concept of mutable is introduced and shows promising behavior. However, there are opportunities for improvement. The mutable diffusion vector is computed based on projected distances, but other parameters can be added to the model to improve the algorithm performance. For instance, the use of the vertex normals of neighbor vertices can be a promising approach to improve the edge awareness of the algorithm.

Intentionally blank page.

Appendix A

Business model proposal

Nowadays, the AM market is growing and, therefore, business opportunities are emerging. Thus, this appendix provides a preliminary business model proposal. Some research regarding market size was performed, being available in the present appendix as an article. A list of opportunities (products needed by industry) and their threats are presented, being present in software's competitors and/or patents. Regarding the business idea and its value proposition, these are briefly presented as well as market implementation, customer segments, needed resources, and possible sources of costs and revenues.

AMISAS: Additive Manufacturing Integrated Solution for Accurate Simulation

Bruno Barroqueiro

Abstract

A summarized and preliminary business model proposal is presented in terms of market size, opportunities and competitors, business idea, value proposition, market implementation, costumers' segments, starting needed resources, and finally, the information is summarized and systematized in a canvas model.

Keywords: Business Model; Additive Manufacturing; Topology Optimization; Simulation;

Business Model Proposal

Market

Metal Additive Manufacturing (MAM) is rapidly growing, exceeding 950M€ in 2016 and, by 2026, a 6600M€ revenue is forecasted [1]. For instance, titanium additive manufactured parts are expected to reach a revenue of 330M€ in 2020 or 950M€ in 2024 [2]. Considering a typical cost breakdown of this technology, the design stage (engineering) represents 15% of the costs involved, which can be reduced with the development of the proper methodologies. Given the new manufacturing freedom given by AM, the current engineering cycle needs to be rethought. A whole new set of lightweight structures can be designed and produced, where variables such as mass reduction or structural stiffness can be maximized. On the one hand, Additive Manufacturing (AM) consists in the construction of a 3D model layer by layer, allowing great design freedom. On the other hand, Topology Optimization (TO) is a type of structural optimization that seeks the optimum material layout [3] and, thus, provides the means for intelligently explore the referred freedom. In the space industry, components with buy to fly ratios of 10:1 or even 20:1 are attractive applications [4]. This aligned with fact that space materials such as titanium are expensive and difficult to process with other technologies (*i.e.* difficult to machine due to hardness and high chemical reactivity - oxygen and high temperature), making AM a suitable candidate. Therefore, the proposed technology has high applicability and importance. In this way, their interconnection has proved to be advantageous [5]. Moreover, Figure 1 illustrates their interplay as well as their main steps and key advantages.

Opportunities Search and Competition

Given the rapid growth of this new market, new opportunities are emerging. In order to identify them in a structured way, a list of problems of the referred industry was listed

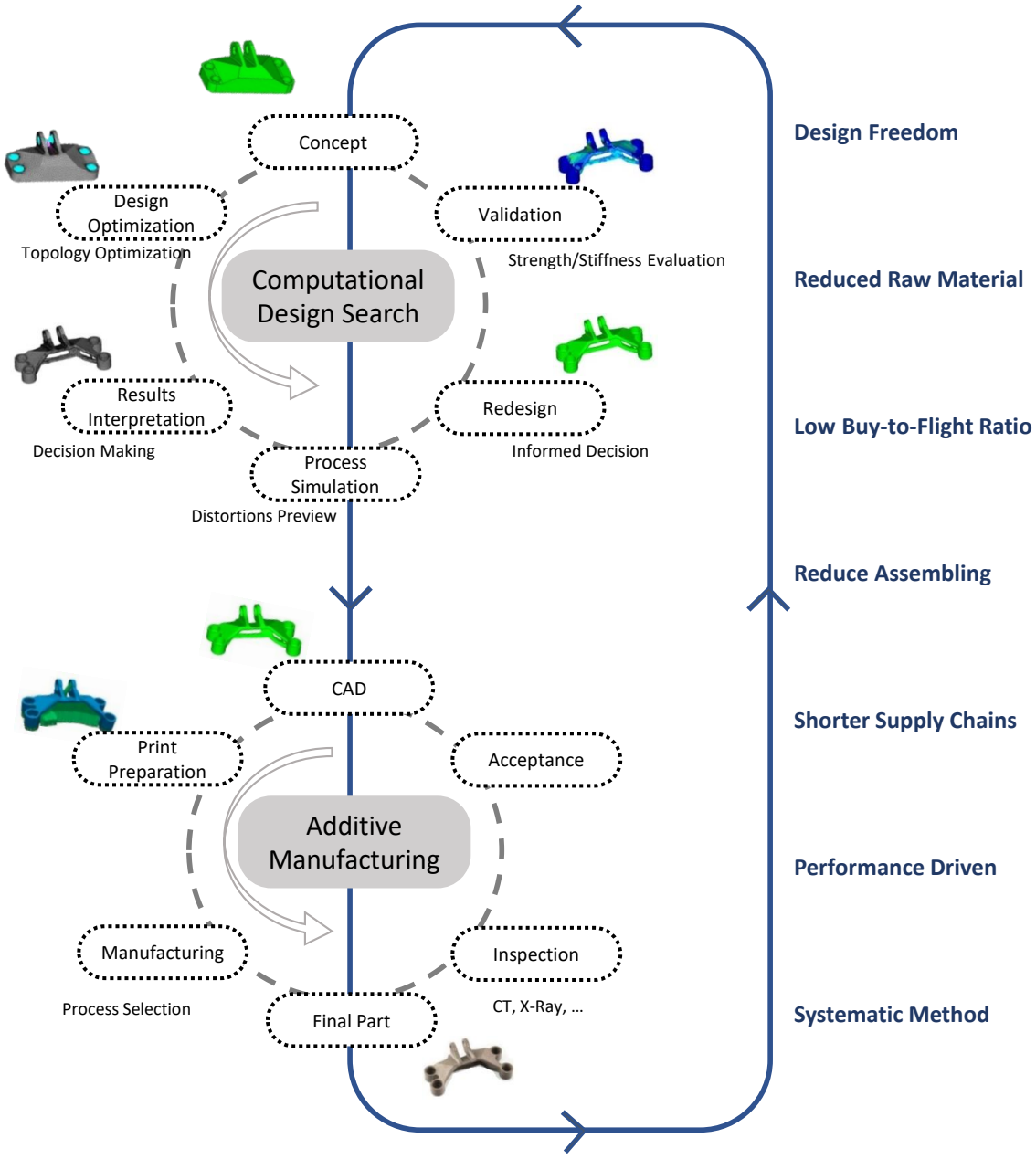

Figure 1: The interplay between Additive Manufacturing and Topology Optimization [6].

and organized. Then, possible solutions for the existent problems were listed as well as the needed technology. Finally, this analysis originated four products. Table 1 summarizes the whole process.

Despite the pertinence of the previous products, the competition may turn it unattractive (*i.e.* the appearance of a patent on the subject or an identical software). In order to address this issue, an enumeration of the possible competitors was performed for software in Table 2 and for Patents in Table 3.

Regarding Metal Additive Manufacturing (MAM) simulation (Product 1 - Table 1),

Table 1: Problem, Solution, Technology and Product (PSTP).

Problem	Solution	Technology	Product
There is the need for reliable solutions from MAM	Improve the knowledge over the process on its defects and limitations (i.e. porosity leads to out-gassing once in vacuum)	Tool describing process, modeling, simulation, typical phenomena, defects and their acceptability and limitations.	Software capable of simulating the MAM process build up and capable of predicting defects and identifying its limitations. Its documentation shall contain the description of the process, its modeling and simulation, typical phenomena, defects and their acceptability, required factors of safety, failure causes and minimum testing sequences
There is the need to establish and document MAM design limitations	Identification of all design MAM limitations	Tool capable of determining the process variability and, therefore, the necessary factors of safety	
There is the need to quantify the repeatability of MAM process and quality consistency	Improve the process understanding and modeling/simulation of MAM in order to understand the origin of the phenomena. Moreover, characterize the process variability (i.e. strength deviations in identical specimens)		
There is the need of increasing confidence of the space industry in MAM parts	Technological demonstration of benchmark problems in order to build heritage and a base of knowledge	Tool that contains examples and typical solutions and their performance.	
There is the need of standards for MAM process quality control in space (ECSS)	Definition of MAM qualification procedures	Tool capable of identifying/listing/consulting failure causes as well as the evaluation each failure cause	
There is the need to understand the structural response of MAM Parts	Thermo-mechanical behavior characterization of parts obtained from MAM	Tool with the constitutive modeling for MAM parts	Software, add-on or just data-sheet properties for reliable modeling and simulation MAM parts
There is the need to verify that a given part will not fail due to the thermo-mechanical loads during testing (vibration and thermal cycling)	Establishing methodologies to verify the existence of enough strength to support a set of given loads	Calculation procedure and failure criteria	Software to perform structural robustness verification
There is the need for reducing the large volumes of fuel for space Aircraft	Weight reduction of components	Tool for structural design optimization of parts	Software that minimizes the mass distribution or maximizes certain phenomena (1st mode resonance) or looks for the best arrangement of materials using optimization algorithms. Nonetheless, the solution would have to comply with certain constraints such as functional and thermo-mechanical specifications, having good manufacturability
There is the need for reducing the number of parts per assembly	Merge functionally of several parts into one		
There is the need of reducing long lead time complex parts (i.e. combustion chamber high buy to fly ratio)	Rethinking the part product cycle from its design to its manufacturing by accepting technologies that can deal with complexity without raising the cost.		
There is the need for reducing the long time frame of design cycles	Reduce user trial error iteration of engineers	Tool that looks automatically for the best parameters given a set of objectives and restrictions	

Table 2: Software competitors.

Name / Supplier	Abstract	Web Page
Dreamcatcher / Autodesk	General propose TO software	https://autodeskresearch.com/projects/dreamcatcher
Netfabb / Autodesk	AM Pre-Processor: Importing, cleaning, editing, refine and repair surface meshes (*e.g.* STL file type). Analysis of build time, supports structures, packing parts, and best fit. Slicing tools, lattice construction. Building simulation, predict stress, distortion, support structure failure.	https://www.autodesk.com/products/netfabb/overview
Tosca / Simulia	General propose TO software	https://www.3ds.com/products-services/simulia/products/tosca/structure/topology-optimization/
Ansys / Ansys	General propose TO software	http://www.ansys.com/products/structures/topology-optimization
Sol 200 / MSC	Topological, size and shape optimization software	http://www.mscsoftware.com/application/design-optimization
Simufact / MSC	Building Simulation tool for distortion residual stress, build-up orientation and support structures	https://www.simufact.com/additive-manufacturing.html
Optistruct / Altair	TO solver included in a general propose solver	http://www.altairhyperworks.com/product/OptiStruct
Amphyon / Additive Works	Building Simulation tool for distortion residual stress, build-up orientation and support structures	https://additive.works/
Creo 4.0 / PTC	Integrated solution for CAD Design, optimization (simple lattices approach with mathematical model), structural verification (simple linear static), Design translation to manufacturing. At moment limited to machines for polymeric printing	https://www.ptc.com/en/products/cad/3d-design/design-for-additive-manufacturing
Virfac / Geonx	Building simulation tool for distortion residual stress, build-up orientation and support structures	http://www.geonx.com/index-3.html
Exasin / 3DSim	Building simulation tool for distortion residual stress, build-up orientation and support structures	http://3dsim.com/product/exasim/

Table 3: Relevant patents.

Title	Inventor(s)	Applicant(s)	Publication Number / Date	Abstract
Manufacturing system using topology optimization design software, novel three-dimensional printing mechanisms and structural composite materials	Nathan Armstrong	FreeSpace Composites INC	US 20150239178 A1 / Aug 27, 2015	Patent mainly focused on a MAM process in particular that highlights its mains advantages. Moreover, it has a section highlighting the importance of the interplay between the topological optimization and MAM technologies and the necessity of one respecting the constraints of the other technologies.
System and method for topology optimization with a plurality of materials	Rajan R. Chakravarty; Weizhang Simon Xu; Kristel E. Corando;	GM Global Technology Operations LLC	US 2015/0103698 A1 / Apr 16,2015	The patent describes the architecture of TO procedure as well as it computer architecture, improving it with the possibility of using different materials at different locations in order to minimize or maximize certain aspects. Topics such as constrains, load vectors, type of material, element variable and objective function (strain energy) are discussed in low detail...
Fatigue-based Topology Optimization Method and Tool	Julian Norato; Chau Le; Chistopher Ha;	Caterpillar INC	US 2014/0156229 / Jun 5 2014	The patent describes the mathematical procedure of fatigue based topological optimization methodology. This document describes some of necessary equations, calculus hypothesis and steps to perform such optimization. The patent is associated with software that implements the described technology. The inventor highlights topics such as density filtering, interpolation and adaptive normalization schemes and fatigue outputs (local and global).
Improved Topology Optimization for Designing Engineering Product	Tushar Goel; Willem J. Roux;	Livermore Software Technology Corporation	EP 2 251 805 A2 / Nov, 17 2010	The patent presents methods and systems topological effectiveness on the engineering product design as well as iterative nature-based structural responses (typically obtained by FEM). Moreover, the inventor highlights that this technology is based on the hybrid cellular Automata Method having different lattices.
Structural Optimization System, Structural Optimization Methodology and Structural Optimization Program	Takajuki Yamada; Shinji Nishiwaki; Kuzuhiro Izui; Masataka Yoshimura;	Kyoto University	US 2011/0270587 A1 / Nov. 3, 2011	This patent describes a topological optimization method and program. It mathematical postulation using level set functions that avoids some problems of the conventional topological optimization.
Method for structure-preserving topology optimization of lattice structures for Additive Manufacturing	Suraj Ravi Musuvathy; Erhan Arisoy;	Siemens Product Life-cycle Management Software Inc	US 9787651 B2 / Oct 17 2017	This patent focus on a method to perform topological optimization of lattice structures, by establishing bounding boxes to each lattice and optimize its topology using level set method.
Additive Topology Optimized Manufacturing for Multi-Functional Components	Aaron T. Nardi; Tahany Ibrahim El-Wardany; Daniel V. Viens; Matthew E. Lynch; Arthur Hsu; Michael A. Klecka; Wenjiong Gu;	Sikorsky Aircraft Corporation	US 2014/0277669 A1 / Sep 18 2014	This patent proposes an architecture of communication between the concept and design stage that accounts for the necessity of topological Optimization, CAD, FEM and their interplay in order to archive a given objective, respecting, some constraints. Moreover, there is the need for multi-physics models in order to capture certain phenomena

there is no interest in competing in the referred market since it is highly developed already. Specialized solutions listed in Table 2 makes it unattractive due to their level specialization. In fact, they heritage knowledge from welding simulation.

About material data (Product 2 - Table 1), there is still a long way to go. Many experimental tests need to be performed due to the immaturity of the technology.

Regarding structural robustness verification (Product 3 - Table 1), there are many general proposed solutions which in principle can be used for the present scope. However, these do not meet the metal additive manufacturing needs (*i.e* anisotropy or porosity) turning it a relevant opportunity.

About design optimization (Product 4 - Table 1), the third patent (see Table 3) proposes an architecture that shall be avoided during development and there are many general propose solutions which in principle can be used for the present scope. However, these do not meet the MAM needs (*i.e* manufacturing restrictions) turning it as a relevant opportunity.

Business Idea

As a result of the previous analysis, the proposed business idea is based on AMISAS (Additive Manufacturing Software for Accurate Simulation - see Figure 2), which is software that intends to reduce costs of the design stage of metal additive manufacturing. As previously

Figure 2: Proposed software's logo.

referred, by 2026, a 6600M€ revenue is forecast for MAM and it is expected that 25% will be generated in the aerospace market. Moreover, if a typical engineering cycle is considered, a cost of 15% is expected. Thus, a market of 250M€ is the initial target of this idea. The software would have three modules, each one intends to address the products 2, 3 and 4 of Table 1. Thus, AMISAS's modules shall be:

- Material Model: Multiscale Accurate Characterization due to the complexity of the involved phenomena (i.e. melting, vaporization, solidification, *etc.*)
- Design Optimization: as an alternative to typical trial error optimization (costly), a mathematical model (Topology Optimization - TO) is proposed in order to perform the design optimization systematically.
- Structural verification: parts produce by MAM raises several challenges (anisotropy, residual stress, porosity, etc.), which need to be accounted for and a model needs to be developed.

Despite the limited interest in competing on Product 1 of Table 1, a competitive business requires a fully integrated solution since the market still wants the referred product. Thus, the idea is to perform a partner alliance with a process simulation company already establish on the market or use a spin approach. The viability of the solution is dependent on its architecture, which needs to be carefully chosen due to the existence of a patent on the subject (last patent of Table 3).

Value Proposition

The value proposition consists of providing the computational tools (software) capable of searching for optimum thermo-mechanical aerospace structures obtained from additive manufacturing. All of the products will include the technical documentation intended to guide users thought various steps of designing for MAM. Thus, increasing reliability and efficiency or decreasing design time, costs and engineering frustration are its many gains. Since it will be capable of providing design tools (guidelines, limitations and constraints) and a systematic design optimization methodology. Moreover, the prediction of structural responses and lifetime assessment is also one key strength. Unlike general propose solutions, this is fully adapted and rethought for MAM specifications in order to release its full potential.

Market Implementation

The market implementation of this idea would have two distinct phases. The first phase would consist of engineering/consulting services to future costumers and European Funding. Thus, the idea would be financing product development while gathering information on the client's real needs. In this way, the project would be financed and developed in a sustainable and meaningful way. Moreover, it would be a great way to advertise the brand and develop a solution according to the market needs.

After reaching a minimum viable product, the second phase would start with its commercialization. Another key step of this phase would be the formation of a partner alliance or spin approach with a process simulation company in order to provide a truly integrated solution. Moreover, this is a great way to finance the company in its second phase.

Costumers

Independently of the phase, the customer's segments are the engineering departments of aerospace companies such as Deimos, GMV, Tekever, LusoSpace, EdiSoft, Omnidea, SpinWorks, HPS. These are just some Portuguese companies (small market), the idea would be the European companies at an initial stage. Additionally, other consulting companies could be potential clients.

Resources

The first phase of the company would require few resources. It would be limited to a few members, computers and subcontracted server services. Since the idea is to use the software under development, the costs of licensing software would be limited but still real due to the needed auxiliaries software (*i.e.* CAD Software).

The second phase would require considerably more resources. The staff members would raise considerably (i.e. human resources, marketing, client support, sales, licensing systems, servers maintenance, interface design and development[1], R&D) as well as IT infrastructures and office space.

Cost and Revenue

In the first phase, the structure of costs is rather low. The salaries and office fees would be paid through engineering/consulting services to future costumers and European Funding (i.e. research projects). The revenue of this first phase would be a direct consequence of the execution of the services.

In the second phase, the costs raise according to the needed resources previously enumerated. The revenues from the first phase would continue at the beginning of the second phase. However, the idea is to progressively change the font of revenue only to software sales and annual maintenance or renting. Additionally, there is the revenue coming from training. In order to maximize the client's envelope, the option of basic, standard and ultimate versions would be important. Thus, the adjustment of the software cost to the company dimension can be an option.

Canvas Model

The Canvas model is according to [7] and represented on Figure 3.

[1]User Friendliness of calculation software has limited relevance for developers, but, crucial for users.

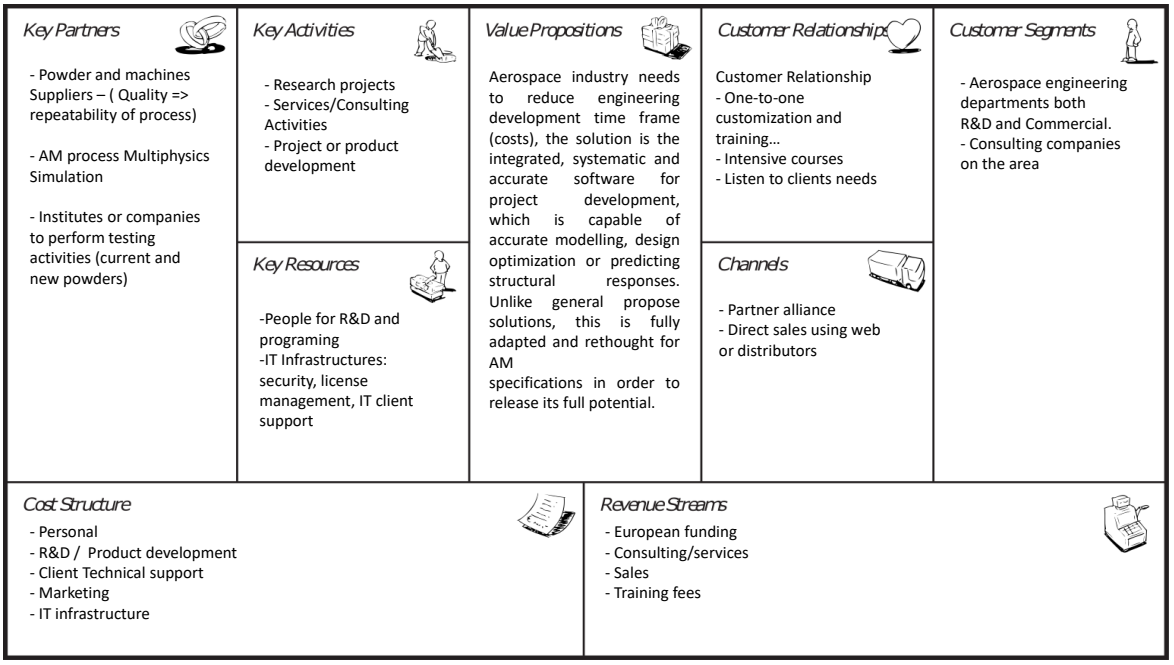

Figure 3: Canvas business model.

Acknowledgements

The authors gratefully acknowledge the financial support of the Portuguese Foundation for Science and Technology (FCT) under the projects CENTRO-01-0145-FEDER-029713 by UE/FEDER through the programs CENTRO 2020 and COMPETE 2020, and UID/EMS/ 00481/2013-FCT under CENTRO-01-0145-FEDER-022083. Financial support of program CENTRO 2020 and UE/FEDER is acknowledged through the project CENTRO-01-0247-FEDER-024039, designated as ADVANSS. B. Barroqueiro also acknowledges the financial support by the FCT through the scholarship SFRH/BD/120779/2016.

References

[1] Susanne Hertenberger (Editor), Market Report ID: 44670015/Global, `https://www.maschinenmarkt.international/english/global/articles/604851/`, accessed: 18-11-2017.
[2] B. Dutta, F. H. Froes, in: B. Dutta, F. H. Froes (Eds.), Additive Manufacturing of Titanium Alloys, Butterworth-Heinemann, 2016.
[3] Aremu A, Ashcroft I, Hague R, Wildman R, Tuck C, Suitability of SIMP and BESO Topology Optimization Algorithms for Additive Manufacture, Wolfson School of Mechanical and Manufacuring Engineering (2010).
[4] E. Incorporated, Measurement science roadmap for metal-based additive manufacturing: workshop summary report, Tech. rep., Maryland Columbia (2013).
[5] A. Clausen, Topology optimization for additive manufacturing, Ph.D. thesis, DTU Mechanical Engineering, Technical University of Denmark (2016).
[6] E. Komi, Topology optimized in design for additive manufacturing, Presentation (2017).
[7] A. Osterwalder, Y. Pigneur, Business Model Generation: A Handbook for Visionaries, Game Changers, and Challengers, Wiley Desktop Editions, Wiley, 2010.

Appendix B

Startups' life-cycle and their funding mechanisms

Any business idea that involves an actual company will need funding to develop a minimal viable product, which allows entering the market and starting to generate revenue. In practice, this task is challenging, and many startups do not flourish. Due to the challenging nature of the referred task, many institutions have been created to help startups during their initial stages. In the scope of this appendix, a compact article, entitled "Grow the idea and start it up", is presented, which performs a succinct overview of the startups' life cycle in a holistic perspective and their funding mechanisms with particular emphasis on the space industry.

Grow the idea and start it up

B. Barroqueiro

Abstract

A Startup company is a human institution designed to create new products and services under conditions of extreme uncertainty. In general, its origin is associated with a good idea, and its funding raises several challenges. The study introduces the startup life cycle (bootstrapping stage, seed-stage and creation stage) and enumerates its funding (governmental, spin activities, crowdfunding, competitions, and venture capital) and supporting mechanisms. Thus, the funding possibilities are high and extensive lists are provided. Although the numerous funding alternatives are available, the task of funding a startup is far trivial.

Keywords: Startup; Life cycle; Funding Mechanisms; Incubators; Accelerators

Introduction

Everything has its life cycle and a startup is not the exception. In fact, its needs change according to its stage. Thus, it is important to understand its stages and be aware of the available mechanisms that increase its chance of success. This study intends to contribute to the overall knowledge of the existent funding mechanisms as well as the supporting mechanisms such as incubators or accelerators. Thus, this work gives the entrepreneur an overall view of existent mechanisms and helps the decision making of each one/ones is/are more adequate to his case. This way, this article briefly (i) introduces the startups' life cycle, (ii) its funding and (iii) supporting mechanisms. Thus, the reader can explore the connection between the three topics.

Startups Life Cycle

A Startup is a human institution designed to create new products and services under conditions of extreme uncertainty [1]. According to [2], the startups' life cycle can be subdivided into three stages considering a holistic perspective:

- Bootstrapping Stage
- Seed Stage
- Creation Stage

The Bootstrapping stage has a strong connection with financial resources, being one of the main reasons for their failure. At this initial stage, the capital raising has proven to be difficult and unfruitful [3], leading to bootstrapping activities. In general, these activities involve personal savings, credit, friends, and family as mechanisms to raise capital. Other mechanisms are loaning equipment or buying it in used condition, delaying payments to suppliers, or selling services [4]. In some cases, angel investors can provide some of the starting capital.

The seed stage is characterized by teamwork, prototype development, market-entry, valuation of the venture, seeking support mechanisms, and average investments [2]. This stage is mainly characterized by product development and consequently people hiring. In fact, "For Seed Stage Startups, It's Hire or Die" [5] and poor choice of new employees lead to failure [3]. The support mechanisms such as accelerators or incubators can give the need support and guidance.

The creation stage begins when the product has entered the market and sales are a reality. At

this stage, organizational arrangements are commonly required and corporate finance is usually the main choice [3]. Venture capital is a way to finance the creation stage.

Funding Mechanisms

There are several funding mechanisms, which may be subdivided in:

- Governmental funding;
- Spin activities;
- Crowdfunding;
- Competitions;
- Venture Capital.

Within Europe, there are several governmental programs to get funding namely: Copernicus Startup Programme [6], Galileo Startup Programme [7], Teck City UK [8], La French Tech [9], Enterprise Ireland [10], Business Finland [11] and, finally, Startup Lisboa [12]. The Copernicus and Galileo programs are related to the space market and the European Space Agency (ESA) is one of its main supporters. Startup Lisboa supports the creation of companies and their first years of activity, being a private non-profit association that provides entrepreneurs office space as well as a support structure - mentoring, strategic partners, access to investment/funding, networking activities and a community based on knowledge and sharing [12].

Companies are increasingly looking for new growth opportunities. Some companies do it by corporate venturing, basically acquiring strategic companies. Others do it by encouraging their employees to take their business idea and start a company, these activities are denominated as spin activities [13]. Thus, new entrepreneurs, who want to develop their ideas, get the needed support. In case the referred company does not have the resources needed to engage in such adventures (too small), there is an European instrument called Horizon 2020 SME instrument [14] that finances such a scenario. The referred Instrument is an open call instrument that has three distinct phases. The first phase evaluates the concept and feasibility of the idea. A successful capital raise of 50K euros can be acquired. The second phase intends to evaluate the product capability of market entry and its maturity. The referred instrument can finance 70% of the total capital needed (something between 0.5 to 2.5 million euros). The last phase focus on business support, coaching, and networking.

Crowdfunding is attractive to startups as an alternative funding source, it encompasses the outsourcing of an organization that requests monetary contributions from a strategically defined crowd towards a commercial or social business goal [15]. Within the crowdfunding category, different typologies can be defined such as:

- Donation Crowdfunding
  - Pure Donation: no reward is expected. Examples: Kopernik [16], Crowdrise [17];
  - Reward Donation: some sort of gift is expected. Example Indiegogo [18].
- Lending Crowdfunding
  - Forgivably Loan: interest is required, only if successful. Examples Quirky [19], TubeStart [20], AppsFunder [21];
  - Presales: finish product is expected. Examples: Kickstarter [22], PledgeMe [23];
  - Traditional Loan: fixed-term interest. Examples: SoMoLend [24], Lending Club [25];
- Equity Crowdfunding: securities, revenue or profit sharing is required. Examples: AngelList [26], Seedrs [27], EquityNet [28], Crowdcube [29], Fundable [30], FundedByMe [31], Invesdor [32], SeedMatch [33], Wised [34].

Crowdfunding is an excellent mechanism to raise capital for a startup in the bootstrapping stage. On the other hand, for seed-stage startups, it has less importance.

Startup competitions are a great way to not only raise funding for your startup but to also increase your startup's brand awareness and receive some useful feedback from experts and potential customers. Slush [35], Tech Crunch [36], Next Step Challenge [37], DLD [38], CPDP [39], Webit [40], Podim [41], Sonar [42], OS!O [43] and Web Summit [44] are competitions worth looking [45].

At a mature level of the startup, VC firms can provide a high investment to grow the company. The main drawback is the owner shares getting diluted to a point, where his autonomy is limited or non-existent. TVM Capital [46], Forbion [47], SEP [48], Partech [49], Endeavour Vision [50], Nothzone [51], Seedcamp [52] and Antemis [53] are some VC firms in Europe [45].

Support Mechanisms

There is no doubt that the number of European startups has increased dramatically in recent years, which also means that the number of startup incubators and accelerators has grown as well [45]. Founder Institute [54], Scout24 [55], Startup Sauna [56], Techstars [57], Telenet Kickstart [58], Eleven [59], StarCube [60], Accelerace [61], GameFounders [62], Startupbootcamp [63], Rockstart [64], INiTS [65], Zip [66], H-Farm [67], Garage [68] and Fongit [69] are several examples of accelerators/incubators across Europe.

Within Space Market, ESA also made available eighteen ESA Business Incubation Centers (ESA BIC) spread across Europe and the Portuguese ESA BIC is located in Instituto Pedro Nunes (IPN) [70].

Conclusion

This study describes and enumerates the main mechanisms either financial either supporting. There is no doubt that the number of European startups has grown at an incredible pace and, consequently, all the mechanisms have grown as well. Despite the long lists presented, many more examples may exist.

Acknowledgements

The authors gratefully acknowledge the financial support of the Portuguese Foundation for Science and Technology (FCT) under the projects CENTRO-01-0145-FEDER-029713 by UE/FEDER through the programs CENTRO 2020 and COMPETE 2020, and UID/EMS/ 00481/2013-FCT under CENTRO-01-0145-FEDER-022083. Financial support of program CENTRO 2020 and UE/FEDER is acknowledged through the project CENTRO-01-0247-FEDER-024039, designated as ADVANSS. B. Barroqueiro also acknowledges the financial support by the FCT through the scholarship SFRH/BD/1207-79/2016.

References

[1] E. Ries, The Lean Startup: How Todays Entrepreneurs Use Continous Innovation to Create Radically Sucessfull Bussiness, New York: Crown Business, 2011.

[2] Aidin Salamzedeh, H.K. Kesim, Startup companies: Life cycle and challenges, SSRN Papers (2015).

[3] N.Q. Hoang, A guide for startups: Using bookndo as a case study, Bachelors Thesis, Degree Programme in Business Management (2015).

[4] Q. Ye, Bootstrapping and new born startups performance: The role of founding team human capital, Global Journal of Entrepreneurship (2017).

[5] For seed stage startups, it's hire or die – visualizing the series a pipeline for 2015, Online :(Jan 2015).

[6] Copernicus start-up programme, Online: `http://www.copernicus.eu/main/start-programmes` (2011).

[7] European satallite navigation competition, Online: `https://www.esnc.eu` (2018).

[8] Tech city: We help ambitious tech founders start, scale and succed, Online: `https://www.techcityuk.com/` (2018).

[9] La french tech: Global movement celebrating french innovation, entrepreneuship and sartups, Online: `https://meetlafrenchtech.com` (2012).

[10] Enterprise ireland where innovation means business, Online: `https://www.enterprise-ireland.com` (2015).

[11] Business finland for finnish customers, Online: `https://www.businessfinland.fi` (2018).

[12] Startup lisboa: Lisbon's incubator, Online: `http://www.startuplisboa.com` (2011).

[13] R. Rohrbeck, M. Dohler, H.M. Arnold, Combining spin-out and spin-in activities – the spin-along approach, MPRA (2007).

[14] Horizon 2020 sme instrument, Online: https://ec.europa.eu/easme/en/sme-instrument (2017).
[15] J. Paschen, Choose wisely: Crowdfunding through the stages of the startup life cycle, Business Horizons 60 (2) (2017) 179 – 188, crowdsourcing.
[16] Kopernik, Online: https://kopernik.info/project/start-up-tech-sales-in-kratie-cambodia (2015).
[17] Crowdrise, Online: https://www.crowdrise.com/ (2018).
[18] Indiegogo, Online: https://www.indiegogo.com/ (2018).
[19] Quirky, Online: https://quirky.com/.
[20] Tubestart, Online: https://www.crunchbase.com/organization/tubestart (2013).
[21] Appsfunder, Online: http://appsfunder.guru/ (2018).
[22] Kickstarter, Online: https://www.kickstarter.com/ (2018).
[23] Pledgeme, Online: https://www.pledgeme.co.nz/.
[24] Somolend, Online: https://www.crunchbase.com/organization/somolend (2014).
[25] Lendingclub, Online: https://www.lendingclub.com/.
[26] Angellist, Online: https://angel.co/.
[27] Seedrs, Online: https://www.seedrs.com/ (2018).
[28] Equitynet, Online: https://www.equitynet.com/ (2005).
[29] Crowdcube, Online: https://www.crowdcube.com/.
[30] Fundable, Online: https://www.fundable.com/ (2018).
[31] Fundedbyme, Online: https://www.fundedbyme.com/en/ (2012).
[32] Invesdor, Online: https://www.invesdor.com/en (2014).
[33] Seedmatch, Online: https://www.seedmatch.de/ (2005).
[34] Wiseed, Online: https://www.wiseed.com/en (2005).
[35] Slush, Online: http://www.slush.org/.
[36] Tech crunch, Online: https://techcrunch.com.
[37] Next step challenge, Online: https://nextstepchallenge.com/.
[38] Dld, Online: http://www.dld-conference.com/.
[39] Cpdp, Online: http://www.cpdpconferences.org/.
[40] Webit, Online: https://www.webit.bg/2018/index.php.
[41] Podim, Online: http://podim.org/en-us.
[42] Sonar, Online: https://sonar.es/en/2016/.
[43] Os!o, Online: http://oiw.no/program.
[44] Web summit, Online: https://websummit.com/.
[45] How to launch a startup in europe, Online :https://fi.co/insight/how-to-launch-a-startup-in-europe (Jan 2018).
[46] Tvm capital, Online: https://www.tvm-lifescience.com/about-us/ (2018).
[47] Forbion, Online: https://forbion.com/en/#/ (2016).
[48] Sep, Online: https://www.sep.co.uk/ (2018).
[49] Partech, Online: https://partechpartners.com (2018).
[50] Endeavourvision, Online: http://www.endeavourvision.com/ (2005).
[51] Northzone, Online: https://northzone.com/ (1996).
[52] Seedcamp, Online: http://seedcamp.com/ (2017).
[53] Anthemis, Online: http://www.anthemis.com/ (2018).
[54] Founder institute, Online: https://fi.co/contents/enrolling# (2018).
[55] Scout24, Online: http://www.scout24.com/en/Home.aspx (2018).
[56] Startup sauna, Online: http://startupsauna.com/.
[57] techstars, Online: https://www.techstars.com/programs/ (2017).
[58] Telenet kick start, Online: https://telenetkickstart.be/ (2018).
[59] Eleven, Online: https://www.11.me/ (2007).
[60] Jic starcube, Online: https://www.jic.cz/en/starcube/ (2014).
[61] Accele race, Online: https://www.accelerace.io/.
[62] Game founders, Online: http://www.gamefounders.com/ (2015).
[63] Startup boot camp, Online: https://www.startupbootcamp.org/accelerator/.
[64] Rock start, Online: https://www.rockstart.com/accelerator/.
[65] Inits, Online :http://www.inits.at/en/.
[66] Zip, Online :http://zipzg.com/en/.
[67] H-farm, Online :http://www.h-farm.com/en.
[68] Garage, Online :http://garage.md/en (2011).
[69] Fongit, Online :https://fongit.ch/ (2011).
[70] Esa business incubation centres, Online: http://www.esa.int/Our_Activities/Space_Engineering_Technology/Business_Incubation/ESA_Business_Incubation_Centres12 (2018 (Last Update)).

Intentionally blank page.

Appendix C

Interactive models

The publications [P4] and [P5] contain interactive models that are not functional in the present document. Thus, Table C.1 provides functional versions of the referred interactive models. It is worth noting that Figure 9 from [P4] corresponds to design T1 in the reference state and Figure 10 corresponds to design T2 in the reference state. Finally, Table 3 from [P5] is identical to Table C.1.

Table C.1: Interactive 3D models of the reference and the smooth designs.

	TO	T1	T2
Reference	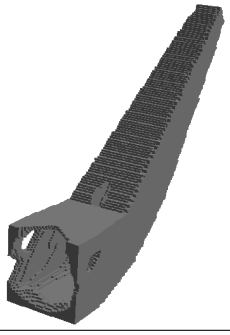	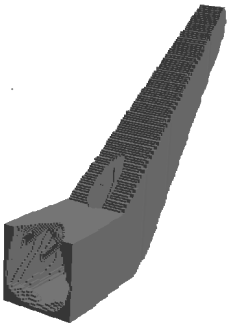	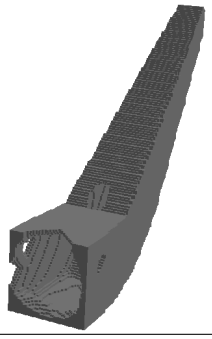
ELA	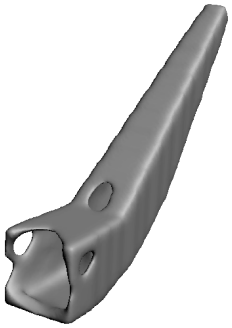	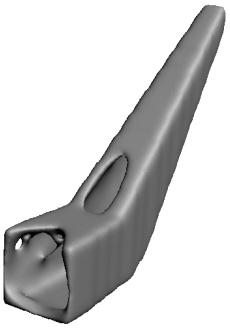	
TL	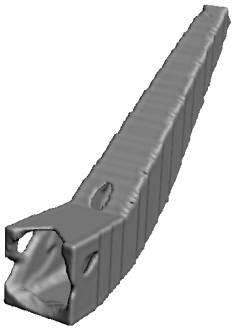	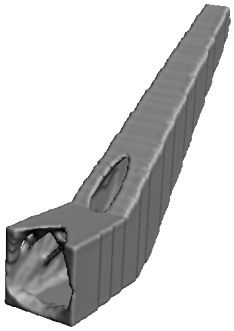	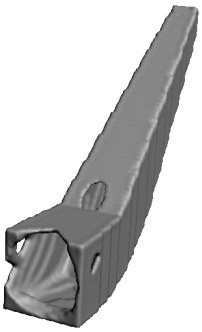
MDLB		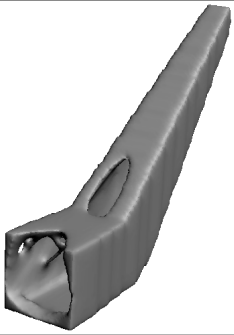	

Additional references

[1] ECSS-E-HB-32-26A. Space engineering: Spacecraft mechanical loads analysis handbook. ECSS Secretariat ESA-ESTEC Requirements Standards Division Noordwijk, Netherlands 2013.

[2] NASA-HDBK-7005. Dynamic environmental criteria: Nasa technical handbook. National Aeronautics and Space Administration 2001.

[3] Dawson-Haggerty et al. Trimesh. Computer Software avaialable in https://trimsh.org/ acessed on 2019-12-8.

Intentionally blank page.